

# Towards a quantitative understanding of chytrid cellular development

by

Davis Jay Laundon

A thesis submitted in partial fulfilment of the degree of

DOCTOR OF PHILOSOPHY

University of East Anglia, School of Environmental Sciences

September 2021



This copy of the thesis has been supplied on condition that anyone who consults it is understood to recognise that its copyright rests with the author and that use of any information derived therefrom must be in accordance with current UK Copyright Law. In addition, any quotation or extract must include full attribution

## Abstract

The current understanding of fungal developmental biology is almost entirely derived from dikaryan hyphae and yeast, neglecting the diversity and prevalence of other major fungal lineages. The 'chytrids' (phylum Chytridiomycota) are a predominantly unicellular group of fungi pervasive throughout aquatic environments. As prominent saprotrophs, parasites, and pathogens, chytrids are integral to biogeochemical cycling in aquatic ecosystems. Additionally, they retain ancestral cellular characteristics present in the last common ancestor of branching (i.e. hyphal and rhizoidal) fungi, making chytrids powerful models to study the evolution of fungal-specific innovations. Despite the evolutionary and ecological importance of chytrids, their basic cell biology and development remains poorly resolved. This fundamental gap must be closed if a proper appreciation for chytrids is to be achieved. To address this, this thesis aimed to present a quantitative picture of chytrid development and identify shifts in biology across the life cycle. Using *Rhizoclosmatium globosum* as a model species for chytrid biology, this thesis set out to 1) establish an experimental toolkit for chytrid developmental biology, 2) identify the cellular and molecular drivers of the chytrid life cycle, and 3) quantify the development of the rhizoid, all of which were achieved. The combination of 3D electron microscopy reconstructions and transcriptomic profiling achieved a holistic developmental atlas for the chytrid life cycle shedding light on lipid metabolism, vacuolisation, and zoospore development in *R. globosum*, and revealing the chytrid apophysis to be a functionally delineated structure governed by intracellular trafficking. Live-cell confocal microscopy and reconstruction of developing rhizoids demonstrated that rhizoid growth was analogous to hyphal morphogenesis, adaptive to resource availability, and capable of spatiotemporal functional differentiation. Overall, this thesis achieved a quantitative characterisation of chytrid development, uncovered previously hidden cellular complexities important for ecological and evolutionary chytrid biology, and will provide a solid foundation for future investigations into chytrid biology.

## **Access Condition and Agreement**

Each deposit in UEA Digital Repository is protected by copyright and other intellectual property rights, and duplication or sale of all or part of any of the Data Collections is not permitted, except that material may be duplicated by you for your research use or for educational purposes in electronic or print form. You must obtain permission from the copyright holder, usually the author, for any other use. Exceptions only apply where a deposit may be explicitly provided under a stated licence, such as a Creative Commons licence or Open Government licence.

Electronic or print copies may not be offered, whether for sale or otherwise to anyone, unless explicitly stated under a Creative Commons or Open Government license. Unauthorised reproduction, editing or reformatting for resale purposes is explicitly prohibited (except where approved by the copyright holder themselves) and UEA reserves the right to take immediate 'take down' action on behalf of the copyright and/or rights holder if this Access condition of the UEA Digital Repository is breached. Any material in this database has been supplied on the understanding that it is copyright material and that no quotation from the material may be published without proper acknowledgement.

## List of contents

<b>Chapter 1 - There is a need for a better understanding of chytrid biology</b> .....	<b>13</b>
1.1 Summary.....	13
1.2 Introduction .....	13
1.3 Why study chytrids? .....	17
1.3.1 Chytrids are a poorly understood branch of fungal diversity.....	17
1.3.2 Chytrids have major ecological impacts .....	18
1.3.3 Chytrids are valuable for understanding fungal evolution .....	19
1.4 What resources do we have to study the biology of chytrids?.....	20
1.4.1 Chytrids are poorly represented in fungal resources .....	21
1.4.2 Chytrid-specific resources are few but increasing .....	23
1.4.3 Chytrid biology has been investigated with comparative genomics .....	24
1.5 What do we know already about chytrid biology? .....	25
1.5.1 Biology of chytrids in terms of the life cycle.....	25
1.5.2 Biology of chytrids in terms of carbon and lipid metabolism .....	26
1.5.3 Biology of chytrids in terms of hyphal and cytoskeletal evolution .....	27
1.6 <i>Rhizoclosmatium globosum</i> JEL800 as model for chytrid developmental biology...	28
1.7 Aims and objectives of this work.....	30
<b>Chapter 2 – General methods and materials</b> .....	<b>34</b>
2.1 Reagents and chemicals .....	34
2.2 Aseptic working procedures.....	34
2.3 Growth media and buffers .....	34
2.3.1 Growth media .....	35
2.3.1.1 PmTG growth medium.....	35

2.3.1.2 Modified Bold's basal medium .....	35
2.3.1.3 F/2 phytoplankton growth medium.....	35
2.3.1.4 CHU-10 growth medium .....	36
2.3.2 Buffers .....	37
2.3.2.1 0.1 M Cacodylate buffer .....	37
2.3.2.2 Reynold's lead citrate buffer .....	37
2.3.2.3 Phosphate buffered saline .....	37
2.3.2.4 PEM buffer .....	37
2.4 Organism culture and maintenance .....	38
2.4.1 <i>Rhizoclostratium globosum</i> JEL800 .....	38
2.4.2 Harvesting zoospores .....	39
2.4.3 Maintenance of the Ast1-Chy1 pathosystem.....	39
2.4.4 <i>Daphnia</i> .....	39
<b>Chapter 3 – Establishing an experimental toolkit to study cellular development in chytrids .....</b>	<b>41</b>
3.1 Summary.....	41
3.2 Introduction .....	41
3.3 Methods and materials .....	43
3.3.1 Using fluorescent vital stains for subcellular chytrid structures.....	43
3.3.2 Non-invasive imaging of the chytrid life cycle.....	44
3.3.3 Imaging chytrid growth on chitin sources .....	45
3.3.4 Imaging of diatom-chytrid interactions.....	46
3.3.5 Cryopreservation and revival of chytrid zoospores.....	47

3.4 Results .....	48
3.4.1 Using fluorescent vital stains for subcellular chytrid structures.....	48
3.4.2 Non-invasive imaging of the chytrid life cycle.....	49
3.4.3 Imaging chytrid growth on chitin sources .....	50
3.4.4 Imaging of diatom-chytrid interactions.....	52
3.4.5 Cryopreservation and revival of chytrid zoospores.....	54
3.5 Discussion.....	55
3.6 Conclusion .....	57
<b>Chapter 4 - A cellular and molecular atlas reveals the basis of chytrid development</b> .....	<b>58</b>
4.1 Summary.....	58
4.2 Introduction .....	59
4.3 Methods and materials .....	62
4.3.1 Cell harvesting for SBF-SEM, transcriptomics, and lipid quantification.....	62
4.3.2 SBF-SEM imaging and reconstruction .....	63
4.3.3 RNA extraction .....	65
4.3.4 Sequencing and bioinformatics.....	65
4.3.5 Confocal and live-cell microscopy of subcellular structures.....	66
4.3.6 Image analysis for live-cell microscopy .....	66
4.3.7 Lipid extraction and quantification .....	67
4.3.8 Data analysis and statistics.....	67
4.4 Results .....	68
4.4.1 A cellular and molecular atlas of <i>R. globosum</i> development .....	68

4.4.2 Changes in lipid-associated structures are linked to variation in lipid composition	76
4.4.3 The apophysis as a compartmentalised junction for intracellular trafficking	80
4.4.4 Developing zoospores display an amoeboid morphology	83
4.5 Discussion	88
4.6 Conclusion	93
4.7 Supplementary figures	94
<b>Chapter 5 - Chytrid rhizoid morphogenesis resembles hyphal development in multicellular fungi and is adaptive to resource availability</b>	<b>96</b>
5.1 Summary	96
5.2 Introduction	97
5.3 Methods and materials	101
5.3.1 General imaging of chytrid rhizoids	101
5.3.2 Imaging 4D rhizoid development	103
5.3.3 Rhizoid tracing, reconstruction, and morphometric analysis	103
5.3.4 Confocal imaging of the rhizoid cell wall and actin	105
5.3.5 Chemical inhibition of rhizoid cell wall and actin dynamics	105
5.3.6 Quantification of chytrid $\beta$ -glucans	106
5.3.7 Identification of putative glucan synthase genes in the JEL800 genome	106
5.3.8 Carbon starvation and growth on chitin beads	106
5.3.9 Data analysis and statistics	107
5.4 Results	107
5.4.1 Quantifying chytrid rhizoid morphogenesis and development	107
5.4.2 Cell wall and actin dynamics are linked to rhizoid branching	109

5.4.3 Rhizoids undergo adaptive development in response to carbon starvation ....	112
5.4.4 Rhizoids spatially differentiate in response to patchy resource environments	114
5.5 Discussion.....	116
5.6 Conclusion .....	121
<b>Chapter 6 - A solid foundation for the future of chytrid developmental biology.....</b>	<b>122</b>
6.1 Thesis summary .....	122
6.2 Implications of thesis results.....	124
6.2.1 Implications for understanding chytrid ecology.....	125
6.2.2 Implications for understanding fungal evolution .....	127
6.3 Limitations of this thesis .....	128
6.4 Future directions.....	130
6.5 Final conclusions.....	131
<b>Appendices .....</b>	<b>133</b>
<b>Appendix A - Environmental sampling to isolate diatom-chytrid parasites .....</b>	<b>133</b>
<b>Appendix B - The impact of a novel selective parasite on the growth dynamics of marine diatoms .....</b>	<b>138</b>
B.1 Summary .....	138
B.2 Introduction.....	139
B.3 Methods and materials.....	140
B.3.1 Isolation and maintenance of the <i>Chaetoceros</i> -Thraul4 symbiosis .....	140
B.3.2 DNA extraction, V4 amplicon sequencing, and bioinformatics .....	141
B.3.3 Fluorescent and electron microscopy of <i>Chaetoceros</i> -Thraul4 .....	143
B.3.4 Quantification of diatom-thraustochytrid growth curves and host range .....	144
B.3.5 Live-cell imaging of <i>Chaetoceros</i> -Thraul4 interactions .....	144



B.3.6 The impact of overall <i>Chaetoceros</i> population health on Thraul4 growth.....	145
B.3.7 The role of individual <i>Chaetoceros</i> cell health on Thraul4 colonisation.....	145
B.3.8 The effect of Thraul4 interaction on the health of diatom populations.....	146
B.3.9 Data analysis and statistics .....	146
B.4 Results.....	147
B.4.1 Isolation of a globally distributed thraustochytrid symbiont of marine diatoms .....	147
B.4.2 Characterisation of the diatom-thraustochytrid interaction cycle .....	151
B.4.3 Thraustochytrids preferentially target unhealthy diatom cells.....	154
B.4.4 Thraustochytrid parasitism increases overall diatom population health.....	155
B.5 Discussion .....	157
B.6 Conclusion .....	159
<b>List of abbreviations</b> .....	161
<b>References</b> .....	162
<b>Peer-reviewed publications associated with this work</b> .....	199

### List of figures

Figure 1.1 Most of what is known about fungal biology comes from dikaryan cell plans .....	14
Figure 1.2 Chytrids represent an important but poorly understood branch of the fungal tree of life .....	16
Figure 1.3 Chytrids are major components of aquatic food webs .....	17
Figure 1.4 Chytrids are underrepresented in fungal resources and databases .....	21
Figure 3.1 Fluorescent vital staining of live <i>R. globosum</i> cells .....	48

Figure 3.2 Lipid and chitin dynamics were imaged non-invasively over the <i>R.globosum</i> life cycle .....	50
Figure 3.3 Growth on chitin by <i>R. globosum</i> was imaged using a suite of microscopy tools .....	51
Figure 3.4 Diatom-chytrid interactions were imaged using live-cell microscopy .....	53
Figure 3.5 <i>R. globosum</i> zoospores were cryopreserved and revived.....	54
Figure 4.1 The chytrid life cycle can be subdivided into four discrete stages .....	60
Figure 4.2 SBF-SEM reconstruction was used to characterise cellular structure .....	62
Figure 4.3 Example subcellular components identified in this study .....	69
Figure 4.4 Volume electron microscopy reconstructions of the <i>R. globosum</i> life cycle.	70
Figure 4.5 Volumetric comparisons of <i>R. globosum</i> life stages .....	71
Figure 4.6 Transcriptome analysis of the <i>R. globosum</i> life cycle.....	73
Figure 4.7 Changes in lipid-associated cell structures between <i>R. globosum</i> life stages .....	77
Figure 4.8 Changes in lipid composition occur with transitions between <i>R. globosum</i> life stages .....	78
Figure 4.9 The apophysis is a pseudo-septated and endomembrane-rich subcellular structure .....	81
Figure 4.10 The apophysis is a subcellular compartment that displays high intracellular trafficking .....	83
Figure 4.11 Developing zoospores display an amoeboid morphology with endocytotic activity .....	85
Figure 4.12 Diagrammatic summary of the <i>R. globosum</i> developmental atlas.....	88
Supplementary figure 4.1 Individual SBF-SEM replicate reconstructions.....	94
Supplementary figure 4.2 Individual SBF-SEM replicate volumetrics.....	95
Figure 5.1 Rhizoids are the basal feeding condition within the fungal kingdom.....	98

Figure 5.2 Scanning electron microscopy (SEM) images of <i>R. globosum</i> rhizoids.....	99
Figure 5.3 Transmission electron microscopy (TEM) images of <i>R. globosum</i> rhizoids	100
Figure 5.4 Neuron tracing was used to reconstruct chytrid rhizoids .....	102
Figure 5.5 Chytrid rhizoids were described using morphometric parameters adapted from neurobiology .....	104
Figure 5.6 Rhizoid morphogenesis was geometrically quantified.....	108
Figure 5.7 Cell wall synthesis and actin dynamics govern rhizoid branching .....	110
Figure 5.8 <i>R. globosum</i> JEL800 cells contain $\beta$ -glucans . .....	111
Figure 5.9 Chytrids are capable of adaptive rhizoid development under carbon starvation (Part 1) .....	113
Figure 5.10 Chytrids are capable of adaptive rhizoid development under carbon starvation (Part 2).....	114
Figure 5.11 Quantification of rhizoids growing on particulate carbon .....	115
Figure 5.12 Rhizoids associated with heterogenous particulate carbon exhibit spatial differentiation.....	116
Figure 5.13 Development of chytrid rhizoids fundamentally resembles mycelial development in hyphal fungi (Part 1) .....	117
Figure 5.14 Development of chytrid rhizoids fundamentally resembles mycelial development in hyphal fungi (Part 2) .....	118
Figure A.1 Location of the tidal mud flat (St. John's Lake) and coastal (Station L4) sampling sites .....	135
Figure A.2 Incubation and harvesting of environmental samples .....	136
Figure B.1 ThrauL4 was originally observed in environmental samples.....	147
Figure B.2 Different stages of the interaction cycle of the <i>Chaetoceros</i> -ThrauL4 symbiosis .....	148

Figure B.3 Scanning electron micrographs (SEMs) of ThrauL4 thalli attached to <i>Chaetoceros</i> diatoms .....	149
Figure B.4 ThrauL4 is a thraustochytrid in the Thraustochytriidae associated with the LAB17 clade.....	150
Figure B.5 Searching of the 2014 and 2015 Ocean Sampling Day dataset for the ThrauL4 V4 sequence revealed the global distribution of this organism .....	151
Figure B.6 Fluorescent labelling of subcellular structures in ThrauL4 .....	152
Figure B.7 Extracellular polysaccharides (EPS) were identified associated with ThrauL4.....	152
Figure B.8. Isolation of ThrauL4 allowed the characterisation of the parasite life cycle .....	153
Figure B.9 Thraustochytrids preferentially target unhealthy diatom cells .....	154
Figure B.10 Selective targeting of unhealthy diatom cells by thraustochytrids improves the overall health of the diatom population .....	156
Figure B.11 This study provides evidence for healthy herd dynamics in a protist-protist interaction .....	157

### List of tables

Table 2.1. List of fluorescent stains for labelling cellular ultrastructure used in this work .....	38
Table 4.1. Volumetric percentages and statistical comparisons of SBF-SEM reconstructions of cellular structures recorded across chytrid life stages.....	72
Table 4.2. Volumetric percentages and statistical comparisons of SBF-SEM reconstructions of cell bodies and their corresponding apophyses in immature thalli....	82
Table 4.3. Volumetric percentages and statistical comparisons of SBF-SEM reconstructions of free-swimming and developing zoospores.....	87
Table A.1. Diatom strains used in environmental co-incubations in an attempt to induce parasitism.....	134

## Acknowledgements

The work presented in this thesis would not have been possible without the support of multiple institutions and individuals. I would first like to thank my supervisory team, Michael Cunliffe, Thomas Mock, Glen Wheeler, and Cock van Oosterhout, for their invaluable feedback and guidance throughout this project. I would like to express my gratitude to The Marine Biological Association (MBA) for providing a supportive research environment and for partly subsidising my attendance at the 2019 MBL Physiology Course, which was vital to my scientific development. I would also like to thank the technical staff at the MBA, particularly Claire Hopkins, Tyrone Roberts, and the crew of the *RV Sepia*, for their tireless work in keeping research running. In addition, I would especially like to say thank you to Angela Ward for her work, support, and our many informative conversations.

Specifically, I would like to thank those individuals who provided direct technical assistance in this research: Colin Brownlee and Serena Flori (MBA) for their instruction using the Mesolens; Angela Ward and Claire Hopkins (MBA) for their direction in culturing diatoms and cryopreservation practices; Glenn Harper, Alex Strachan, and the team at the Plymouth Electron Microscopy Centre (PEMC) for their assistance with electron microscopy; Jingwen Pan (University of British Columbia) and Javier del Campo (University of Miami) for providing the reference sequences used in building phylogenetic trees; Daniel Vaultot (Station Biologique de Roscoff) for help in interpreting the Ocean Sampling Day dataset; and Chris Neal and the team at the Wolfson Bioimaging Facility (University of Bristol) for SBF-SEM optimisation and imaging throughout the project. The Ast1-Chy1 pathosystem was kindly gifted by Silke van den Wyngaert (IGB, Berlin), and we are indebted to Joyce Longcore (University of Maine) for providing *R. globosum* JEL800 from her chytrid culture collection (now curated by the Collection of Zoosporic Eufungi at the University of Michigan). This research was supported by an EnvEast Doctoral Training Partnership (DTP) PhD studentship funded from the UK Natural Environment Research Council (NERC grant no. NE/L002582/1).

## **Chapter 1 – There is a need for a better understanding of chytrid biology**

**Published as:** Laundon D and Cunliffe M. 2021. A call for a better understanding of aquatic chytrid biology. *Front Fungal Biol* **2**:1-8. doi:10.3389/ffunb.2021.708813

**Author contributions:** DL and MC wrote the manuscript together.

### **1.1 Summary**

The phylum Chytridiomycota (the 'chytrids') is a major, mostly unicellular, lineage of fungi. Chytrids are ecologically significant as saprotrophs, parasites, and pathogens, and of evolutionary interest due to their retention of biological traits considered ancestral in the fungal kingdom. While the existence of chytrids has long been known, their fundamental biology has received relatively little attention compared to dikaryan fungi. In recent years, chytrids have generated increased interest due, in part, to their widespread detection in molecular ecology surveys and role as the agents of the global amphibian panzootic. As such, we are beginning to establish a detailed understanding of chytrid environmental distribution and insight into their ecological functions and prominence. The underlying biology governing these ecological activities and core developmental processes remains largely understudied and therefore unresolved. Major biological questions are outstanding for chytrids: What are the foundational biological mechanisms that control their development and life cycle? Which core biological processes underpin their ecological influence? What can their biology tell us about the evolution of fungi and the wider eukaryotic tree of life? These are questions that must be resolved if a comprehensive understanding of chytrids is to be achieved.

### **1.2 Introduction**

Fungi are well-known for their ecological and evolutionary importance, distinctive cell biology, and long-term service as model organisms for the biological sciences. Most of our comprehension of fungal developmental and cell biology is derived from dikaryan (Ascomycota and Basidiomycota) hyphal and yeast cell types (Figure 1.1A-E), which have often been isolated from terrestrial or human-associated environments. This knowledge

base does not cover the full diversity of habitats, ecologies, and cell types found throughout the Kingdom Fungi and neglects the prevalence and diversity of non-dikaryan fungal groups.

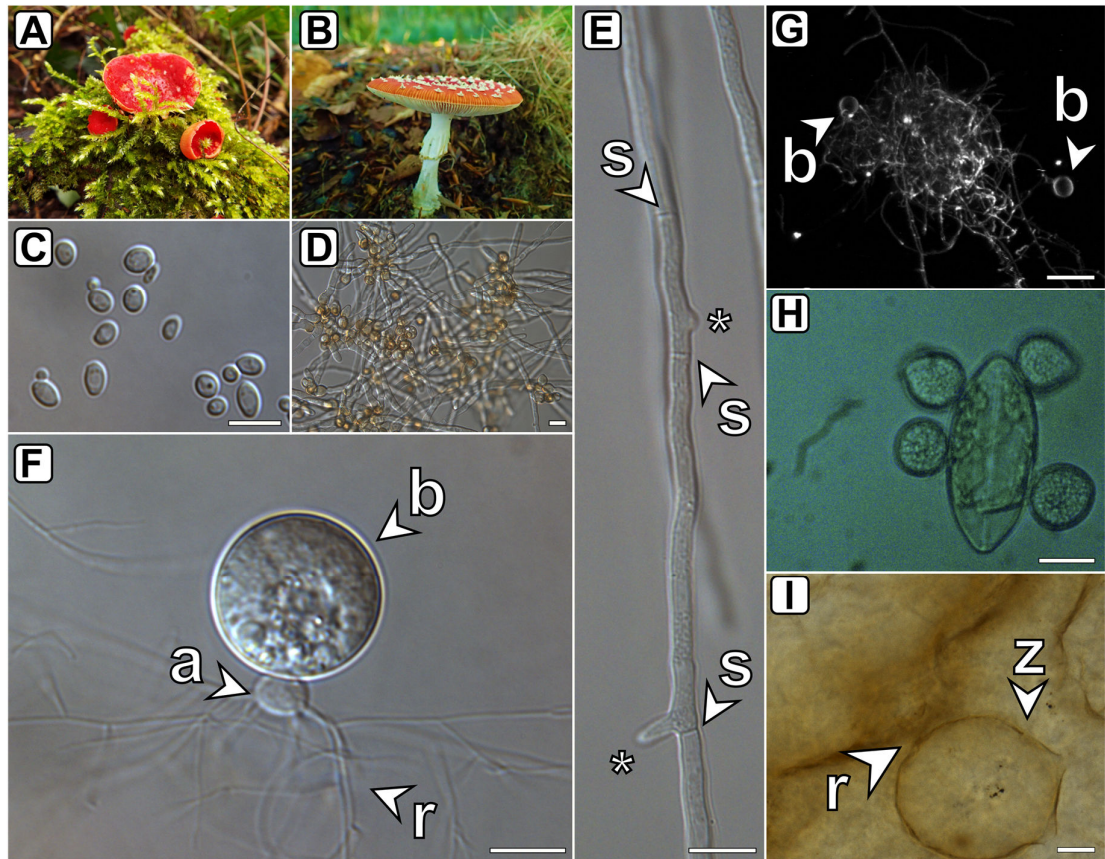


**Figure 1.1 Most of what is known about fungal biology comes from dikaryan cell plans.** The Dikarya is a fungal taxon consisting of the phyla Ascomycota (A) and Basidiomycota (B), and its members dominate our understanding of fungal cell biology. Pictured are the terrestrial species *Sarcoscypha coccinea* (A) and *Amanita muscaria* (B). The Dikarya are predominantly represented by yeast (C) and mycelial (D) cell plans. Pictured are the yeast *Metschnikowia zobellii* (C) and the mycelium of the marine fungus *Paradendryphiella salina* (D). The fundamental units of the mycelium are elongating, branching structures called 'hyphae' (E). Pictured are the hyphae of *P. salina* (E). Chytrids are widespread, ecologically prominent fungi but their fundamental biology is poorly understood (F). Pictured is the freshwater fungus *Rhizoclostridium globosum* (F). (G) Chytrids are prominent saprotrophs of recalcitrant biopolymers. Pictured is a maximum intensity projected z-stack confocal image of two *R. globosum* cells growing attached to a chitin particle. (H) Ecologically important taxa such as microalgae can be parasitised by

aquatic chytrids. Pictured is a sea ice diatom infected by an unknown chytrid species.

Image courtesy of Brandon Hassett (Arctic University of Norway). (l) Extant chytrids retain ancestral cellular characteristics conserved from their last common ancestor with hyphal fungi. Identical cell plans can be observed in fossil chytrids, such as the 407-million-year-old *Cultoraquaticus trewini* pictured. Image courtesy of Christine Strullu-Derrien (Natural History Museum) (Strullu-Derrien et al., 2016). apophysis (a), cell body (b), rhizoids (r), hyphal septa (s), zoosporangium (z), hyphal branching points (asterisks). Scale bars = 10  $\mu\text{m}$ .

The phylum Chytridiomycota (the 'chytrids') is an major, predominantly unicellular group of mostly aquatic fungi that use anucleate rhizoids to attach and feed on substrates, and reproduce by motile uniflagellate zoospores (Hurdeal et al., 2021; Naranjo-Ortiz and Gabaldón, 2019a; Sparrow, 1960) (Figure 1.1F&G, Figure 1.2A&B). Chytrids are significant components of aquatic ecosystems (Gleason et al., 2017; Grossart et al., 2019). In addition, they retain cellular characteristics and biological traits shared from their last common ancestor with hyphal fungi, making them of interest to evolutionary biologists (Berbee et al., 2017; Nagy et al., 2017) (Figure 1.2C). Even though chytrids have been known to science since the mid-19<sup>th</sup> century (Braun, 1856), their fundamental biology has received relatively little attention compared to other fungi, particularly dikaryans. In recent years, chytrids have generated increased attention due, in part, to their widespread detection in culture-independent molecular ecology surveys (Comeau et al., 2016; Jeffries et al., 2016; Kiliyas et al., 2020; Taylor and Cunliffe, 2016) and their role as the agents of the global amphibian panzootic (Fisher et al., 2020; Scheele et al., 2019). As such, we are beginning to establish a detailed understanding of chytrid environmental distribution and insight into their ecological functions and prominence (Figure 1.3).



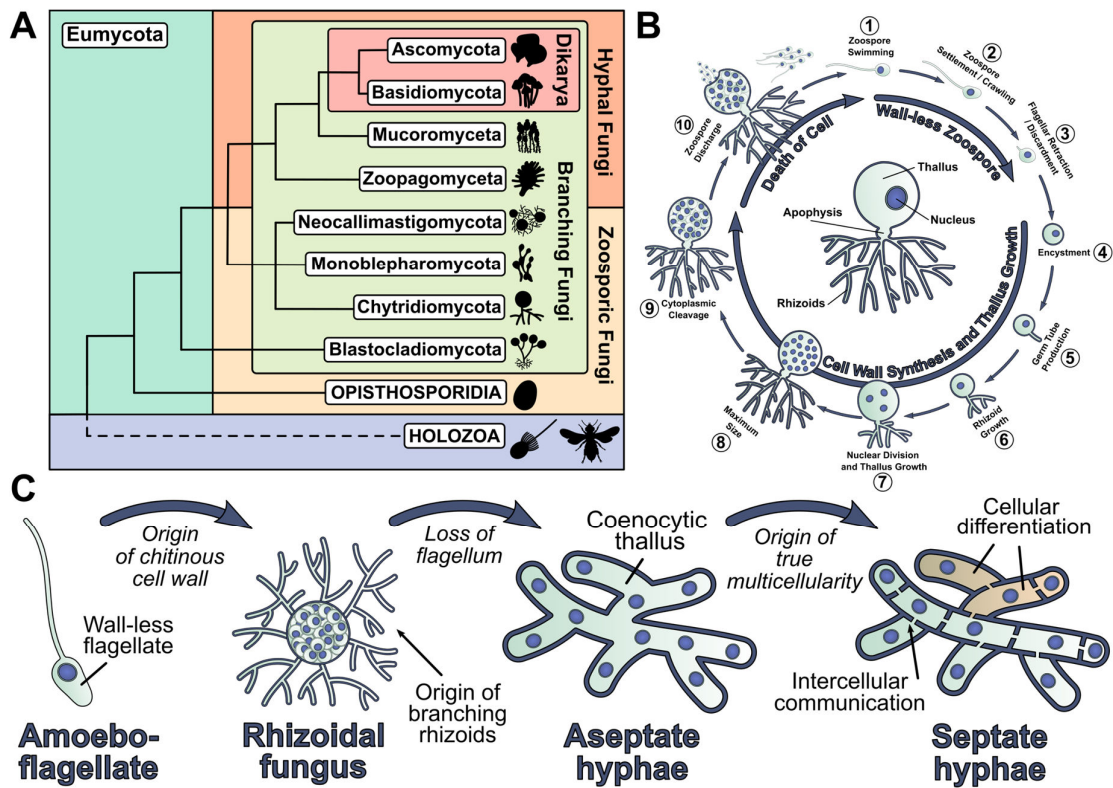


**Figure 1.2 Chytrids represent an important but poorly understood branch of the fungal tree of life.** (A) Phylogenetic tree of the Kingdom Fungi, adapted from the phylogeny outlined in (Naranjo-Ortiz and Gabaldón, 2019a; Tedersoo et al., 2018). (B) Key events in the archetypal dimorphic chytrid lifecycle. The centre of the circle highlights key features of the chytrid cell anatomy. (C) Major evolutionary milestones in the evolution of multicellular hyphal fungi. Chytrids retain many ancestral characteristics of the last common ancestor of branching fungi.

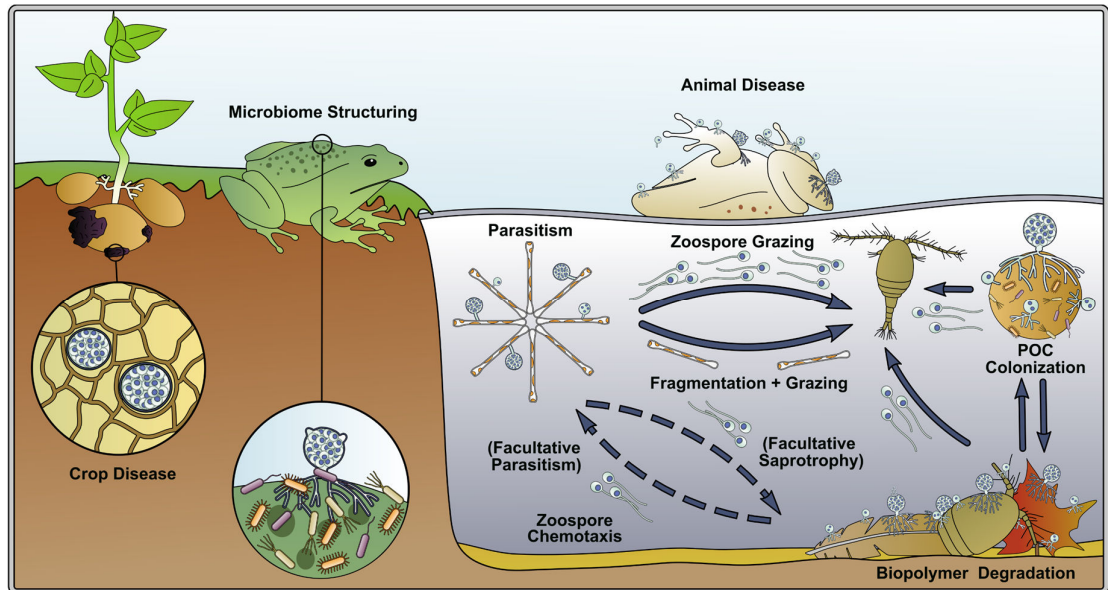


**Figure 1.3 Chytrids are major components of aquatic food webs.** Summary of the ecological roles played by chytrids in aquatic ecosystems.

### 1.3 Why study chytrids?

#### 1.3.1 Chytrids are a poorly understood branch of fungal diversity

Chytrids and their close relatives (Blastocladiomycota, Neocallimastigomycota, and Monoblepharomycota) are a significant component of the eukaryotic tree of life, situated between the predominantly multicellular hyphal fungi (Zoopagomycota, Mucoromycota, Ascomycota and Basidiomycota) and ‘protist-like’ organisms (Opisthosporidia) at the base of the fungal tree (Naranjo-Ortiz and Gabaldón, 2019a; Tedersoo et al., 2018) (Figure 1.2A). This work considers Chytridiomycota, Blastocladiomycota, Neocallimastigomycota, and Monoblepharomycota as separate phyla as described by (Tedersoo et al., 2018).

These groups of zoosporic fungi are fascinating in their own right, however they are not considered further in this project. At present understanding, they do not appear to share the ecological prominence of the Chytridiomycota (*detailed below*) and also exhibit major unrepresentative cellular traits not thought to be present in the last common ancestor of branching fungi, such as hydrogenosomes and an anaerobic metabolism in the Neocallimastigomycota (Gruninger et al., 2014) and convergent hyphal morphogenesis in the Monoblepharomycota (Dee et al., 2015).

### **1.3.2 Chytrids have major ecological impacts**

The ecology of aquatic chytrids has been recently reviewed (Frenken et al., 2017; Gleason et al., 2017; Grossart et al., 2019). Here, the ecological prominence of chytrids is only briefly highlighted as a context in which to understand their cell biology. Historically, chytrids have been identified from aquatic habitats by microscopy-based surveys, including their association with algae and particulate substrates, such as pollen and arthropod exuviae (Canter and Lund, 1948; Sparrow, 1960). The recent application of high-throughput amplicon sequencing has allowed the widespread surveying of diverse aquatic habitats, showing that chytrids are a ubiquitous, and in many cases dominant, fungal group. In addition, sequencing has allowed researchers to overcome the poor culturability of many environmental microbes, particularly from marine systems (Gladfelter et al., 2019), where chytrids can dominate the fungal communities in polar, coastal, and benthic habitats (Amend et al., 2019).

Recent studies using traditional microscopy or metabarcoding surveys have detected abundant chytrid communities in marine sediments (Hassett and Gradinger, 2016; Picard, 2017; Wang et al., 2017), seawater (Comeau et al., 2016; Jeffries et al., 2016; Kiliyas et al., 2020; Taylor and Cunliffe, 2016), sea ice (Comeau et al., 2016; Hassett and Gradinger, 2016), hydrothermal vents (Le Calvez et al., 2009), rivers (Maier and Peterson, 2017), and ponds (Davis et al., 2018; Khomich et al., 2017). Chytrid signatures have also been detected from soil (Duo Saito et al., 2018; Freeman et al., 2009) and snow (Brown et al., 2015; Duo Saito et al., 2018; Naff et al., 2013). This makes chytrids a major component of otherwise uncultured environmental fungal taxa termed 'dark matter fungi' (Grossart et al., 2016). Some marine chytrid signatures represent entirely novel lineages such as Basal Clone Group 1 (Nagahama et al., 2011) and Novel Chytrid-Like-Clades (NCLC) 2-3 (Richards et al., 2015). Chytrid signatures from marine habitats also appear to be some of the most deep-branching (Naranjo-Ortiz and Gabaldón, 2019b).

Chytrids influence ecosystem structure through their interactions with other organisms, ranging from putative mutualism with microalgae (Picard et al., 2013), to competition with bacteria (Wurzbacher et al., 2014), and structuring animal (Bates et al.,

2018; Walke et al., 2015) and particulate organic matter (Roberts et al., 2020) microbiomes (Figure 1.3). Chytrids are prominent parasites of phylogenetically distant hosts, causative agents of devastating wildlife diseases (Figure 1.1H) (Fisher et al., 2020; Scheele et al., 2019), and even hyperparasites of other parasitic chytrids (Gleason et al., 2014). Chytrid parasites also impact engineered ecological systems when they infect commercially important algae in artificial habitats, such as *Haematococcus* (Carney and Lane, 2014; Longcore et al., 2020).

As saprotrophs, chytrids contribute to biogeochemical cycling by degrading recalcitrant biological substrates such as chitin (Czeczuga et al., 2004; Murray and Lovett, 1966; Reisert and Fuller, 1962), cellulose (Dogma, 1969; Mitchell and Deacon, 1986), pollen (Goldstein, 1960; Kagami et al., 2017; Wurzbacher et al., 2014), and keratin (Czeczuga et al., 2004; Piotrowski et al., 2004). This is particularly important as chytrid zoospores are consumed by grazing zooplankton in aquatic ecosystems (Batko and Hassan, 2014; Farthing et al., 2020; Searle et al., 2013). Zoospores are lipid-rich with 'ecologically high-value' sterols and polyunsaturated fatty acids (Akinwale et al., 2014; Gerphagnon et al., 2019), and therefore upgrade nutritionally deficient or otherwise inaccessible substrates to higher trophic levels in processes such as the 'mycoloop' (Agha et al., 2016; Kagami et al., 2014) and the 'fungal shunt' (Klawonn et al., 2021).

### **1.3.3 Chytrids are valuable for understanding fungal evolution**

Chytrids are of interest to evolutionary biologists due to their placement within the eukaryotic tree of life. Fossil records show that the ecological niches and cell plans of chytrids are ancient (Figure 1.1I). Fossils assigned to the Chytridiomycota have been described from the ~410-million-year-old deposits from the Devonian Rhynie Chert that are similar to extant chytrids in terms of their sporangial-rhizoidal cell plan (Krings and Taylor, 2014; Strullu-Derrien et al., 2016) and ecological niches (Krings et al., 2018; Taylor et al., 1992). Fossil chytrids have been documented interacting with plant and fungal matter (Krings et al., 2018, 2009; Krings and Taylor, 2014; Millay and Taylor, 1978), crustacean eggs (Strullu-Derrien et al., 2016) and protists (Krings and Kerp, 2019) as saprotrophs or putative parasites. These fossil chytrids physically interact with trophic

substrates using rhizoid systems similar to extant chytrids (Krings and Taylor, 2014; Strullu-Derrien et al., 2016). The conservation of ancient ecology and cell biology makes chytrids 'living fossils'.

Chytrids retain many of the ancestral characteristics of the last common ancestor of branching fungi (i.e. fungi exhibiting branching rhizoidal or hyphal growth) such as anucleate rhizoids and motile zoospores (Berbee et al., 2017) (Figure 2C). This ancestor existed ~850-750 MYA (Tedersoo et al., 2018) and marked a radical evolutionary transition towards cell biology dedicated to osmotrophy, chitinous cell walls, and elongating and bifurcating cellular growth (Berbee et al., 2017). Fungi that later diverged from this group developed multicellularity via hyphal septation (Nagy et al., 2017). Chytrids are therefore powerful models to explore the origin and evolution of innovations in fungal cell biology and reconstruct the putative biology of the last common ancestor of branching fungi.

#### **1.4 What resources do we have to study the biology of chytrids?**

Web of Science (WoS) searches highlight how little research has been devoted to chytrid fungi relative to dikaryan species, using dikaryan-specific search terms as a proxy for fungal biology overall (Figure 1.4A&B). However, when literature results are scaled as a percentage of total, there has been a sharp relative increase in chytrid research in recent decades (Figure 1.4C), coinciding with the discovery of the global amphibian panzootic chytrid *Batrachomyces dendrobatidis* (Longcore et al., 1999).

Despite the ecological and evolutionary importance of chytrids summarised above, understanding of their underpinning biology is lacking. The reasons for this are likely to include methodological limitations due to the historic lack of cultured and characterized chytrid species and limited molecular and cellular tools for chytrids.

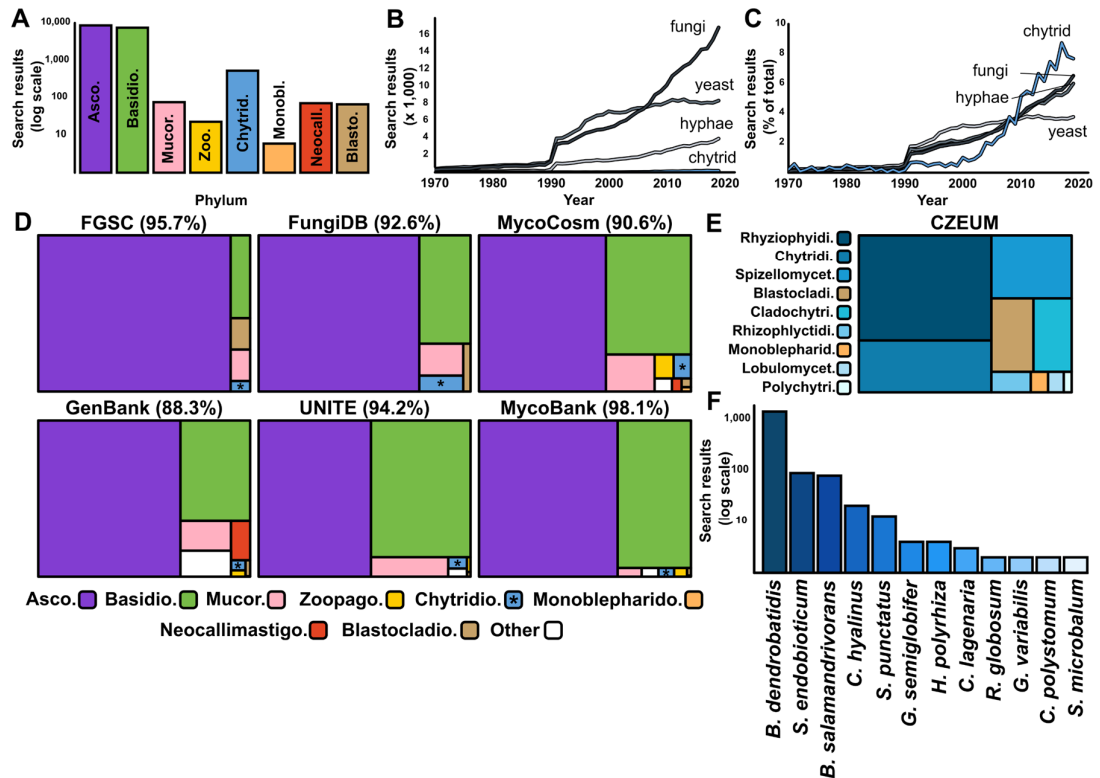


**Figure 1.4 Chytrids are underrepresented in fungal resources and databases. (A)**

Web of Science (WoS) counts for fungal phyla search terms since 1970. Phylum colours as in (D). (B) WoS for search terms associated with mycology. Chytrids suffer low representation next to other mycological terms. However, when scaled as a percentage of total results, chytrids have experienced a sharp increase in attention in the past couple of decades (C). (D) Online fungal resources are dominated by dikaryan species. Numbers in brackets indicate percentage of dikaryan representation. Asterisk marks the chytrids. (E) Taxonomic composition of the CZEUM culture collection at the level of taxonomic order. Abbreviated orders end with '-ales' in full. (F) WoS results for selected chytrid species with sequenced genomes.

### 1.4.1 Chytrids are poorly represented in fungal resources

Dikaryan fungi are well established as model organisms for molecular and cell biology. The ascomycete *Neurospora crassa* has been developed as a model organism for genetics research since the early 1920's, with work on mutagenesis awarded the Nobel Prize in Physiology or Medicine in 1958 (Aramayo and Selker, 2013). Dikaryan fungi are still key models for modern cell biology, with three Nobel Prizes awarded to researchers

using yeast (*Saccharomyces cerevisiae* and *Schizosaccharomyces pombe*) since 2001 alone (Hohmann, 2016). We have an excellent understanding of dikaryan cell biology, and a large number of resources and tools are available to study them even further. Biologists that work with model organisms tend to form communities that facilitate the increased development and centralization of protocols and resources, and therefore naturally develop comprehensive research infrastructures (Leonelli and Ankeny, 2013).

Model dikaryan fungi cultures are widely accessible. For example, there are dedicated culture collections for yeasts, such as the National Collection of Yeast Cultures (NCYC) in the UK. The Fungal Genetics Stock Centre was founded in 1960 and serves to preserve, validate, and distribute mutant and wild type strains of model fungi. At the time of writing, the centre contained 95 species (excluding strain variation) of which only one is a chytrid (*B. dendrobatidis*) (Figure 1.4D).

In terms of genomic resources, dikaryans are also well represented. The first sequenced fungal genome was from *S. cerevisiae* (Goffeau et al., 1996), followed by *S. pombe* (Wood et al., 2002) and then *N. crassa* (Galagan et al., 2003). The first non-dikaryan genome was not published until 2004 (Slamovits et al., 2004) from the microsporidians *Antonospora locustae* and *Encephalitozoon cuniculi*. The first chytrid genome was not completed until 2008 from *B. dendrobatidis*.

The FungiDB (Stajich et al., 2012) is an integrated genomics resource for fungi under the EuPathDB umbrella that combines multiple, annotated DNA/RNA-Seq datasets under a navigable graphic user interface. It is also dominated by dikaryan representation (Figure 1.4D). Model dikaryans often even have their own dedicated integrated genome resources, such as the *Saccharomyces* Genome Database (SGD) for *S. cerevisiae* (Cherry et al., 2012), the *Aspergillus* Genome Database (AspGD) for *Aspergillus* spp. (Cerqueira et al., 2014), and the *Candida* Genome Database (CGD) (Arnaud et al., 2005) for *C. albicans*. The dominance of genomes of dikaryan models and pathogens is being addressed by the more inclusive Joint Genome Institute 1000 Fungal Genomes project available through MycoCosm (Grigoriev et al., 2014) developed with the aim of sequencing diverse species from across the fungal kingdom. A time of writing, MycoCosm

contains 1,609 genomes with 20 from chytrids (Figure 1.4D). A similar dikaryan dominance is observed for the GenBank and UNITE nucleotide resources (Figure 1.4D).

#### **1.4.2 Chytrid-specific resources are few but increasing**

The discrepancies outlined above highlight how both substantial supportive resources for fungal biology have become in recent years and how underrepresented chytrids are. Chytrid biology should address this resource gap by increasing the representation of chytrids in fungal databases and through the development of chytrid-specific tools, resources, and models.

Such resources are starting to emerge. For example, <http://chytrids.org/> is a website dedicated to centralizing and developing tools for chytrids research. Sites such as chytrids.org will prove invaluable as chytrid-specific tools become available. Similar online informational resources available from the Longcore Lab at the University of Maine <https://umaine.edu/chytrids/> provide educational resources for chytrid ecology, including instructions for the isolation of environmental chytrids. ‘Chytrid Fungi Online’ <http://nsfpeet.as.ua.edu/> is an online informational resource associated with a US National Science Foundation (NSF) funded Partnerships for Enhancing Expertise in Taxonomy (PEET) project known as ‘Chytrid-PEET’, a collaborative project to characterize the biodiversity of chytrids through taxonomic investigation.

Chytrid cultures from projects like Chytrid-PEET and other isolation endeavours form a major part of an important chytrid resource, ‘The Collection of Zoosporic Eufungi at the University of Michigan’ (CZEUM) (Simmons et al., 2020) <https://czeum.herb.lsa.umich.edu/HistoryofCZEUM.php>. CZEUM was set up with support from the NSF’s Collections in Support of Biological Research (CSBR) program to protect chytrids collected from over three decades and currently contains 934 chytrid isolates (Figure 1.4E).

Chytrid culturing is now established. Detailed protocols for chytrid cryopreservation (Boyle et al., 2003; Gleason et al., 2007; Rad-Menéndez et al., 2018) are available to researchers and investigations into the physiology of chytrids in the laboratory have established culturing procedures (Barr, 1969; Goldstein, 1960; Hassan and Catapane,



2000; Piotrowski et al., 2004). However, despite this, WoS surveys still show chytrid research is dominated by the amphibian pathogen *B. dendrobatidis*, and to a lesser extent *Synchytrium endobioticum* and *Batrachochytrium salamandrivorans* (Figure 1.4F).

### **1.4.3 Chytrid biology has been investigated with comparative genomics**

Several recent advances are a consequence of the expansion of genome sequencing, including from single-cell genomes (Ahrendt et al., 2018), across the fungal kingdom. The increase in complete chytrid genomes has allowed greater coverage of non-dikaryan fungi in phylogenomic analyses and provided hints into chytrid biology relative to other fungi, including for hyphal evolution (Kiss et al., 2019), cytosine and adenine methylation (Bewick et al., 2019; Mondo et al., 2017), TOR (Target Of Rapamycin) signalling (Shertz et al., 2010), phytohormone sensing (Hérivaux et al., 2017), cell cycle regulation (Medina et al., 2016) and secondary metabolism (Ahrendt et al., 2018).

Sequenced genomes have also provided insight into the evolution of the amphibian parasites *B. dendrobatidis* and *B. salamandrivorans* and factors driving their pathogenicity. Genome sequencing across biogeographical scales has shed light on the origin of the ancestral population of *B. dendrobatidis* that seeded the global panzootic (O'Hanlon et al., 2018) and selective pressures acting on genome evolution in this pathogen (Rosenblum et al., 2013). Comparative genomics, transcriptomics, and proteomics have allowed the identification of genes associated with pathogenicity in these chytrids (Ellison et al., 2017; Farrer et al., 2017; Fisher et al., 2009; Joneson et al., 2011; Refsnider et al., 2015; Rosenblum et al., 2012, 2008; Thekkiniath et al., 2015), which generally show the expansion or upregulation of protease enzymes and Crinkler (CRN)-like effectors.

Comparative genomics have also identified molecular signatures associated with the obligate biotrophy and pathogenicity of the crop pest *S. endobioticum*, such as the loss of purine pathway components, reduction in plant cell-wall degrading enzymes, and novel effector proteins (Van de Vossenberg et al., 2019a). The *S. endobioticum* genome was used to characterize the first effector protein (*AvrSen1*) in the Chytridiomycota, which

triggers a hypersensitive response when expressed in resistant potato populations (Van De Vossen et al., 2019b).

### **1.5 What do we know already about chytrid biology?**

Although the availability of chytrid genomes has stimulated chytrid research, genomes alone cannot be relied on to completely resolve chytrid biology. These analyses highlight key molecular signatures from which biological function can be inferred, but they are limited in terms of understanding chytrids at the cellular level. For example, genomic-based approaches provide limited understanding of how chytrid cells are assembled on a structural basis and how they develop and grow through time. To solve these kinds of problems, it is necessary to bring chytrids into the lab and interrogate their biology at a cellular level.

#### **1.5.1 Biology of chytrids in terms of the life cycle**

We currently possess a generally descriptive understanding of cell development and the dimorphic life cycle of chytrids (i.e. wall-less, motile zoospore and walled, non-motile sporangium) (Figure 1.2B), however a systematic and quantitative understanding of these cell types and the transition between them has not yet been achieved. Chytrid development (Berger et al., 2005; Doggett and Porter, 1996; Greenspan et al., 2012; Powell, 1975) and zoospore ultrastructure (Barr and Désaulniers, 1988; Beakes et al., 1988; Longcore, 1995; Longcore et al., 1999) have mainly been characterized by electron and light microscopy, all of which has been mostly for taxonomic purposes and largely qualitative. These studies characterized and demarcated chytrid life stages and have formed a baseline from which to now develop more quantitative approaches. Studies have shown that chytrids can reproduce both sexually and asexually (discussed by Frenken et al., 2017). Although some chytrid species, such as *Chytrium mycelium*, frequently reproduce sexually via rhizoidal anastomoses (Miller, 1977; Miller and Dylewski, 1981), in general sexual reproduction is only rarely reported in chytrids and zoospore reproduction is the result of asexual cleavage (Frenken et al., 2017).

More recent studies on chytrid development have started to apply novel tools, such as genetic transformation (Medina et al., 2020). Fluorescently-tagged lectins revealed that cell wall *N*-acetyl-D-glucosamine, the monomer of chitin, was predominantly localized to the currently poorly understood subsporangial apophysis in developed sporangia (Ota and Kawano, 2015). Labelling over the life cycle of *Staurastromyces oculus* with the viability stain FUN™ 1 found high metabolic activity in early encysted stages while later stages had lower activity (Van den Wyngaert et al., 2017). However, these fluorescent stain studies are again largely qualitative and descriptive.

Culture-based studies have also shed some light on the regulation of chytrid growth. Assessment of *B. dendrobatidis* growth using chemical analysis, gene transcription, and culture-based phenotyping found that population development was regulated by the fungal quorum-sensing aromatic tryptophol (Verbrugghe et al., 2019), and that monolayer formation over aggregation was promoted by high-nutrient regimes (Silva et al., 2019).

### **1.5.2 Biology of chytrids in terms of carbon and lipid metabolism**

A crucial distinction between chytrids and hyphal fungi are motile zoospores, which enable the targeting of trophic substrates by reproductive propagules in a way not possible by dikaryan spores. Dissolved organic molecules act as chemoattractants for zoospores (Moss et al., 2008; Muehlstein et al., 1988; Scholz et al., 2017). *B. dendrobatidis* zoospores are attracted to amphibian thyroid hormone (Thekkiniath et al., 2013), and are repelled by antifungal metabolites produced by bacteria associated with amphibian skin (Lam et al., 2011). Zoospores have also been shown to exhibit positive phototaxis (Kazama, 1972; Muehlstein et al., 1987). The cellular mechanisms of environmental sensing and guided motility in chytrid zoospores are unknown.

While the trophic range and ecological niches are established in some chytrids, we know little about the degradation pathways (i.e. enzymes), mechanical degradation processes, and physiology of nutrient assimilation. This is particularly important for degraders of recalcitrant biopolymers and hosts that are poorly accessible to other heterotrophs (Agha et al., 2016; Kagami et al., 2014). Comparative genomics of chytrids

suggest that they use a diverse range of extracellular enzymes as part of their secretome, including carbohydrate-active enzymes (CAZymes) (Lange et al., 2019), that are yet to characterised in any biological detail.

The biochemical development of lipid-rich zoospores is of great interest to aquatic ecologists (Kagami et al., 2014). Lipid profiling of zoospores has shown them to be rich in polyunsaturated fatty acids (PUFAs) and sterols (Akinwole et al., 2014; Kagami et al., 2007). Parasitic chytrids have PUFA profiles that are similar to their hosts, indicating direct assimilation, and new sterols that are likely synthesized *de novo* (Gerphagnon et al., 2019). These details have been instrumental in quantitative ecology, allowing the modelling of C:N:P stoichiometry and nutrient flux through aquatic systems (Kagami et al., 2017, 2007; Velthuis et al., 2017). The biochemistry of chytrid lipid anabolism and intracellular transport during zoosporogenesis, and lipid catabolism during zoospore free-swimming and encystment (Figure 1.2B), is currently unknown.

### **1.5.3 Biology of chytrids in terms of hyphal and cytoskeletal evolution**

The chytrids and their close relatives represent a key transition in the fungal kingdom from generally unicellular and rhizoidal growth towards multicellularity and hyphal growth (Berbee et al., 2017; Nagy et al., 2017). As extant chytrids exhibit ancestral characteristics of the progenitors of the hyphal fungi (Berbee et al., 2017; Nagy et al., 2017), insights into their cell biology can help evolutionary biologists infer traits associated with the origin of hyphae in fungi. Of prominence are investigations into the biology of chytrid rhizoids, as it has been hypothesized that rhizoids or rhizoid-like structures were the evolutionary precursors to hyphae (Dee et al., 2019, 2015; Harris, 2011; Ivarsson et al., 2020; Kiss et al., 2019; Nagy et al., 2018) and comparative genomics has suggested that hyphae evolved in the rhizoid-bearing Chytridiomycota-Blastocladiomycota-Zoopagomycota phylogenetic nodes of the fungal tree (Kiss et al., 2019).

Investigations into the cell biology of rhizoids have been lacking until recent years. Monoblepharids, a sister group to the chytrids (Figure 1.2A), have aseptate coenocytic hyphal growth as their predominant cell plan (Dee et al., 2015). Cytoskeletal, cytoplasmic, and vesicular organization in the hyphae of zoosporic and dikaryan fungi suggests

multiple convergent origins of hyphae from rhizoid-bearing lineages (Dee et al., 2015). In chytrids, actin polymerization has been shown to guide rhizoid morphogenesis (Dee et al., 2019; Medina et al., 2020), as it does in hyphal growth (Gow et al., 2017; Riquelme et al., 2018; Steinberg et al., 2017). Cortical actin patches and actin cables are also present throughout the rhizoid system of several chytrid species (Dee et al., 2019; Medina et al., 2020). However, these observations are largely descriptive and no proper morphometric quantification of rhizoidal growth has been conducted, unlike in hyphal fungi (Trinci, 1974), perhaps due to their small size. A protocol for live-cell imaging and quantification of rhizoid development is desperately needed to geometrically compare their growth with hyphal morphogenesis and resolve their shared origin.

Chytrids also provide insight into the evolution of the cytoskeleton in eukaryotic cells (Prostak et al., 2021; Velle and Fritz-Laylin, 2019). Phylogenetic analysis and live-cell microscopy have shown that actin-associated Arp2/3 activator proteins WASP and SCAR in *B. dendrobatidis* zoospores conferred crawling by pseudopodal  $\alpha$ -motility (Fritz-Laylin et al., 2017). The link between WASP and SCAR and  $\alpha$ -motility has also been shown in *Spizellomyces punctatus* zoospores (Medina et al., 2020). The retention of ancestral amoeboid cell biology and flagellar motility in chytrid zoospores makes them different from how dikaryan spores function and more reminiscent of the common ancestor between animals and fungi (Richter and King, 2013). For example, centrioles are lacking from hyphal fungi, having been lost at least four separate times across the kingdom from their flagellated ancestor (Azimzadeh, 2014). However, centrioles are retained in chytrid zoospores (Azimzadeh, 2014), which share the same molecular mechanisms for centriole biogenesis with animals (Ito et al., 2019).

### **1.6. *Rhizoclosmatium globosum* JEL800 as a model for chytrid developmental biology**

A sequenced, annotated and openly available genome, relatively easy laboratory culture (ideally under axenic conditions), a relatively fast life cycle, experimental and genetic tractability, and ecological representativeness (e.g. of a major functional group, such as a phytoplankton parasite) are important factors to consider for model organisms (Leonelli

and Ankeny, 2013; Yarden, 2016). As unicellular organisms, chytrids are often overlooked in collections of model fungi (Yarden, 2016), and as fungi they are also neglected in initiatives to develop model protists. For example, unicellular fungi were not included in the Environmental Model Systems (EMS) (Faktorová et al., 2020; Waller et al., 2018) or the Emerging Model Organisms (EMO) projects (Yarden, 2016). Yet developing model species from enigmatic groups can benefit cell biology (Goldstein and King, 2016).

Numerous dikaryan fungi have served as model organisms in cell biology, but no chytrid has thus far achieved the formal status, even though some have features that make them candidates. The majority of chytrid publications concern batrachochytrids and *S. endobioticum* due to their pathogenicity (Figure 1.4F). Research into their biology is vital for the protection of global biodiversity and food security, however their choice as models for chytrid biology should be cautioned against if the aim is to understand chytrids generally. As their success as global pathogens (i.e. vertebrate and plant parasites) is unusual amongst the chytrids, it is unlikely that their biology would be completely representative. Restrictive biosafety regulations in many countries also place limits on working with them in many laboratories.

*Rhizoclosmatium globosum* is a widespread, freshwater saprotrophic chytrid in the order Chytridiales and is naturally chitinophilic, typically associated with chitin-rich particulate organic matter such as arthropod exuviae (Sparrow, 1960). It is frequently isolated from freshwater habitats (Canter, 1953; Davis et al., 2018; Mahmoud and Abou Zeid, 2002) and is likely of ecological importance through biopolymer degradation and recycling. *R. globosum* JEL800 was isolated by chitin baiting from a lake on the East coast of the USA. *R. globosum* reproduction is via asexual zoosporogenesis, and sexual reproduction is not observed in *R. globosum* JEL800 (Powell et al., 2019). As an experimental organism, *R. globosum* JEL800 is easy to axenically culture, amenable to live-cell microscopy (*this work*), and has a rapid life cycle as fast as ~11-13 h growing at 22 °C on rich media (*this work*), making it an excellent choice for a model to study chytrid developmental biology. The annotated genome of *R. globosum* JEL800 is available via MycoCosm, with an assembly size of 57 Mbp and average of 16,990 gene models (Mondo et al., 2017) (full genome statistics available at:

<https://mycocosm.jgi.doe.gov/Rhihy1/Rhihy1.info.html>), permitting easy transcriptomic profiling of this organism. The JEL800 genome further supports the role of *R. globosum* as a chitin degrader, due to its high ratio of chitinase genes (glycoside hydrolases 18, GH18) relative to total glycoside hydrolase genes (Michael Cunliffe, *pers. comm.*). As a result of its experimental tractability, *R. globosum* JEL800 has been used as a model in recent studies to understand flagellar retraction (Venard et al., 2020) and chytrid-bacteria interaction (Roberts et al., 2020).

### **1.7 Aims and objectives of this work**

Analysing the current state of the field above, there appears to be large gaps in our understanding of the most fundamental processes in chytrid cellular and developmental biology, our understanding of which is mainly descriptive and qualitative. In order to truly resolve the ecological and evolutionary importance of chytrid fungi, these oversights must be initially addressed. As such, the overarching ambition of this thesis is to present a quantitative understanding of chytrid cellular development and contribute to a shift in priorities in chytrid research. In addition, it is the intention to move away from solely bioinformatics approaches and couple molecular tools to cellular development. From evaluating the literature, three areas stand out for immediate investigation and form the three major aims of this thesis, employing *R. globosum* JEL800 as a model species for chytrid biology:

#### **1. Establish an experimental ‘toolkit’ for live-cell chytrid experimentation**

**(Chapter 3).** As discussed above, the methodologies available to cell biologists working on understudied organisms have never been greater and we should not rely solely on bioinformatic approaches to resolve chytrid biology. The application of quantitative live-cell microscopy in particular will be central to bringing chytrids to the cutting edge of fungal cell biology and quantifying their cellular development. However, such tools must first be tested on *R. globosum* JEL800. The results of this aim will serve as the platform from which to investigate further aims. This will involve the realisation of the following objectives:

- i. Applying fluorescent vital staining to label *R. globosum* JEL800 subcellular structures, with a focus on the cell wall, intracellular lipids, and endomembrane. As *R. globosum* is ecologically important as a degrader of environmental chitin (Sparrow, 1960), this will then be tested in the context of growth on chitin.
- ii. Following the previous objective, it will then be necessary to refine live-cell microscopy conditions for non-invasive imaging of the entire *R. globosum* JEL800 life cycle, which will be central to any research into chytrid cellular development. This will focus on the dynamic quantification of lipid and chitin anabolism/catabolism, shedding light on these biogeochemically important cellular processes.
- iii. Although *R. globosum* JEL800 is not a parasitic chytrid, chytrid parasitism is a major ecological phenomenon. However, imaging two organisms simultaneously as components of a pathosystem presents additional challenges. Therefore, protocols previously applied to *R. globosum* JEL800 will be then used to image the development and subcellular organisation of the diatom-chytrid pathosystem Ast1-Chy1, consisting of the diatom *Asterionella formosa* and an undescribed chytrid isolate.
- iv. Establishing a reliable cryopreservation protocol for *R. globosum* JEL800 zoospores. For downstream cell and developmental biology experiments, it will be necessary to create a cryopreserved back stock that can remain viable when revived.

## 2. Identify the major cellular and molecular drivers of the chytrid life cycle

**(Chapter 4).** The shifts between chytrid life stages are not only important in understanding the ecological importance of chytrids (e.g the settlement of zoospores on substrates and the onset of feeding), but uncovering the fundamental drivers of chytrid development will be invaluable at reconstructing the biology of the last common ancestor of branching fungi. However, a robust and quantitative understanding of fundamental chytrid development is lacking.

Addressing this will involve the realisation of the following objectives:



- i. Generating full 3D reconstructions of the subcellular ultrastructure of each *R. globosum* JEL800 life stage from volume electron microscopy (vEM) for quantitative volumetric characterisation and comparison.
- ii. Mapping the differential gene expression of each *R. globosum* JEL800 life stage using transcriptome profiling to identify the molecular drivers of transitions between life stages.
- iii. Using the information from the previous two objectives, targeted investigations employing live-cell microscopy will further characterise life cycle changes in ecologically and biogeochemically important processes, such as lipid synthesis and intracellular trafficking.

### 3. Quantify chytrid rhizoidal growth in comparison to hyphal morphogenesis

**(Chapter 5).** Due to the complex organisation of the rhizoidal system, and the fact some chytrid life stages lack rhizoids, the developmental biology of the chytrid rhizoid will be treated separately from the previous aim. As the feeding subsection of the chytrid cell plan, rhizoids are of obvious ecological importance, and their proposed role as the precursors of hyphae is of huge evolutionary interest. However, their development and biology are poorly understood, which must be overcome if any true appreciation of the chytrid cell is to be achieved. This will involve the realisation of the following objectives:

- i. Developing a protocol to image developing rhizoids and quantify their morphometrics, for comparison with hyphal geometry in dikaryan fungi.
- ii. Interrogating the subcellular control of rhizoid growth through chemical inhibition, with a focus on cell wall and actin dynamics.
- iii. Investigating whether rhizoid development can adapt differently to resource availability through carbon starvation and resource heterogeneity experiments.

Taken together, achievement of these objectives and realisation of these aims will constitute a major step forward in understanding fundamental chytrid cell and developmental biology and act as a solid foundation for future investigations into non-dikaryan fungal lineages.

During the initial phases of this research, environmental sampling was conducted to isolate a chytrid parasite of marine diatoms. This sampling was carried out to investigate the cell and developmental biology of a representative of this ecologically important chytrid group. As these efforts ultimately proved unsuccessful, they are not included in the main body of the thesis and are instead described in Appendix A. However, during environmental sampling a novel thraustochytrid (Stramenopila; Labyrinthulomycota; Thraustochytrida) symbiont of marine diatoms was isolated that was shown to preferentially target senescent and dead diatom cells and, as a result, strengthen the overall health of the phytoplankton population. As this organism is distantly related to true chytrids, this work is also not included in the main body of the thesis. However, the results of the ecophysiological experiments concerning this organism are presented in Appendix B.

## **Chapter 2 – General methods and materials**

This chapter outlines basic laboratory procedures common to all research chapters, presents the recipes for common media and buffers, and details protocols for cell culture. Experimental methodologies specific to research projects are presented in their corresponding chapters.

### **2.1 Reagents and chemicals**

All general laboratory chemicals described in this chapter were obtained from either Sigma-Aldrich or ThermoFisher Scientific unless stated otherwise.

### **2.2 Aseptic working procedures**

Aseptic work was conducted using sterilised laboratory consumables (as designated by the manufacturer) at a workbench sterilised with 70 % (v/v) Industrial Methylated Spirit (IMS). Lab coats and nitrile gloves were worn at all times. All culture media was sterilised by autoclaving for 15 min at 121 °C, and liquid media was additionally 0.22 µm filtered. Re-usable glassware and plasticware were cleaned by soaking for 24 h in 1,000 ppm chlorine disinfectant solution, Decon90 2 % (v/v), and hydrochloric acid solution 1 % (v/v) prior to rinsing in distilled water (ddH<sub>2</sub>O). All cell culture manipulation and processing were conducted in an IMS-sterilised laminar flow hood (ScanLaf Fortuna, Labogene). Cell cultures were visually inspected for contamination with a Nikon inverted phase contrast microscope (TMS, Nikon) using a 10 x air objective.

### **2.3 Growth media and buffers**

All media was either used as a liquid or as 1 % agar plates. pH was measured using a benchtop pH meter (SevenExcellence, Mettler Toledo) and adjusted using 1 mM NaOH (pH ↑) or 1 mM HCl (pH ↓).

### **2.3.1 Growth media**

#### 2.3.1.1 PmTG growth medium (Barr, 1986)

Add into 1 L ddH<sub>2</sub>O and autoclave prior to pouring:

- Peptonised milk – 1.00 g
- Tryptone – 1.00 g
- D-glucose – 5.00 g

#### 2.3.1.2 Modified Bold's basal medium (BBM)

Add into 1 L ddH<sub>2</sub>O and autoclave prior to pouring:

- Bold basal medium (50X) (Sigma-Aldrich) – 2 ml
- (NH<sub>4</sub>)<sub>2</sub>SO<sub>4</sub> (ammonium sulphate) – 0.25 g
- F/2 vitamin stock (Guillard and Ryther, 1962) – 500 µl (*add after autoclaving*)

The base medium was supplemented with different carbon sources for trophic experiments:

10 mM *N*-Acetylglucosamine (NAG) BBM

- *N*-Acetylglucosamine – 2.21 g

Colloidal chitin (CC) BBM

- Colloidal Chitin – 0.5 g

No carbon (NOC) BBM

- *Not supplemented with carbon*

#### 2.3.1.2 F/2 phytoplankton growth medium (Guillard and Ryther, 1962)

Add to 1 L autoclaved 30 kDa-filtered seawater. All stocks are 0.22 µm filtered in ddH<sub>2</sub>O:

1 ml phosphate stock

- 5 g/L NaH<sub>2</sub>PO<sub>4</sub> H<sub>2</sub>O (monosodium phosphate monohydrate)

1 ml nitrate stock

- 75 g/L NaNO<sub>3</sub> (sodium nitrate)

1 ml silicate stock

- 30 g/L Na<sub>2</sub>SiO<sub>3</sub> 9H<sub>2</sub>O (sodium metasilicate nonahydrate)

1 ml trace metal solution

- 3.15 g/L FeCl<sub>3</sub> 6H<sub>2</sub>O (iron(III) chloride hexahydrate)
- 4.36 g/L Na<sub>2</sub>EDTA 2H<sub>2</sub>O (ethylenediaminetetraacetic acid disodium salt dihydrate)
- 9.8 g/L CuSO<sub>4</sub> 5H<sub>2</sub>O (copper(II) sulfate pentahydrate)
- 6.3 g/L Na<sub>2</sub>MoO<sub>4</sub> 2H<sub>2</sub>O (sodium molybdate dihydrate)
- 22 g/L ZnSO<sub>4</sub> 7H<sub>2</sub>O (zinc sulfate heptahydrate)
- 10 g/L CoCl<sub>2</sub> 6H<sub>2</sub>O (cobalt(II) – chloride hexahydrate)
- 180 g/L MnCl<sub>2</sub> 4H<sub>2</sub>O (manganese(II) chloride tetrahydrate)

0.5 ml vitamin solution

- 0.2 g/L thiamine HCl (vitamin B<sub>1</sub>)
  - 1 g/L biotin (vitamin B<sub>7</sub>)
  - 1 g/L cyanocobalamin (vitamin B<sub>12</sub>)

### 2.3.1.3 CHU-10 growth medium (Gerloff et al., 1950)

Add to 1L ddH<sub>2</sub>O:

- 0.039 g Na<sub>2</sub>SiO<sub>3</sub> (sodium metasilicate)
- 0.015 g Ca(NO<sub>3</sub>)<sub>2</sub> (calcium nitrate)
- 0.006 g K<sub>2</sub>HPO<sub>4</sub> (dipotassium phosphate)
- 0.002 g MgSO<sub>4</sub> (magnesium sulfate)
- 0.011 g Na<sub>2</sub>CO<sub>3</sub> (sodium carbonate)

Adjust pH to 6.4 with HCl or NaOH, autoclave and then add:

- 1 ml Fe-EDTA (ethylenediamine tetraacetic acid iron(III) sodium salt) solution
- 1 ml F/2 vitamin stock

*Fe-EDTA Solution:*

- 5.2 g L<sup>-1</sup> EDTA (ethylenediaminetetraacetic acid)
- 5.4 g L<sup>-1</sup> FeSO<sub>4</sub> (iron(II) sulfate)

**2.3.2 Buffers**

2.3.2.1 0.1 M Cacodylate buffer

Add to 1 L MilliQ ddH<sub>2</sub>O:

- 21.4 g (CH<sub>3</sub>)<sub>2</sub>AsO<sub>2</sub>H (cacodylic acid)

Adjust to pH 7.2

2.3.2.2 Reynold's lead citrate buffer

Add to 1 L MilliQ ddH<sub>2</sub>O:

- 26.6 g Pb(NO<sub>3</sub>)<sub>2</sub> (lead nitrate)
- 35.2 g Na<sub>3</sub>C<sub>6</sub>H<sub>5</sub>O<sub>7</sub> (sodium citrate)

2.3.2.3 Phosphate buffered saline

Add to 1 L MilliQ ddH<sub>2</sub>O:

- 13.559 g Na<sub>2</sub>HPO<sub>4</sub> (disodium phosphate)
- 80 g NaCl (sodium chloride)
- 2 g KCl (potassium chloride)
- 2 g KH<sub>2</sub>PO<sub>4</sub> (monopotassium phosphate)

Adjust to pH 7.4

2.3.2.4 PEM buffer

Add to 1L of MilliQ ddH<sub>2</sub>O:

- 30.25 g PIPES (piperazine-N,N'-bis(2-ethanesulfonic acid))
- 0.76 g EGTA (ethyleneglycol-bis(2-aminoethylether)-N,N',N'-tetraacetic acid)

- 0.245 g  $\text{MgSO}_4$  (magnesium sulfate)

Adjust to pH 6.9

**Table 2.1. List of fluorescent stains for labelling cellular ultrastructure used in this work.**

Fluorescent Stain	Target	Max Ex. (Å)	Max Em. (Å)	Product Code	Manufacturer
Nile Red	Neutral lipids	552	636	N3013	Sigma-Aldrich
Calcofluor White	Chitin/cellulose	355	433	18909	Sigma-Aldrich
FM 1-43 Dye	Endomembrane	510	626	T35356	ThermoFisher
Rhodamine Phalloidin	F-Actin	540	565	R415	ThermoFisher
Hoechst 33342	Double-stranded DNA (dsDNA)	350	361	H3570	ThermoFisher
Texas Red conjugated Wheat Germ Agglutinin	N-acetylglucosaminyl residues	595	615	W6748	ThermoFisher
MitoTracker Red CMXRos	Mitochondria	579	599	M7512	ThermoFisher
LysoTracker Yellow HCK-123	Acidic intracellular vacuoles	465	535	L12491	ThermoFisher

## 2.4 Organism culture and maintenance

### 2.4.1 *Rhizoclostratium globosum* JEL800

*Rhizoclostratium globosum* JEL800 was grown axenically on PmTG agar. Agar plugs were excised from established cultures using a sterile scalpel, inverted onto fresh agar plates (four plugs per plate), and incubated in the dark for 48 h at 22-23 °C. Cultures were then sporulated by immersing each plug in 100 µl of autoclaved ddH<sub>2</sub>O and incubated at

room temperature for 30 min. Agar plates were then agitated to evenly distribute ddH<sub>2</sub>O across the agar surface to create a lawn of settled zoospores, air-dried for 10 min in a laminar flow hood, and further incubated for 48 h at 22-23 °C. Agar plates were sealed with Parafilm M during both incubations. Planktonic cultures were established by implanting a single agar plug into 25 ml 0.22 µm-filtered liquid PmTG and incubated in the dark at 22-23 °C.

#### **2.4.2 Harvesting zoospores**

To harvest zoospores, plates were flooded with 1-4 ml of ddH<sub>2</sub>O 48-72 h post-sporulation. To exclude later life stages, this suspension was harvested and passed through a 10 µm (43-50010, pluriSelect) cell strainer prior to use. Zoosporic density was quantified using a Sedgewick Raft Counter (02C00415, Pyser SCGI) under a Leica DM1000 (10 x objective) using 50 µl aliquots fixed in 2 % formaldehyde at a dilution of 1:1,000.

#### **2.4.3 Maintenance of the *Ast1-Chy1* pathosystem**

The chytrid Chy-1 is an obligate parasite on *Asterionella* sp. (*Ast-1*) and must be maintained growing on host cultures. Unparasitized host stocks were cultured in 0.22 µm-filtered CHU-10 media at ~40 µM s<sup>-1</sup> m<sup>-2</sup> irradiance at 19 °C under a 18:6 h light:dark photoperiod. 1 ml of established culture was subcultured into 35 ml of fresh growth medium weekly. Chy-1 was maintained by subculturing 1 ml of parasitized culture (~7-14 d post-inoculation) in a flask containing 5 ml 7 d old uninfected *Ast-1* culture and 17 ml 0.22 µm-filtered CHU-10 media.

#### **2.4.4 Daphnia**

*Daphnia* sp. Were acquired from a local aquarium supplier and maintained in 500 ml of Bold's basal medium. *Daphnia* cultures were aerated with a Koi Air pump (KA25, Blagdon), and fed every other day with 2 ml of dense *Chlamydomonas reinhardtii* culture.



Media was changed weekly. *Daphnia* exoskeletons were cleaned of organic matter prior to chitin degradation experiments. Whole harvested *Daphnia* were incubated in 10 % sodium dodecyl sulfate (SDS) solution for 30 min, then 100 % ethanol for 1 h, and autoclaved in ddH<sub>2</sub>O. Exoskeletons were washed twice in ddH<sub>2</sub>O between each step.

## **Chapter 3 – Establishing an experimental toolkit to study cellular development in chytrid fungi**

### **3.1 Summary**

To investigate the cellular development of chytrids, physiological experiments must be conducted in live cells. However, due to the previous neglect of chytrids in cell biology, protocols for imaging developing cells are largely lacking in these organisms. To address this gap, this chapter set out to establish an experimental toolkit focussed on bioimaging protocols for chytrid development, using the saprotrophic chytrid *Rhizoclostridium globosum* JEL800. From these investigations, protocols centred on fluorescent vital staining, live-cell development, particulate carbon degradation, diatom-parasite interaction, and zoospore cryopreservation were applied to developing chytrid cells. These tested protocols will serve as the foundation for future efforts to image and quantify the cellular development of chytrid fungi.

### **3.2 Introduction**

To understand the dynamic nature of chytrid development, it is necessary to investigate live cells. For this, experiments involving live-cell growth and imaging must be applied to chytrids in the laboratory. However, due to the relative lack of investigation into these organisms, protocols for live-cell experimentation in chytrids are poorly developed. In this chapter, the saprotrophic chytrid *Rhizoclostridium globosum* JEL800 was used to establish a series of protocols, predominantly focussed on live-cell bioimaging of labelled subcellular structures, that would serve as an experimental toolkit for future investigations in chytrid cell biology in the context outlined below. Given the ecological prominence of chytrids, these investigations centred around the roles of chytrids as saprotrophs of recalcitrant biopolymers, lipid-rich cells, and algal parasites.

These investigations were built around five distinct protocols:

1. *Using fluorescent vital stains for subcellular chytrid structures* – The synthesis of neutral lipids by chytrids is integral to the release of inaccessible carbon back into aquatic food webs (Kagami et al., 2014). Given the biogeochemical importance of chytrids, fluorescent vital stains for neutral storage lipids and the chitin cell wall (in addition to endomembrane) were applied to live *R. globosum* cells.
2. *Non-invasive imaging of the chytrid life cycle* – Based on the successful results of the previous experiments, the next methodological hurdle was to refine live-cell imaging conditions for the entire *R. globosum* life cycle. This allowed the dynamic quantification of lipid and chitin synthesis, shedding light on these biogeochemically important cellular processes.
3. *Imaging chytrid growth on chitin sources* – In aquatic systems, chytrids are key degraders of recalcitrant organic carbon (Sparrow, 1936; Gleason et al., 2008). These protocols set out to image the saprotrophic growth of *R. globosum* on *Daphnia* exuviae and colloidal chitin. This was predominantly conducted to trial protocols for mesocopy and 3D confocal reconstruction in imaging chytrid growth. Mesocopy represents a novel tool to image thousands of cells in a single image (McConnell et al., 2016), which could allow the large scale investigation of chytrid population dynamics. 3D confocal reconstructions highlighted the complexity of chytrid rhizoids growing associated with chitin.
4. *Imaging of diatom-chytrid interactions* – As prominent parasites of phytoplankton in aquatic systems (Frenken et al., 2017; Scholz et al., 2016a), imaging chytrid interactions with their hosts has importance in understanding their ecology. However, imaging two organisms simultaneously as components of a pathosystem presents additional challenges. Therefore, the live-cell imaging conditions applied to *R. globosum* development above were used to image the development of the diatom-chytrid pathosystem Ast1-Chy1. In addition, fluorescent vital stains for nuclei, vacuoles, and mitochondria were applied to both the host and parasite.
5. *Cryopreservation and revival of chytrid zoospores* – To work with *R. globosum* in the laboratory, it is necessary to create cryopreserved back stocks that remain viable when revived. Therefore, protocols for the cryopreservation of *R. globosum*

zoospores were optimised to allow the conservation and revival of experimental lineages.

From these preliminary investigations, protocols concerning fluorescent vital staining, live-cell development, growth on particulate carbon, diatom-parasite interaction, and zoospore cryopreservation were established in the context of chytrid cell biology and development. Taken together, these results will serve as a foundation from which to explore the biology of chytrid development.

### **3.3 Methods and materials**

#### ***3.3.1 Using fluorescent vital stains for subcellular chytrid structures***

500  $\mu\text{l}$  of planktonic *R. globosum* cultures (48 h in age) were applied to poly-L-lysine coated glass-bottom dishes (IBL) and incubated in the dark at room temperature for 30 min to promote cell adhesion. Culture supernatant was then removed, and adhered cells were incubated in 250  $\mu\text{l}$  of 0.22  $\mu\text{m}$ -filtered ddH<sub>2</sub>O impregnated with vital stains. Cells were incubated with 432 nM Nile Red (NR) solution to label neutral lipids for 30 min after which the supernatant was removed. Cells were then immersed in ice-cold 4.09  $\mu\text{M}$  FM 1-43 Dye to label endomembrane and 1.1  $\mu\text{M}$  Calcofluor White (CFW) to label cell wall chitin and imaged immediately. Optimised concentrations were determined from tested trial ranges: 0.29- 5.76  $\mu\text{M}$  (NR), 0.82-8.18  $\mu\text{M}$  (FM 1-43) and 0.11-11  $\mu\text{M}$  (CFW).

Epifluorescent microscopy was conducted using a Leica Dmi8 microscope (Leica, Germany) under a 100 x oil-immersion objective lens. Image acquisition settings were: excitation at 395 nm and emission at 435-485 nm (Intensity 15 %, FIM 100 %) for CFW; excitation at 470 nm and emission at 500-550 nm (Intensity 15 %, FIM 100 %) for FM 1-43; excitation at 575 nm and emission at 575-615 nm for NR (intensity 5 %, FIM 55 %); and DIC (intensity 221, exposure = 304 ms). Images were captured using an ORCA-Flash4.0 digital camera (Hamamatsu Photonics, Japan). Background fluorescence was controlled for by imaging no-stain controls (*not shown*) using only 1  $\mu\text{l ml}^{-1}$  of the stain

solvent dimethyl sulfoxide (DMSO) (D4540, Sigma-Aldrich). No auto- or background fluorescence was identified for *R. globosum* JEL800.

### **3.3.2 Non-invasive imaging of the chytrid life cycle**

To qualitatively illustrate the relative chitin and lipid content in different *R. globosum* life stages, chitin and neutral lipids were labelled for four major stages of the *R. globosum* lifecycle. Live-cell time lapse imaging of chitin and lipid dynamics in *R. globosum* was optimised for vital stain concentrations and light intensity which did not negatively impact growth. For these experiments, a stain load of 2.75  $\mu\text{M}$  CFW and 432 nM NR was chosen from screening the stain concentrations mentioned above at LED intensities <15 % (FIM 100 %, LED 15 %) for an optimal signal over a 13 h imaging period under a 20 x objective lens using the Leica Dmi8 microscope as previously described. Zoospores were harvested and diluted to a working concentration of  $1.6 \times 10^4$  in ddH<sub>2</sub>O. 500  $\mu\text{l}$  of this suspension was added to a glass bottom dish coated with 250  $\mu\text{l}$  of PmTG agar, incubated in the dark for 15 min at room temperature, and the supernatant removed. 3 ml of ddH<sub>2</sub>O was then added to the dish and imaged following 15 min of additional incubation. All ddH<sub>2</sub>O used for the above steps was labelled with the above stain concentrations (imaged populations  $n = 3$ ), but not for control treatments ( $n = 3$ ). Development was imaged at 30 min intervals for 13 h. To prevent thermal and hypoxic stress during the imaging period, the dish was placed into a P-Set 2000 CT stage (PeCon, Germany) where temperature was controlled at 22 °C by an F-25 MC water bath (Julabo, Germany), and the dish was covered by an optically clear film which permits gas exchange.

From each of the imaging population replicates ( $n = 3$ ), individual cells ( $n = 5$ ) were assigned numerical values and chosen at random by random number generator (total sample size per treatment  $n = 15$ ). Single cell growth was quantified by measuring cell area as a growth proxy for each timepoint in Fiji. To assess the relative change in chitin and lipid cellular content, average intensity for a 50-pixel radius around a cell was

quantified using the Fiji Plugin 'Time Series Analyzer V3'. To assess the potential toxicity of this stain load on *R. globosum* growth, 15 ml culture flasks of PmTG labelled with the above concentrations of either CFW; NR; or NR+CFW (or the equivalent volume of ddH<sub>2</sub>O as a positive control) were inoculated with 500 µl of harvested zoospores. Flasks ( $n = 3$ ) were inoculated for each stain treatment for 24 h timepoints ranging from 24-120 h. Biomass at each timepoint was quantified by pelleting the contents of the culture flasks at 4,600 rpm for 10 min at 4 °C, removing the supernatant and freezing the pellets at -80 °C overnight. Frozen pellets were then freeze-dried for 7 h using a CoolSafe freeze-dryer (Labogene, Denmark) and dry mass quantified in grams using an Entris benchtop balance (Sartorius, USA). Three flasks were inoculated and processed immediately to ground the growth curves at a  $T_0$  baseline mass. The toxicity of LED exposure during the imaging duration was assessed by comparing the growth and the onset of major developmental stages (time to reach maximum size and time of sporulation) between stain-labelled (imaged by LED) and control (imaged by DIC only) cells. Differences between treatments were assessed using an Analysis of Variance (ANOVA) test for each time point. Shapiro-Wilk and Levene's tests were used to assess normality and homogeneity of variance respectively, and data were transformed if they did not meet these assumptions. Differences between treatments within a time point were assessed with a Tukey's Post-Hoc test. All statistical analyses were conducted using R v3.3.1 implemented in Rstudio v0.99.903.

### **3.3.3 Imaging chytrid growth on chitin sources**

Imaging of chytrid growth on chitin sources was conducted in culture dishes containing 3 ml of Bold's basal medium (BBM), supplemented with either a single cleaned *Daphnia* carapace or 0.5 g L<sup>-1</sup> colloidal chitin as a carbon source. Dishes were inoculated with 500 µl of *R. globosum* zoospore suspensions (inoculum concentration =  $1.03 \times 10^6$  zoospores ml<sup>-1</sup>), incubated at 22 °C, and imaged at 24 h, 72 h and 96 h.

For mesoscopy imaging, cultures were incubated for 30 min in 3 ml of 5  $\mu$ M CFW and 1.57  $\mu$ M NR. Cultures were placed under a coverslip and imaged using an epifluorescent Mesolens system (McConnell et al., 2016) at 4x magnification. Stains were imaged as: excitation at 365 nm and emission at 410-450 nm (CFW); and excitation at 550 nm and emission at 570-610 nm (for NR). Images were captured with a Vieworks VNP-29MC (Stemmer Imaging) (exposure 800 ms). Background fluorescence was controlled for by imaging no-stain controls (*not shown*) using only the stain solvents DMSO and methanol (34860, Sigma). No background fluorescence was identified for *R. globosum* JEL800. Mesoscopy images of the colonised chitin particle were deconvolved with a Richardson-Lucy algorithm in the Fiji (Schindelin et al., 2012) plugin DeconvolutionLab2 (Sage et al., 2017) based on a theoretical point spread function generated using a Gibson and Lanni model in the plugin PSF Generator (Kirschner et al., 2013).

For confocal images of *R. globosum* rhizoid architecture, cells were immersed in 250  $\mu$ l ice-cold 8.18  $\mu$ M FM 1-43 to label the membrane and imaged immediately using a Zeiss LSM 510 Meta confocal laser scanning microscope (Carl Zeiss, Germany) under a 40 x oil-immersion objective. Membranes were imaged by excitation at 488 nm and emission at 500-530 nm. Z-stacks were taken at 0.5  $\mu$ m intervals, and a surface mesh was generated automatically in Vaa3D (Peng et al., 2014). To highlight the chitin particle, the z-stack was manually segmented in the Fiji plugin TrakEM2 (Cardona et al., 2012) and reconstructed automatically by merging traced features along the z-axis. Meshes were imported into the 3D rendering software Blender v2.77 for final presentation.

### **3.3.4 Imaging of diatom-chytrid interactions**

To image diatom-chytrid interactions, the *Asterionella*-chytrid system Ast1-Chy1 was used. Chytrid sporulation was recorded using DIC time lapse microscopy. Prior to imaging, infected *Asterionella* cultures were washed in CHU-10 media using a 40  $\mu$ m cell strainer. 500  $\mu$ l of this culture was introduced into a glass bottom dish containing 3 ml of

CHU-10 media and allowed to settle for 1 h prior to imaging. Images were recorded with a 20 x objective lens using the Leica Dmi8 wide field microscope and live-cell imaging setup as described in *Non-invasive imaging of the chytrid life cycle*. Images were recorded at 2.5 min intervals.

To label intracellular organelles, washed cultures were incubated for 30 min at room temperature in the dark with 4.9  $\mu\text{M}$  Hoechst 33342 (to label nuclei), 1  $\mu\text{M}$  LysoTracker Yellow HCK-123 (LTY) (to label acidic vacuoles) and 250 nM MitoTracker™ Red CM-H<sub>2</sub>Xros (MTR) (to label mitochondria). Epifluorescent microscopy was conducted using the Leica Dmi8 microscope under a 63 x oil-immersion objective lens. Stains were imaged by excitation at 395 nm and emission at 435-485 nm for Hoechst 33342; excitation at 470 nm and emission at 500-550 nm for LTY; and excitation at 575 nm and 575-615 nm for MTR. Chlorophyll autofluorescence was excited at 470 nm and detected at 412-448, 495-535, 575-615 and 670-770 nm using a Sp-X filter. Images were captured using a CMOS Camera (Prime 95B™, Photometrics). Background fluorescence and coexcitation was controlled for by imaging no-stain controls (*not shown*) using only the stain solvent DMSO. Images were captured as z-stacks (z-interval = 0.5  $\mu\text{m}$ ) and deconvolved as described in *Imaging chytrid growth on chitin sources*. Images are presented as maximum intensity projections.

### **3.3.5 Cryopreservation and revival of chytrid zoospores**

Zoospore suspensions ( $n = 8$ ) were pelleted at 5,000 rpm for 10 min and resuspended in 500  $\mu\text{l}$  of PmTG liquid medium supplemented with four differential cryoprotectant treatments: PmTG only (control); 10 % Foetal Calf Serum (FCS) (A3160401, Gibco) only; 10 % FCS and 10 % DMSO; and 10 % FCS and 10 % glycerol (H5433, Promega). All cryoprotectant treatments were 0.22  $\mu\text{m}$ -filtered prior to use. These cryoprotectant treatments were selected from a review of cryopreservation of chytrid zoospores (Gleason et al., 2007).



Zoospore suspensions were transferred to 1.6 ml cryotubes (72.380.004, Sarstedt), placed in a Nalgene Mr. Frosty Freezing Container (C1562, Sigma-Aldrich) and then frozen at  $-1\text{ }^{\circ}\text{C min}^{-1}$  in a  $-80\text{ }^{\circ}\text{C}$  freezer. Survival was assessed prior to freezing (control), after 1 month, and after 3 months at  $-80\text{ }^{\circ}\text{C}$ . To quantify survival, cells were thawed by immersion in a  $40\text{ }^{\circ}\text{C}$  water bath for 2 min, serially diluted from  $10^{-1}$ - $10^{-4}$  in PmTG liquid medium, and plated on PmTG agar in  $5 \times 10\text{ }\mu\text{l}$  drops per dilution. Plates were incubated in the dark for 72 h at  $22\text{ }^{\circ}\text{C}$  and survival was quantified in CFU (Colony Forming Units)  $\text{ml}^{-1}$ . Differences in zoospore survival between the differential cryoprotectant treatments were assessed using ANOVA analysis as described above in *Non-invasive imaging of the chytrid life cycle*.

### 3.4 Results

#### 3.4.1 Using fluorescent vital stains for subcellular chytrid structures

Application of vital stains to live *R. globosum* cells labelled intracellular lipids, the cell wall, and endomembrane (Figure 3.1). It should be noted, however, that NR coexcites with FM 1-43 at 470 nm and is a poor choice for multichannel imaging. The settled zoospore stage did not stain positive for CFW, due to a lack of a cell wall. The endomembrane of the cell body and rhizoids in the immature thallus could not be imaged simultaneously at the same focal plane, highlighting the need for z-stacking in future imaging. The internalisation of FM 1-43 in the cell body indicated endocytosis in *R. globosum* cells.

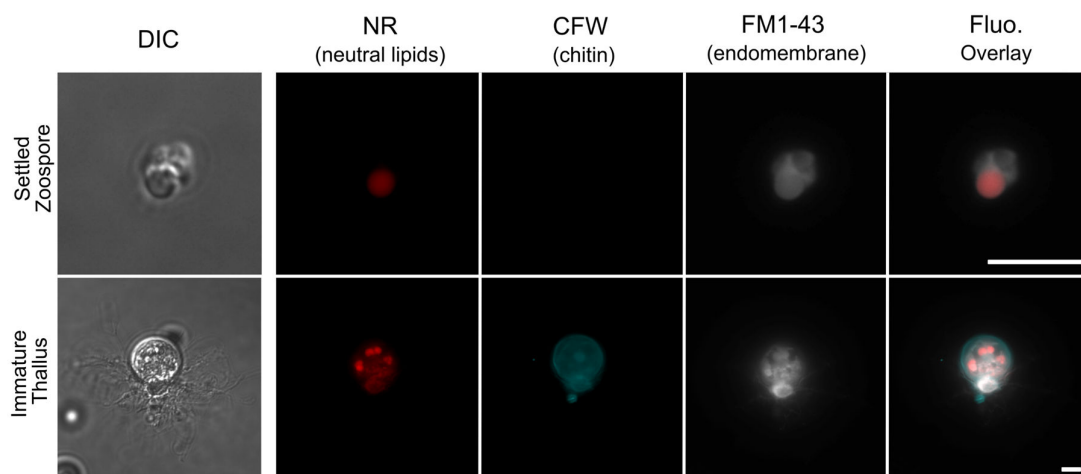


**Figure 3.1 Fluorescent vital staining of live *R. globosum* cells.** Labelled subcellular structures in the chytrid *Rhizoclosmatium globosum* JEL800 settled zoospore and immature thallus. NR = Nile Red. CFW = Calcofluor White. Scale bar = 5  $\mu$ m.

### **3.4.2 Non-invasive imaging of the chytrid life cycle**

Labelling of the chitin cell wall and intracellular lipids showed that these components varied considerably across the *R. globosum* life cycle (Figure 3.2A&B). Qualitatively, these changes in chitin-lipid content were delineated between the four major *R. globosum* life stages. Zoospores lack a cell wall and possess a prominent, single lipid globule. During encystment (<1 h post-settlement), the lipid globule fluorescence decreases alongside the onset of chitin synthesis, resulting in the germling stage. Exponential growth of the thallus is evident by the exponential growth of chitin synthesis and cell area between 1-11 h. However, NR fluorescence does not increase as rapidly at this stage and decreases between 6-7.5 h, which appears to be a result of lipid redistribution throughout the cell. The stage at which cell growth by chitin synthesis dominates lipid synthesis characterises the immature thallus. The cell body becomes a mature sporangium once the thallus has reached maximum size at 11 h and lipid synthesis reaches asymptote prior to sporulation at 12.5 h. After this, the maternal sporangium is dead and only the chitinous cell wall remains. There was no difference between stain treatments in terms of *R. globosum* dry biomass at any of the tested timepoints ( $p>0.05$ ) (Figure 3.2C). There was also no difference in the growth rate or development between stain-labelled and control cells (Figure 3.2D). These findings provide evidence that the developed imaging method is non-invasive and does not negatively interfere with cell growth.

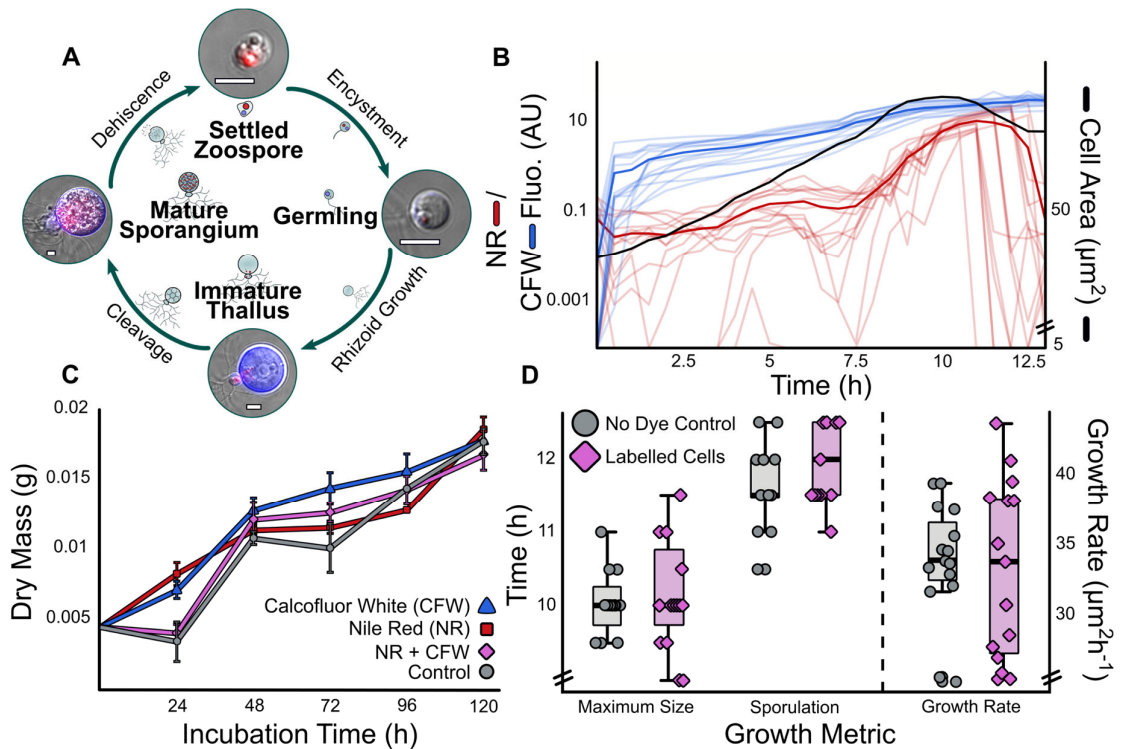


**Figure 3.2** Lipid and chitin dynamics were imaged non-invasively over the *R.*

*globosum* life cycle. (A) Intracellular lipids (red) and chitin (blue) labelled with fluorescent vital stains in different life stages of *R. globosum*. (B) Live-cell time lapse imaging ( $n = 15$ ) of chitin and lipid fluorescence across the *R. globosum* life cycle. Individual replicates are plotted with low opacity. The opaque line represents the mean of the treatment. Mean cell area growth curve is shown for reference. AU = arbitrary units. (C) Dry mass over time of vital stained *R. globosum* cultures ( $n = 3$ ) versus control to assess toxicity. (D) Comparison of the onset of developmental milestones and growth rate of labelled and non-labelled *R. globosum* cells ( $n = 15$ ) to assess toxicity. There were no significant differences between either treatment therefore the stain load was designated non-toxic.

### 3.4.3 Imaging chytrid growth on chitin sources

*R. globosum* was able to grow using chitin as the only carbon source in the form of both colloidal chitin (Figure 3.3A&B) and *Daphnia* exuviae (Figure 3.3C&D). Qualitatively, *Daphnia* exuviae incubated with *R. globosum* for 96 h noticeably exhibited increased lipid fluorescence and less chitin fluorescence than those incubated for only 24 h (Figure

3.3E), suggesting that chitin degradation and lipid production by chytrids was driving this change. Mesoscopic imaging of entire *Daphnia* carapaces permitted the imaging of all attached chytrids at various developmental stages at subcellular resolution, even showing freshly released zoospores in *Daphnia* carapaces incubated for 96 h (Figure 3.3E). Qualitatively, chytrids growing on colloidal chitin did not grow as densely or as large as those growing on *Daphnia* exuviae, suggesting that the former may have presented a more recalcitrant carbon source to *R. globosum* (Figure 3.3F). 3D confocal reconstruction of *R. globosum* growing associated with colloidal chitin showed heavy rhizoid branching around and inside the particle (Figure 3.3G-I) that appeared to be much denser than that not in contact with the chitin.

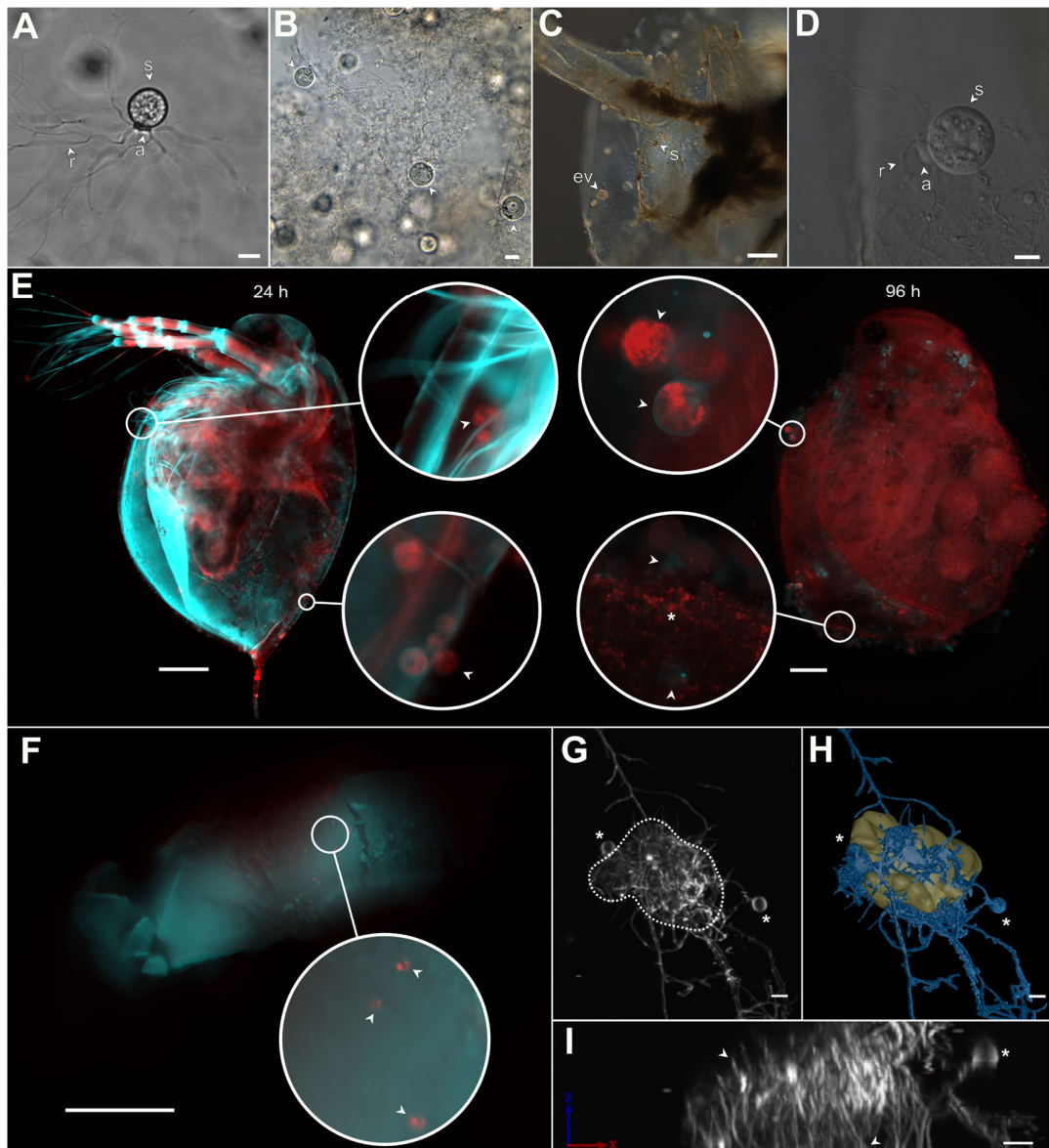


**Figure 3.3 Growth on chitin by *R. globosum* was imaged using a suite of microscopy tools.** (A-D) Transmitted light micrographs of *R. globosum* illustrating cell plan and growth on chitin sources. (A) Bright field (BF) image of the *R. globosum* cell plan. Labelled is the apophysis (a), rhizoidal system (r) and sporangium (s). Scale bar = 10  $\mu\text{m}$ . (B) BF image of *R. globosum* JEL800 growing on a particle of colloidal chitin. Cells are marked by arrowheads. Scale bar = 10  $\mu\text{m}$ . (C) Differential interference contrast (DIC) image of *R. globosum* growing on a *Daphnia* exoskeleton. Labelled are developing sporangia (s) and recently sporulated zoospores contained within an ephemeral vesicle (ev). Scale bar = 250  $\mu\text{m}$ . (D) High-magnification image of an *R. globosum* sporangium developing on a *Daphnia* exoskeleton. Labels and scale bar as in (A). (E&F) Fluorescent mesoscopy of *R. globosum* growing on chitin. Labelled are chitin (cyan) and neutral lipids (red). Scale bars = 250  $\mu\text{m}$ . (E) *R. globosum* thalli (arrowheads, insets) growing on cleaned *Daphnia* exoskeleton examples from 24 h (left) and 96 h (right) incubations. Note the difference in chitin and lipid coverage between the treatments. Bottom right inset shows discharged sporangia (arrowheads) and a lawn of recently settled zoospores (asterisk). (F) *R. globosum* cells (arrowheads, insets) growing on a particle of colloidal chitin after 72 h. (G-I) Confocal z-stacks show the rhizoidal architecture of *R. globosum* cells growing on colloidal chitin particles. Scale bar = 5  $\mu\text{m}$ . Maximum intensity projection (G) and 3D surface mesh (blue) reconstruction (H) of *R. globosum* cells growing on a colloidal chitin particle (yellow) after 72 h. Cell bodies labelled by asterisks. Particle is demarked by the dashed line in (G) and shown in yellow in (H). Orthogonal projection of the confocal stack in (G) in the ZX axes shows that rhizoids (arrowheads) appear to penetrate throughout the chitin particle. Cell body labelled with an asterisk.

#### **3.4.4 Imaging of diatom-chytrid interactions**

To image the development of a diatom-chytrid interaction, the live cell bioimaging protocol previously applied to *R. globosum* was applied to the diatom-chytrid pathosystem (Ast1-Chy1). Live cell time lapse imaging in the short term captured key life events such as sporulation (Figure 3.4A), however the rapid growth of concomitant bacteria within the

culture smothered the host and prevented any kind of growth after ~ 24 h (*not shown*). Nuclei, vacuoles, mitochondria, were labelled by fluorescent vital staining and all had discrete localisation in both the host and the parasite, suggesting no co-excitation was present (Figure 3.4B).

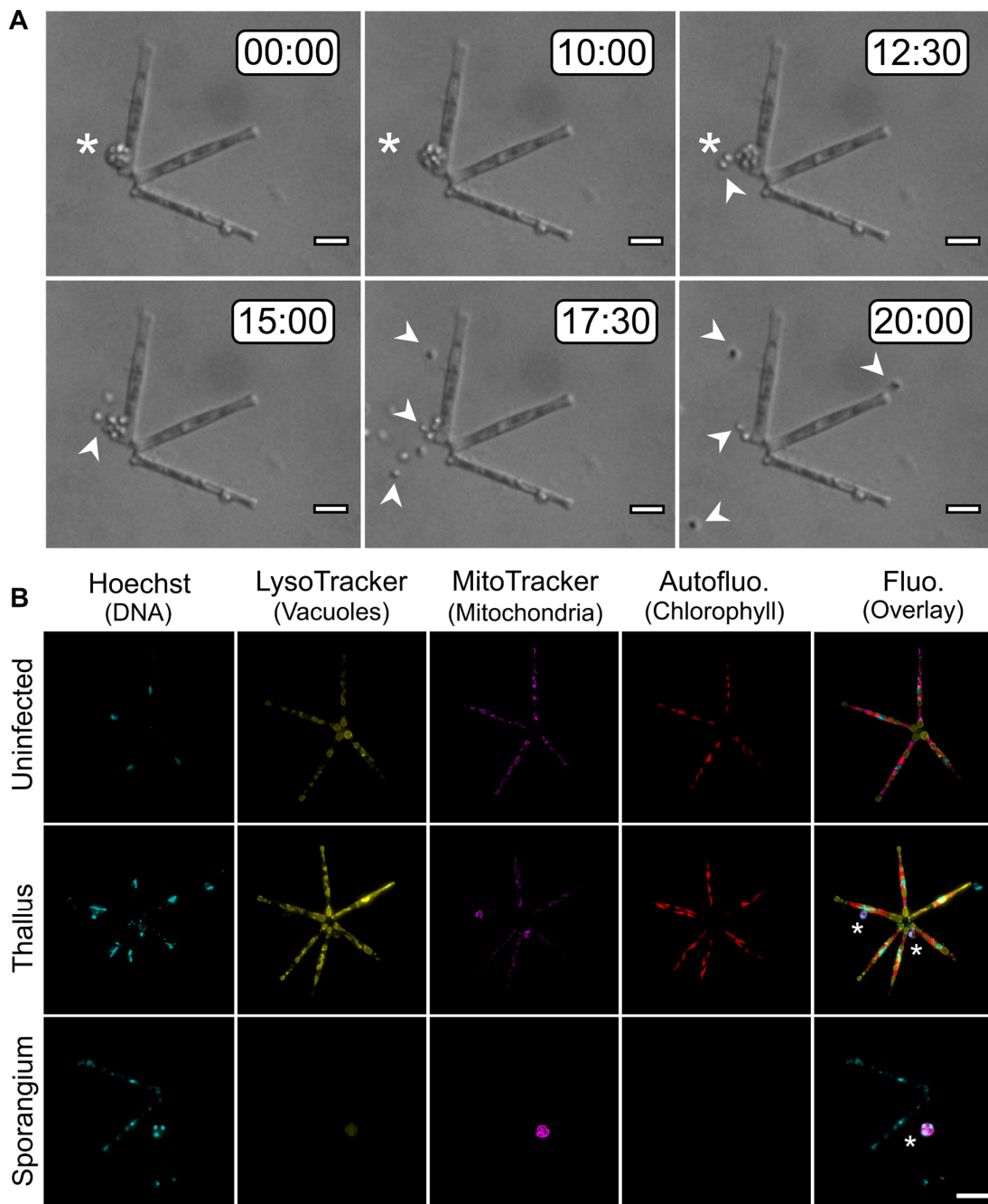


**Figure 3.4** Diatom-chytrid interactions were imaged using live-cell microscopy. Time lapse imaging and characterisation of major organelles using vital staining in Ast1-Chy1 life stages. (A) DIC time series of a sporulating chytrid sporangium (asterisk) parasitizing

an *Asterionella* diatom. Time stamp = MM:SS. Arrowheads point to newly released zoospores. Scale bar = 10  $\mu\text{m}$ . (B) Labelling of major organelles in Ast1-Chy1 using vital stains. Scale bar = 50  $\mu\text{m}$ .

### 3.4.5 Cryopreservation and revival of chytrid zoospores

*R. globosum* zoospores had a slightly lower survival rate prior to freezing in the presence of dimethyl sulfoxide (DMSO) and/or foetal calf serum (FCS) relative to the control (Figure 3.3) ( $p > 0.05$ ). However, no *R. globosum* zoospores survived freezing unless supplemented with cryoprotectants. There was no difference between cryoprotectant treatments after 1 month ( $p = 0.08$ ). However, after three months, different cryoprotectant treatments yielded differential zoospore survival ( $p < 0.05$ ). DMSO performed better as cryoprotectant than glycerol ( $p < 0.05$ ).

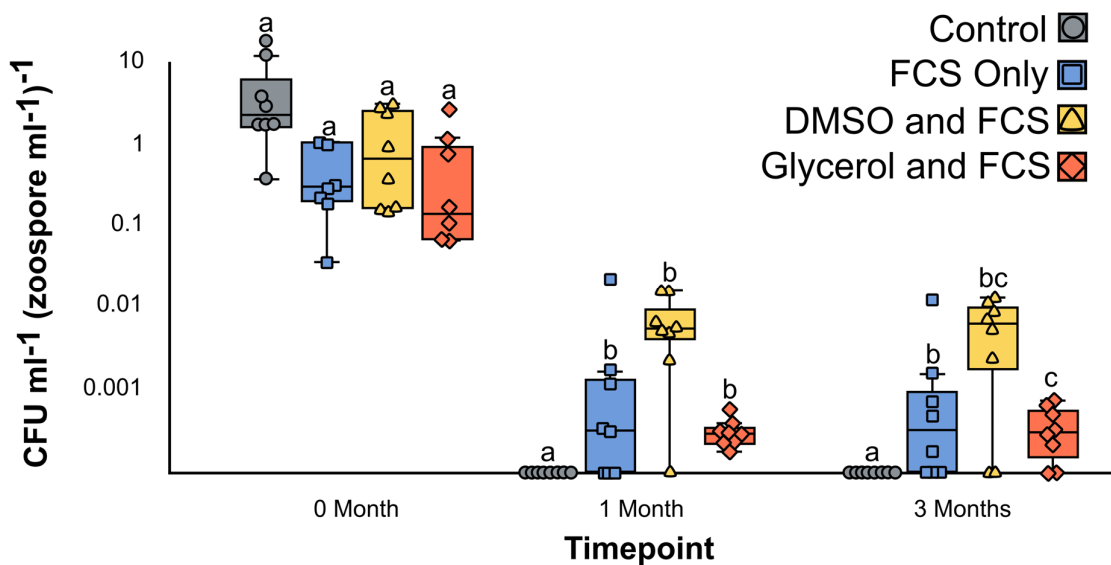


**Figure 3.5** *R. globosum* zoospores were cryopreserved and revived. Mean CFU (Colony Forming Units)  $\text{ml}^{-1}$  (zoospore  $\text{ml}^{-1}$ ) $^{-1}$  for zoospore viability following cryopreservation with different cryoprotectants across three timepoints. DMSO and FCS emerges as the optimal cryoprotectant treatment.

### 3.5 Discussion

This series of preliminary experiments provides a toolkit for future experiments in chytrid development using *R. globosum*. Firstly, fluorescent vital stains were used to label subcellular structures in *R. globosum*. The targeted labelling of the biogeochemically important lipid globules and the chitin-containing cell wall are important markers for studies into the functional ecology and impact on carbon cycling played by chytrids. Previous studies have employed CFW labelling of the chytrid cell wall (Gerphagnon et al., 2013; Rasconi et al., 2009; Sime-Ngando et al., 2013) and Nile Red labelling of chytrid lipid reserves (Buck et al., 2011; Gutman et al., 2009; Kagami et al., 2004), however these have predominantly been employed for the positive identification of chytrids in fixed environmental samples.

The application of these stains to live cells presented the opportunity to quantify the real-time synthesis and degradation of lipids and chitin across the *R. globosum* life cycle using developmental imaging. These data quantified for the first time lipid and chitin dynamics in chytrids, which before was only known from single timepoint images. Given the ecological impact of lipid synthesis in chytrids (Kagami et al., 2014), these data will serve as a promising foundation on which to build future investigations into the biology underpinning the ecological context of chytrids.

Imaging of *R. globosum* growing on various chitin sources supported that *R. globosum* is a proficient chitinophilic chytrid and can grow on both arthropod exuviae and crystalline chitin sources. The Mesolens was shown to be a powerful tool in imaging developing chytrids on *Daphnia* exuviae and colloidal chitin particles by allowing the characterisation of entire populations while maintaining subcellular resolution. The Mesolens is a custom 4 x objective lens with a numerical aperture of 0.5 and a field of view of 3 x 6 mm (McConnell et al., 2016). This enables the characterisation of either large objects, or populations of thousands of cells, at high resolution to identify population heterogeneity and rare events (McConnell et al., 2016; McConnell and Amos, 2018). While the results of these investigations are qualitative at this point, they form the baseline from which to develop future quantitative investigations into chytrid growth dynamics and



cell biology taking advantage of the large population sizes and statistical power offered by the Mesolens.

Qualitative 3D reconstruction of the chytrid rhizoid growing associated with particulate chitin appeared to show that rhizoids associated with the carbon source were denser and more branched than those outside the particle. This hints at a form of developmental plasticity in rhizoid growth. In dikaryan fungi, branching associated with hyphal feeding and development is well understood (Harris, 2008; Riquelme et al., 2018). However, despite the ecological importance of chytrids, little is known about the cell biology and development of the feeding structures of chytrids. It is now necessary to develop a methodological workflow to morphometrically quantify rhizoid development robustly in the future to investigate this preliminary observation further.

Subcellular structures in the Ast1-Chy1 pathosystem were labelled with fluorescent vital stains. Although this selection of stains proved useful in successful multichannel imaging of major subcellular organelles, Ast1-Chy1 did not take well to long-term culture and could not be kept viable due to bacterial overgrowth that could not be treated with antibiotics or serial dilution. Therefore, Ast1-Chy1 is not selected here as a promising pathosystem to pursue. Despite the unsuitability of Ast1-Chy1 for future investigation, the live cell imaging and staining protocol applied here will be built upon and applied to future diatom-chytrid interactions. *A. formosa* has long been understood as an ecologically relevant host for fresh water chytrid parasites (Canter and Lund, 1948), however the cell biology of this interaction is poorly understood. It is therefore unfortunate that long term culturing of Ast1-Chy1 was not possible. The lack of success with this pathosystem was likely exaggerated by the obligate nature of the parasite, which cannot be cultured independently from the host. However, the experimental intractability of Ast1-Chy1 is not a serious loss as it is only an environmental isolate at this stage, where the parasite lacks both a curated species binomial and genome. Therefore, future efforts to establish a long term algal-chytrid pathosystem should focus on securing a chytrid that exhibits facultative parasitism for robust comparison between saprotrophic and parasitic lifestyles, as well as the presence of a host and parasite genome.

Refinement of *R. globosum* cryopreservation showed this species to be a hardy and robust laboratory organism with great potential as an emerging model for chytrid biology. Previous studies have successfully optimised chytrid cryopreservation for different species (Gleason et al., 2007; Rad-Menéndez et al., 2018), however the specific optimisation of preservation and revival for *R. globosum* will prove useful during future investigations. These data will also provide a valuable baseline in the long-term storage of environmental isolates.

### **3.6 Conclusion**

Taken together, these preliminary investigations produced an experimental ‘toolkit’ for studying the development and cell biology of chytrids. Although largely qualitative at this stage, they have also provided insights into previously lacking fundamental chytrid biology, including the dynamics of lipid and chitin synthesis, the architecture of rhizoids during particulate feeding, and the subcellular localisation of major organelles. The protocols presented herein will prove vital in downstream experiments into the developmental biology of chytrids in this thesis and beyond and are an important step forward in the establishment of *R. globosum* JEL800 as a tractable laboratory model organism.

## Chapter 4 – A cellular and molecular atlas reveals the basis of chytrid development

**Preprinted as:** Laundon D, Christmas N, Bird K, Thomas S, Mock T, and Cunliffe M. 2021. A cellular and molecular atlas reveals the basis of chytrid development. *bioRxiv*. doi:10.1101/2021.09.06.459148

**Author contributions:** *KB extracted the RNA and prepared for transcriptome sequencing. ST performed the lipid analysis. NC processed the transcriptome sequence data and supported associated data interpretation. TM and MC provided supervision and manuscript feedback. SBF-SEM imaging was conducted by Chris Neal at the Wolfson Bioimaging Facility (University of Bristol). All other experimentation, analysis, and writing was conducted by DL.*

### 4.1 Summary

Despite the ecological and evolutionary importance of chytrids, our understanding of their fundamental developmental and cell biology remains poorly understood. To address these knowledge gaps, quantitative volume electron microscopy and comparative transcriptome profiling were combined to create an ‘atlas’ of the cellular and molecular basis of the chytrid life cycle, using the archetypal chytrid *Rhizoclostridium globosum* JEL800. From this developmental atlas, it is shown that zoospore biology is dominated by ribosome aggregates and that encystment is associated with a transition from neutral glycolipids to polar lipids. It is further demonstrated that the chytrid apophysis is a distinct subcellular structure characterised by high intracellular trafficking, providing evidence for division of labour in the chytrid cell plan, and it is shown that intrasporangial zoospore development is governed by amoeboid cell morphologies resulting from endocytotic cargo transport from the interstitial maternal cytoplasm. Taken together, these results reveal hidden insights into chytrid developmental biology and provide an integrated platform for future investigations into non-dikaryan fungal cell biology.

## 4.2 Introduction

Central to chytrid cell biology is their distinctive dimorphic life cycle, consisting of a motile free-swimming unflagellate zoospore that transforms into a sessile walled thallus with anucleate attaching and feeding rhizoids (Figure 4.1A). The cell body component of the thallus develops into the zoosporangium from which the next generation of zoospores is produced (Figure 4.1A). Any biological life cycle inherently represents a temporal progression, yet the chytrid life cycle can be categorised into four distinctive and contiguous life stages (Berger et al., 2005) (Chapter 3). The first stage is the motile 'zoospore' which lacks a cell wall, does not feed, and colonises substrates or hosts. The second stage is the sessile 'germling' which develops immediately after zoospore settlement following flagellar retraction (or sometimes detachment), undergoes cell wall production (encystment), and initiates rhizoid growth from an initial germ tube. The third stage is the vegetative 'immature thallus' which is associated with the highest levels of rhizoid development and overall cellular growth. The cell plan of the immature thallus can be divided into three parts (Figure 4.1A): the cell body which is ultimately destined for reproduction (zoosporogenesis), the rhizoid for attachment and feeding, and (in some chytrid species) a bulbous swelling between the cell body and rhizoid termed the 'apophysis', the function of which is currently poorly understood. The final life stage is the reproductive 'mature zoosporangium', which appears once the immature thallus has reached maximum cell size and the cell body cytoplasm is cleaved into the next generation of zoospores (Figure 4.1A).

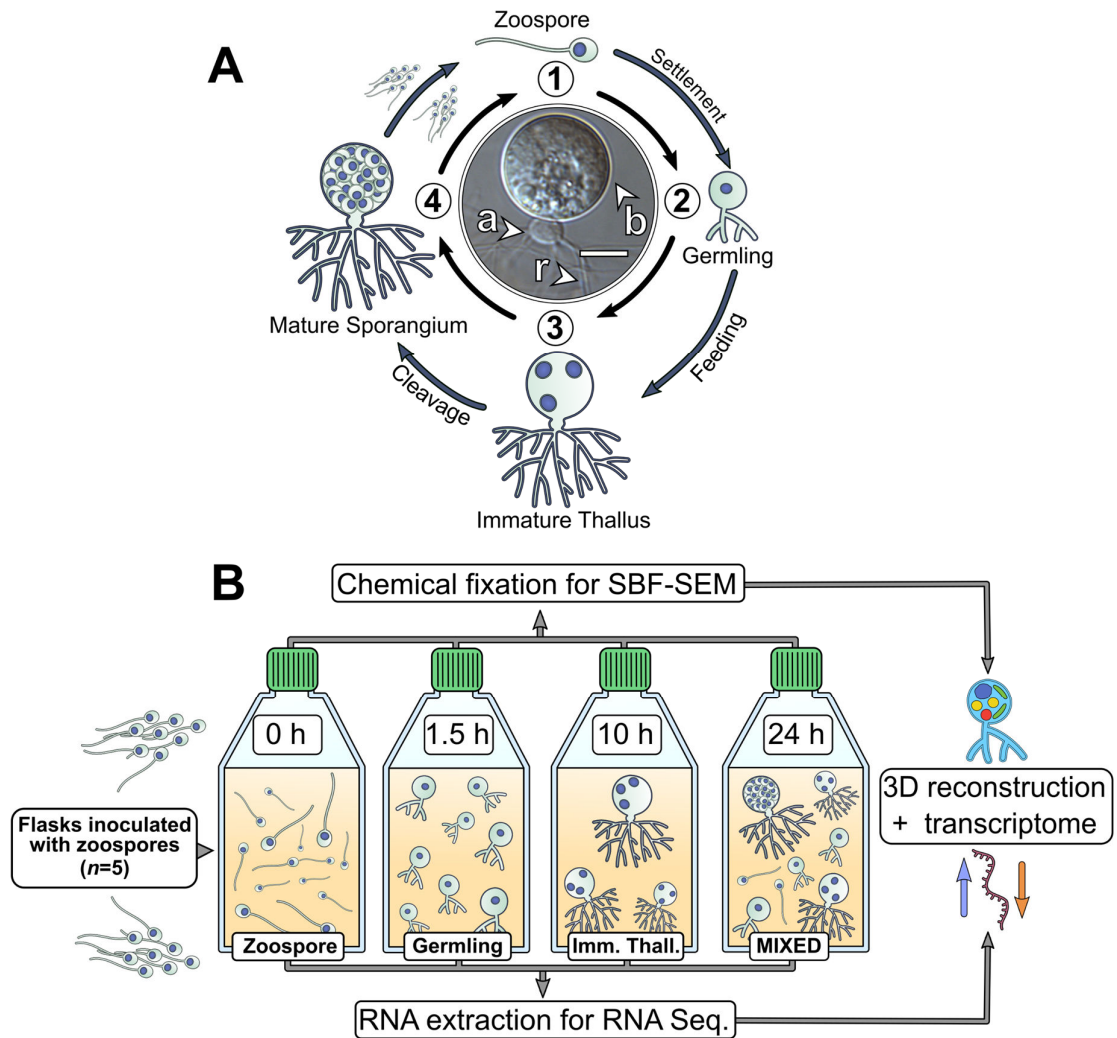


**Figure 4.1** The chytrid life cycle can be subdivided into four discrete stages. (A) The chytrid *Rhizoclostridium globosum* exhibits an archetypal chytrid life cycle and cell plan delineated here into four discrete major stages. Labelled is the apophysis (a), cell body (b), and rhizoids (r). Scale bar = 10  $\mu$ m. (B) Diagrammatic workflow of the experimental setup used in this study for comparative cellular Serial Block Face Scanning Electron Microscopy (SBF-SEM) and molecular (transcriptome) analysis.

The chytrid life cycle has so far been characterised with largely descriptive approaches (e.g Berger et al., 2005) with only a few quantitative studies focusing on targeted processes, such as rhizoid morphogenesis (Dee et al., 2019) and actin formation (Medina et al., 2020; Prostack et al., 2021). These important studies provide a foundation on which to develop a quantitative approach to understand the biology of the chytrid cell

plan and the drivers of the transitions between the life stages. To investigate the cellular and molecular underpinnings of the chytrid life cycle and associated cell biology, this chapter studied the four major life stages of the *R. globosum* cell cycle by combining quantitative volume electron microscopy and transcriptomics (Figure 4.1B), with the addition of supplementary targeted live-cell fluorescent microscopy and lipid analysis. The aim of this approach was to quantify the cellular traits that define the major chytrid life stages and identify the biological processes that take place during the developmental transitions between them. As such, this work constitutes a developmental 'atlas' with *R. globosum* for the archetypal chytrid lifecycle, which in turn generated specific avenues for targeted investigation of important biological processes, namely lipid biology, apophysis function, and zoosporogenesis.

By culturing *R. globosum* and sampling the populations at different stages through their temporal development (Figure 4.1B), this work examined chytrid populations with both 3D reconstructions by Serial Block Face Scanning Electron Microscopy (SBF-SEM) and mRNA sequencing. Single-cell SBF-SEM reconstructions ( $n = 5$ ) (Figure 4.2) were used to quantify the cellular structures at each life stage and population-level transcriptomic analysis of significant KEGG pathway categories ( $n = 3$ , Differentially Expressed Genes (DEGs)) was used to identify the major biological differences between the life stages through temporal development (Figure 4.1B). As these stages represent key time points in the progression of the linear temporal chytrid life cycle, pairwise comparison of transcriptomes from contiguous life stages achieved an account of the major putative biological transitions (e.g. germling vs. zoospore, immature thallus vs. germling). These findings provide insights into chytrid developmental processes and serve as a resource from which to resolve the biology of this ecologically and evolutionary important fungal lineage.

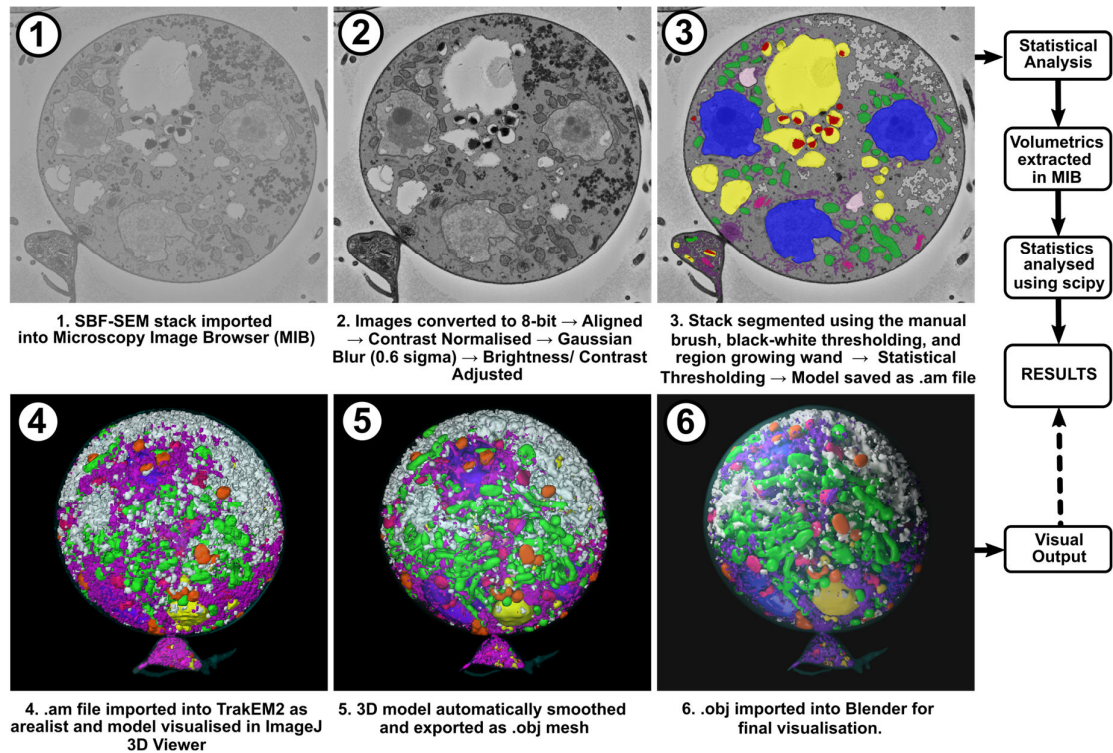


**Figure 4.2 SBF-SEM reconstruction was used to characterise cellular structure.**

Workflow of the image analysis protocol used to generate and visualise 3D reconstructions of chytrid cells from SBF-SEM stacks.

## 4.3 Methods and materials

### 4.3.1 Cell harvesting for SBF-SEM, transcriptomics, and lipid quantification

*R. globosum* was grown to progress through the life cycle and sampled ( $n = 5$ ) at key time points: 0 h (zoospore), 1.5 h (germling), 10 h (immature thalli), and at 24 h when the population was a mix of stages including mature zoosporangia (Figure 4.1B). For zoospores, each replicate was harvested from 10 ml of undiluted cell suspension immediately after plate flooding. For germlings, each culture flask (83.3910, Sarstedt) contained 40 ml of liquid PmTG and was inoculated with 10 ml of zoospore suspension, incubated for 1.5 h, and pelleted after scraping the flask with an inoculation loop to dislodge adherent cells. Immature thalli replicates were pooled from 10 x culture flasks of 25 ml liquid PmTG inoculated with 50  $\mu$ l zoospore suspension and incubated for 10 h. Finally, mixed 24 h populations containing mature zoosporangia were harvested and

strained through a 40 µm cell strainer (11587522, FisherBrand) to remove smaller life stages. All incubations were conducted at 23 °C and cells were pelleted at 4,700 rpm for 5 min. For SBF-SEM, cell pellets were resuspended and fixed in 2.5 % glutaraldehyde in 0.1 M cacodylate buffer pH 7.2. Cells were harvested identically for RNA Seq ( $n = 3$ ) with the exception that the supernatant was removed before being flash frozen in liquid nitrogen and stored at -80 °C. Sub-samples from cell pellets were diluted 1:1,000, fixed in 0.2 % formaldehyde, and stained with FM 1-43FX to visualise cell membranes in order to qualitatively confirm the synchronicity of cultures under a confocal microscope (*see further below*) before being processed further. Cell pellets were harvested for lipid extraction and quantification as per RNA samples ( $n = 3$ ).

#### **4.3.2 SBF-SEM imaging and reconstruction**

Samples were further fixed in buffered glutaraldehyde, pelleted, and embedded in Bovine Serum Albumin (BSA) gel. Blocks were processed into resin using a modified protocol by Deerinck and colleagues (<https://tinyurl.com/ybdtwedm>). Briefly, gel-embedded chytrids were fixed with reduced osmium tetroxide, thiocarbohydrazide, and osmium tetroxide again, before being stained with uranyl acetate and lead aspartate. Stained blocks were dehydrated in an ethanol series, embedded in Durcupan resin, and polymerised at 60 °C for 24-48 h. Blocks were preliminarily sectioned to ascertain regions of interest (ROIs) using transmission electron microscopy (FEI Tecnai T12 TEM). ROIs were removed from the resin blocks and remounted on aluminium pins, which were aligned using scanning electron microscopy (Zeiss GeminiSEM) on a Gatan 3 view serial block face microtome and imaged.

Stacks of chytrid cells were acquired at 75 nm z-intervals with an XY pixel resolution of 2 nm (zoospore, germling, and developing zoospore inside a mature zoosporangium), 4 nm (immature thallus), and 8 nm (mature zoosporangium). Although XY pixel size differed between life stages, 2-4 nm resolutions were above the minimum sampling limits for quantitative comparison of reconstructed organelles. Due to the lack of



replication, the mature zoosporangium was only considered qualitatively. Acquired stacks were cropped into individual cells and imported into Microscopy Image Browser (MIB) (Belevich et al., 2016) for reconstruction. Prior to segmentation, images were converted to 8-bit, aligned, contrast normalised across z-intervals using default parameters, and then were processed with a Gaussian blur filter ( $\sigma = 0.6$ ). Stacks were segmented using a combination of manual brush annotation and the semi-automated tools available in MIB (Figure 4.2). Briefly, flagella, lipids, microbodies, nuclei, ribosomal clusters, rumposomes, peripheral bodies, striated inclusions, vacuoles, and vesicles (Figure 4.3) were segmented manually using interpolation every 3-5 slices where appropriate; the discharge plug, endomembrane, glycogen granules, Golgi apparatuses, and mitochondria (Figure 4.3) were masked by coarse manual brushing and then refined by black-white thresholding; and cell boundaries were segmented using the magic wand tool. All models were refined by erosion/dilation operations and manually curated. Models were also refined by statistical thresholding at size cut-offs for each structure consistent across all life stages (either 500 or 1,000 voxels).

Structures were volumetrically quantified within MIB. For visualisation of reconstructed cells .am model files were resampled by 33 % in XY and imported as arealists into the Fiji (Schindelin et al., 2012) plugin TrakEM2 (Cardona et al., 2012), smoothed consistently across life stages, and exported as 3D .obj meshes for final rendering in Blender v2.79. All quantification was conducted on unsmoothed models scaled by 50 %. Flagella and rhizoids were excluded from quantification as they are not a component of the cell body, and their total length were not imaged in this study. The unassigned cytosol fraction was defined as the total volume of assigned organelles subtracted from the total cell volume and is inclusive of small structures such as ribosomes, vesicles, and small endomembrane and glycogen objects that could not be confidently assigned and were conservatively excluded. Only endomembrane not considered to be predominantly structural (i.e. an organelle or cell-compartment boundary) was reconstructed in the endomembrane category.

### **4.3.3 RNA extraction**

RNA was extracted from the cell pellets using the RNeasy extraction kit (Qiagen) following the manufacturer's instructions with minor modifications. Cell pellets were thawed in 600 ml RLT lysis buffer containing 10  $\mu\text{l ml}^{-1}$  of 2-mercaptoethanol and lysed at room temperature for 5 min with periodic vortexing. Cell debris was removed by centrifuging at 8,000 xg for 1 min, before the lysate was recovered and passed through a QIA shredder (Qiagen). An equal volume of 100 % ethanol was added to the homogenised lysate before being transferred to an RNeasy extraction column. RNA was then extracted following the manufacturer's protocol and included an on-column DNase digestion step using the RNase-Free DNase (Qiagen). RNA was quantified using both a NanoDrop 1000 spectrophotometer (ThermoFisher) and the RNA BR assay kit (Invitrogen) on the Qubit 4 fluorometer (Invitrogen). RNA quality was assessed using the RNA 6000 Nano kit total RNA assay (Agilent) run on the 2100 Bioanalyzer instrument (Agilent).

### **4.3.4 Sequencing and bioinformatics**

Sequencing was carried out by Novogene ([www.novogene.com](http://www.novogene.com)) using Illumina NovaSeq 6000 technology and base calling by CASAVA, yielding 20,122,633 – 23,677,987 raw reads. Raw reads were filtered for adaptor contamination and low-quality reads (ambiguous nucleotides >10 % of the read, base quality <5 for more than 50 % of the read) resulting in 19,665,560 – 22,917,489 clean reads. Reads were mapped against the JEL800 genome using HISAT2 before differentially expressed genes (DEGs) between life stages were determined as part of the Novogene pipeline using DESeq2 (Love et al., 2014). Transcriptomic profiles were highly conserved between replicates within each of the three life stages. All further analyses were performed in house in R v3.6.1 (R Core Team) using output from the Novogene analysis pipeline. Shared genes between life history stages were displayed using UpSetR (Conway et al., 2017). Volcano plots of differentially expressed genes were produced using ggplot2 based upon a conservative threshold of  $\log_2\text{FoldChange} >0$ ,  $\text{padj} <0.05$ . Gene Ontology (GO) and Kyoto

Encyclopedia of Genes and Genomes (KEGG) enrichment analysis was carried out using the enricher function in the R package clusterProfiler v3.12 (Yu et al., 2012) with a threshold of  $p_{adj} < 0.05$ . Differentially expressed KEGG categories were plotted using the dotplot function and GO maps generated using the emapplot function. For the purposes of this study, analysis and discussion of KEGG pathways was favoured over GO categories as KEGG pathways allow for a more process-oriented interpretation of activity.

#### ***4.3.5 Confocal and live-cell microscopy of subcellular structures***

Cell structures were labelled in a 24 h mixed population with 5  $\mu\text{M}$  calcofluor white (CFW, chitin), 1  $\mu\text{M}$  Nile red (NR, neutral lipid), and 5  $\mu\text{M}$  FM 1-43 (membranes). Cells were imaged under a 63 x oil immersion objective lens with a Leica SP8 confocal microscope (Leica, Germany). Image acquisition settings were as follows: for cell wall excitation at 405 nm and emission at 410-500 nm (intensity 0.1 %, gain 20); for lipids excitation at 514 nm and emission at 550-710 nm (intensity 0.1 %, gain 50); and for membranes excitation at 470 nm and 500-650 nm (intensity 5 %, gain 50). All life stages were imaged under identical acquisition settings. Cell wall and lipid images are maximum intensity projections at 0.3  $\mu\text{m}$  z-intervals and membrane images are single optical sections. Live-cell microscopy was conducted as in Chapter 3.

#### ***4.3.6 Image analysis for live-cell microscopy***

Developmental time series of fluorescently labelled subcellular structures were analysed with a custom workflow based around scikit-image v0.16.2 (Van Der Walt et al., 2014) run with Python v3.7.3 implemented in Jupyter Notebook v6.0.3. Briefly, cells were segmented using the bright-field channel by Sobel edge detection (Kanopoulos et al., 1988) and Otsu thresholding (Otsu, 1979). This mask was used to quantify normalised intensity in the fluorescence channel. For lipid tracking during single-cell development, images from the lipid channel were converted to maximum intensity projections and lipid globules were automatically detected using differences of Gaussian (DoG) detection in the Fiji plugin

TrakMate (Tinevez et al., 2017). Tracking of the initial lipid globule was conducted using a simple LAP tracker.

#### **4.3.7 Lipid extraction and quantification**

Lipids were extracted using the Bligh and Dyer method (Bligh and Dyer, 1959). Lyophilised culture pellets were submersed in 2:1:0.8 (v/v/v) methanol (MeOH), dichloromethane (DCM) and phosphate buffered saline (PBS) and sonicated for 10 min in an ultrasonic bath before being centrifuged at 3,000 rpm for 2 min. The supernatant was collected, and the pellet was re-extracted twice. The combined supernatant was phase separated via addition of DCM and PBS (giving an overall ratio of 1:1:0.9 (v/v/v)) and centrifugation at 3,000 rpm for 2 min. The lower solvent phases were extracted prior to washing the remaining upper phase twice with DCM. The three lower solvent phases were collected and gently evaporated under oxygen-free nitrogen (OFN) in a water bath held at 25 °C (N-EVAP, Organomation, USA). The initial lipid extracts were weighed to quantify total lipid biomass before being dissolved in 9:1 (v/v) DCM:MeOH and loaded onto preactivated silica gel (4 h at 150 °C) columns for fractionation. Lipid fractions were separated by polarity via washing the column with one volume of DCM, followed by one volume of acetone and two volumes of MeOH. Each fraction was collected separately and evaporated to dryness under OFN and weighed.

#### **4.3.8 Data analysis and statistics**

All data were tested for normality and homogeneity assumptions using a Shapiro and Levene's test respectively. If assumptions could be met, then differences between zoospore, germling, and immature thallus volumetric proportions were assessed using ANOVA followed by Tukey HSD posthoc testing or, if not, then by a Kruskal-Wallis followed by a Dunn's posthoc test. If a structure was entirely absent from a life stage (e.g. no cell wall in the zoospore stage) then the life stage was eliminated from statistical analysis to remove zero values and the remaining two life stages were compared using a

*t*-test or Mann-Whitney U test depending on assumptions, and then the removed life stage qualitatively assigned as different. The differences between cell bodies and apophyses in the immature thallus life stage, and between mature zoospores and developing zoospores, were compared using either a *t*-test or a Mann-Whitney U test depending on assumptions. All statistical analysis was conducted using the scipy package (Virtanen et al., 2020) run with Python v3.7.3 implemented in Jupyter Notebook v6.0.3.

## **4.4 Results**

### **4.4.1 A cellular and molecular atlas of *R. globosum* development**

The orientation, subcellular localisation, and ultrastructural morphology determined with SBF-SEM of the *R. globosum* zoospore, germling, and immature thallus life stages are shown in Figure 4.4, with the volumetric transition from zoospore ( $20.7 \pm 1.7 \mu\text{m}^3$ ) (mean $\pm$ SD) to germling ( $33.0 \pm 2.0 \mu\text{m}^3$ ) to immature thallus ( $1,116.3 \pm 206.2 \mu\text{m}^3$ ) exceeding an order of magnitude. The volumetric differences in the cell patterns at each life stage (Figure 4.5; Table 4.1) are complemented with differential gene expression analysis focusing on characterising the transitions between life stages (Figure 4.6). Full statistical details of cell volumetric comparisons are provided in Tables 4.1-3. All reconstructed SBF-SEM replicates are shown in Supplementary Figures 4.1&2 at the end of this chapter. As the mature zoosporangium samples were taken from a mixed population of cell stages (Figure 4.1B), they were conservatively excluded from comparison with the first three stages and will be treated separately in this analysis.

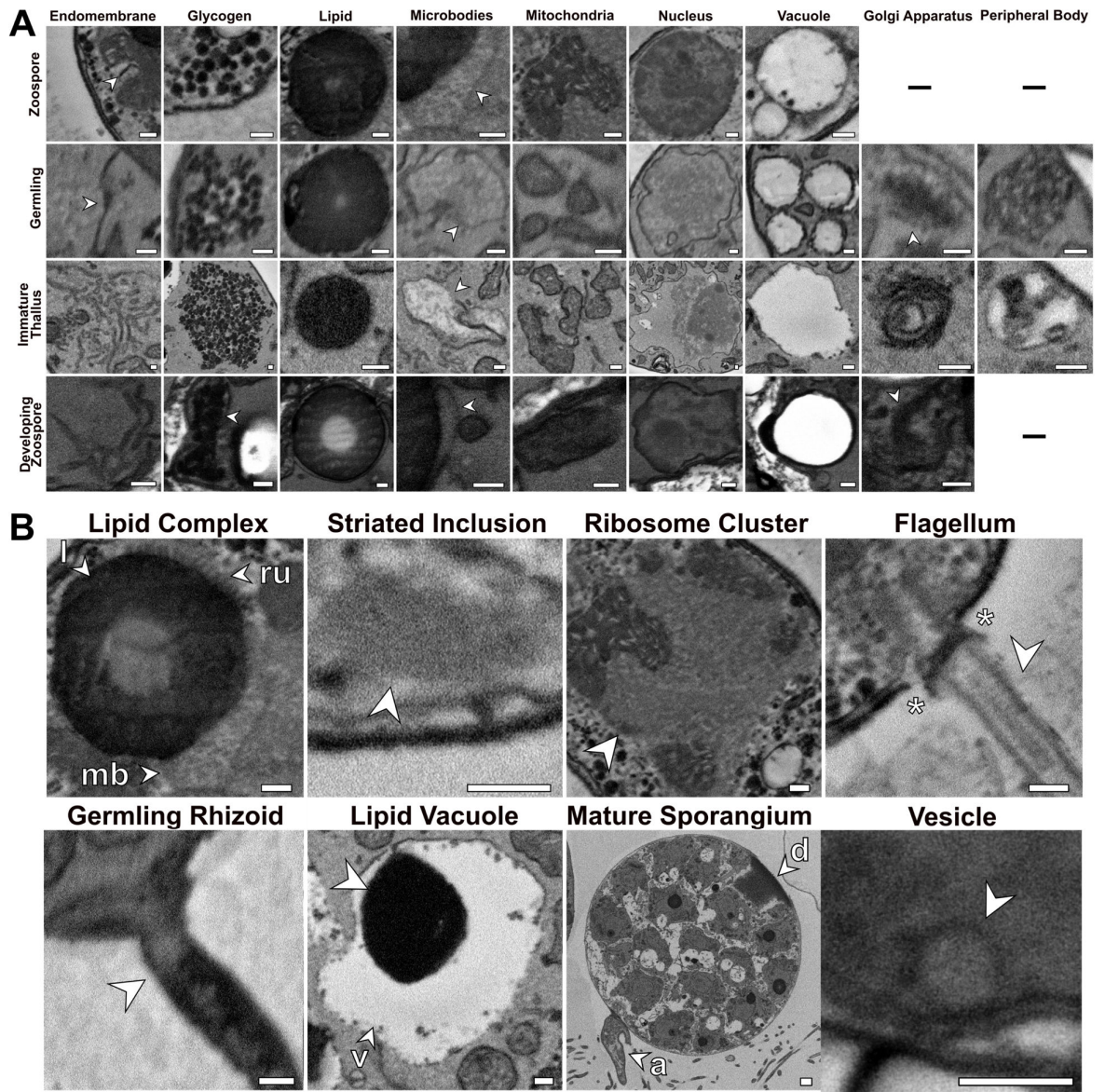


**Figure 4.3 Example subcellular components identified in this study.** (A) High magnification example images of individual subcellular structures identified across life stages, where present, taken from single SBF-SEM images. (B) Individual subcellular structures largely unique to individual life stages. a = apophysis, d = discharge plug, l = lipid globule, mb = microbodies, ru = rumposome, v = vacuoles. Asterisks in (B) show electron-dense plate at the base of the zoospore flagella. Scale bars = 0.2  $\mu\text{m}$ .

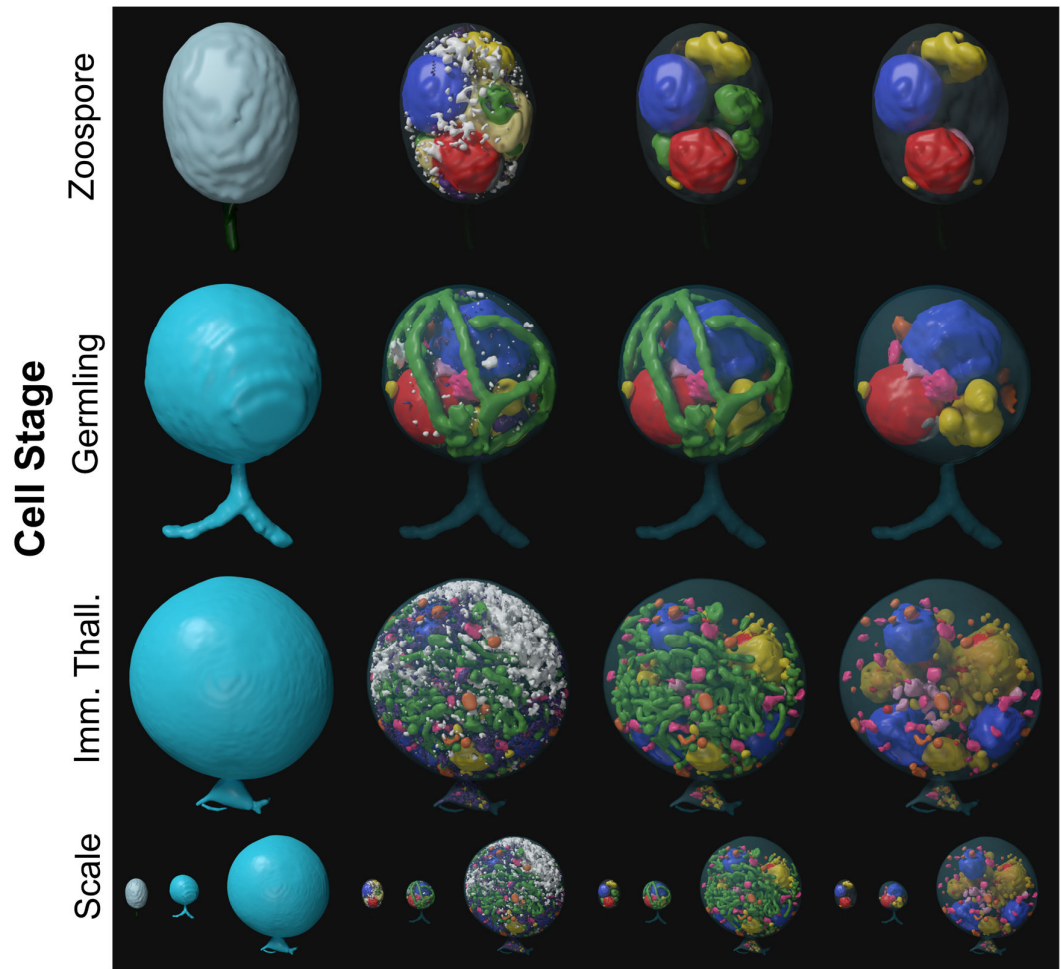


**Figure 4.4** Volume electron microscopy reconstructions of the *R. globosum* life cycle. Representative SBF-SEM reconstructions of the first three life stages of the *R. globosum* lifecycle. Bottom row shows the stages to scale. Organelle colours as in Figure 4.5 and conserved throughout.

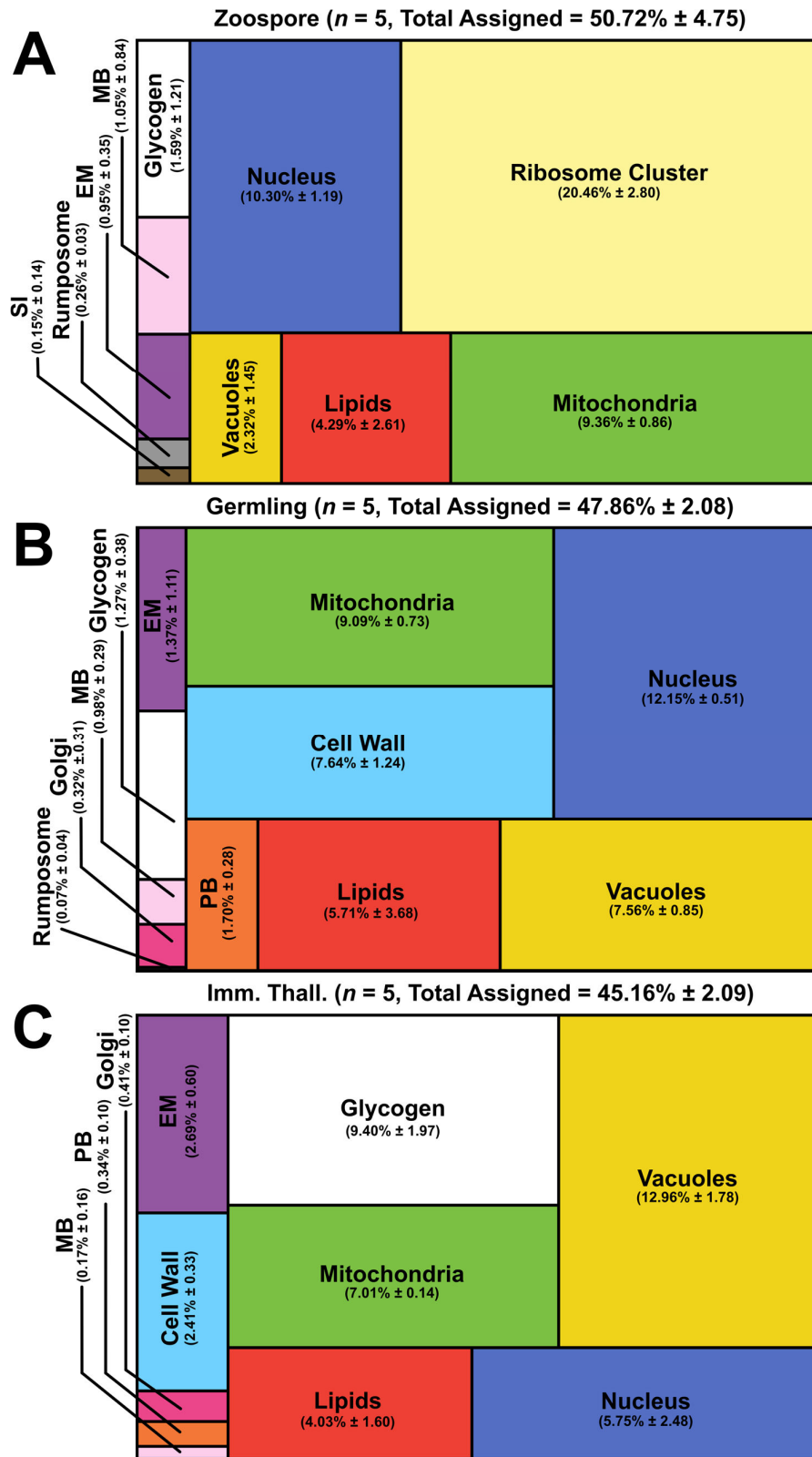


**Figure 4.5 Volumetric comparisons of *R. globosum* life stages.** (A-C) Volumetric composition of assigned organelles in SBF-SEM reconstructions ( $n = 5$ ) of zoospores (A), germlings (B), and immature thalli (C). EM = endomembrane, MB = microbodies, PB = peripheral bodies, SI = striated inclusion.



**Table 4.1 Volumetric percentages and statistical comparisons of SBF-SEM**

**reconstructions of cellular structures recorded across chytrid life stages.** Data given to 3 decimal places.

Cellular Structure	Chytrid Life stage – Volumetric %						Statistical Test used	p-Value	Posthoc Annotation
	Zoospore (n = 5)	± S.D	Germling (n = 5)	± S.D	Immature Thallus (n = 5)	± S.D			
Total Volume	100.000	0	100.000	0	100.000	0.000	NA	NA	NA
Cell Wall	0.000	0.000	7.644	1.245	2.409	0.328	Mann Whitney U	<0.01	A B C
Cytosolic Lipid	4.290	2.610	5.714	3.678	0.341	0.159	Kruskal	<0.01	A A B
Endomembrane	0.948	0.353	1.371	1.112	2.691	0.597	ANOVA	<0.01	A A B
Glycogen	1.590	1.213	1.265	0.376	9.399	1.969	Kruskal	<0.01	A A B
Golgi Apparatus	0.000	0.000	0.321	0.313	0.414	0.104	Mann Whitney U	>0.05	A B B
Microbodies	1.052	0.836	0.978	0.293	0.167	0.156	ANOVA	<0.05	A AB B
Mitochondria	9.363	0.861	9.086	0.732	7.005	0.143	ANOVA	<0.001	A A B
Nucleus	10.297	1.187	12.151	0.512	5.749	2.477	ANOVA	<0.001	A A B
Peripheral Bodies	0.000	0.000	1.696	0.278	0.336	0.100	Mann Whitney U	<0.01	A B C
Ribosome Cluster	20.457	2.798	0.000	0.000	0.000	0.000	NA	NA	A B B
Rumposome	0.258	0.030	0.095	0.071	0.000	0.000	T-Test	<0.001	A B C
Striated Inclusion	0.147	0.139	0.000	0.000	0.000	0.000	NA	NA	A B B
Vacuole-bound Lipid	0.000	0.000	0.000	0.000	3.689	1.596	NA	NA	A A B
Vacuoles excl. Lipid Contents	2.322	1.453	7.560	0.852	12.958	1.780	ANOVA	<0.001	A B C
Total Assigned Organelles	50.724	4.754	47.857	2.082	45.159	2.087	ANOVA	>0.05	A AB B
Unassigned Cytosol	49.276	4.754	52.143	2.082	54.841	2.087	ANOVA	<0.05	A AB B
Vacuoles incl. Lipid Contents	2.322	1.453	7.560	0.852	16.647	0.930	Kruskal	<0.01	A A B
Total Lipid Fraction	4.290	2.610	5.714	3.678	4.030	1.604	Kruskal	>0.05	A A A
Total Endomembrane Fraction	4.322	1.113	11.745	1.719	20.255	1.248	ANOVA	<0.001	A B C

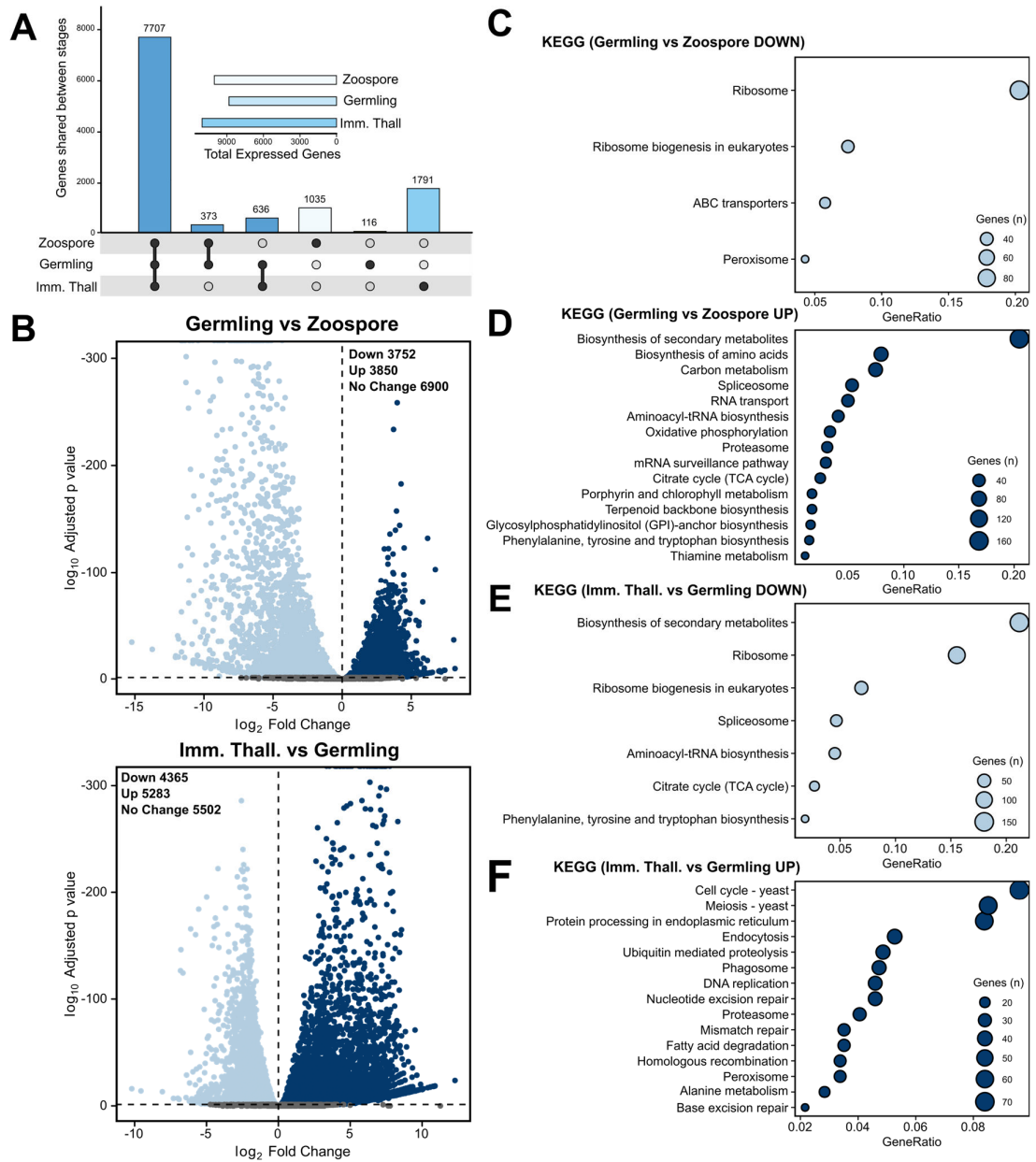


**Figure 4.6** Transcriptome analysis of the *R. globosum* life cycle. (A) Shared and unique gene expression counts between life stages. Inset shows total expressed genes per life stage. (B) Pairwise comparison of differentially expressed genes (DEGs) between germlings and zoospores, and immature thalli and germlings. (C-F) Pairwise comparison of significant ( $p < 0.05$ ) differentially expressed KEGG categories between germlings and zoospores (C&D), and immature thalli and germlings (E&F). GeneRatio = ratio of input genes annotated within a KEGG term between life stages.

The zoospore cell body is a prolate spheroid with an posterior flagellum that is volumetrically dominated by a structurally distinct ribosome cluster ( $20.5 \pm 2.8$  %) in the cell interior which was not detected in the other life stages (Figure 4.5A). The loss of the ribosome cluster in the germling from the zoospore stage matched a downregulation of ribosome and ribosome biogenesis KEGG categories in the germling relative to the zoospore (Figure 4.6C). There was no observed significant molecular signature associated with elevated protein synthesis in zoospores, suggesting that ribosome presence and aggregation, but not activity, govern chytrid zoospores. Only two other KEGG categories were downregulated in germlings relative to zoospores. These were linked to peroxisomes and ATP-binding cassette (ABC) transporters (Figure 4.6C), both of which are associated with lipid metabolism (*discussed further below*).

The germling stage marks the origin of a complete cell wall, Golgi apparatuses (3 out of 5 replicates), and peripheral bodies i.e. vesicular structures bound to the cell periphery putatively associated with cell wall deposition (Figure 4.5B), as well as the beginning of rhizoid growth from a posterior germ tube. Transcriptome analysis indicated that the germling exhibits a greater range of active processes compared to the zoospore, with upregulation of primary and secondary metabolism (e.g. amino acid and secondary metabolite biosynthesis), feeding and energy release (e.g. carbon metabolism and Tricarboxylic Acid Cycle), and transcription and translation (e.g. spliceosome and aminoacyl-tRNA biosynthesis) KEGG categories (Figure 4.6D). A similar pattern is shown when comparing KEGG categories downregulated in immature thalli relative to germlings (Figure 4.6E). In the germling stage, the upregulation of genes associated with proteasome activity was also observed (Figure 4.6D). Taken together, these data show that the transition from zoospore to germling is characterised by the apparent activation of diverse biological processes including central metabolic pathways, cellular anabolism, and feeding.

Compared to the germling, immature thalli devoted a smaller volumetric proportion to the cell wall (IT  $2.4 \pm 0.3$  % vs G  $7.6 \pm 1.2$  %,  $p < 0.01$ ) and peripheral bodies (IT  $0.3 \pm 0.1$  % vs G  $1.7 \pm 0.3$  %,  $p < 0.01$ ) (Figure 4.5C). Similarly, nuclei (IT  $4.8 \pm 2.5$  % vs G  $12.2 \pm 0.5$  %,

$p < 0.01$ ) and mitochondria (IT  $7.0 \pm 0.1$  % vs G  $9.1 \pm 0.7$ %,  $p < 0.001$ ) occupied a smaller volumetric proportion (Figure 4.5C). Conversely, immature thalli displayed larger glycogen stores (IT  $9.4 \pm 2.0$  % vs G  $1.3 \pm 0.4$ %,  $p < 0.01$ ) and vacuole fractions (IT  $13.0 \pm 1.8$  % vs G  $7.6 \pm 0.9$  %,  $p < 0.001$ ) than germlings (Figure 4.5C). Quantification of the increased vacuolisation of immature thalli in the SBF-SEM images was correlated with upregulation of related KEGG categories including endocytosis and phagosomes relative to germlings (Figure 4.6F). Within these categories are genes related to microtubules and actin, including actin-related proteins-2/3 (Arp2/3), indicating that the immature thalli are associated with higher cytoskeletal activity compared to germlings. Some immature thallus replicates were multinucleate ( $1.8 \pm 1.3$  nuclei per cell), indicating the onset of nuclear division (Figure 4.4), which matched the upregulation of cell cycle and DNA replication KEGG categories relative to germlings. The apophysis ( $12.2 \pm 6.0 \mu\text{m}^3$ ) was observed at the immature thallus stage (*discussed further below*). Overall, these data show that the biological shift from germling to immature thallus is characterised by a move from general metabolic activity to intracellular trafficking and the initiation of zoosporogenesis.

As anticipated, the SBF-SEM reconstructions showed that the zoospore is wall-less unlike the germling and immature thallus stages (Figure 4.4). Single cell fluorescent-labelling of chitin (the primary wall component) however showed that some precursory material is produced by zoospores at the posterior pole near the flagellum base (Figure 4.7A) suggesting that cell wall production is initiated to some extent during the free-swimming zoospore stage of the *R. globosum* cell cycle. Later in Chapter 5, twenty-eight candidate genes for glycosyltransferase (GT2) domain containing proteins putatively involved in chitin synthesis are identified in *R. globosum* and are searched for their individual regulation in the transcriptome data here. There was no clear pattern of differential regulation of these genes between the life stages overall, however five putative chitin synthase genes were upregulated during the zoospore stage. Nine genes were only found upregulated in the immature thallus relative to the germling, six of which had >5-fold change increase in abundance. Six genes were not recovered in any of the

transcriptomes. Interestingly, a putative  $\beta$ -1,6-glucan synthase gene (ORY39038) identified as having a possible role in wall formation in *R. globosum* was downregulated in germlings relative to wall-less zoospores. Together, this suggests that cell wall formation is a dynamic process throughout the chytrid life cycle, with alternative synthesis enzymes employed at different stages.

#### **4.4.2 Changes in lipid-associated structures are linked to variation in lipid composition**

Fluorescent labelling and SBF-SEM reconstructions showed that zoospores and germlings possess a single lipid globule (Z  $0.9 \pm 0.6$  and G  $1.9 \pm 1.1 \mu\text{m}^3$ ) whereas immature thalli have multiple ( $68.8 \pm 55.2$ ) but smaller ( $0.5 \pm 0.8 \mu\text{m}^3$ ) globules scattered throughout the cell body (Figure 4.7A&B). The lipid globule (red) in the zoospore and germling stages was associated with an posteriorly oriented structure called the rumposome (grey), which is a chytrid-specific organelle putatively associated with cell signalling (Powell, 1983), and an anteriorly oriented microbody (pink) that likely functions as a lipid-processing peroxisome (Powell, 1976) (Figure 4.7B&C). Together these structures form the lipid-rumposome-microbody (LRM) complex. The rumposome was larger in zoospores than in germlings (Z  $0.3 \pm 0.0$  % vs G  $0.1 \pm 0.1$  %,  $p < 0.001$ ), indicating increased activity in zoospores. In immature thalli, LRM complexes were not detected. Unlike in zoospores and germlings, the bulk of the lipids in the immature thalli were intravacuolar ( $89.8 \pm 8.5$  % total lipids) (Figure 4.7D). There was no proportional volumetric difference in lipid fractions determined with SBF-SEM reconstructions between the three life stages (Z  $4.3 \pm 2.6$  % vs G  $5.7 \pm 3.7$  % vs IT  $4.0 \pm 1.6$  %,  $p > 0.05$ ) (Figure 4.5).

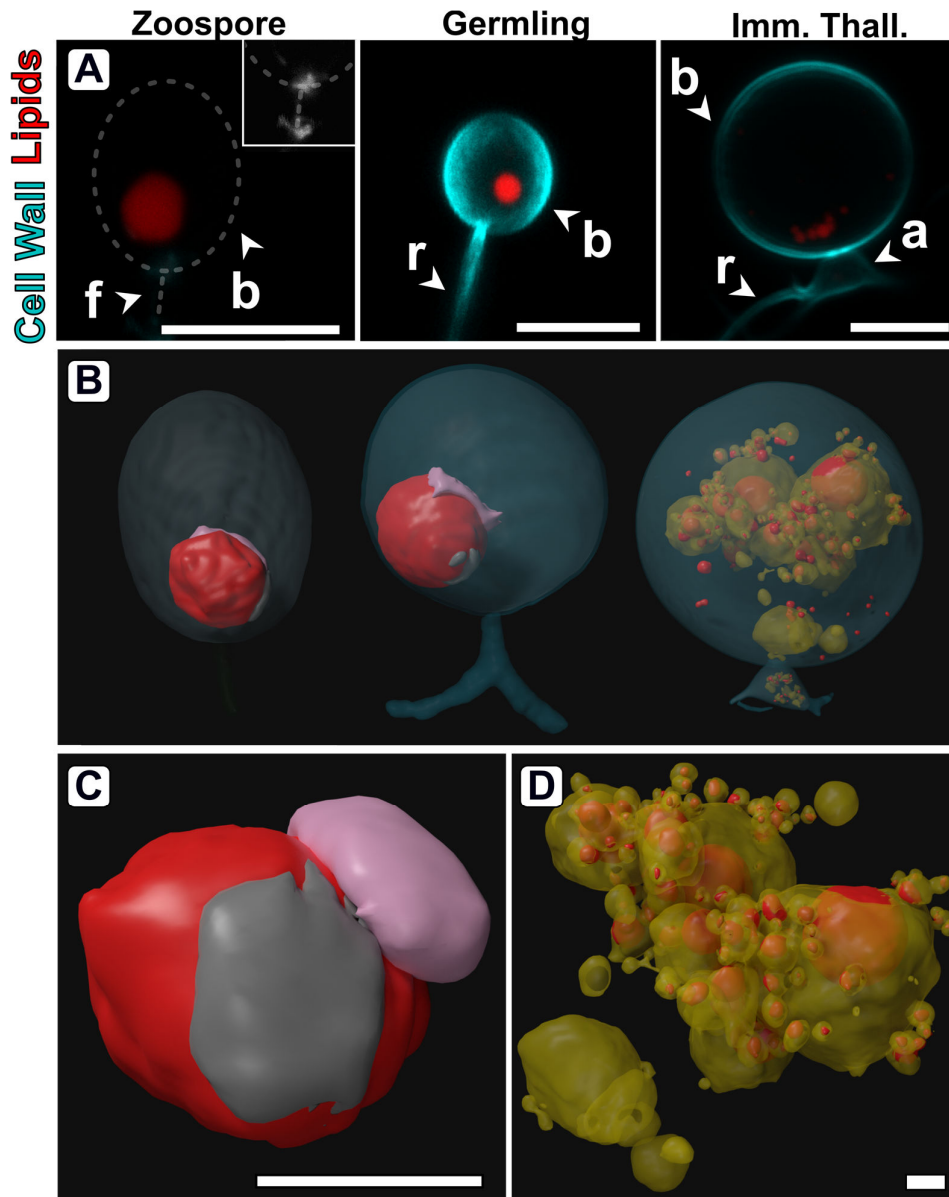


**Figure 4.7 Changes in lipid-associated cell structures between *R. globosum* life stages.** (A) Fluorescently labelled confocal images of *R. globosum* showing qualitative shifts in lipid structures and cell wall across the chytrid life cycle. Dashed line demarks cell boundary where not labelled in the zoospore. Zoospore inset shows precursory cell wall material at the flagellar base contrast-brightness adjusted for visualisation. Apophysis (a), cell body (b), flagellum (f), rhizoid (r). Scale bars = 5 μm. (B) Representative SBF-SEM reconstructions of lipid globules and lipid-associated structures across chytrid life stages. (C&D) SBF-SEM reconstructions of the lipid-rumposome-microbody (LRM) complex from zoospores (also seen in germlings) (C) and intravacuolar lipid globules from immature thalli (D). Scale bars = 1 μm.

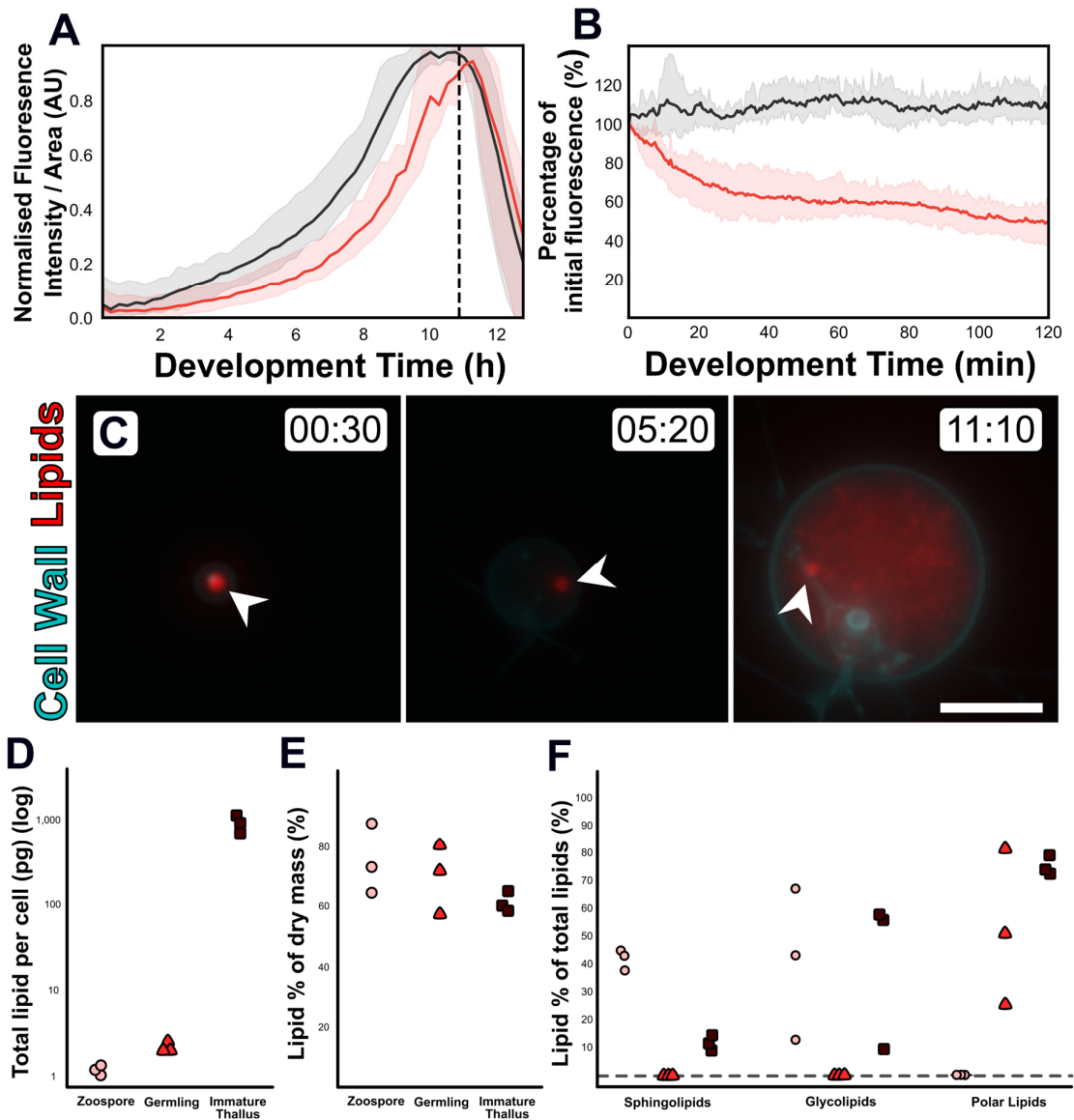


**Figure 4.8** Changes in lipid composition occur with transitions between *R.*

*globosum* life stages. (A) Live-cell imaging ( $n = 5$ ) of *R. globosum* population-level Nile red-stained lipid dynamics. Red = mean lipid fluorescence ( $\pm$ min/max), black = mean total cell area ( $\pm$ min/max), dashed line = mean sporulation time of population. (B) Immediately following zoospore settlement, the population-level ( $n = 5$ ) lipid fluorescence (red) decreases relative to fixed photobleaching control populations (black). (C) Live-cell imaging revealed differential lipid dynamics across the chytrid life cycle. Note that the initial lipid globule (arrowhead) remains intact up to the point of lipid anabolism. Timestamp = HH:MM. Scale bar = 10  $\mu$ m. (D-F) Lipid analysis shows shifts in lipid composition of the chytrid lifecycle. Lipid quantities as total mass per cell (D) and as a

percentage of total dry mass (E) between chytrid life stages. Changes in lipid fractions were found between chytrid life stages (F). Dashed line = below analytical detection.

Live-population imaging of NR-labelled storage lipids showed that initially the chytrid life cycle (0-2 h) was characterised by a decrease ( $-49.7 \pm 9.8$  %) in lipid fluorescence suggesting that neutral storage lipid catabolism was taking place, before fluorescence increased suggesting that lipid anabolism was occurring up to zoospore release (Figure 4.8A&B). Initial lipid fluorescence decreased even in the presence of a carbon replete growth medium in line with the non-feeding habit of zoospores (Figure 4.8B). Live single cell imaging revealed a similar response as shown at the population level, and additionally showed that the original zoospore lipid globule remains intact and detectable until at least the point of visible lipid anabolism in the developing cell before it is incorporated into the new lipid fraction (Figure 4.8C).

Extraction and quantification of lipids from cells harvested at the major life stages showed shifts in lipid profiles. Individual zoospores possessed  $1.2 \pm 0.1$  pg, germlings  $2.2 \pm 0.3$  pg, and immature thalli  $904.5 \pm 201.0$  pg of lipid per cell (Figure 4.8D), however lipid composition as a percentage of dry mass (Z  $74.8 \pm 11.8$  % vs G  $69.5.0 \pm 11.5$  % vs IT  $61.0 \pm 3.3$  %) was similar across the life stages (Figure 4.7E). Sphingolipids were present in both zoospores and immature thalli (Z  $41.6 \pm 3.6$  % and IT  $11.5 \pm 2.6$  %), but below detection in germlings (Figure 4.8F). Likewise, glycolipids were present in both zoospores ( $40.7 \pm 27.1$  %) and immature thalli ( $40.6 \pm 27.3$  %), but below detection in germlings. Conversely, polar lipids were below detection in zoospores yet present in germlings ( $51.7 \pm 27.5$  %) and immature thalli ( $74.0 \pm 3.4$  %).

The differences in lipid composition between the zoospore and germling stages (Figure 4.8F) correlated with higher expression of genes in KEGG categories associated with peroxisome activity and ABC-transporters in zoospores compared to germlings (Figure 4.6C). Most of the genes identified under the peroxisome category are involved lipid oxidation and acyl-CoA metabolism, and therefore likely involved in the catabolic



processing of the lipid globule. Lipid reductases were also detected and have previously been identified with phospholipid anabolism (Lodhi and Semenkovich, 2014) and, together with the increase in endomembrane between germlings and zoospores determined with SBF-SEM (Figure 4.5A&B), point to increased phospholipid synthesis for membrane production. ABC-transporters are also involved in lipid transport into peroxisomes from lipid stores (Tarling et al., 2013). Together, these results suggests that glycolipid, and possibly sphingolipid, catabolism likely form part of storage lipid utilisation from the globule via the peroxisome, and polar lipid anabolism associated with endomembrane production are biological characteristics of the transition from zoospore to germling.

The upregulation of genes associated with fatty acid degradation and peroxisomes was observed in the immature thallus stage compared to the germling stage (Figure 4.6F) coinciding with new lipids being produced (Figure 4.8). The genes were associated with similar acyl-CoA pathways as the zoospore peroxisome category, in addition to alcohol and aldehyde dehydrogenation. Interestingly, although the peroxisome category was also upregulated in immature thalli, the associated genes were not identical to those in zoospores. Many similar acyl-CoA metabolic signatures were shared (16 genes), but with the addition of alcohol and isocitrate dehydrogenation and superoxide dismutase activity. This suggests that in immature thalli lipid production is driven by an interplay of fatty acid degradation and lipid anabolism, illustrating that some aspects of lipid catabolism and conversion in zoospores are bidirectionally repurposed for anabolism in immature thalli.

#### **4.4.3 The apophysis as a compartmentalised junction for intracellular trafficking**

The apophysis is ubiquitous across the Chytridiomycota (James et al., 2006b), but its function remains poorly understood. This chapter shows that the apophysis exhibits high endomembrane density and active intracellular trafficking between the feeding rhizoid and cell body (Figure 4.9&10). Live-population imaging of FM 1-43 labelled endomembrane in *R. globosum* cells (excluding apophysis and rhizoids) showed stability in fluorescence at the beginning of the life cycle (0-2 h), before a constant increase to the point of

sporulation (Figure 4.9A). Matching this, SBF-SEM reconstruction revealed that immature thalli devoted a larger proportion of cell body volume to endomembrane than zoospores and germlings (Z  $2.3 \pm 1.5$  % vs G  $7.6 \pm 0.9$  % vs IT  $13.0 \pm 1.8$  %,  $p < 0.001$ ), as well as vacuoles (Figure 4.5). The associated upregulation of KEGG categories such as protein processing in the endoplasmic reticulum (ER) and ubiquitin mediated proteolysis (Figure 4.6F) with the transition from the germling to the immature thallus stage suggests that this structural endomembrane is at least in part ER and associated with protein turnover.

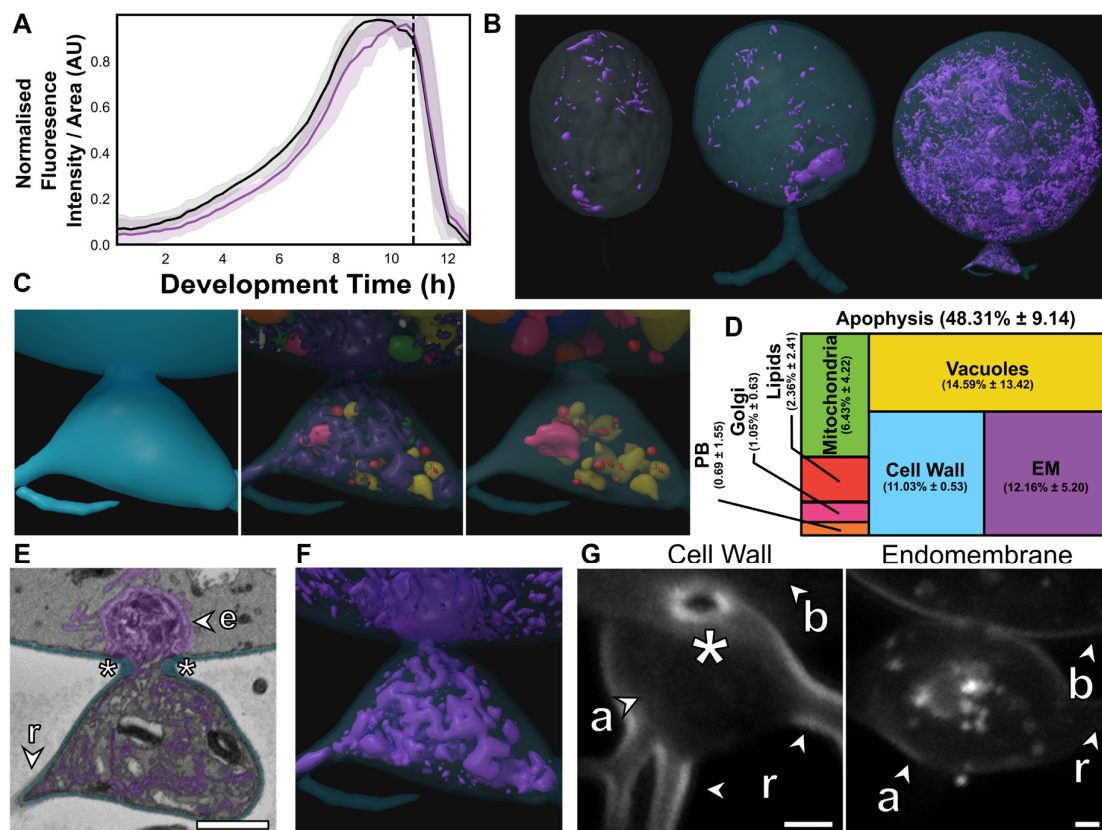


**Figure 4.9 The apophysis is a pseudo-septated and endomembrane-rich subcellular structure.** (A) Live-cell imaging ( $n = 5$ ) of *R. globosum* population-level FM 1-43-stained endomembrane dynamics. Purple = mean endomembrane fluorescence ( $\pm$ min/max), black = mean total cell area ( $\pm$ min/max), dashed line = mean sporulation time of population. (B&C) Representative SBF-SEM reconstructions of endomembrane across chytrid life stages (B) and the apophysis from immature thalli (C). Volumetric composition of SBF-SEM reconstructions ( $n = 5$ ) of immature thallus apophyses (D). Representative single false-coloured SBF-SEM slice (E) and reconstruction (F) of the endomembrane and chitinous pseudo-septum (asterisk) at the apophysis-cell body junction. (G) Fluorescent

labelling of the chitin rich wall around the apophysis-cell body connecting pore and associated endomembrane structures. Labels as in Figure 4.6A. All scale bars = 1  $\mu\text{m}$ .

**Table 4.2 Volumetric percentages and statistical comparisons of SBF-SEM reconstructions of cell bodies and their corresponding apophyses in immature thalli.** Data given to 3 decimal places.

Cellular Structure	Cellular Structure – Volumetric %					
	Cell Body (n = 5)	$\pm$ S.D	Apophysis (n = 5)	$\pm$ S.D	Statistical Test used	p- Value
Total Volume	100.000	0.000	100.000	0.000	NA	NA
Cell Wall	2.409	0.328	11.034	0.534	Mann Whitney U	<0.01
Cytosolic Lipid	0.341	0.159	1.308	2.318	Mann Whitney U	>0.05
Endomembrane	2.691	0.597	12.155	5.202	Mann Whitney U	<0.01
Glycogen	9.399	1.969	0.000	0.000	NA	NA
Golgi Apparatus	0.414	0.104	1.047	0.627	Mann Whitney U	>0.05
Microbodies	0.167	0.156	0.000	0.000	NA	NA
Mitochondria	7.005	0.143	6.429	4.215	Mann Whitney U	>0.05
Nucleus	5.749	2.477	0.000	0.000	NA	NA
Peripheral Bodies	0.336	0.100	0.693	1.551	Mann Whitney U	>0.05
Vacuole-bound Lipid	3.689	1.596	1.056	0.350	Mann Whitney U	<0.05
Vacuoles excl. Lipid Contents	12.958	1.780	14.589	13.420	Mann Whitney U	>0.05
Total Assigned Organelles	45.159	2.087	48.312	9.136	Paired T- Test	>0.05
Unassigned Cytosol	54.841	2.087	51.688	9.136	Paired T- Test	>0.05
Vacuoles incl. Lipid Contents	16.647	0.930	15.645	13.371	Mann Whitney U	>0.05
Total Lipid Fraction	4.030	1.604	2.364	2.407	Paired T- Test	>0.05
Total Endomembrane Fraction	20.255	1.248	29.542	9.135	Mann Whitney U	<0.05

The immature thallus SBF-SEM reconstructions showed that apophyses displayed even greater structural endomembrane than their corresponding cell bodies (apophysis 12.2 $\pm$ 5.2 % vs cell body 2.7 $\pm$ 0.6 %,  $p$ <0.01) (Figure 4.9C&D; Table 4.2). Apophyses also had comparatively more cell wall than the larger cell bodies (A 11.0 $\pm$ 0.5 % vs CB 2.4 $\pm$ 0.3 %,  $p$ <0.01) (Figure 4.9D). In *R. globosum* the cytoplasm between the apophysis and the cell body was connected through an annular pore (0.40 $\pm$ 0.07  $\mu\text{m}$  in diameter) with a distinctive chitin-rich pseudo-septum (Figure 4.9E&G), causing spatial division within the immature thallus cell plan. Live single cell imaging showed heavy dynamic endomembrane activity in the apophysis linking the intracellular traffic between the rhizoid

system and posterior base of the cell body (Figure 4.10). Given the disproportionate endomembrane activity in the apophysis, it is proposed that a function of the apophysis is to act as a cellular junction sorting intracellular traffic and channelling material from feeding rhizoids through the pseudo-septal pore to the cell body dedicated for reproduction.

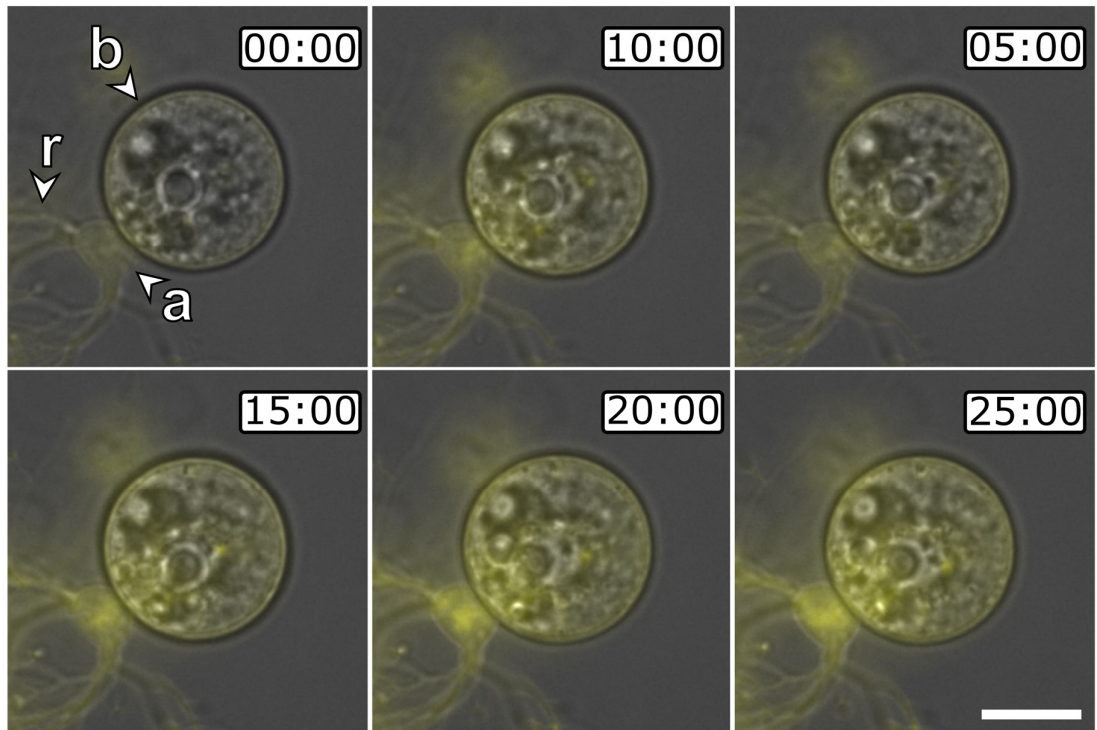


**Figure 4.10 The apophysis is a subcellular compartment that displays high intracellular trafficking.** Representative DIC time series of an *R. globosum* cell with FM 1-43-stained endomembrane (overlay, yellow). Labels as in Figure 4.6A. Scale bar = 10  $\mu\text{m}$ . Time stamp = MM:SS.

#### ***4.4.4 Developing zoospores display an amoeboid morphology***

Understanding zoosporogenesis, including how the immature thallus cell body differentiates into the next generation of zoospores, is integral to closing the chytrid life cycle. A synchronised population of mature zoosporangia was not achieved, however imaging and sequencing of mixed populations (~4 % cells mature zoosporangia) still allowed structural characterisation of this life stage, including the SBF-SEM reconstruction

of an entire mature zoosporangium containing 82-developing zoospores (Figure 4.11). Mature zoosporangia are characterised by internal membrane cleavage (Figure 4.11A) where coenocytic immature cytoplasm and organelles are allocated into nascent zoospores. The volume of the SBF-SEM reconstructed mature zoosporangium was  $3,651.5 \mu\text{m}^3$ , indicating that a single chytrid cell volumetrically increases by more than two orders of magnitude over its entire life cycle. The developing zoospores were flagellate, with the flagellum coiled round the cell body in two neat and complete rotations (Figure 4.11B&D). Zoospores are held within the cell wall of the zoosporangium during zoosporogenesis (Figure 4.9B), before exiting through the anteriorly oriented discharge pore (an aperture in the cell wall) when developed. During development, the pore is obstructed by a fibrillar discharge plug ( $49.7 \mu\text{m}^3$  in volume) (Figure 4.11C).

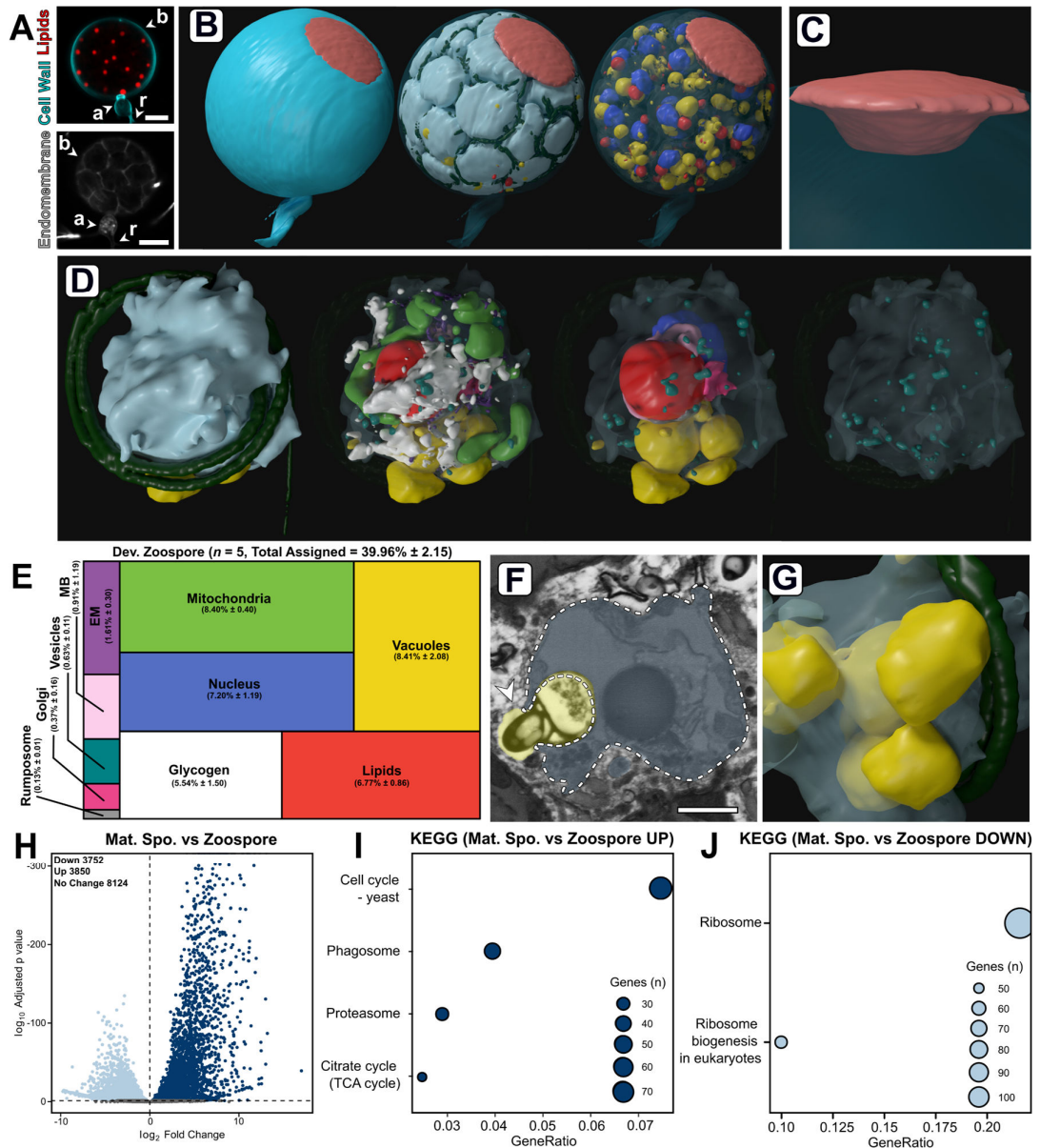


**Figure 4.11 Developing zoospores have an amoeboid morphology with endocytotic activity.** (A) Fluorescently-labelled confocal images of lipids, cell wall, and endomembrane in an *R. globosum* mature zoosporangium. Scale bar = 5  $\mu$ m. (B&C) SBF-SEM reconstructions of an 82-zoospore containing mature zoosporangium (B) highlighting the discharge plug, shown in coral (C). (D) Representative SBF-SEM reconstructions of a developing zoospore. Organelle colours as in (E). (E) Volumetric composition of SBF-SEM reconstructions of developing zoospores ( $n = 5$ ). (F&G) Representative single false-coloured SBF-SEM slice (F) and reconstruction (G) of the endocytotic vacuoles in developing zoospores. Dashed line delineates the zoospore cell boundary in (F). Scale bar = 1  $\mu$ m. (H) Pairwise comparison of differentially expressed genes (DEGs) between

mature zoosporangia and the free-swimming zoospore life stage. (I&J) Pairwise comparison of significant differentially expressed KEGG categories between mature zoosporangia and the free-swimming zoospore life stage.

The single zoosporangium reconstruction (Figure 4.11B) allowed the visualisation of developing zoospores in context, but to understand the detailed structural basis of this process it was necessary to reconstruct individual zoospore cells in the zoosporangium at higher resolution for comparison with 'mature' free-swimming zoospores (Figure 4.11D-G). This was coupled with comparison of transcriptomes from the mature zoosporangia (taken from the mixed populations) with transcriptomes from the free-swimming zoospores. Relative to free-swimming zoospores, developing zoospores in the zoosporangium displayed an amoeboid morphology (irregular morphologies characterised by numerous cellular protrusions, not to be confused with amoeboid motility) and had greater intracellular trafficking, characterised by a larger volumetric proportion of endomembrane (developing zoospores  $1.7 \pm 0.3$  % vs mature zoospores  $0.9 \pm 0.4$  %,  $p < 0.05$ ), vacuoles, (DZ  $8.4 \pm 2.1$  % vs MZ  $2.3 \pm 1.5$  %,  $p < 0.001$ ) and the presence of Golgi apparatuses and a vesicle class not observed in mature free-swimming zoospores (Figure 4.11D&E). Developing zoospores in the zoosporangium also exhibited larger glycogen stores (DV  $5.5 \pm 1.5$  % vs MV  $1.6 \pm 1.2$  %,  $p < 0.01$ ), indicating that glycogen utilisation occurs between the two stages, and a smaller rumposome (DV  $0.1 \pm 0.0$  % vs MZ  $1.3 \pm 0.0$  %,  $p < 0.001$ ) (Figure 4.11D&E) than their mature free-swimming counterparts.

**Table 4.3 Volumetric percentages and statistical comparisons of SBF-SEM reconstructions of free-swimming and developing zoospores.** Data given to 3 decimal places.

Cellular Structure	Chytrid Life stage – Volumetric %					
	Mature Zoospore (n = 5)	± S.D	Developing Zoospore (n = 5)	± S.D	Statistical Test used	p- Value
Total Volume	100.000	0.00	100.000	100.000	NA	NA
Cytosolic Lipid	4.290	2.610	6.766	0.859	Mann Whitney U	>0.05
Endomembrane	0.948	0.353	1.607	0.296	T-Test	<0.05
Glycogen	1.590	1.213	5.536	1.494	T-Test	<0.01
Golgi Apparatus	0.000	0.000	0.367	0.156	NA	NA
Microbodies	1.052	0.836	0.909	1.191	Mann Whitney U	>0.05
Mitochondria	9.363	0.861	8.400	0.403	T-Test	>0.05
Nucleus	10.297	1.187	7.202	0.361	T-Test	<0.001
Ribosome Cluster	20.457	2.798	0.000	0.000	NA	NA
Rumpsome	0.258	0.030	0.129	0.013	T-Test	<0.001
Striated Inclusion	0.147	0.139	0.000	0.000	NA	NA
Vacuoles	2.322	1.453	8.410	2.082	T-Test	<0.001
Vesicles	0.000	0.000	0.630	0.113	NA	NA
Total Assigned Organelles	50.724	4.754	39.956	2.145	Mann Whitney U	<0.05
Unassigned Cytosol	49.276	4.754	60.044	2.145	Mann Whitney U	<0.05
Total Endomembrane Fraction	4.322	1.113	11.923	1.856	T-Test	<0.001

The amoeboid morphology of the developing zoospores was in part a result of endocytotic engulfment activity, where vacuoles extended from within the zoospore cell interior to the interstitial maternal cytoplasm of the zoosporangium (Figure 4.11F&G). Such vacuoles were found in every replicate ( $2.0 \pm 0.7$  vacuoles per replicate). The transcriptome of the mature zoosporangia stage showed an upregulation of phagosome genes relative to the free-swimming zoospore stage (Figure 4.11I). The zoospore vacuoles contained electron-dense cargo similar to lipids (Figure 4.11F). The prominence of this engulfment across replicates suggests that endocytosis is the primary mode by which resources are trafficked from the maternal cytoplasm into developing zoospores post-cleavage, and that zoospore development does not cease once cleavage has been completed. Notably, developing zoospores did not yet display a detectable ribosomal cluster, as in the mature free-swimming zoospores (Figure 4.4), and the only KEGG categories higher in free-swimming zoospores than in the mature zoosporangia samples were associated with ribosomes (Figure 4.11J), indicating that this structure is formed later in zoospore development than captured here. The apparent importance of maintaining ribosomes in the biology of zoospores closes the chytrid life cycle when



considered with the earlier discussion on the distinctiveness of zoospores in the zoospore-germling transition.

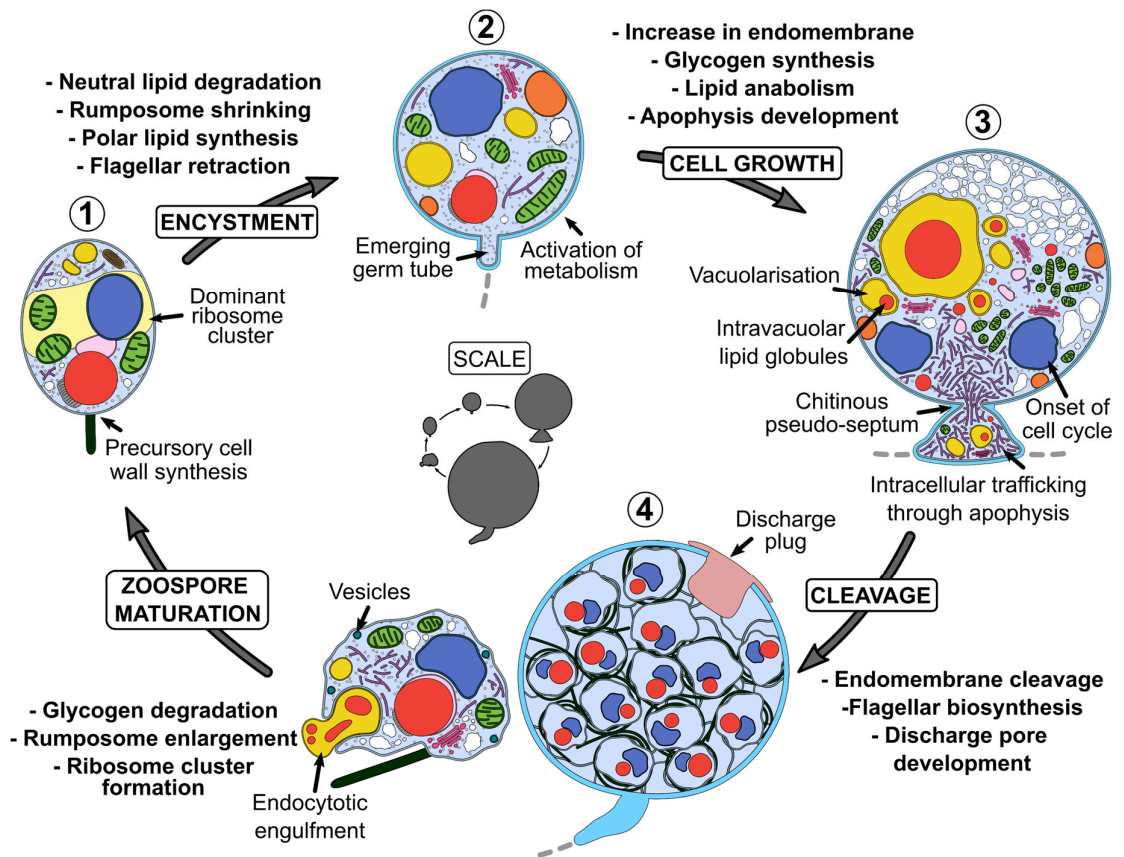


**Figure 4.12** Diagrammatic summary of the *R. globosum* developmental atlas. Inner life cycle shows life stages to scale. Grey dashed lines indicate the beginning of the rhizoid system.

#### 4.5 Discussion

This study into the cellular and molecular biology of *R. globosum* has generated a developmental atlas of an archetypal chytrid life cycle, shedding light on the biological processes governing each major life stage and the transitions between them (Figure 4.12). Although a ribosome cluster is a common structure in chytrid zoospores (Barr and Hartmann, 1976; Beakes et al., 1992), it is proposed that ribosomes in chytrid zoospores are translationally inactive (Medina and Buchler, 2020). Lovett (1968; 1963) related the *Blastocliadiella* zoospore ribosome cluster and subsequent dissipation with the biological

activity of the cell during the zoospore-germling transition, proposing the role of the cluster was to maintain the ribosomes through the zoospore stage and to spatially isolate the ribosomes to prevent translation occurring until when the cluster dissipates during the germling stage, and protein synthesis is initiated. Investigations into protein synthesis in chytrids (Léjohn and Lovett, 1965) and their close cousins the blastocladiomycetes (Lovett, 1968; Schmoyer and Lovett, 1969) suggest that translation does not begin until germination and that the zoospore is at least partially dependent on maternally-provisioned mRNA and ribosomes. Similarly, Rosenblum et al. (2008) detected high levels of transcripts associated with posttranslational protein modification in *Batrachochytrium dendrobatidis* zoospores but low transcriptional activity, and therefore high posttranslational modification may also be a dominant factor in the biology of *R. globosum* zoospores. Similar translational activity is seen in dikaryan spore germination (Brambl and Van Etten, 1970; Mirkes, 1974; Rado and Cochrane, 1971). The findings of this work not only support these proposals but go further to suggest that the inherited ribosomal cluster is the dominant feature in zoospores at both the structural and molecular level, indicating that the zoospore life stage represents a niche biological repertoire optimised for dispersal to new growth substrates rather than general metabolism, which is only initiated at the germling stage.

The germling stage is characterised by major cell plan remodelling, including rhizoid growth, and concomitant activation of diverse metabolic pathways. Similar upregulation of metabolic pathways has been observed at the transcriptional level associated with conidial germination in dikaryan fungi (Sharma et al., 2016; Zhou et al., 2018). Interestingly, proteasome genes were upregulated in the germling relative to the zoospore, which are also necessary for dikaryan germination (Seong et al., 2008; Wang et al., 2011). A previous study into flagellar retraction in *R. globosum* showed that the internalised flagellum is disassembled and degraded in the germling stage, at least partially by proteasome-dependent proteolysis (Venard et al., 2020). The findings of increased proteasome expression here may likewise be associated with flagellar degradation and the recycling of redundant zoospore machinery in the germling.

The immature thallus displayed increased cellular and molecular signatures associated with the reproductive cell cycle, intracellular trafficking, and protein processing. A key structural development was the vacuolisation of the cell body. Highly vacuolated dikaryan cells (El Ghaouth et al., 1994; Gow and Gooday, 1987) are associated with diverse cellular processes including general homeostasis, protein sorting, cell cycling, and intracellular trafficking (Veses et al., 2008), any of which could at least partially explain the high vacuolisation of immature chytrid thalli. Noticeable in the context of chytrid cell biology however is the upregulation of actin-driven cytoskeletal genes, including those assigned to the Arp2/3 complex. The role of actin in vacuolisation and endocytosis has been demonstrated in yeast (Eitzen et al., 2002; Gachet and Hyams, 2005), similar to the observations here in *R. globosum*. Arp2/3-dependent actin dynamics drive crawling  $\alpha$ -motility in some chytrid zoospores (Fritz-Laylin et al., 2017; Medina et al., 2020) and the presence of animal-like actin components that have been lost in multicellular fungi makes chytrids important in understanding evolution of the fungal cytoskeleton (Prostak et al., 2021). Although *R. globosum* zoospores do not crawl, the immature thallus has actin patches, cables, and perinuclear shells (Prostak et al., 2021). Here it is shown that, for a non-crawling chytrid, actin-associated genes are upregulated in immature thalli and are associated with a cell stage with high vacuolisation and endocytosis.

No clear molecular differences in cell wall synthesis between the different life stages were observed at the higher categorical level in *R. globosum*, instead individual differentially expressed genes were identified suggesting that the process is dynamic and complex. Higher levels of putative chitin synthase gene transcripts (e.g. ORY39038) in wall-less zoospores was coupled with the detection of precursory cell wall material at the base of the flagellum. *B. dendrobatidis* transcriptomes also show specific transcripts associated with chitin synthesis to be higher in zoospores than in sessile thalli (Rosenblum et al., 2008). Chitin synthase activity has been shown associated with the *Blastocladiella emersonii* zoospore membrane (Dalley and Sonneborn, 1982). Early initiation of cell wall synthesis warrants further study and may explain why early chemical inhibition induces phenotypic disruptions to normal development in chytrids (Chapter 5).

This emphasises the need to include the wall-less zoospore stage in investigations into chytrid cell wall biology.

This study has highlighted the complexity of lipid dynamics across the *R. globosum* lifecycle. These data show that the volume of the lipid globule, total lipid by volume, and lipid as a percentage of dry mass remain unchanged between zoospores and germlings. Yet a shift in lipid type was demonstrated, moving from sphingolipids and neutral glycolipids (putatively storage triacylglycerides) to polar lipids (putatively membrane-associated phospholipids) between zoospores and germlings. Similarly, during the *B. emersonii* zoospore-germling transition glycolipids decrease and phospholipids increase (Dalley and Sonneborn, 1982). Previous research has characterised fatty acid profiles in chytrids (Akinwole et al., 2014; Gerphagnon et al., 2019; Rasconi et al., 2020) and shown differences between chytrid zoospores and sessile thalli of the same species (Taube et al., 2019). As the NR emission spectrum undergoes a red shift in increasingly polar environments (Bertozzini et al., 2011), the live-cell data do not quantify the structural degradation of the lipid globule *per se* but rather biochemical polarisation as neutral storage lipids are catabolised for energy mobilisation and polar phospholipids are synthesised. The larger volumetric proportion of glycogen stores in developing zoospores over mature free-swimming zoospores also indicates that glycogen catabolism between the two stages contributes to energy mobilisation during zoospore motility as previously suggested (Powell, 1979).

Changes in lipid profiles were coupled with subcellular ultrastructure in *R. globosum*. The enzymatic function of LRM-associated microbodies as lipolytic organelles has been previously proposed (Powell, 1979, 1977, 1976), where evidence suggests that enzymatic activity increases following germination (Powell, 1976). From the data presented here, this organelle may have bidirectional function and be associated with lipid conversion as well as catabolism. A key component of the LRM is the enigmatic rumposome, which was larger in zoospores than germlings. Previous hypotheses have proposed that this organelle is associated with environmental reception and signal transduction in flagellar regulation (Dorward and Powell, 1983). An enlarged rumposome

in motile zoospores would support a flagellar role, but its retention in germlings implies additional functions. The bulk of lipids in immature thalli during anabolism were intravacuolar and comparable intravacuolar inclusions have been identified in chytrid and dikaryan fungi in the past (Beakes et al., 1992; Bourett and Howard, 1994; Lösel, 1990). Intravacuolar lipid droplets have been previously investigated in yeast but in a catabolic capacity (Van Zutphen et al., 2014; Vevea et al., 2015). Although *de novo* storage lipid synthesis is associated with the ER (Veeva et al., 2015), the vacuoles identified here may cache and aggregate nascent globules as part of the lipid anabolic pathway.

The function of the chytrid apophysis has long been overlooked, despite its ubiquity in the Chytridiomycota (Powell, 1974; Powell and Gillette, 1987; Taylor and Fuller, 1980). The results here provide evidence that the apophysis is a distinct subcellular structure that acts as a hub for dynamic intracellular trafficking from the rhizoids into the cell body. The ability of multicellular dikaryan fungi to translocate assimilated nutrients through their hyphal network from the site of uptake is sophisticated (Van't Padjé et al., 2021; Whiteside et al., 2019), and the observed endomembrane flow from feeding rhizoids to the cell body in chytrids is not surprising. However, the localisation of high endomembrane activity to the apophysis and through the pseudo-septum into the cell body implicates this structure as a sorting intermediary junction.

The pseudo-septation of the apophysis and rhizoids from the cell body is evidence for functional compartmentation within the thallus of a unicellular fungus. Comparable structures are also present in other chytrid species (Barr, 2011; Beakes et al., 1992). Division of multicellular dikaryan fungi by septa, where continuity between distinct cytoplasmic compartments is maintained by septal pores, is integral to multicellularity, cellular differentiation, and resilience (Bleichrodt et al., 2015, 2012). The origin of hyphal septa was a major innovation in fungal evolution (Berbee et al., 2017; Nagy et al., 2020) occurring at the phylogenetic node shared by hyphal and rhizoidal fungi (Berbee et al., 2017). The role of the apophysis pseudo-septum (or an analogous structure) in chytrids in delineating functionally dedicated subcellular compartments may represent an evolutionary precursor to dikaryan septa and differentiation. This makes investigating the

chytrid apophysis not only important for understanding intracellular trafficking biology, but also the evolution of fungal multicellularity.

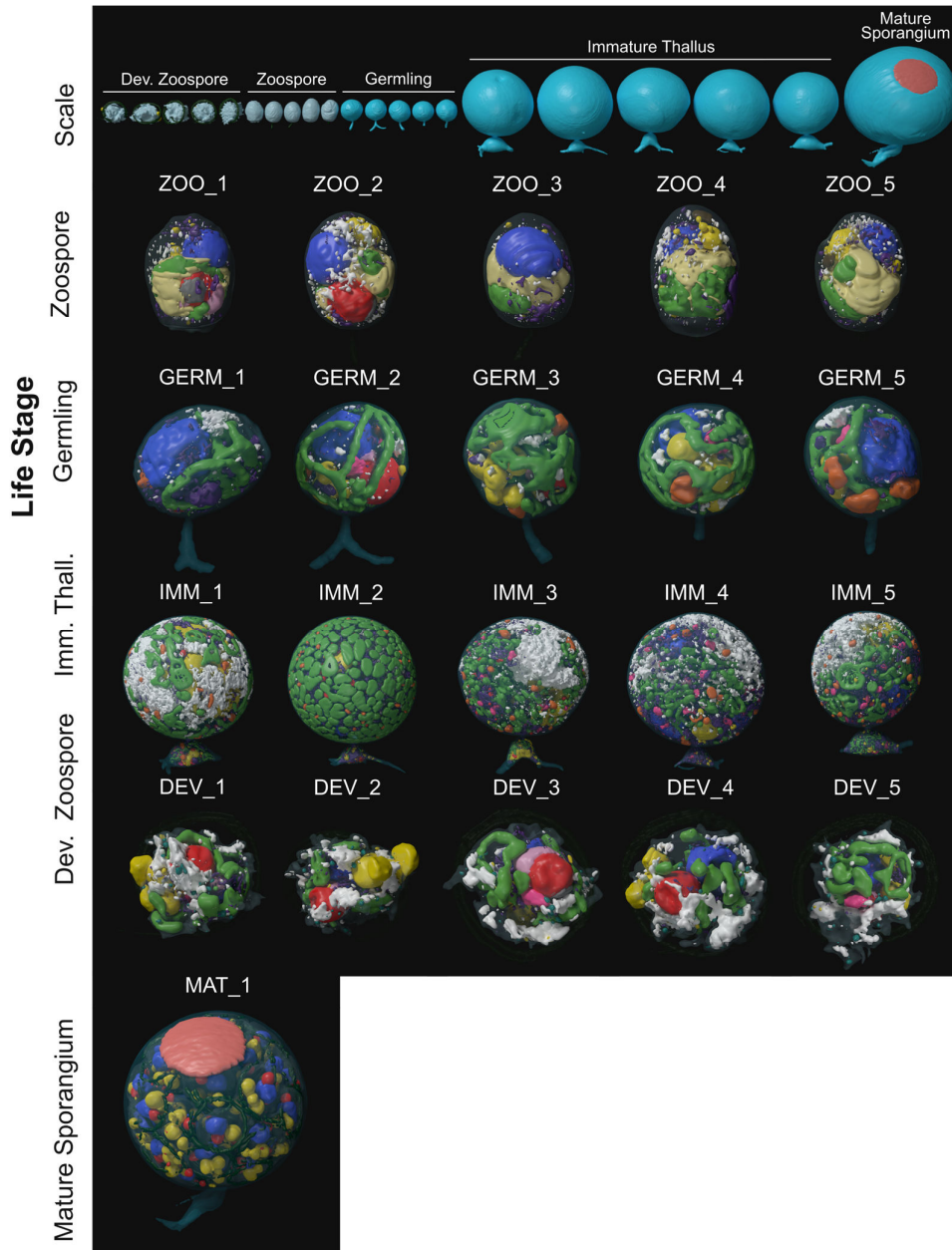
Finally, the quantitative reconstructions of individual developing zoospores in the zoosporangium and comparison with their free-swimming counterparts have added to understanding the underpinning biology of zoosporogenesis. Perhaps the most striking finding here is the amoeboid morphology of developing zoospores, resulting from engulfment and trafficking structures, suggesting that developing zoospores assimilate material from the maternal cytoplasm post-cleavage. Although dikaryan sporogenesis is complex and diverse, it typically involves the septation of hyphal cytoplasm via cell wall synthesis (Cole, 1986; Money, 2016). As walled cells, dikaryan spores are incapable of such engulfment activity, and amoeboid chytrid zoospores therefore have more in common with their more distant opisthokont relatives in this regard. Nucleariid amoebae (Yoshida et al., 2009), choanoflagellates (Laundon et al., 2019), and various animal cell types (Bayne, 1990) exhibit analogous endocytotic engulfment behaviour as shown here in chytrid zoospores. This conservation may indicate that such engulfment behaviour existed in the last common ancestor of branching fungi to assimilate subcellular cargo during sporogenesis of wall-less zoospores and was lost in dikaryan fungi as spores became walled.

#### **4.6 Conclusion**

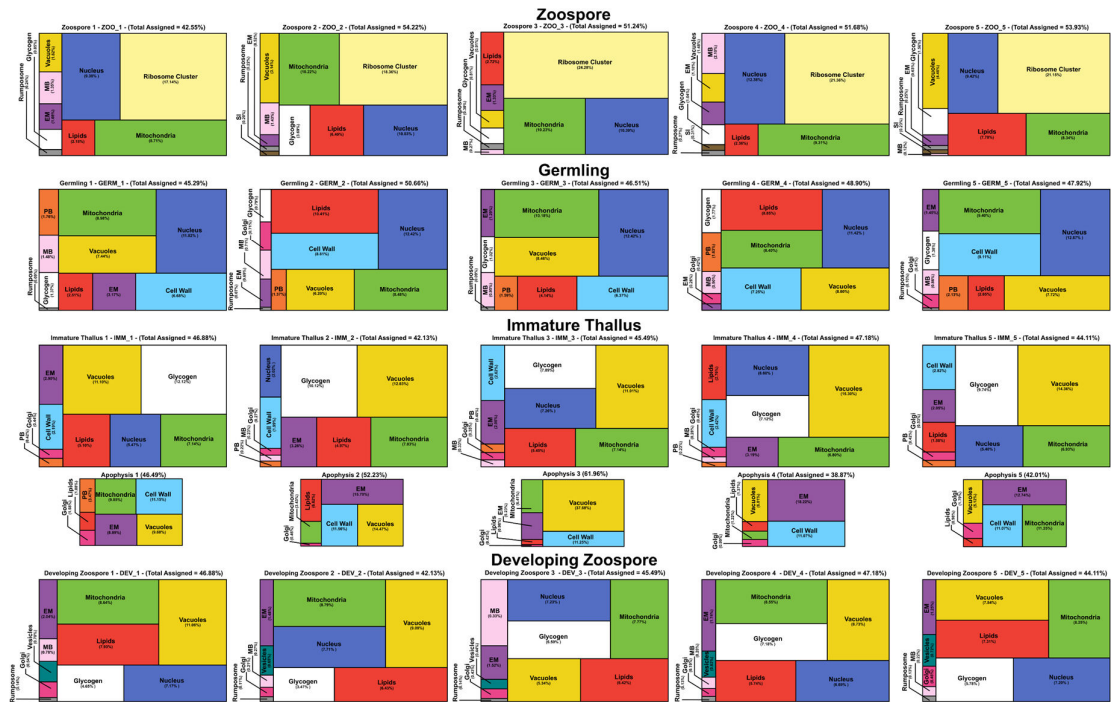
In conclusion, this characterisation of the *R. globosum* life cycle has revealed changes in cell structure and associated biological processes driving chytrid development, some of which show analogies in dikaryan fungi and animal cells. As important saprotrophs, parasites, and pathogens in aquatic ecosystems, these findings provide information into the cellular processes that underpin the ecological importance of chytrids. In addition, this characterisation of an fungus that retains cellular characteristics from the last common ancestor of branching fungi is an important step forward in reconstructing the putative biology of this organism. This study demonstrates the utility of developmental studies with

model chytrids such as *R. globosum* and reiterates the need for fundamental biology in investigating the function of chytrid cells.

#### 4.7 Supplementary figures



**Supplementary figure 4.1 Individual SBF-SEM replicate reconstructions.** Individual 3D SBF-SEM reconstructions of *R. globosum* cells (not to scale) across life stages labelled with replicate ID's. Organelle colours as in Figure 4.5. Top row shows all replicates to scale.



**Supplementary figure 4.2 Individual SBF-SEM replicate volumetrics.** Individual volumetric compositions of assigned organelles from *R. globosum* SBF-SEM reconstructions across life stages labelled with replicate ID's. Organelle colours as in Figure 4.5.



## **Chapter 5 - Chytrid rhizoid morphogenesis resembles hyphal development in multicellular fungi and is adaptive to resource availability**

**Published as:** Laundon D, Christmas N, Wheeler G, and Cunliffe M. 2020. Chytrid rhizoid morphogenesis resembles hyphal development in multicellular fungi and is adaptive to resource availability. *Proc Royal Soc B* **287**(1928): p.20200433.

doi:10.1098/rspb.2020.0433

**Author contributions:** *NC analysed the sequence data. GW and MC provided supervision and manuscript feedback. All other experimentation, analysis, and writing was conducted by DL. TEM/SEM was conducted by DL at the Plymouth Electron Microscopy Centre (PEMC).*

### **5.1 Summary**

Unlike dikaryan hyphae, chytrids typically attach to substrates and feed osmotrophically via anucleate rhizoids. The evolution of fungal hyphae appears to have occurred from rhizoid-bearing lineages and it has been hypothesized that a rhizoid-like structure was the precursor to multicellular hyphae. Here, it is shown in a unicellular chytrid, *Rhizoclosmatium globosum* JEL800, that rhizoid development exhibits striking similarities with dikaryan hyphae and is adaptive to resource availability. Rhizoid morphogenesis displays analogous patterns to hyphal growth and is controlled by  $\beta$ -glucan-dependent cell wall synthesis and actin polymerization. Rhizoids growing from individual cells also demonstrate adaptive morphological plasticity in response to resource availability, developing an apparent 'searching' phenotype when carbon starved and spatial differentiation when interacting with particulate organic matter. Such differentiation indicates division of labour in the rhizoid system of a unicellular fungus. These results demonstrate that the adaptive cell biology and associated developmental plasticity considered characteristic of hyphal fungi are shared more widely across the Kingdom Fungi and therefore could be conserved from their most recent common ancestor.

## 5.2 Introduction

Hyphae are polarised, elongating, and bifurcating cellular structures that many fungi use to forage and feed (Figure 5.1A&B). Chytrids produce filamentous hyphae-like structures called rhizoids (Figure 5.1-3) (Stajich et al., 2009), which are important in their ecological functions, in terms of both attachment to substrates and osmotrophic feeding (Berbee et al., 2017). Unlike coenocytic or multicellular hyphae, the diameter of which is typically measured at the micron scale (e.g. Harris, 2011), rhizoids consist of a subsection of a single cell, are anucleate, and are typically only a few hundred nanometres in diameter (e.g. Dee et al., 2019).

407-million-year-old fossils from the Devonian Rhynie Chert deposit show chytrids in freshwater aquatic ecosystems physically interacting with substrates via rhizoids in a comparative mode to extant taxa (Strullu-Derrien et al., 2016). Yet surprisingly, given the importance of rhizoids in both contemporary and paleo- chytrid ecology, there remains a limited understanding of chytrid rhizoid biology, including possible similarities with functionally analogous hyphae in other fungi and the potential for substrate-dependent adaptations.

Character mapping of the presence of cellular growth plans against established phylogenies reveals the multicellular hyphal form to be a derived condition, whereas rhizoid feeding structures are the basal condition within the true fungi (Eumycota) (Figure 5.1A&B). Hyphal cell types are sometimes observed outside of the Eumycota, such as within the Oomycota (Stramenopila), however the origin of fungal hyphae within the Eumycota was independent (Dee et al., 2015; Kiss et al., 2019) and has not been reported in their closest relatives the Holozoans (animals, choanoflagellates, etc.). Comparative genomics has indicated that hyphae originated within the rhizoid-bearing Chytridiomycota-Blastocladiomycota-Zoopagomycota phylogenetic nodes of the fungal tree (Kiss et al., 2019), which is supported by fossil Blastocladiomycota and extant Monoblepharidomycetes having hyphae (Dee et al., 2015; Strullu-Derrien et al., 2018). This has led to the proposition that rhizoids, or rhizoid-like structures, were the evolutionary precursors of fungal hyphae (Dee et al., 2015; Harris, 2011; Kiss et al.,

2019), however investigation into such hypotheses have been hindered by a relative lack of understanding of rhizoid developmental biology.

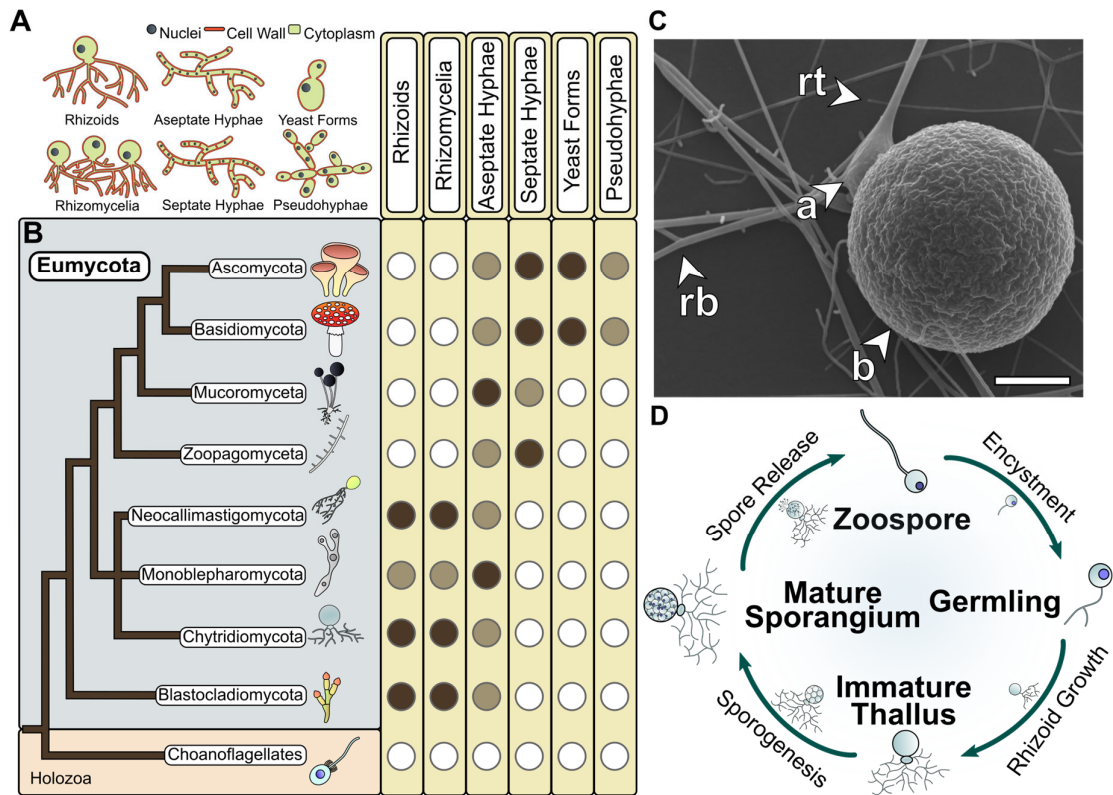


**Figure 5.1 Rhizoids are the basal feeding condition within the fungal kingdom.**

(A&B) Correlating the major feeding types in fungi (A) to phylogeny (B) shows rhizoids to be the basal feeding condition in the true fungi (Eumycota). Tree adapted from (Tedersoo et al., 2018). (C) *R. globosum* cell plan. Shown is the cell body (b) anchored to the substrate by threadlike rhizoids. Rhizoids emanate from the apophysis (a). Also shown are rhizoid bifurcations (rb) and tips (rt). Scale bar = 5  $\mu$ m. (D) *R. globosum* lifecycle.

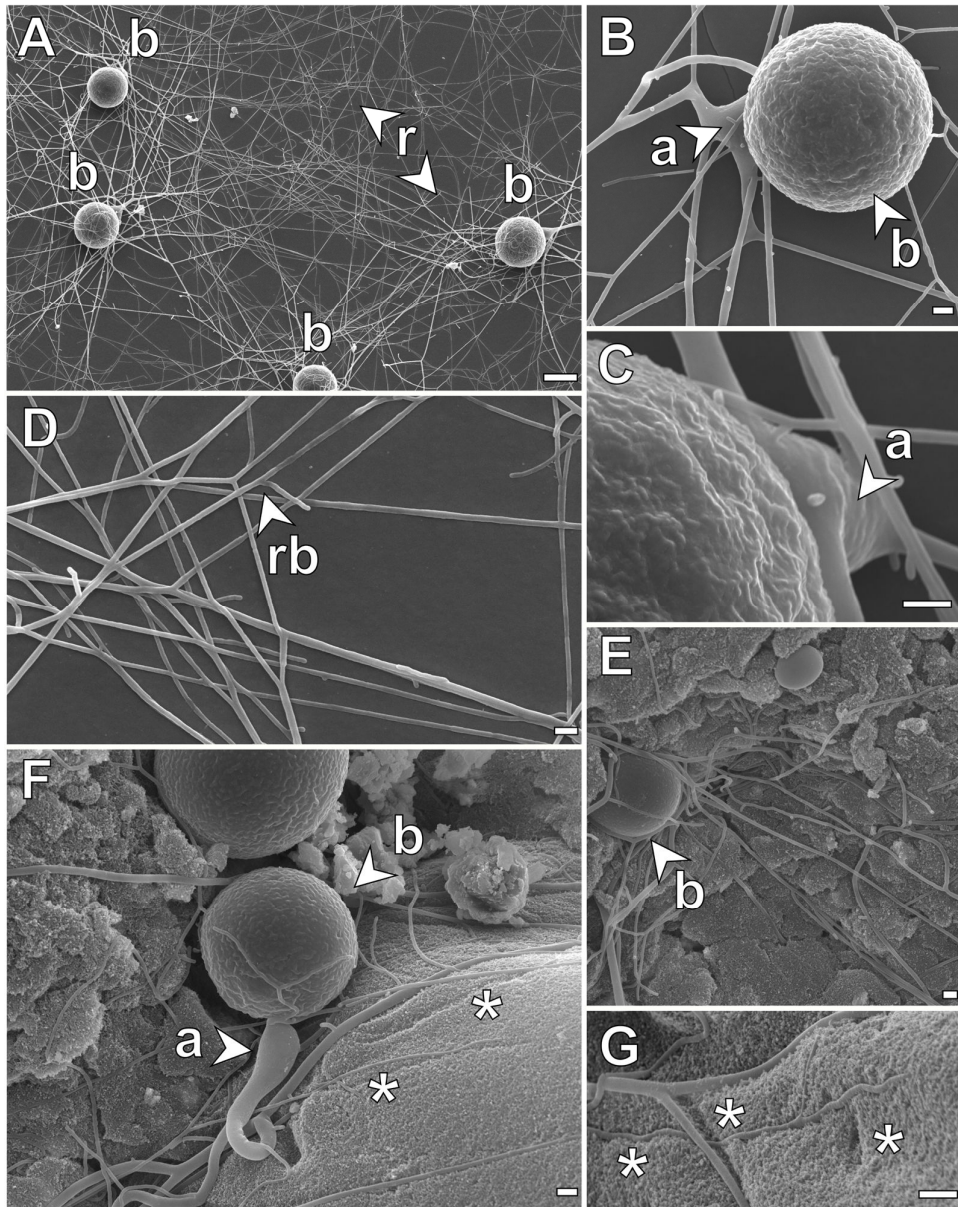


**Figure 5.2. Scanning electron microscopy (SEM) images of *R. globosum* rhizoids.**

(A-D) *R. globosum* cells grown on a 2D, inert surface (Aclar) in *N*-Acetylglucosamine

(NAG) supplemented media. (A) Shown are multiple cells anchored to the surface by

threadlike rhizoids. (B) The spherical cell body of *R. globosum* is connected to the rhizoid

system via an apophysis (subsporangial swelling). (C) High-magnification image of the

apophysis. (D) Rhizoids are branched and bifurcating structures that frequently overlap.

The fusion of rhizoids (anastomoses) was never observed from SEM images. (E-G)

Chytrid cells growing on chitin beads. (F&G) External rhizoids growing along the surface

of the particle formed superficial lacerations (indicated by asterisks). Apophysis (a); cell

body (b), rhizoid bifurcation (rb). Scale bar (A&E) = 10  $\mu$ m. Scale bar (B-D, F&G) = 1  $\mu$ m.

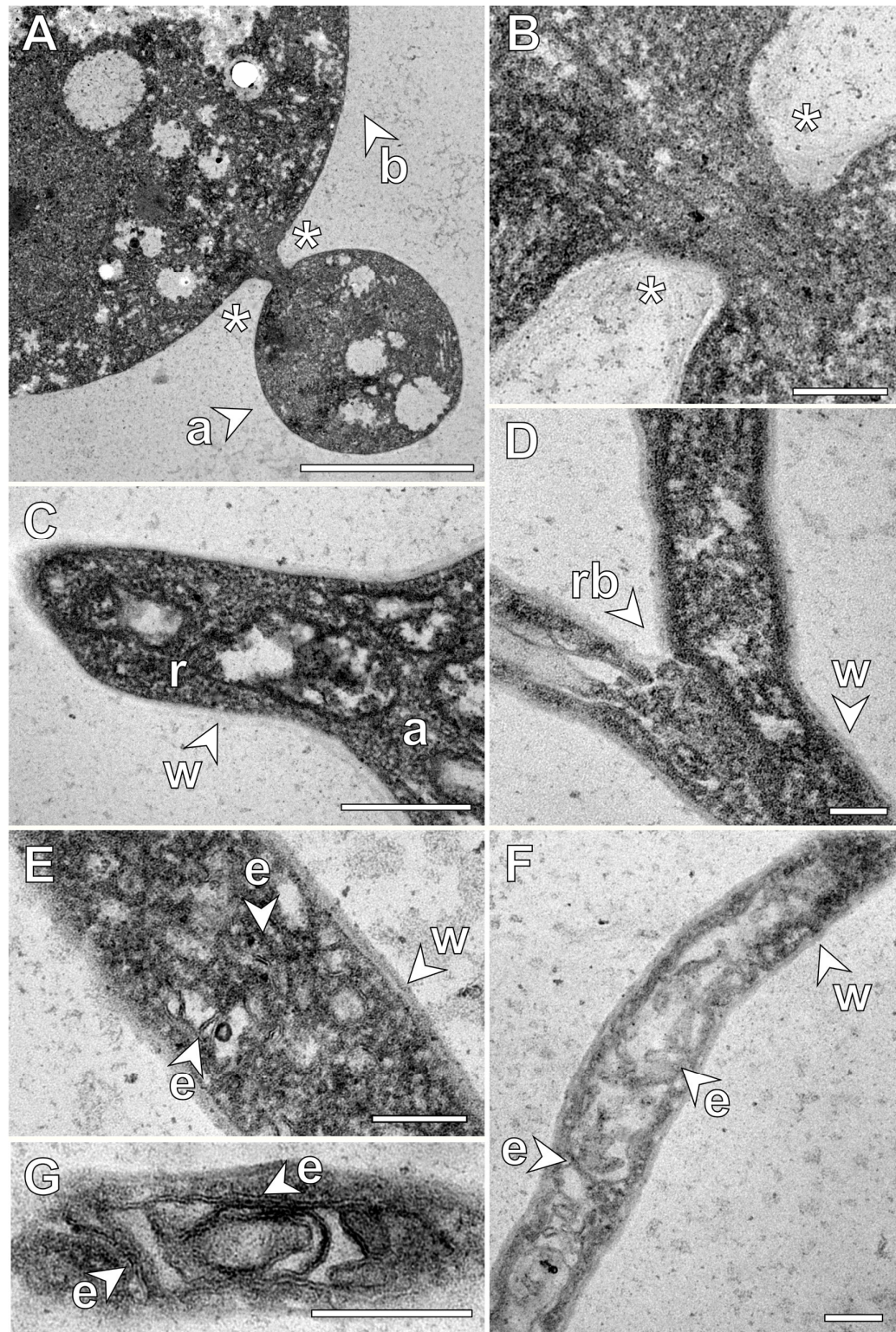


**Figure 5.3 Transmission electron microscopy (TEM) images of *R. globosum* rhizoids.** (A-C) TEM images of the apophysis. The apophysis is pseudo-septated from the cell body and the two are connected by continuous cytoplasm (A&B), as are the apophysis and the rhizoid (C). (D-F) TEM images of the apophysis. The rhizoid is always enveloped by a cell wall and no structure was observed to demarcate rhizoid branches at

bifurcation nodes (D). Although no formal subcellular organelles could be identified within the rhizoid, a dense and complex endomembrane system permeated the entire rhizoid (E&F). This suggested that the rhizoid is governed by high levels of trafficking and endomembrane reorganisation. apophysis (a), cell body (b), endomembrane (e), rhizoid (r) bifurcations (rb), cell wall (w). Asterisks mark the connection between the apophysis and the cell body. Scale bar (A) = 2  $\mu$ m. Scale bar (B-F) = 200 nm.

Rhizoids were purposefully overlooked in the previous chapter to focus on cell body development and comparison between arhizoidal life stages. As before, the archetypal cell plan and lifecycle (Sparrow, 1960) of *Rhizoclostridium globosum* JEL800 were exploited to investigate the cell and developmental biology of rhizoid-bearing aquatic fungi. To characterise the developing rhizoid system for morphometric analyses, a live-cell 3D/4D confocal microscopy approach in combination with the application of neuron tracing software was established to 3D reconstruct developing cells (Figure 5.4). This methodology generated a series of cell morphometrics to describe and quantify rhizoid development (Figure 5.5) under a range of experimental conditions in terms of geometric organisation, morphogenesis, and underlying cellular control mechanisms (investigated by chemical inhibition). In addition, substrate-dependent adaptations, particularly in the ecological context of carbon starvation and aquatic particulate organic matter (POM) interaction, were also characterised.

## **5.3 Methods and materials**

### **5.3.1 General imaging of chytrid rhizoids**

*R. globosum* membranes were labelled with 8.18  $\mu$ M FM 1-43 and imaged using a Zeiss LSM 510 Meta confocal laser scanning microscope (CLSM) (Carl Zeiss) under a 40 x oil-immersion objective lens. For Scanning electron microscopy (SEM) of rhizoids growing along a 2D surface, culture dishes were lined with EtOH-sterilised Aclar discs and filled with 3 ml of Bold's basal medium (BBM) with 10 mM *N*-Acetylglucosamine (NAG), before inoculation with zoospores and incubation for 24 h at 22 °C. For SEM of cells growing on chitin beads, dishes were prepared as described below and were also inoculated and

incubated for 24 h. Cells from both treatments were fixed in 2.5 % glutaraldehyde and then rinsed twice in 0.1 M cacodylate buffer (pH 7.2). Fixed samples were dehydrated in a graded alcohol series. Cells were then dried in a Critical Point Drier (K850, Quorum) and attached to SEM sample stubs using carbon infiltrated tabs prior to Cr sputter-coating using a sputter coating unit (Q150T, Quorum). Samples were imaged with a Field Emission Gun Scanning Electron Microscope (JSM-7001F, JEOL) operating at 10 kV. For Transmission Electron Microscopy (TEM), 24 h cells grown in suspension were fixed as previously described. The samples were secondarily fixed with osmium tetroxide (1 %, in 0.1 M cacodylate buffer pH 7.2) for 1 h, rinsed, and alcohol dehydrated as above. The alcohol was replaced with agar low viscosity resin through a graded resin series. Blocks were sectioned at 50 nm intervals with an ultramicrotome (Ultracut E, Leica) and the sections stained using a saturated solution of uranyl acetate (for 15 min) and Reynold's lead citrate (15 min) before being examined using a transmission electron microscope (JEM-1400, JEOL).

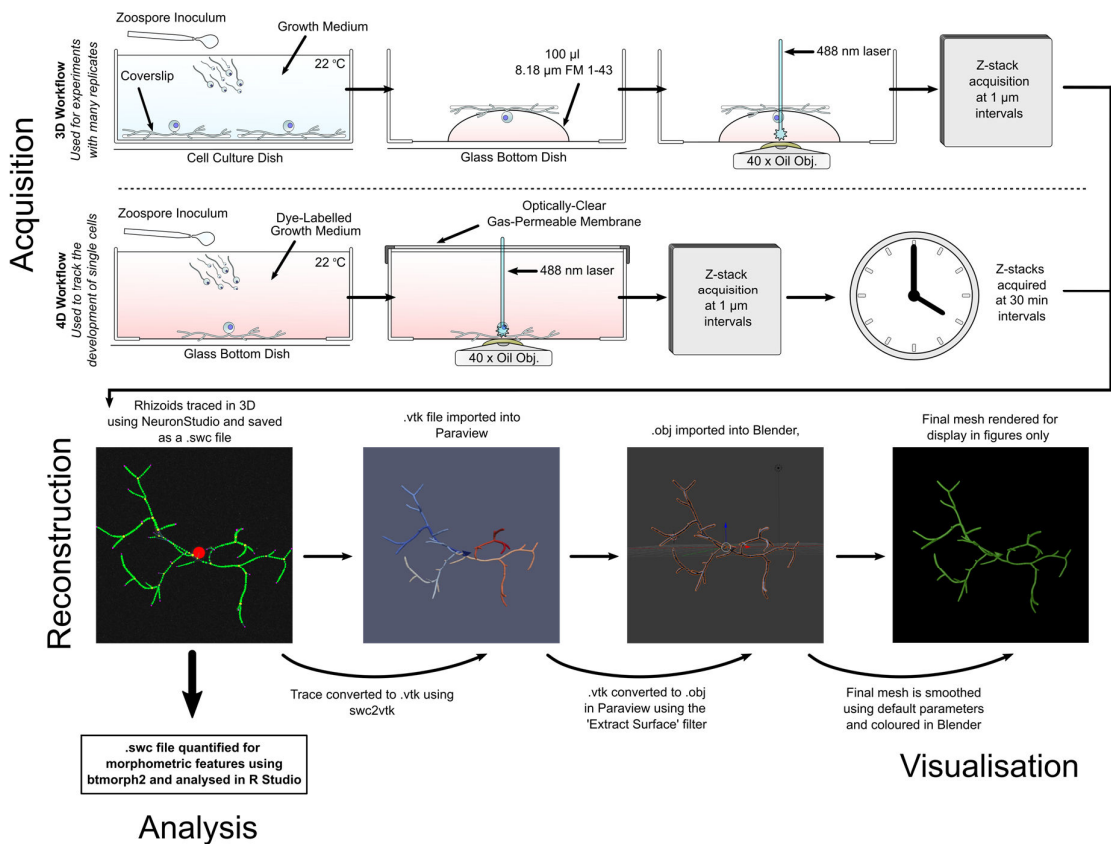


**Figure 5.4 Neuron tracing was used to reconstruct chytrid rhizoids.** Flow-diagram protocol for the acquisition, reconstruction, analysis, and visualisation of *R. globosum* rhizoids based on neuron tracing.

### **5.3.2 Imaging 4D rhizoid development**

Glass bottom dishes (IBL) ( $n = 5$ ) containing 3 ml BBM with 10 mM NAG were inoculated with 500  $\mu$ l zoospore suspension. Zoospores settled for 1 h prior to imaging before z-stacks to 50  $\mu$ m depth were acquired at 30 min time intervals for 10 h at 22 °C. An optically clear film permitting gas exchange covered the dish. Branches were counted manually from maximum intensity projected z-stacks. To quantify rhizoid fractal dimensions, cells were grown on glass bottom dishes for 24 h. Due to the large size of the 24 h cells, z-stacks were stitched together in Fiji from four individual stacks. Stitched stacks ( $n = 5$ ) were converted to maximum intensity projections, processed into binary masks by default thresholding and denoised. Local Connected Fractal Dimension (LCFD) analysis was conducted using default parameters on binary masks with the Fiji plugin Fraclac (Karperien et al., 2013).

### **5.3.3 Rhizoid tracing, reconstruction, and morphometric analysis**

Z-stacks of rhizoids were imported into the neuron reconstruction software NeuronStudio (Rodriguez et al., 2008, 2006). Rhizoids were semi-automatically traced with the 'Build Neurite' function using the apical point of the cell body as the rhizoidal origin (Figure 5.4). Cells grown for 24 h in BBM 10 mM NAG or on chitin beads were too dense to be manually curated and therefore were automatically traced using dynamic thresholding with a minimum neurite length of 2  $\mu$ m, although due to their high-density tracings should be considered imperfect. For 4D image stacks, the rhizoid was reconstructed in 3D at each 30 min interval. For particle associated and non-associated rhizoids, traced rhizoid systems from individual cells were manually split into their respective categories.

Rhizoids were exported as .swc file extensions (Stockley et al., 1993) and morphometrically quantified using the btmorph2 library (Torben-Nielsen, 2014) run with Python v3.6.5 implemented in Jupyter Notebook v4.4.0. Reconstructed rhizoids were



visualised by converting the .swc files first to .vtk files using the swc2vtk Python script (Daisuke Miyamoto: [github.com/ DaisukeMiyamoto /swc2vtk/](https://github.com/DaisukeMiyamoto/swc2vtk/)) and then to .obj files using the 'Extract Surface' filter in ParaView (Ahrens et al. 2005). .obj files were then imported into Blender v2.79, smoothed using automatic default parameters and rendered for display. .obj meshes were used for final display only and not analysis. To visualise chitin beads, z-stacks were imported into the Fiji plugin TrakEM2. Chitin beads were manually segmented, and 3D reconstructed by automatically merging traced features along the z-axis. Meshes were then preliminarily smoothed in TrakEM2 and exported as .obj files into Blender for visualisation.

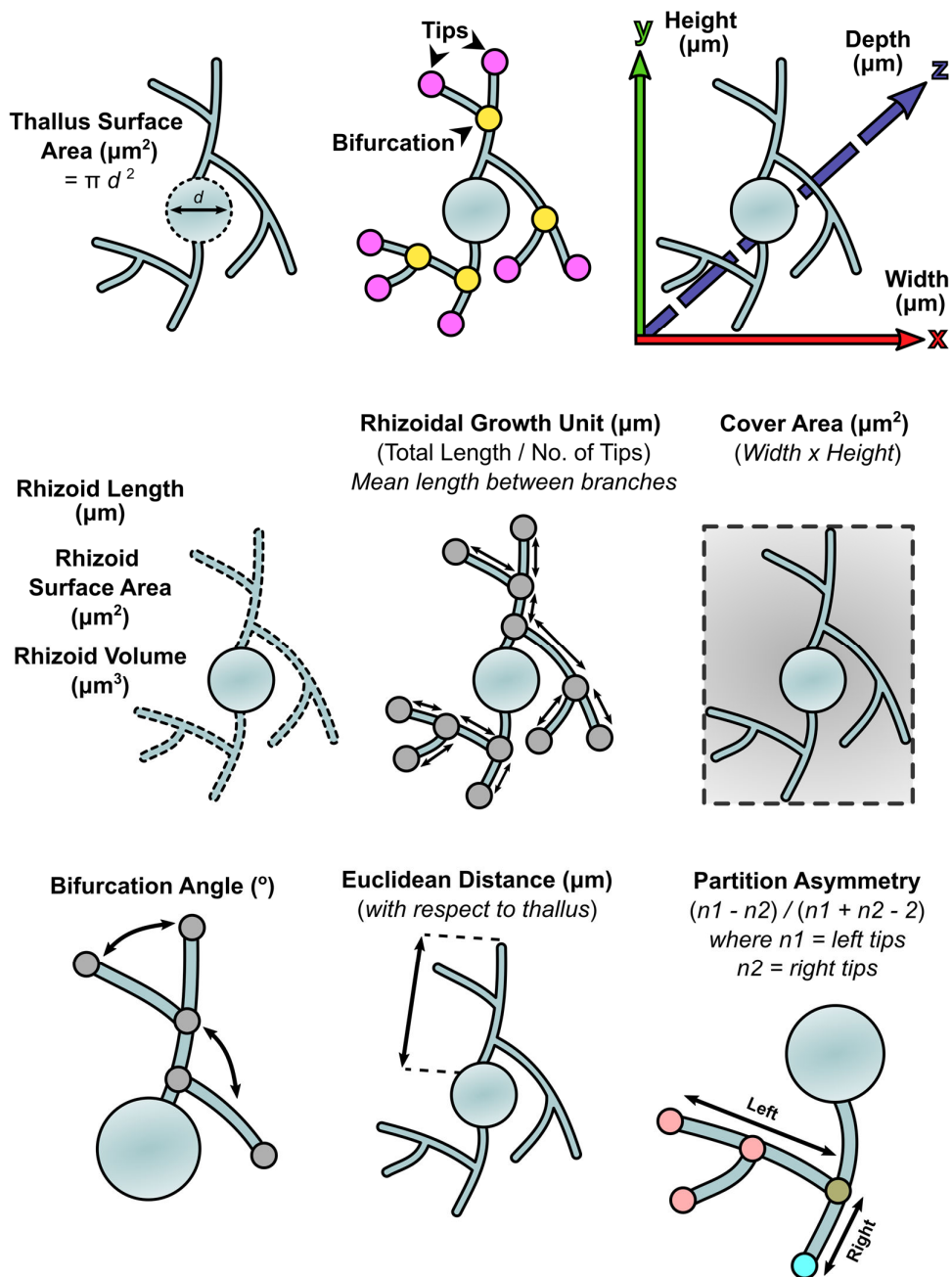


**Figure 5.5 Chytrid rhizoids were described using morphometric parameters adapted from neurobiology.** Diagrammatic glossary of neuronal morphometric parameters used to describe 3D reconstructed chytrid rhizoids from growth experiments. Chytrids are represented by an aerial 2D diagram, as if from a z-stack maximum intensity projection.

#### **5.3.4 Confocal imaging of the rhizoid cell wall and actin**

To label the cell wall and F-actin throughout the rhizoid system, cells were grown for 24 h in 3 ml BBM with 10 mM NAG on glass bottom dishes. The culture medium was aspirated from the cells, which were then washed three times in 500  $\mu$ l 1 x phosphate buffered saline (PBS). Cells were subsequently fixed for 1 h in 4 % formaldehyde in 1 x PBS and then washed three times in 1 x PBS and once in 100 mM PIPES (piperazine-N,N'-bis(2-ethanesulfonic acid)) buffer at pH 6.9, 1 mM EGTA (ethylene glycol tetraacetic acid), and 0.1 mM MgSO<sub>4</sub> (PEM). Fixed cells were stained with 1:50 rhodamine phalloidin in PEM for 30 min, washed three times in PEM, and finally stained with 5  $\mu$ g/ml Texas Red-conjugated wheat germ agglutinin (WGA) in PEM for 30 min. Stained cells were further washed three times in PEM and mounted under a glass coverslip with one drop of ProLong™ Gold Antifade Mountant (ThermoFisher). Cells were imaged using the same CLSM as described above with a 63 x oil immersion objective lens. F-Actin was imaged by excitation with a 543 nm HeNe laser and emission at 535-590 nm, and the cell wall by excitation with a 633 nm HeNe laser and emission at 650-710 nm. No stain controls were run for each excitation/emission channel (*not shown*).

#### **5.3.5 Chemical inhibition of rhizoid cell wall and actin dynamics**

Autoclaved glass coverslips (VWR) were placed in a culture dish and submerged in 3 ml BBM with 10 mM NAG. Following 1 h of incubation to allow normal zoospore settlement and germination, 1 ml of growth medium was removed from the dish and 1 ml of poison-containing medium was introduced. Caspofungin diacetate (an inhibitor of 1,3- $\beta$ -glucan synthase, working concentration 1-50  $\mu$ M) was used to inhibit cell wall synthesis and cytochalasin B (an inhibitor of actin polymerization, working concentration 0.1-10  $\mu$ M) was used to inhibit actin filament formation. Cells were further incubated for 6 h, which was

found to be sufficient to observe phenotypic variation before being removed from the incubator and held at 4 °C prior to imaging. Coverslips were removed from the dishes using EtOH-cleaned forceps and placed cell-side down into a glass bottom dish containing 100 µl of membrane stain.

### **5.3.6 Quantification of chytrid $\beta$ -glucans**

*R. globosum* was grown to 250 ml in BBM with 10 mM NAG ( $n = 5$ ) for 7 d before harvesting by centrifugation at 4,700 rpm for 10 min in 50 ml aliquots and washed in 50 ml MilliQ H<sub>2</sub>O. The cell pellet from each flask was processed for  $\beta$ -glucans in duplicate using a commercial  $\beta$ -Glucan assay (Yeast & Mushroom) (K-YBGL, Megazyme) following the manufacturer's protocol. A sample of shop-bought baker's yeast was used as a positive control. Glucans were quantified spectrophotometrically using a CLARIOstar Plus microplate reader (BMG Labtech).

### **5.3.7 Identification of putative glucan synthase genes in the *R. globosum* JEL800 genome**

All glycosyl transferase group 2 (GT2) domain-containing proteins within the *R. globosum* genome were identified using the JGI MycoCosm online portal. GT2 functional domains were identified using DELTA-BLAST (Boratyn et al., 2012) and aligned with MAFFT (Kato and Standley, 2013).

### **5.3.8 Carbon starvation and growth on chitin beads**

To quantify differential rhizoidal growth under carbon replete and carbon deplete conditions, coverslips were placed in a culture dish and submerged in 3 ml growth medium (either carbon-free BBM or BBM with 10 mM NAG). Dishes were then inoculated with zoospores and incubated for either 1, 4, 7 or 24 h, with the 24 h cell z-stacks stitched as described in the fractal analysis. For both sets of experiments, cells were imaged as per the chemical inhibition experiments above.

Chitin beads of approximately 50-70 µm in diameter (New England Biolabs) were washed three times in carbon-free BBM using a magnetic Eppendorf rack and suspended

in carbon-free BBM at a working concentration of 1:1,000 stock concentration. Glass bottom dishes containing 3 ml of the diluted beads were inoculated with zoospores and incubated for either 1, 4, 7 or 24 h prior to imaging. For imaging, the culture medium was aspirated off and beads were submerged in 100  $\mu$ l FM 1-43. To understand rhizoid development in a starved cell that had encountered a chitin bead, cells that contacted a chitin bead following development along the glass bottom of the dish were imaged.

### **5.3.9 Data analysis and statistics**

The comparison between apical and lateral branching was conducted using a Wilcoxon Rank Sum test. Univariate differences in rhizoid morphometrics between experimental treatments were evaluated using Welch's *t*-tests unless stated otherwise. Shapiro-Wilk and Levene's tests were used to assess normality and homogeneity of variance respectively. If these assumptions could not be met, then Wilcoxon Rank Sum was used as a nonparametric alternative. Univariate morphometric differences between particle-associated and non-associated rhizoids were evaluated using paired *t*-tests. All data were analysed in RStudio v1.1.456.

## **5.4 Results**

### **5.4.1 Quantifying chytrid rhizoid morphogenesis**

Electron microscopy (Figure 5.3&4) confirmed that rhizoids in *R. globosum* were thin (~200 nm in diameter) and anucleate, and also showed rhizoids to contain dense endomembrane structures and to lack organelles such as mitochondria. This implies chemical energy generation must occur in the cell body and can only reach the rhizoids through translocation. The confocal imaging workflow employed in this study resulted in 3D reconstructions of rhizoids for quantification (Figure 5.6A). During rhizoid development a continuous increase in rhizoid length ( $110.8 \pm 24.4 \mu\text{m h}^{-1}$ ) ( $n = 5$ , mean $\pm$ SD) and the number of rhizoid tips ( $4.6 \pm 1.2 \text{ tips h}^{-1}$ ) was observed (Figure 5.6B), with an increase in the total cell surface area ( $21.1 \pm 5.2 \mu\text{m}^2 \text{ h}^{-1}$ ), rhizoid bifurcations ( $4.2 \pm 1.0 \text{ bifurcations h}^{-1}$ ), cover area ( $2,235 \pm 170.8 \mu\text{m}^2 \text{ h}^{-1}$ ) and maximum Euclidean distance ( $5.4 \pm 0.1 \mu\text{m h}^{-1}$ ). The hyphal growth unit (HGU) has been used previously to describe hyphal development in

dikaryan fungi and is defined as the distance between two hyphal compartments (Trinci, 1974). Adapting this metric for the chytrid rhizoid, the rhizoidal growth unit (RGU) (i.e. the distance between two rhizoid compartments, Figure 5.5) increased continuously during the first 6 h of the development period (i.e. cells became relatively less branched) before stabilising during the later phase of growth (Figure 5.6B). The local rhizoid bifurcation angle remained consistent at  $81.4^{\circ} \pm 6.3$  after  $\sim 2$  h, and lateral branching was more frequent than apical branching during rhizoid development (Figure 5.6C&D). Fractal analysis (fractal dimension =  $Db$ ) of 24 h grown cells showed that rhizoids approximate a 2D biological fractal (Mean  $Db = 1.51 \pm 0.24$ ), with rhizoids relatively more fractal at the centre of the cell (Max  $Db = 1.69$ - $2.19$ ) and less fractal towards the growing periphery (Min  $Db = 0.69$ - $1.49$ ) (Figure 5.6E).

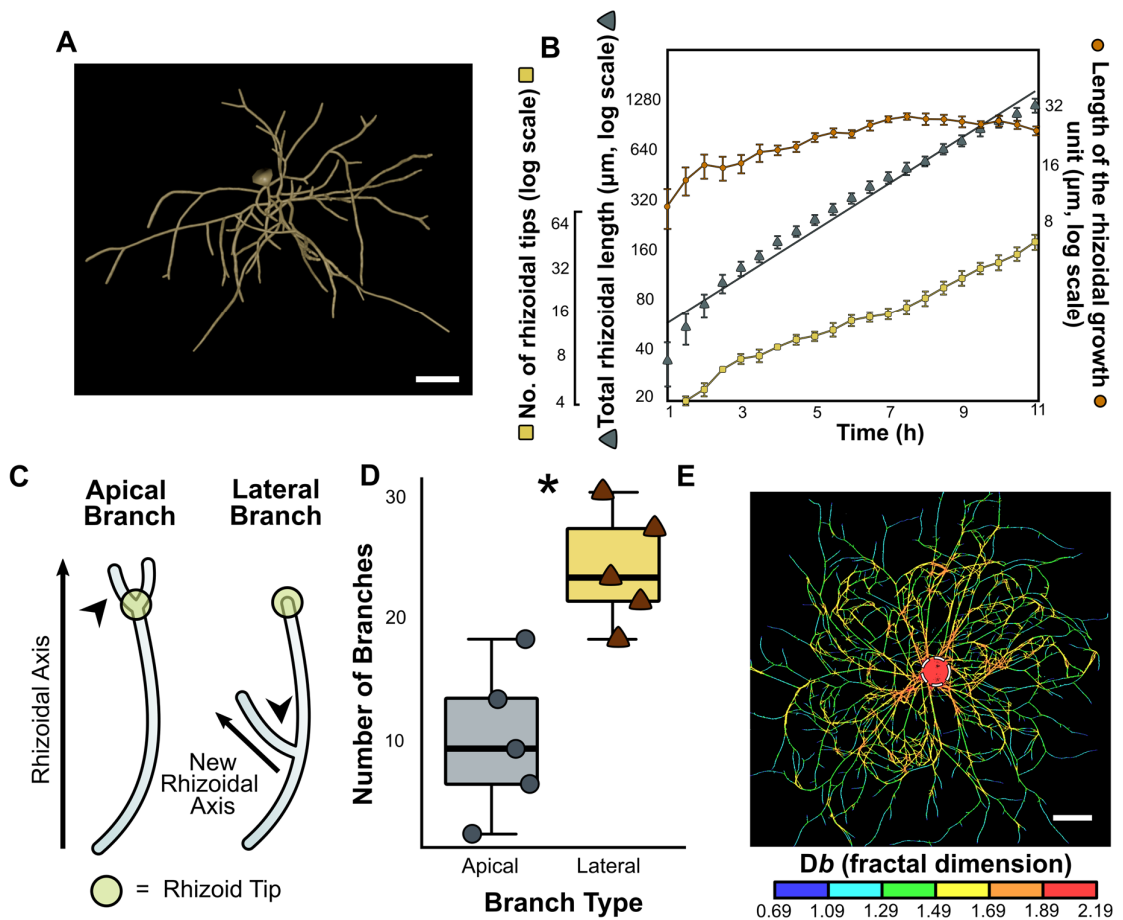


**Figure 5.6 Rhizoid morphogenesis was geometrically quantified.** (A) Chytrid rhizoids were reconstructed using the neuron tracing workflow (Figure 5.4). Example of a 3D reconstructed *R. globosum* rhizoid system taken from a 10 h time series. Scale bar = 20

$\mu\text{m}$ . (B) Rhizoid growth trajectories for 4D confocal time series ( $n = 5$ , mean  $\pm$ SE) of rhizoidal growth unit, total length, and number of tips. (C) Apical and lateral branches occur in chytrid rhizoids. Apical branching occurs when a branch is formed at the rhizoid tip parallel to the established rhizoidal axis. Lateral branching occurs when a branch is formed distally to the rhizoidal tip, establishing a new rhizoidal axis. (D) 4D confocal imaging ( $n = 5$ ) revealed that lateral branching dominates over apical branching  $*p < 0.05$ . (E). Fractal analysis of chytrid rhizoid systems shows a decrease in fractal dimension ( $D_b$ ) towards the growing edge. Cell body demarked by dashed circle. Scale bar = 50  $\mu\text{m}$ .

#### **5.4.2 Cell wall and actin dynamics are linked to rhizoid branching**

The cell wall and actin patches are present throughout the chytrid rhizoid (Figure 5.7A). Inhibition of cell wall  $\beta$ -1,3-glucan synthesis and actin polymerisation with caspofungin and cytochalasin B respectively induced a concentration-dependent decrease in the RGU, with the development of atypical hyperbranched rhizoids (Figure 5.7B-D). However, as with *Batrachochytrium dendrobatidis* (Richards et al., 2017; Ruiz-Herrera and Ortiz-Castellanos, 2019, 2010), it was confirmed that *R. globosum* JEL800 lacks an apparent  $\beta$ -1,3-glucan synthase FSK1 gene homolog, the target of caspofungin. Despite this, quantification of glucans in *R. globosum* showed that they are present (Figure 5.8), with  $58.3 \pm 7.6$  %  $\beta$ -glucans and  $41.6 \pm 7.6$  %  $\alpha$ -glucans of total glucans.

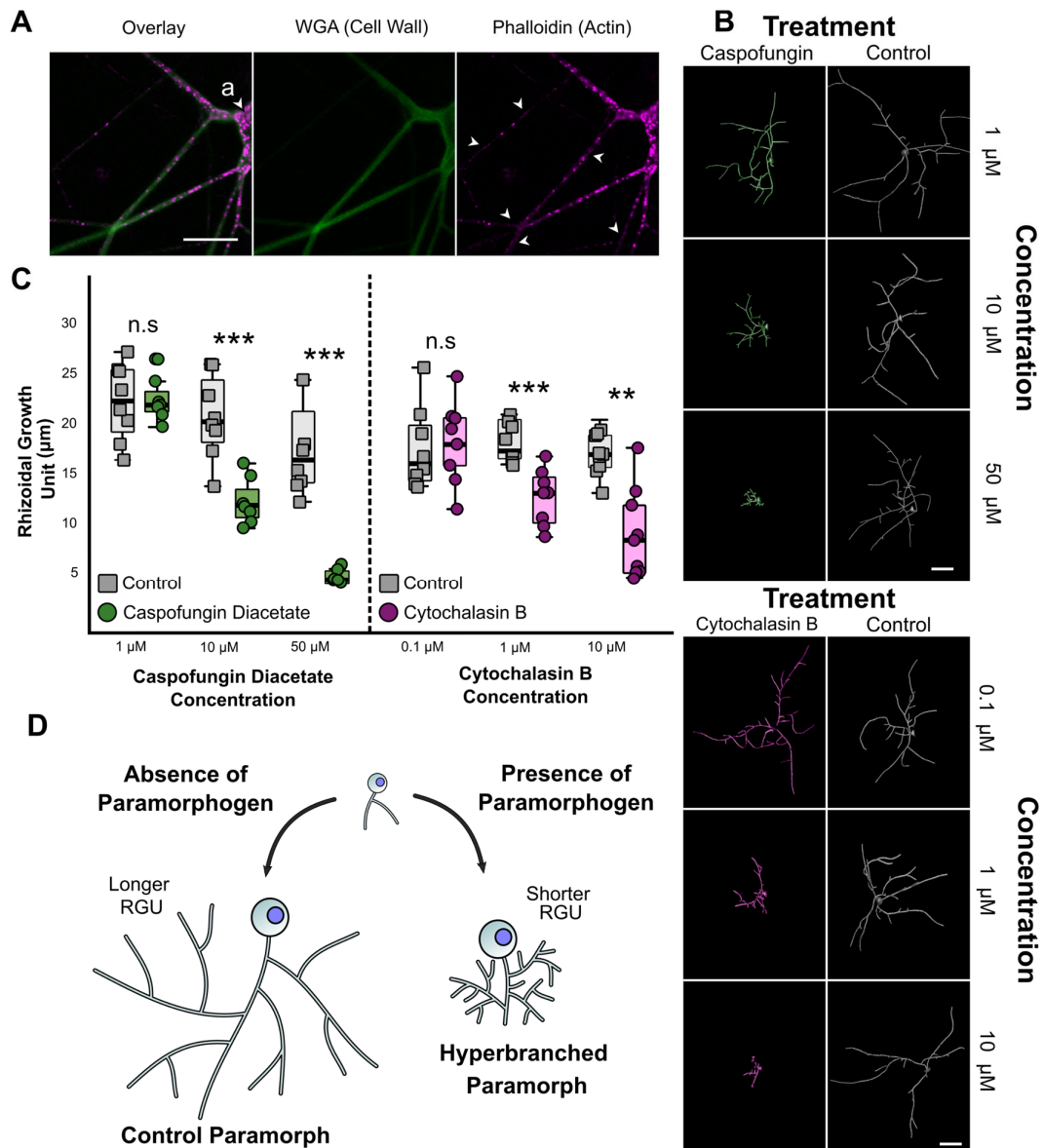


**Figure 5.7 Cell wall synthesis and actin dynamics govern rhizoid branching.** (A)

Fluorescent labelling of cell wall and actin structures in 24 h *R. globosum* cells. The cell wall and actin patches were found throughout the rhizoid. WGA = conjugated Wheat Germ Agglutinin. Scale bar = 10  $\mu\text{m}$ . (B) Representative 3D reconstructions of 7 h *R. globosum* cells following treatment with caspofungin diacetate and cytochalasin B at stated concentrations to inhibit cell wall and actin filament biosynthesis respectively, relative to solvent only controls. Scale bar = 20  $\mu\text{m}$  (C) Application of caspofungin diacetate and cytochalasin B resulted in a concentration-dependent decrease in the rhizoidal growth unit, resulting in atypical hyperbranched rhizoids ( $n = \sim 9$ ). n.s  $p > 0.05$  (not significant), \* $p < 0.05$ , \*\* $p < 0.01$ , \*\*\* $p < 0.001$ . This differential growth is diagrammatically summarised in (D).

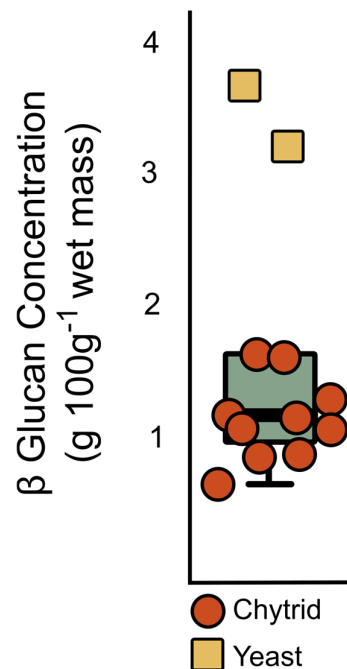


**Figure 5.8 *R. globosum* JEL800 cells contain  $\beta$ -glucans.**  $\beta$ -glucan concentration of *R. globosum* ( $n = 10$ ) relative to a baker's yeast control ( $n = 2$ ).

To identify alternative putative  $\beta$ -glucan synthesis genes in *R. globosum* JEL800, the genome was surveyed with a focus on glycosyltransferase family 2 (GT2) encoding genes, which include typical glucan synthases in fungi. A total of 28 GT2 domains were found within 27 genes. Of these genes, 20 contained putative chitin synthase domains and many contained additional domains involved in transcriptional regulation. Nine encode chitin synthase 2 family proteins and 11 encode chitin synthase 1 family proteins (with two GT2 domains in ORY48846). No obvious genes for  $\beta$ -1,3-glucan or  $\beta$ -1,6-glucan synthases were found within the genome. However, one chitin synthase 2 gene ORY39038 included a putative SKN1 domain (Figure 5.8B), which has been implicated in  $\beta$ -1,6-glucan synthesis in the ascomycete yeasts *Saccharomyces cerevisiae* (Roemer et al., 1993) and *Candida albicans* (Han et al., 2019). These results indicate a yet uncharacterised  $\beta$ -glucan-dependent cell wall production process in chytrids (also targeted by caspofungin), putatively employing ORY39038, that is not currently apparent using gene/genome level assessment and warrants further study.



### **5.4.3 Rhizoids undergo adaptive development in response to carbon starvation**

To examine whether chytrids are capable of modifying rhizoid development in response to changes in resource availability, *R. globosum* was exposed to carbon starvation (i.e. development in the absence of exogenous carbon). When provided with 10 mM NAG as an exogenous carbon source, the entire life cycle from zoospore to sporulation was completed and the rhizoids branched densely, indicative of a feeding phenotype. Carbon-starved cells did not produce zoospores and cell growth stopped after 14-16 h. Using only endogenous carbon (i.e. zoospore storage lipids and glycogen), starved cells underwent differential rhizoid development compared to cells from the exogenous carbon replete conditions to form an apparent adaptive searching phenotype (Figure 5.9A&B). Under carbon starvation, *R. globosum* invested less in cell body growth than in carbon replete conditions and developed longer rhizoids with a greater maximum Euclidean distance (Figure 5.10). Carbon starved cells were also less branched, had wider bifurcation angles and subsequently covered a larger surface area. These morphological changes in response to exogenous carbon starvation (summarised in Figure 5.9B) suggest that individual chytrid cells are capable of differential reallocation of resources away from reproduction (i.e. the production of the zoosporangium) and towards an extended modified rhizoidal structure indicative of a resource searching phenotype.

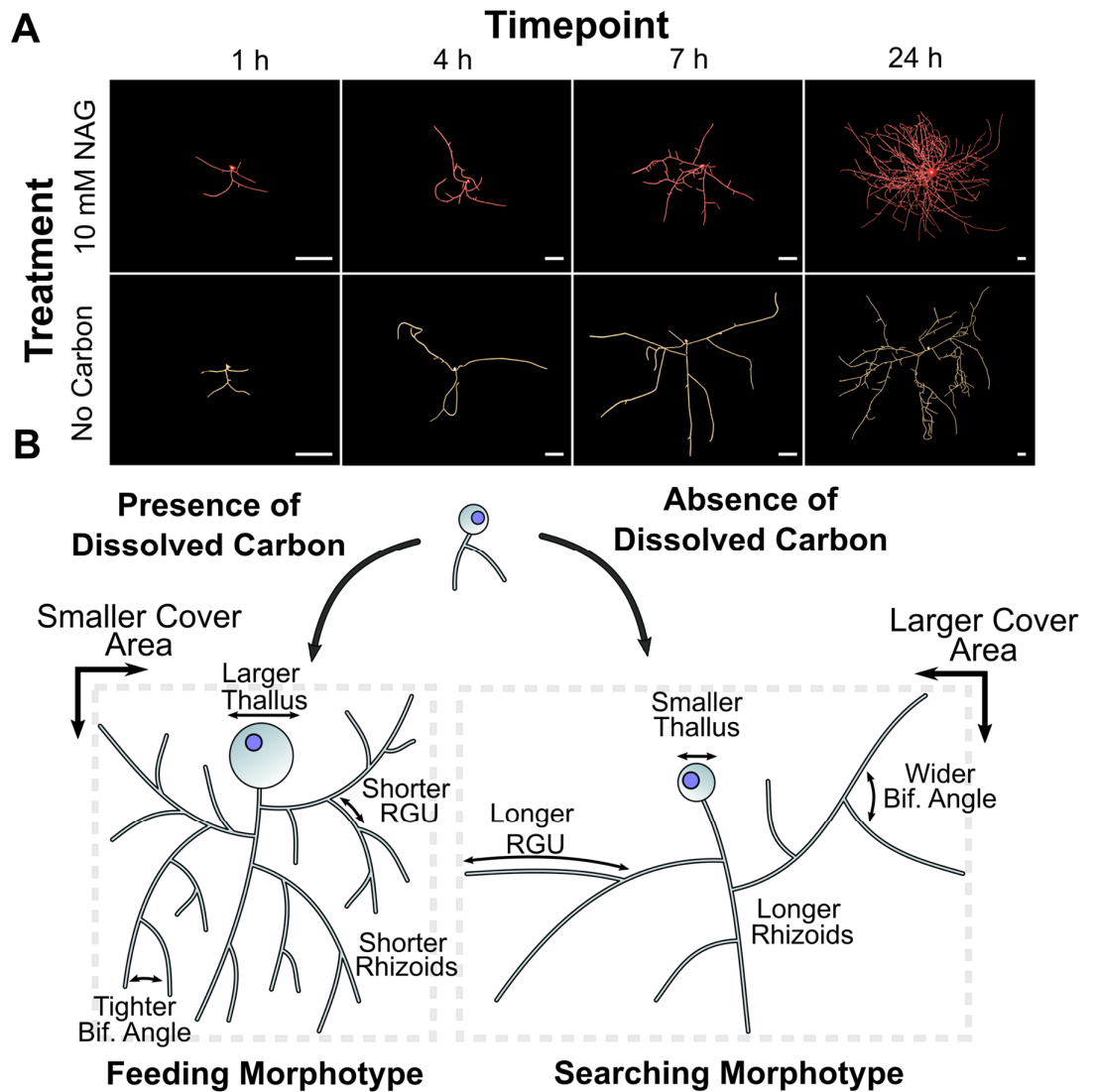


**Figure 5.9 Chytrids are capable of adaptive rhizoid development under carbon starvation (Part 1).** (A) Representative 3D reconstructions of *R. globosum* cells grown under carbon replete or carbon deplete conditions at different timepoints. Scale bar = 20  $\mu\text{m}$ . When exposed to carbon starvation, chytrids are capable of differential adaptive growth to produce a searching phenotype. This differential growth is summarised in (B).

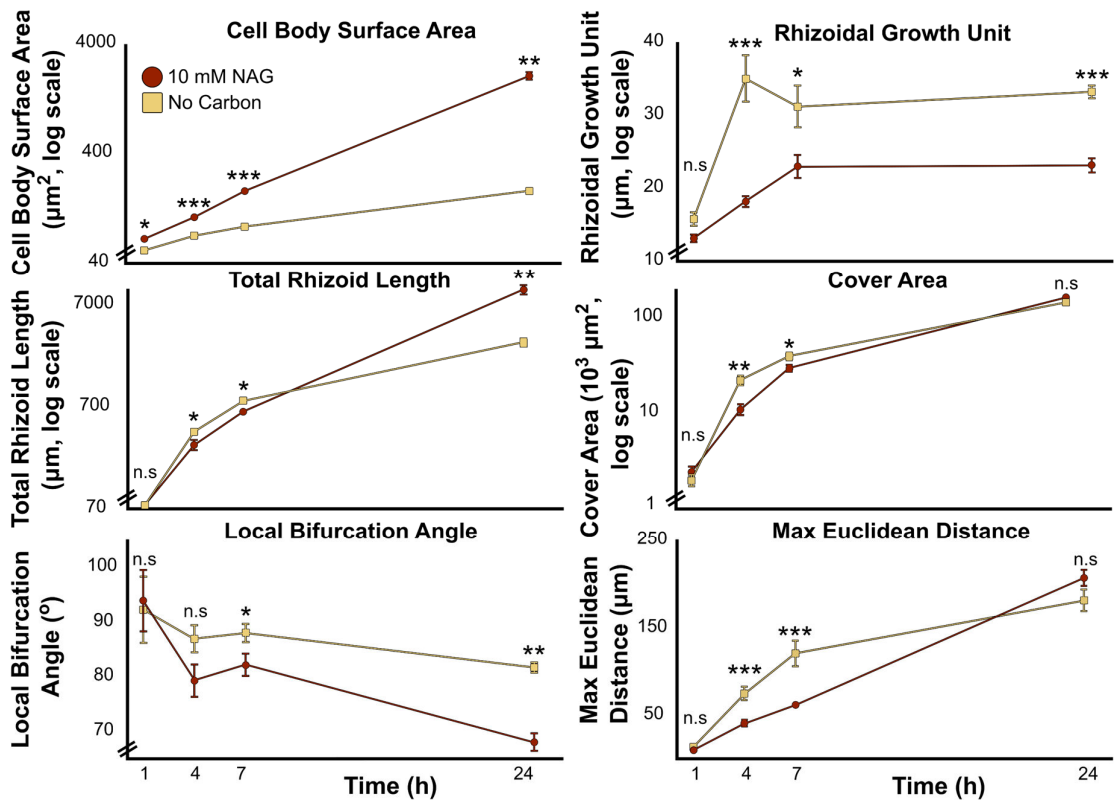


**Figure 5.10 Chytrids are capable of adaptive rhizoid development under carbon starvation (Part 2).** Differential growth trajectories of major morphometric traits between *R. globosum* cells ( $n = \sim 9$ , mean  $\pm$ SE) grown under carbon replete and carbon deplete conditions over time. n.s  $p > 0.05$  (not significant), \*  $p < 0.05$ , \*\*  $p < 0.01$ , \*\*\*  $p < 0.001$ .

#### 5.4.4 Rhizoids spatially differentiate in response to patchy resource environments

Rhizoid growth of single cells growing on chitin microbeads was quantified as experimental POM (Figure 5.11A&B). Initially, rhizoids grew along the outer surface of the bead and were probably used primarily for anchorage to the substrate. Scanning electron microscopy (SEM) showed that the rhizoids growing externally on the chitin particle formed grooves on the bead parallel to the rhizoid axis (Figure 5.2F&G), suggesting extracellular enzymatic chitin degradation by the rhizoid on the outer surface. Penetration of the bead occurred during the later stages of particle colonisation (Figure 5.11A). Branching inside the bead emanated from 'pioneer' rhizoids that penetrated the particle (Figure 5.11C).

Given the previous results of the searching rhizoid development in response to carbon starvation, a patchy resource environment was created using the chitin

microbeads randomly distributed around individual developing cells in otherwise carbon-free media to investigate how encountering POM affected rhizoid morphology (Figure 5.12A). Spatial differentiation of single cell rhizoid systems in association with POM contact was observed. Particle-associated rhizoids were shorter than rhizoids not in particle contact, were more branched (i.e. lower RGU), had a shorter maximum Euclidean distance and covered a smaller area (Figure 5.12B). These rhizoid morphometrics closely resembled the feeding and searching modifications of the cells grown under carbon replete and carbon deplete conditions previously discussed (Figure 5.9B), but instead are displayed simultaneously with spatial regulation in individual cells linked to POM-associated and non-associated rhizoids respectively.

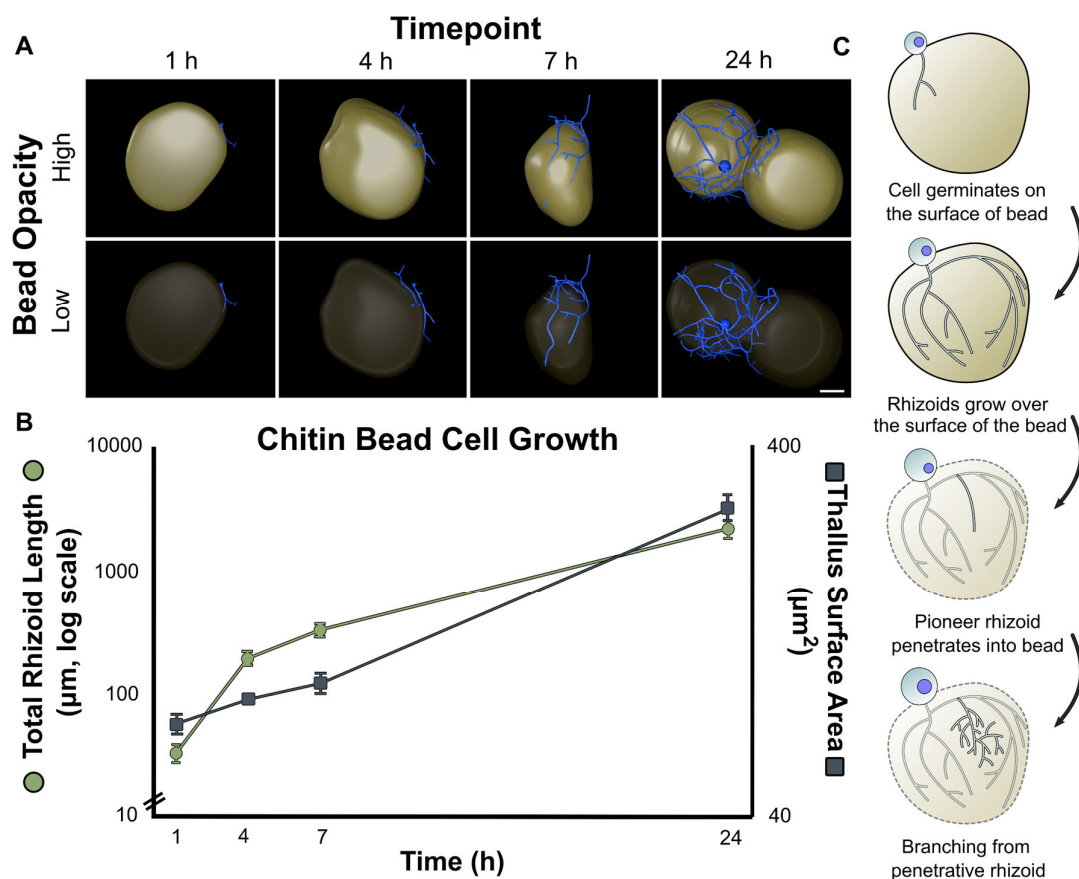


**Figure 5.11 Quantification of rhizoids growing on particulate carbon. (A)**

Representative 3D reconstructions of *R. globosum* cells (blue) growing on chitin beads (beige) at different timepoints. Scale bar = 20 μm. (B) Growth trajectories for total rhizoid length and cell body surface area for *R. globosum* cells growing on chitin beads ( $n \sim 9$ , mean  $\pm$  SE). (C) Diagrammatic summary of *R. globosum* rhizoid development on chitin beads.

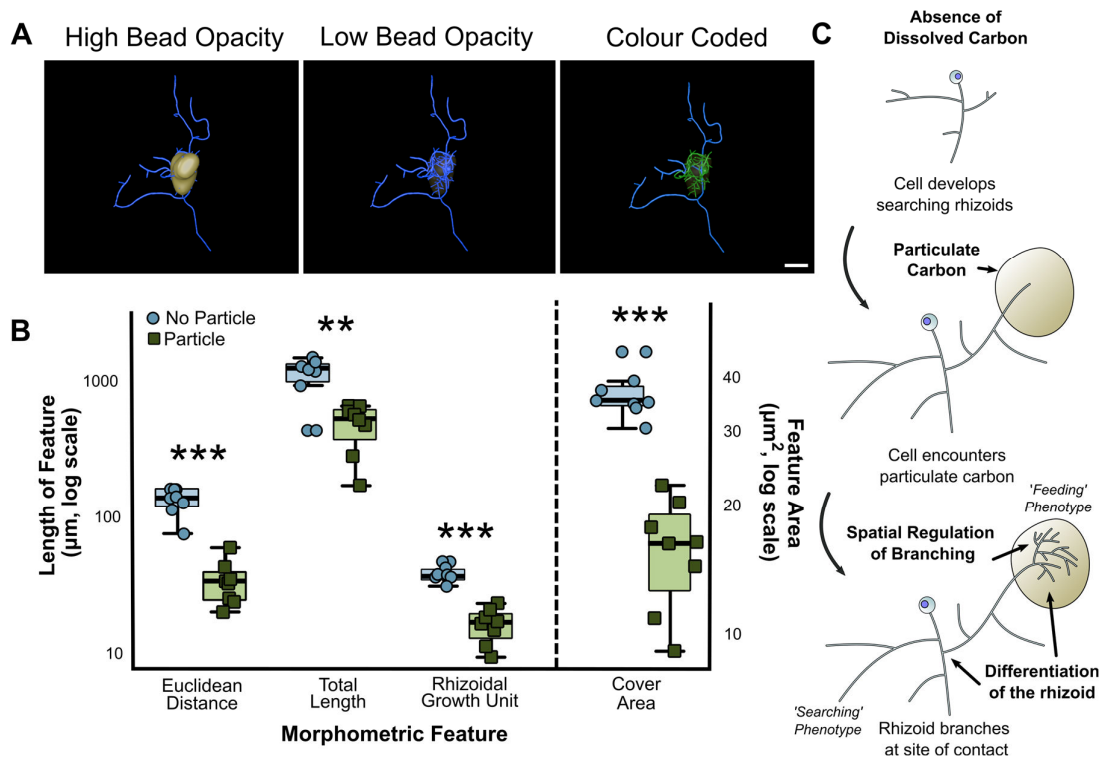


**Figure 5.12 Rhizoids associated with heterogeneous particulate carbon exhibit spatial differentiation.** (A) Representative 3D reconstruction of a 24 h searching *R. globosum* cell (blue) that has encountered a chitin bead (beige). The colour coded panel shows parts of the rhizoid system in contact (green) and not in contact (blue) with the bead. Scale bar = 20 µm. (B) Comparison of rhizoids in contact or not in contact with the chitin bead ( $n = 8$ ). n.s  $p > 0.05$  (not significant), \* $p < 0.05$ , \*\* $p < 0.01$ , \*\*\* $p < 0.001$ . (C) Diagrammatic summary of spatial differentiation in a starved, searching rhizoid that has encountered a particulate carbon patch.

## 5.5 Discussion

These results provide new insights into the developmental cell biology of chytrid fungi and highlight similarities between the organisation of anucleate rhizoids and multicellular hyphae. The fundamental patterns of rhizoid morphogenesis reported here for a unicellular non-hyphal fungus are comparable to those previously recorded for dikaryan fungi (Figure 5.13&14) (Trinci, 1974). Trinci (1974) assessed hyphal development in three major fungal lineages (Ascomycota, Basidiomycota, and Mucoromycota) and observed that the growth patterns of major morphometric traits (HGU, total length, and number of

tips) were similar across the studied taxa. When the data from this study are directly compared to that of Trinci (1974), hyphal growth patterns are analogous to the rhizoids of the unicellular Chytridiomycota (Figure 5.13&14).

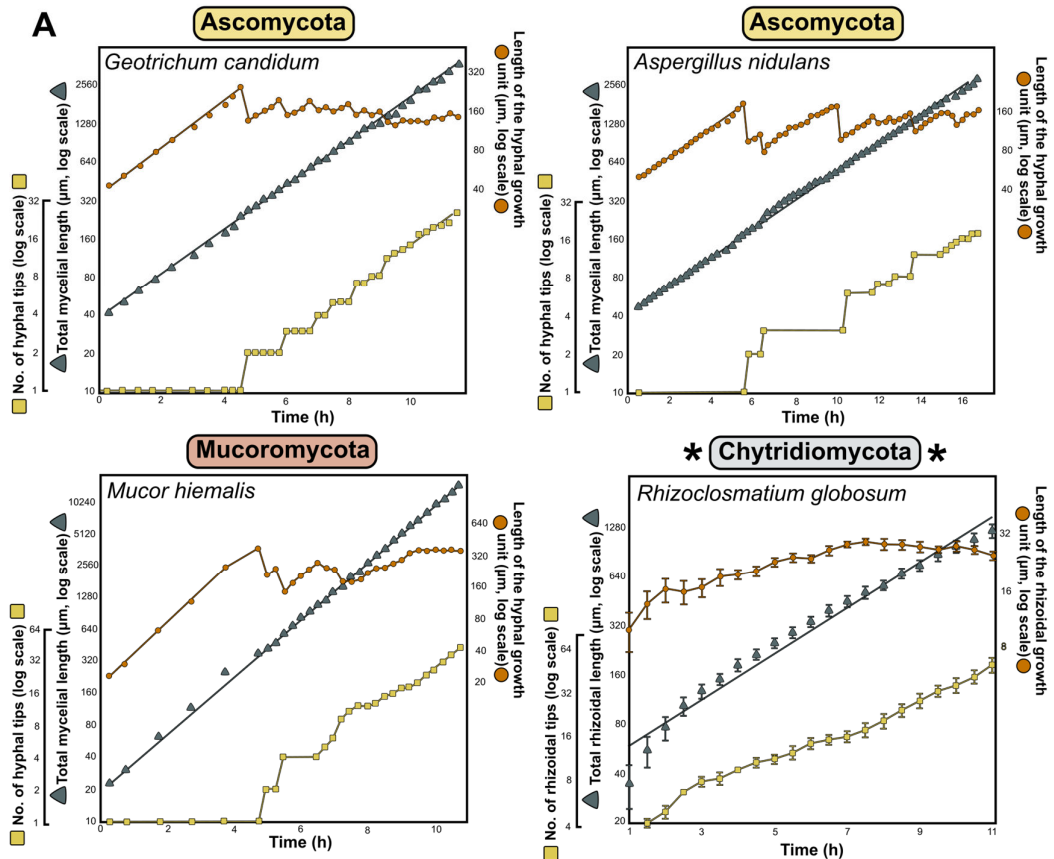


**Figure 5.13 Development of chytrid rhizoids fundamentally resembles mycelial development in hyphal fungi (Part 1).** Comparison of rhizoid development from this study (asterisks) with other studies on hyphal fungi (López-Franco et al., 1994; Trinci, 1974). Growth trajectories of the growth unit, total length, and number of tips of rhizoids and hyphae. Data for other fungi are reproduced as new figures directly from (Trinci, 1974). For *R. globosum* ( $n = 5$ ). Error bars denote  $\pm$ SE.

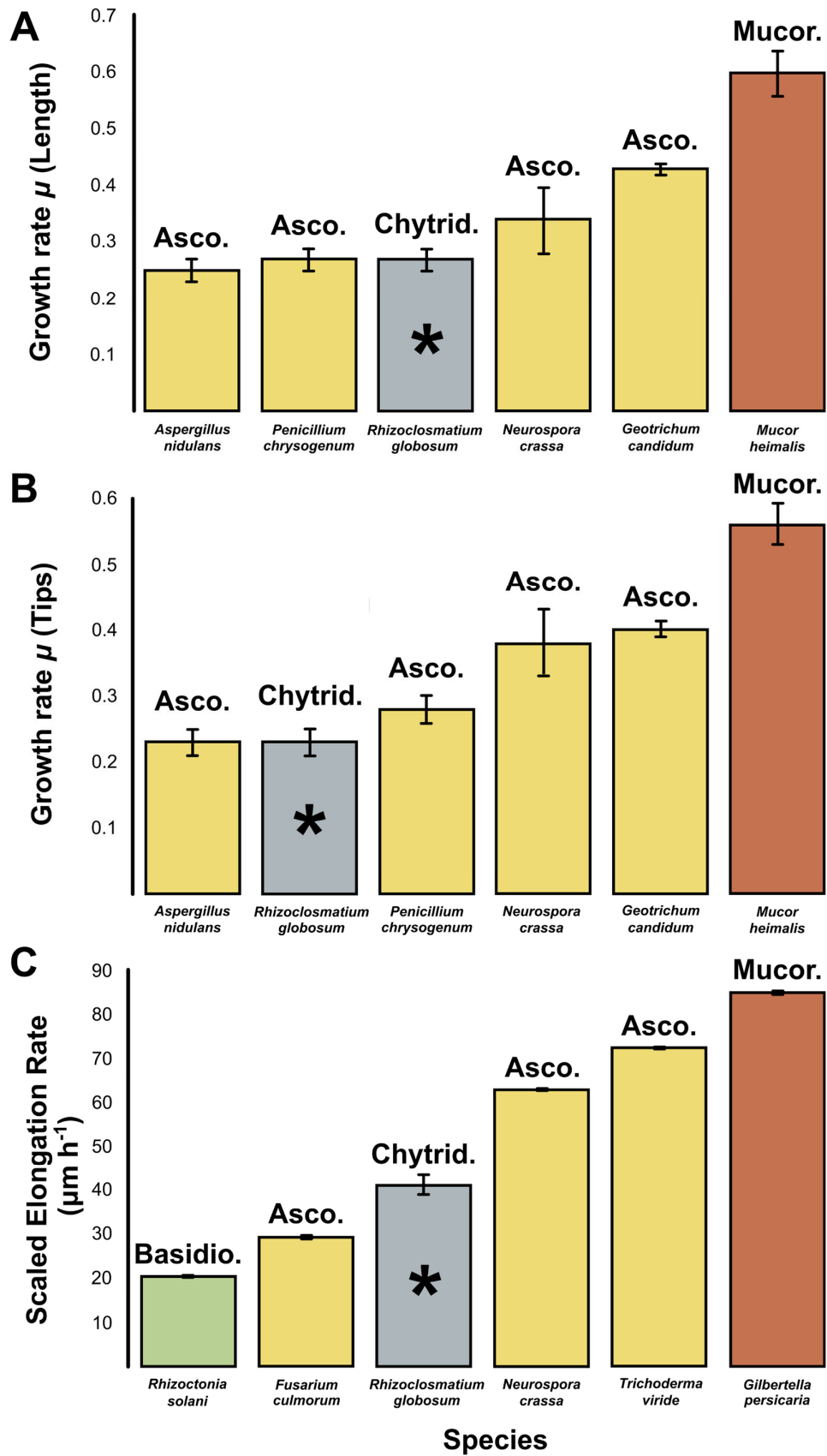


Figure 5.14 Development of chytrid rhizoids fundamentally resembles mycelial

development in hyphal fungi (Part 2). (A&B) *R. globosum* has similar growth rates

regarding total length (A) and tip production (B) to hyphal fungi. Rhizoid growth rates ( $\mu$ )

calculated as increase in the total rhizoid length or tip number as in (Trinci, 1974). Data for Ascomycota and Mucoromycota fungi are from (Trinci, 1974). For *R. globosum* ( $n = 5$ ). Mean  $\pm$ SD (C) *R. globosum* rhizoids when scaled by diameter have a comparable elongation rate to hyphae. Rhizoid elongation rates (the speed at which individual rhizoid compartments extend) were quantified by measurement of extending rhizoid compartments (10 rhizoids for each biological replicate) separated by a 30 min interval on maximum intensity projected z-stacks in Fiji. Data for other fungi are from (López-Franco et al., 1994). For *R. globosum* ( $n = 5$ ). Mean  $\pm$ SE.

Such similarities also extend to rhizoid branching patterns, where lateral branching dominates over apical branching. This branching pattern is also the predominant mode of hyphal branching, where apical branching is suppressed by a process termed ‘apical dominance’ (Harris, 2019). The mechanisms of apical dominance are unknown, but reactive oxygen species (ROS) and calcium ( $\text{Ca}^{2+}$ ) gradients are thought to be involved (Harris, 2019). These findings suggest that a form of apical dominance at the growing edge of rhizoid tips may suppress apical branching to maintain rhizoid network integrity as in dikaryan hyphae (Harris, 2019; Semighini and Harris, 2008). Chytrid rhizoids also become less fractal towards the growing edge in terms of their overall morphology, and similar patterns of fractal organisation are also observed in hyphae-based mycelial colonies (Obert et al., 1990). Taken together, these results show strong geometric analogies in the fundamental organisation of unicellular chytrid rhizoid and multicellular hyphal morphogenesis.

Given the apparent hyphal-like properties of rhizoid development, a greater understanding of the potential subcellular machinery underpinning rhizoid morphogenesis in *R. globosum* was sought. Normal rhizoid branching was disrupted by inhibition of cell wall synthesis and actin polymerisation, both of which are known to control branching and growth in hyphal biology (Gow et al., 2017; Steinberg et al., 2017). These effects in *R. globosum* are similar to disruption of normal hyphal branching reported in *Aspergillus fumigatus* (Ascomycota) in the presence of caspofungin (Moreno-Velásquez et al., 2017), and in *Neurospora crassa* (Ascomycota) in the presence of cytochalasins (Allen et al.,



1980). Recent studies have shown the presence of actin in the rhizoids of soil chytrids (Dee et al., 2019; Medina et al., 2020) and inhibition of actin in *Chytrium hyalinus* similarly disrupts normal rhizoid branching (Dee et al., 2019). Although the specific action of actin in rhizoid organisation is unknown, it may be associated with regulating vesicle deposition at the tip as is the case during hyphal development (Riquelme et al., 2018). In this study, the quantitative characterisation of cell wall and actin inhibited rhizoid paramorphs provides support that  $\beta$ -1,3-glucan-dependent cell wall synthesis and actin dynamics also govern branching in chytrid rhizoids as in multicellular hyphae.

Rhizoid development was also shown to be plastic to resource availability, with chytrid cells displaying an adaptive searching phenotype under carbon starvation. Adaptive foraging strategies are well described in multicellular hyphae (Boddy, 1999; Vinck et al., 2005) and the data here support the existence of analogous strategies in rhizoidal fungi. Dense branching zones in dikaryan mycelia are known to improve colonisation of trophic substrates and feeding by increasing surface area for osmotrophy, while more linear 'exploring' zones cover greater area and search for new resources (Vinck et al., 2005). Similar morphometrics are displayed by *R. globosum* exhibiting feeding and searching phenotypes respectively. In addition, exogenous carbon starvation has also been shown to be associated with a decrease in branching in the multicellular dikaryan fungus *Aspergillus oryzae* (Ascomycota) (Pollack et al., 2008). Overall, these results highlight that adaptive search strategies are more widely spread than previously known in the Kingdom Fungi.

Finally, these results show the spatial and functional differentiation of feeding and searching sections of anucleate rhizoid systems from individual cells. The simultaneous display of both rhizoid types in the same cell indicates a controlled spatial regulation of branching and differentiation of labour within single chytrid rhizoid networks. Functional division of labour is prevalently seen in multicellular mycelial fungi (Boddy, 1999; Vinck et al., 2005), including the development of specialised branching structures for increased surface area and nutrient uptake, as in the plant symbiont mycorrhiza (Glomeromycota) (Bago et al., 1998). The observation of similarly complex development in a unicellular

chytrid suggests that multicellularity is not a prerequisite for adaptive spatial differentiation in fungi.

## 5.6 Conclusion

The cell biology focused approach employed here advances our understanding of fungal ecology and evolution by showing that a representative unicellular rhizoid-bearing chytrid displays hyphal-like morphogenesis, with evidence that the cell structuring mechanisms (e.g. apical dominance) underpinning chytrid rhizoid development are equivalent to reciprocal mechanisms in dikaryan fungi. Perhaps the key discovery of this study is that the anucleate chytrid rhizoid shows considerable developmental plasticity. *R. globosum* can control rhizoid morphogenesis to produce a searching form in response to carbon starvation and, from an individual cell, is capable of spatial differentiation in adaptation to patchy substrate availability indicating functional division of labour. The potential for convergent evolution aside, I propose by parsimony from the presence of analogous complex cell developmental features between chytrid and dikaryan fungi that adaptive rhizoids are a shared feature of their most recent common ancestor.

## Chapter 6 – A solid foundation for the future of chytrid developmental biology

### 6.1 Thesis summary

Despite the ecological and evolutionary importance of chytrids highlighted in the opening chapter of this thesis (Chapter 1), a quantitative literature search highlighted how overlooked chytrids are in a field of fungal biology dominated by dikaryan model species (Figure 1.4). Although interest in chytrids has spiked in the past two decades (Figure 1.4C), investigations into chytrid development have been largely qualitative prior to this work. Analysis of this oversight highlighted how little is currently understood about the fundamentals of chytrid cell and developmental biology and presented the three major aims that constituted this thesis.

The initial aim was to establish experimental protocols for live-cell imaging in chytrids, the results of which are outlined in Chapter 3. The rationale behind this was twofold: to generate central protocols for the future use of *R. globosum* as a model for developmental chytrid biology and to highlight methodological alternatives to counteract the previous overreliance on bioinformatics tools (Chapter 1.4.3). These preliminary investigations consisted of protocols for the fluorescent imaging (Figure 3.1-4) and cryopreservation (Figure 3.5) of *R. globosum*, which were used to investigate chitin and lipid dynamics. While the results of this chapter were largely methodological and qualitative, they formed a foundation to support the research aims of the subsequent two chapters. Specifically, fluorescent labelling and microscopy of lipid structures across the *R. globosum* life cycle (Figure 3.1&2) generated hypotheses regarding anabolism and catabolism expanded on in Chapter 4, and the imaging protocols developed here were used in their exploration (Figure 4.7). Additionally, the fluorescent membrane labelling and confocal imaging of *R. globosum* rhizoids interacting with particulate chitin (Figure 3.3G-I) hinted at the complexity of rhizoid architecture and provided the impetus for Chapter 5.

Building on these methodological trials, this work next set out to identify the key cellular and molecular drivers of the chytrid lifecycle (Chapter 4). Before the ecological

and evolutionary importance of chytrids can be fully appreciated, these most fundamental gaps in our understanding of chytrid biology must be closed. Due to how little was previously known about these processes, this research employed a multimethodological and non-targeted approach (Figure 4.1) to identify the overarching biological motifs of the *R. globosum* life cycle. By combining 3D electron microscopy reconstruction with transcriptomic profiling, this research generated a holistic atlas of chytrid development (Figure 4.4-6) from which to launch further, targeted investigations. These initial findings included, but were not limited to, the dominance of the ribosome cluster in zoospore biology, the onset of germling metabolic pathways and proteasome activity, and the vacuolisation of immature thalli driven by cytoskeletal organization (Figure 4.4&6). Lipid metabolism was then investigated, revealing that a qualitative shift from neutral glycolipids to polar lipids characterised lipid dynamics from zoospores to germlings, but not a change in lipid quantity or structure, and that intravacuolar lipid globules were associated with lipid anabolism in immature thalli (Figure 4.7&8). The enigmatic apophysis structure in immature thalli, that previously lacked any proposed function, was shown to be a distinct subcellular structure delineated by a chitinous pseudo-septum and governed by intracellular trafficking between the rhizoids and cell body (Figure 4.9&10). Finally, it was discovered that intrasporangial developing zoospores exhibited an amoeboid morphology as a result of endocytotic activity between the zoospore cell body and the interstitial maternal cytoplasm (Figure 4.11). Taken together, this investigation succeeded in identifying the major biological drivers of the chytrid life cycle (Figure 4.12) and quantified for the first time the structural and molecular basis of archetypal chytrid life stages.

As some chytrid life stages lack rhizoids, rhizoids were excluded from the previous aim to focus on the development of the cell body. Quantification of rhizoid growth was treated separately in Chapter 5 with a focus on imaging dynamic growth in 3D. The geometry and causative subcellular machinery of mycelial morphogenesis in dikaryan fungi is well understood (Riquelme et al., 2018) but an analogous understanding of rhizoid development in chytrids was previously lacking, despite the proposed role of rhizoids as evolutionary precursors of hyphae. This lack of understanding may have been partly

methodological, due to the difficulty in quantifying thin rhizoids that are at least an order of magnitude thinner than hyphae. To study developing rhizoids, a customized protocol was designed based on membrane labelling, 3D/4D confocal microscopy, and neuron tracing (Figure 5.4) to morphometrically quantify rhizoid growth (Figure 5.5). It was found that rhizoid morphogenesis was governed by cell wall synthesis and actin dynamics (Figure 5.7) and was adaptive to resource availability (Figure 5.9-12), becoming spatially differentiated in the presence of heterogeneous particulate carbon (Figure 5.12). In summary, these results display striking similarities between rhizoidal and hyphal growth (Figure 5.13&14), which hints at a common evolutionary origin of the two structures and quantifies the fundamentals of chytrid rhizoid development.

## **6.2 Implications of thesis results**

The overarching ambition of this thesis was to apply cellular tools to the growth of a representative chytrid in order to establish a quantitative understanding of chytrid development, which has been achieved. It is my hope that these quantitative investigations are the first of many to come and that chytrids move from just outgroups and pathogens to central subjects in both cellular and fungal biology. The identification of fundamental developmental processes described herein will serve as a valuable foundation for future research in the field. Additionally, the results of this thesis demonstrate the power of *R. globosum* as a model for chytrid developmental biology and the insights it can provide into general chytrid biology. If chytrid cell biology is to progress robustly, it will be necessary to develop a few species as models for chytrid cell biology to centralize resources in laboratory investigations. It is not necessary to repeat what makes a good model for developmental chytrid biology or why *R. globosum* is a strong candidate (outlined in Chapter 1.6), but the work in this thesis has further validated the versatility and amenability of *R. globosum* to laboratory experimentation. The experimental imaging protocols (Chapter 3) and developmental atlas (Chapter 4) that have now been created for *R. globosum* will further contribute to the nascent research infrastructure surrounding this chytrid as an emerging model organism. However, to discuss the implications of the

specific biological results uncovered by this work it is necessary to place chytrids back into the ecological and evolutionary contexts in which they are most impactful.

### **6.2.1 Implications for understanding chytrid ecology**

Chytrids serve integral biogeochemical roles in aquatic food webs, from saprotrophs to parasites (Figure 1.3), and upgrade inaccessible carbon to higher trophic levels through the production of lipid-rich zoospores (Kagami et al., 2014). *R. globosum* is a prominent saprotroph of chitin, associated with arthropod exuviae in the wild (Sparrow, 1960), and fluorescent labelling of subcellular structures was conducted to visualize lipid production when grown on particulate chitin (Figure 3.3). Although qualitative at this stage, these images demonstrated the capacity of chitinophilic chytrids to convert recalcitrant biopolymers to intracellular lipids. Live-cell imaging of chitin and lipid dynamics quantified lipid distribution across the chytrid life cycle (Figure 3.2), highlighting shifts in anabolism versus catabolism and beginning to outline the trophic priorities of individual life stages. However, as the work in Chapter 3 was largely methodological and preliminary, these findings simply paved the way for ecological insights in further chapters.

The insights provided by Chapter 4 were a valuable advance in resolving the cell biology underpinning chytrid lipid metabolism. These data revealed the three-dimensional ultrastructure of intracellular lipid globules and their associated organelles, from contiguous peroxisome-like microbodies and rumposomes associated with lipid conversion and catabolism, to the intravacuolar location of anabolic lipid globules (Figure 4.7B-D). This was coupled to biochemical lipid profiling which revealed that, contrary to previous assumptions, the zoospore lipid globule is not structurally or quantifiably degraded during the transition to germlings, but rather the lipid profile shifts from being dominated by neutral glycolipids in zoospores towards polar lipids in germlings, providing evidence for lipid conversion, but not catabolism *per se*, upon zoospore settlement (Figure 4.8). On a molecular level, transcriptomic profiling identified genes that control zoospore lipid conversion (associated with peroxisomes and ABC-transporters) and showed that

some are also associated with lipid anabolism in immature thalli, suggesting bidirectional function (Figure 4.6). Taken together, these data expose key intracellular processes governing lipid metabolism and synthesis in chytrids and outline the biology underpinning arguably the greatest biogeochemical contribution of chytrids to aquatic food webs.

Of course, given the contribution of chytrids to carbon flow in aquatic systems, anything that sheds light on their central metabolism and feeding dynamics provides insight into their ecological impact. For example, the transcriptomic comparison of germlings and zoospores identified the key metabolic pathways that are activated following zoospore encystment, including carbon metabolism, which provided the molecular basis for chytrid feeding (Figure 4.6D). In addition, the live-cell imaging of fluorescently labelled endomembrane in the immature thallus apophysis revealed high levels of endomembrane cycling (Figure 4.10) in this structure and illustrated how intracellular traffic is directed from the rhizoids (presumably with cargo assimilated from feeding) to the cell body, hinting at a role for this structure in the directional sorting of flow (Figure 4.9). These findings pointed out cellular and molecular processes associated with carbon uptake in chytrid cells and characterised the intracellular fate of assimilated ecological substrates.

Perhaps the greatest contribution of this thesis towards an understanding of chytrid ecological function was the quantification of *R. globosum* rhizoid development presented in Chapter 5. These data revealed that geometric 'foraging' behaviour in chytrids is comparably complex to hyphal fungi, with rhizoid growth being plastic to resource availability. The uncovered ability of chytrids to enact a 'searching' morphology in the absence of a carbon source was a striking finding (Figure 5.9&10), as was the targeted branching at the feeding site in differentiated rhizoid systems growing on particulate chitin (Figure 5.11&12). The sheer sophistication of rhizoid growth in unicellular chytrids and their dynamic capability to adapt to resource changes uncovered here likely is a major explanatory factor in their ecological success.

### **6.2.2 Implications for understanding fungal evolution**

Due to their position in the fungal and eukaryotic trees of life (Figure 1.2), it is unavoidable to study chytrid cell biology without shedding light on evolutionary biology. Chytrids retain ancestral cellular traits thought to have been present in the last common ancestor of branching fungi, making them powerful models to investigate and reconstruct the putative biology of this organism (Figure 1.2). Therefore, the holistic characterization of *R. globosum* development presented in Chapter 4 is an important step forward in this direction. In Chapter 4.4, comparisons were made between the findings of this study and dikaryan cell biology, including the onset of transcription/translation, vacuolar activity, resource trafficking, and amoeboid cell development, however the most impactful contributions of this study to fungal evolution will likely come in the future as other authors employ the dataset in more targeted investigations.

However, the discovery of the apophysis as a distinct subcellular structure characterized by intensive intracellular trafficking and delineated from the cell body by a chitinous pseudo-septum raises immediate implications for fungal evolution (Figure 4.9). Hyphal septation and division of labour are key innovations associated with multicellularity in dikaryan evolution (Berbee et al., 2017; Nagy et al., 2020), however this thesis presents evidence that they, or at least their precursors, are also present in a unicellular chytrid fungus. If so, it is reasonable to suggest by parsimony that they were too present in their last common ancestor. Dedication of a discrete subcellular compartment to membrane trafficking, and its intracellular segregation, may be the precursory condition to hyphal septation and differentiation in dikaryan evolution. Characterization of such differentiation in an extant chytrid not only reiterates the intricacy of the chytrid cell plan but raises the future possibility for chytrids as models in studying the evolution of fungal septation and compartmentalization.

A similar illustration of the sophistication of chytrid development was presented in Chapter 5. Despite being only a subsection of a single cell, rhizoid development was shown to function analogously to large multicellular dikaryan fungi in morphometric complexity and adaptability. Most striking in this regard was the simultaneous display of



both feeding and searching rhizoids during interaction with particulate carbon, demonstrating spatial differentiation and division of labour within the unicellular chytrid rhizoidal system (Figure 5.12). These results not only again validate the previously hidden complexity of chytrid development but reveal that multicellularity is not required for spatial differentiation in fungi. The highly sophisticated capabilities of rhizoids uncovered by this chapter imply by parsimony that they were too present in the last common ancestor of branching fungi. These data support the proposal that rhizoids, or rhizoid-like structures, were the evolutionary precursors to dikaryan hyphae and solidify the role of chytrids as models in hyphal evolution.

### **6.3 Limitations of this thesis**

While this thesis has made important contributions to the fields of chytrid cell and developmental biology, it is not without limitations. The first constraints that must be addressed are the drawbacks of working with *R. globosum* as a model for chytrid biology generally. While *R. globosum* is still an ideal candidate model for chytrid development and possesses an annotated genome, its major drawback is its current lack of genetic tractability limiting our current scope in potential experiments and toolkit components. Only one chytrid at time of writing, *Spizellomyces punctatus*, has been genetically transformed (Medina et al., 2020), which shed light on actin organization and nuclear dynamics. The genetic tractability of *S. punctatus* will undoubtedly yield more important findings in chytrid cell biology, but the rapid archetypal life cycle of *R. globosum* and experimental amenability still places it as a forerunner model system for chytrid developmental biology. Future directions to achieve a transgenic *R. globosum* line are proposed below in Chapter 6.4. Additionally, the use of any single species, archetypal or otherwise, cannot fully be representative of the entirety of chytrid diversity so caution should be placed in overgeneralization. Only through broader investigation can the universality of these findings be confidently asserted.

The holistic approach taken in Chapter 4 was successful in identifying key overarching themes characterizing the chytrid life cycle. However, such a comprehensive approach naturally comes at the expense of a detailed understanding of any individual process. This was partly remedied by targeted investigations into processes of interest (lipid metabolism, apophysis trafficking, and zoospore development), but certain findings were only superficially described (e.g the nature of the cell cycle or changes in mitochondrial structure). It is also important to recognize that the four discrete life stages chosen for this study cannot fully represent the entire continuity of the life cycle and the intervals between could only be filled by extrapolation. As a result, some biological processes have undoubtedly been missed. Likewise, certain dynamic processes (e.g endocytotic engulfment) uncovered from electron microscopy reconstructions could only be inferred from static images. Even so, these results have shed light on previously unknown drivers of the chytrid life cycle and generated major avenues for further investigation.

The novel combination of 3D/4D confocal microscopy and reconstruction by neuron tracing in Chapter 5 (Figure 5.4) provided a robust contribution towards understanding rhizoid development. However, a shortcoming of this approach was a lack of understanding of the genetics underpinning rhizoid development. Hyphal developmental studies using model dikaryans such as *Neurospora crassa* have long used genetic knockouts and transformation to identify genes associated with hyphal morphogenesis (Riquelme et al., 2018; Watters et al., 2011). Although this was not attempted in this thesis, such manipulation would have been wasted without an appropriate methodology for morphometric quantification. The protocol developed by this thesis will lay a solid foundation for future investigations into the genetic underpinnings of rhizoid development. Finally, an unfortunate reality of imaging chytrid rhizoids relative to developing hyphae is their small size, making subcellular tip architecture difficult to resolve. Organization of the hyphal tip is central to understanding mycelial development (Riquelme et al., 2018), however at ~200 nm in width the chytrid rhizoid is too small to resolve subcellular structures with standard light microscopy. Even with transmission

electron microscopy no rhizoid tip was found. Therefore, while a good understanding of rhizoid development was achieved in total, this work did not shed light on the architecture of the rhizoid tip.

#### **6.4 Future directions**

The most pressing future work needed to build on the findings of this thesis will be an expansion of the *R. globosum* experimental toolkit to solidify its place as a model for chytrid development. First and foremost will be the genetic transformation of *R. globosum*. This should first be attempted by the application (and modification, if necessary) of the agrobacterium-mediated transformation developed by Medina and colleagues (Medina et al., 2020). If this does not prove fruitful, electroporation protocols have been optimized for chytrid zoospores (Swafford et al., 2020) and plasmid delivery by electroporation has been successful in transforming choanoflagellates, close relatives of the chytrids (Booth et al., 2018). These protocols provide immediate routes towards achieving a transgenic *R. globosum* line that will prove invaluable in interrogating protein localization and organelle dynamics during chytrid development.

The broad scale characterization of the chytrid life cycle presented in Chapter 4 has generated abundant avenues for pursuit, too numerous to fully describe here. The depth of pursuit into any individual genetic or cellular marker identified here will depend on the biological aims of the future researchers, but in general dynamic imaging of static subcellular reconstructions would provide a more detailed understanding of structural function. Of note, dynamic imaging of developing zoospores inside the maternal sporangium will be vital to understand the nature of vacuole engulfment and cargo uptake. In addition, genetic manipulation of differentially expressed genes will greatly expand on the findings of this study. For example, the function of individual genes of interest could be better elucidated by knockout and phenotypic characterization, and fluorescent tagging (or in lieu of transgenic capabilities, immunolocalisation) will help identify subcellular

localization of proteins. This approach would be advantageous in resolving the specific components of the lipid metabolic pathway and pinpoint its most important components.

Similarly, genetic knockout of developing rhizoids is the natural next step in rhizoid research, elevating our understanding for their underpinning genetics to a comparable footing with hyphal research. This will be particularly important in direct comparison of genes previously identified to control hyphal morphogenesis, to see if their knockout results in analogous phenotypes. This will be of great evolutionary significance if conserved genes provide identical functions in both hyphal and rhizoidal development. Additionally, future work should aim to better characterize the subcellular architecture of the chytrid rhizoid, particularly the tip. To overcome their small size, the application of super-resolution or electron microscopy will be necessary to resolve their ultrastructure in any detail. Ultrastructural comparison of rhizoids and hyphae could provide insights into the evolution of dikaryan hyphae (as has been similarly done in monoblepharids (Dee et al., 2015)), otherwise missed by overreliance on genomics alone.

## **6.5 Final conclusion**

In conclusion, this thesis has provided an important step forward in chytrid biology. Prior to this work, investigations into chytrid development were largely descriptive and chytrid cell biology was dominated by bioinformatics-only approaches. By focusing on the fundamentals of chytrid development, and coupling cellular phenotypes to molecular analysis, this work has identified overarching drivers of the chytrid life cycle. This will provide a valuable contribution to the understanding of chytrids in the ecological and evolutionary contexts they are most frequently considered, and act as a solid foundation for future investigations in these areas. Despite the natural limitations of this thesis, and the fact that some of these findings will only be truly understood following future research, these results are an important addition to chytrid cell biology. These data have demonstrated just how complex chytrid development can be, and how sophisticated

chytrid behaviour is. Subsequent work will undoubtedly uncover even more secrets held by these enigmatic microbes. The future of chytrid research is exciting.

## Appendices

### Appendix A - Environmental sampling to isolate diatom-chytrid parasites

A tidal mud flat and coastal site (Figure A.1) were sampled regularly to isolate and characterise diatom-parasite interactions within the first year of the project (December 2017-18). This allowed the identification of diatom-parasite interactions from both benthic and planktonic habitats. Both habitats were sampled for DNA extraction and molecular barcoding as well as to subculture viable diatom-protist parasites. Once the samples had been returned to the lab, they were visually inspected for examples of diatom-protist parasitism with a Nikon inverted phase contrast microscope (TMS, Nikon). In addition, 24 well plates containing 2 ml of diatoms listed in Table A.1 were incubated with 20  $\mu$ l of environmental samples in an attempt to induce parasitism in the cultured algae. Single cell isolation was conducted using a flame-pulled 150 mm VOLAC glass Pasteur pipette (D 810, Poulten and Graf) and cells of interest were transferred to 2 ml F/2 wells in a 24 well plate and incubated at 15 °C with a 16:8 light:dark cycle at 30-80  $\mu$ M s<sup>-1</sup> m<sup>-2</sup> irradiance.

**Table A.1. Diatom strains used in environmental co-incubations in an attempt to induce parasitism.**

<b>Species Name</b>	<b>Strain</b>	<b>Genome Reference (<i>not strain specific</i>)</b>	<b>Culture Collection</b>
<i>Achnanthes sp</i>	1095/1	-	Roscoff Culture Collection
<i>Amphora coffeaeformis</i>	PLY 547	-	MBA Culture Collection
<i>Asterionellopsis glacialis</i>	PLY 607	-	MBA Culture Collection
<i>Coscinodiscus granii</i>	PLY 8536	-	MBA Culture Collection
<i>Coscinodiscus sp.</i>	-	-	MBA Culture Collection
<i>Ditylum brightwellii</i>	PLY 897	-	MBA Culture Collection
<i>Nitzschia sp.</i>	RCC 2600	-	Roscoff Culture Collection
<i>Odontella mobiliensis</i>	PLY 618	-	MBA Culture Collection
<i>Odontella sinensis</i>	PLY 8537	-	MBA Culture Collection
<i>Phaeodactylum tricornutum</i>	PLY 100	(Bowler et al., 2008)	MBA Culture Collection
<i>Skeletonema dohrnii</i>	PLY 612	-	MBA Culture Collection
<i>Thalassiosira oceanica</i>	PLY 692	(Lommer et al., 2012)	MBA Culture Collection
<i>Thalassiosira pseudonana</i>	PLY 695	(Armbrust et al., 2004)	MBA Culture Collection
<i>Thalassiosira weissflogii</i>	PLY 541	-	MBA Culture Collection

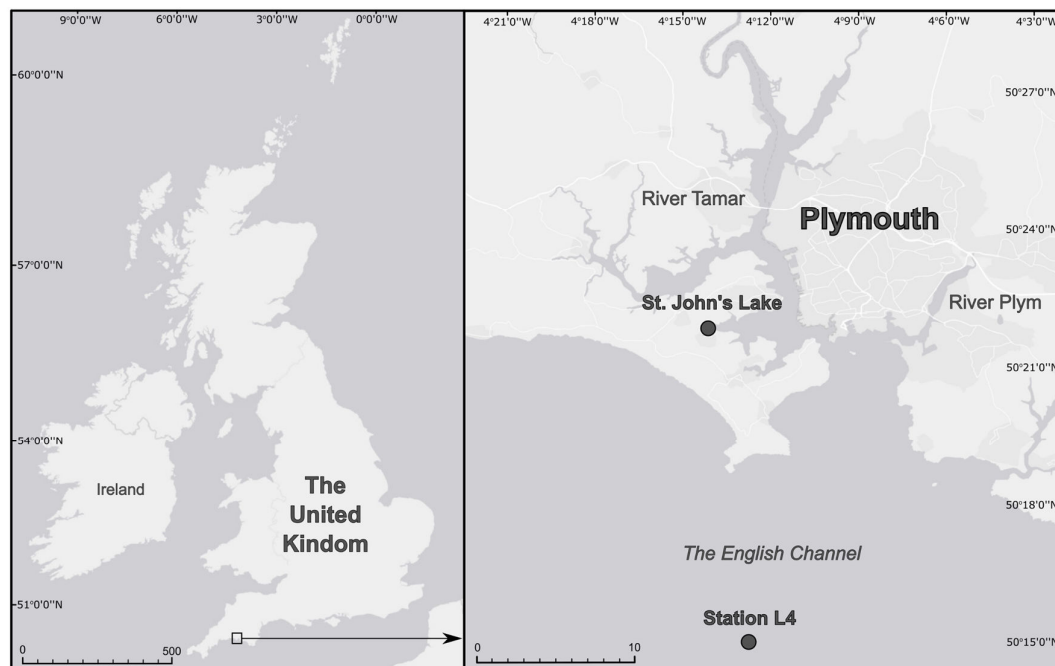


**Figure A.1** Location of the tidal mud flat (St. John's Lake) and coastal (Station L4) sampling sites. Scalebars in kilometres.

The tidal mud flat was located at St. John's Lake, Cornwall UK (50° 21'51.1" N 4° 14' 08.3" W). This station was sampled monthly at low tide between December 2017 and August 2018. The surface of the mud flat was scraped with a disposable inoculation loop and transferred to 2 ml Eppendorf tubes ( $n = 3$ ). Eppendorf tubes were transported back to the laboratory at ~4 °C in a Stratacooler Benchtop Cooler (Agilent, USA) and stored at -20 °C prior to DNA extraction. Sections of the phytobenthos were extracted each month and brought to the laboratory to promote diatom growth and parasite proliferation. This also facilitated weekly subsampling. The upper surface of the mud was excised using a shovel and placed into clip-lid plastic storage containers (13.5 x 13.5 x 5 cm,  $n = 6$ ), giving an exposed phytobenthic area of 182 cm<sup>2</sup>.

These containers were placed into a controlled mesocosm environment (Figure A.2A) associated with a continuously flowing seawater aquarium. This environment consisted of two discrete treatments - Tanks A and B – which approximated the summer conditions of a Northern European mud flat (based on physiochemical data from (Scholz et al., 2016b)) to promote host and parasite growth. Each tank (63.5 x 38.5 x 21.5 cm)



contained  $n = 3$  sediment samples, which were elevated to  $\sim 3$  cm below the surface. Tank A mimicked a gently flowing ( $2 \text{ L min}^{-1}$ ) mud flat and was heated during winter to  $\sim 18 \pm 1$  °C using a Deltatherm Heater 300 W (Interpet, UK). Tank B mimicked a stagnant tidal pool and was left at ambient temperature with no seawater flow. Natural evaporation aerielly exposed portions of the mud surface. Both tanks were exposed to  $30\text{-}70 \mu\text{M s}^{-1} \text{ m}^2$  of overhead light generated by an Aquarium Overhead LED Strip (Luffy Pets, UK). Overall, the phytobenthic sampling efforts from December 2017 to August 2018 failed to yield a single parasitized diatom and were therefore discontinued from August 2018.

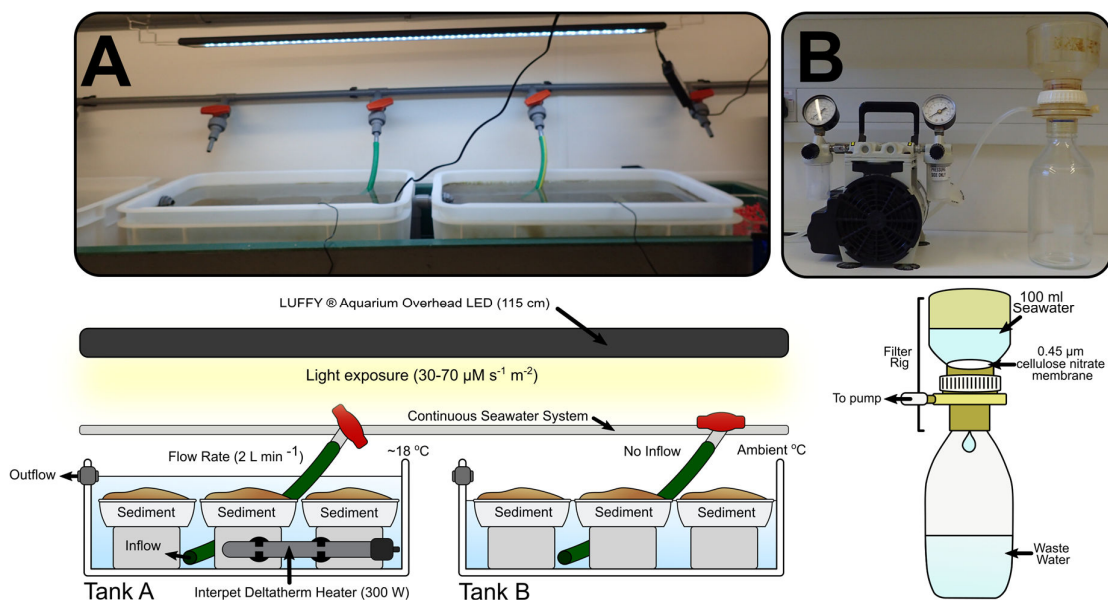


**Figure A.2 Incubation and harvesting of environmental samples.** Photographic (top) and diagrammatic (bottom) representations of the tidal mud flat mesocosm (A) and seawater filter rig (B).

The coastal sampling site was sampled at the Western Channel Observatory Station L4 ( $50^{\circ} 15' \text{ N } 4^{\circ} 13' \text{ W}$ ). The plankton at the site was sampled weekly by a vertical plankton tow using a  $61 \mu\text{m}$  drift net. The net was lowered to depth and retrieved after 10 min. At deck, the samples were washed with a deck hose into the cod end of the net, returned to the laboratory in a dark esky box containing ambient seawater to buffer against large temperature fluctuations, and stored at  $4$  °C prior to processing. Sea surface temperature (SST) and Secchi depth were also recorded. In addition, 100 ml of this

plankton sample was vacuum filtered through a 0.45 µm nitrocellulose membrane (Figure A.2B). Membrane filters were placed into Eppendorf tubes and stored at -20 °C prior to DNA extraction. Sampling began in December 2017 and was terminated in November 2018. These sampling efforts were successful in isolating a stable co-culture of *Chaetoceros* diatoms and an associated thraustochytrid parasite (see Appendix B). However, I was unable to extract and amplify DNA of sufficient quality for downstream environmental analysis from the filters.

## **Appendix B – The impact of a novel selective parasite on the growth dynamics of marine diatoms**

**Published as:** Laundon D, Mock T, Wheeler G, and Cunliffe M. 2021. Healthy herds in the phytoplankton: the benefit of selective parasitism. *ISME J* **15**:2163-2166.

doi:10.1038/s41396-021-00936-8

**Author contributions:** *TM, GW, and MC provided supervision and manuscript feedback.*

*All other experimentation, analysis, and writing was conducted by DL. SEM was conducted by DL at the Plymouth Electron Microscopy Centre (PEMC).*

### **B.1 Summary**

Protist-protist interactions are ubiquitous, yet poorly understood, ecological processes that regulate the structure and function of microbial communities. Of these interactions, parasitism of marine diatoms has major implications on global biogeochemical cycling due to their essential role as primary producers. Environmental DNA sequencing studies have indicated that such interactions are widespread across the global oceans, however, our understanding of the underpinning physiology of diatom-protist parasitism is limited because of the relatively few cultured examples of these systems. Culture-based experiments are therefore vital in gaining a comprehensive understanding of the trophic ecology and the impact of diatom parasitism on biogeochemical cycles in marine systems. Here, the isolation, stable co-culture, and characterisation of a widespread thraustochytrid symbiont (herein designated 'ThrauL4') of the ecologically important diatom *Chaetoceros* is described, including the development of an experimentally tractable pathosystem. These physiological experiments characterise the *Chaetoceros*-ThrauL4 interaction cycle and show that ThrauL4 preferentially targets and thrives on senescent and 'unhealthy' diatom cells. Surprisingly, these results show that the selective targeting of 'unhealthy' diatoms manipulates the overall diatom population to be healthier, revealing the hidden complexities of protist parasitism on marine phytoplankton communities. This study provides support for the 'healthy herd hypothesis' in a protist-protist interaction, a phenomenon typically associated with animal predators and their prey. These results caution against the implicit assumption that protist-protist parasitism is always detrimental

to the host populations and highlight the intricacies of marine protist-protist interactions for future investigations

## **B.2 Introduction**

Spatial and temporal molecular ecology surveys of the global oceans have unveiled widespread protist-protist interactions (De Vargas et al., 2015; Krabberød et al., 2017; Lima-Mendez et al., 2015), the prevalence of which adds to the complexity in our understanding of marine ecosystem structure and biogeochemical functioning (Worden et al., 2015). Due to the poor culturability of marine microbes (Connon and Giovannoni, 2002) and the difficulty in maintaining protist-protist dual cultures, our knowledge of the physiology underpinning these interactions and their ecological ramifications remains poorly understood. Culture-based experiments are therefore vital in gaining a more holistic understanding of how the microbial oceans operate. This is particularly true of parasitism, one of the most prevalent interactions within the plankton (Lima-Mendez et al., 2015) that is assumed to inevitably be of detriment to host populations (Jephcott et al., 2016; Skovgaard, 2014).

Thraustochytrids (Stramenopila; Labyrinthulomycota; Thraustochytrida) are a group of cosmopolitan marine protists (Cavalier-Smith et al., 1994; Fossier Marchan et al., 2018; Leyland et al., 2017; Raghukumar, 2002). Thraustochytrids have been reported from a wide range of marine habitats, ranging from the water column (Damare and Raghukumar, 2008) to sediments (Bongiorni, 2012; Bongiorni et al., 2004; Cathrine and Raghukumar, 2009), hydrothermal vents (Raghukumar et al., 2008), and mangrove forests (Leaño et al., 2001). In these ecosystems, thraustochytrids have established roles in the marine carbon cycle as saprotrophs (Leaño et al., 2001; Damare and Raghukumar, 2008; Phuphumirat, Ferguson and Gleason, 2016,) bacterivores (Raghukumar, 1992), and parasites and pathogens of algae and invertebrates (Jones and O'Dor, 1983; McLean and Porter, 1982; Sathe-Pathak et al., 1993).

Diatoms are among the most ecologically and biogeochemically important photosynthetic organisms on Earth, responsible for ~45 % of marine primary production (Mann, 1999) and one fifth of total primary production worldwide (Nelson et al., 1995),

making diatoms larger contributors to global carbon fixation than all of the terrestrial rainforests combined (Field et al., 1998). Parasitism on diatoms by zoosporic protists therefore has the potential for major biogeochemical impacts, yet this phenomenon remains poorly understood and represents an ecological 'black box' in need of investigation (Scholz et al., 2016a).

Here the isolation and stable co-culture of a globally distributed thraustochytrid diatom symbiont from a coastal marine environment is described. Through culture-based studies, the interaction cycle of the diatom-thraustochytrid symbiosis is characterised, and it is shown that thraustochytrid symbionts preferentially target and feed on unhealthy diatom cells. These results demonstrate that co-culture with thraustochytrids and the resulting targeting of unhealthy diatom cells surprisingly improves the health of the overall diatom population. These results provide evidence of the 'healthy herd hypothesis' in a microbe-microbe symbiosis, an ecological phenomenon characteristically associated with predatory animals. Taken together, these data provide an important step forward into the characterisation of a potentially globally distributed ecological interaction, challenge the assumption that protist parasitism is inexorably negative for the host population as a whole, and lay the foundations for future investigations into the underpinning ecophysiology of diatom-thraustochytrid symbioses.

### **B.3 Methods and materials**

#### ***B.3.1 Isolation and maintenance of the *Chaetoceros-Thraul4* symbiosis***

Epibionts of *Chaetoceros* were first observed in a 61 µm net plankton sample collected at 10:14 BST on the 16<sup>th</sup> July 2018 at Station L4 in the Western English Channel (Figure B.1&2). At the time of sampling, the Secchi Depth was 12 m and the sea surface temperature (SST) was 19.7 °C. This sample was taken from 54.6 m below the surface. Both colonised and non-colonised single *Chaetoceros* chains (approx. 4-5 cells) were isolated by single cell picking under an inverted phase-contrast microscope (TMS, Nikon) at a magnification of 25-400 x using a flame-pulled 150 mm VOLAC glass Pasteur pipette (D 810, Poulten and Graf). Isolated chains were washed at least three times in 0.22 µm-

filtered F/2 medium (Guillard and Ryther, 1962) and transferred to a 24-well plate (83.3922, Sarstedt), with each well containing 2 ml of F/2.

Cells were subsequently grown, isolated, and successively transferred to new wells over 14 d, following treatment with 20  $\mu$ l antibiotic cocktail (working concentration = 100 mg L<sup>-1</sup> penicillin G, 25 mg L<sup>-1</sup> dihydrostreptomycin sulfate and 25 mg L<sup>-1</sup> gentamicin sulfate (Kawachi and Noël, 2005)) for 48 h to prevent bacterial overgrowth. Following antibiotic treatment, cells were transferred to 20 ml F/2, incubated for 7 d, and then diluted again into 35 ml of F/2 in culture flasks (83.3910, Sarstedt). Once stabilised, unparasitized *Chaetoceros* cultures were maintained by transferring 1 ml of 7 d old culture into 35 ml of fresh F/2 media. Parasitized cultures were maintained by transferring 3 ml of *Chaetoceros*-Thraul4 culture (~7-14 d post-inoculation) into 35 ml of 7 d old unparasitized host culture. Cultures of all stages were maintained at 15 °C with a 16:8 light:dark cycle at 30-80  $\mu$ M s<sup>-1</sup> m<sup>-2</sup> irradiance.

A culture of Thraul4 growing without *Chaetoceros* was generated by inoculating 25 ml of EtOH-washed autoclaved pine pollen (PP) suspended in F/2 medium (with 200  $\mu$ g ml<sup>-1</sup> chloramphenicol) with 5 ml of 10 d *Chaetoceros*-Thraul4 co-culture and incubating the culture at 15 °C in the dark to cause the death of concomitant diatoms. Thraul4 temporarily grew attached to PP, however not for longer than ~14 d. For the long-term growth of Thraul4, 5 ml of 6 d Thraul4-PP was transferred to 25 ml Honda's Medium (HM; 2 g L<sup>-1</sup> glucose, 0.2 g L<sup>-1</sup> yeast extract, 0.5 g L<sup>-1</sup> monosodium glutamate in 50 % seawater) (Honda et al., 1998; Rosa et al., 2011)), grown for 7 d and treated with a thraustochytrid-specific antibiotic cocktail optimised from (Rosa et al., 2011) for 48 h (working concentration = 500 mg L<sup>-1</sup> penicillin G, 500 mg L<sup>-1</sup> dihydrostreptomycin sulfate, 30 mg L<sup>-1</sup> chloramphenicol and 50 mg L<sup>-1</sup> kanamycin sulphate). This culture (Thraul4-HM) was maintained by subculture every 14 d into 0.22  $\mu$ m-filtered HM and kept in the dark at 15 °C.

### **B.3.2 DNA extraction, V4 amplicon sequencing, and bioinformatics**

20 ml of *Chaetoceros*-Thraul4 co-culture was centrifuged for 10 min at 4,500 rpm. The resulting pellet (wet weight ~ 400 mg) was resuspended in 500  $\mu$ l of Tris-HCl-EDTA-NaCl

(TEN; 10 mM Tris-Cl, 10 mM EDTA, 150 nM NaCl) buffer, vortexed, and spun down again under the same conditions. The resulting pellet was resuspended in 300 µl of sodium-dodecyl-sulfate extraction buffer (SDS-EB; 2 % SDS, 100 mM Tris-HCl, 400 mM NaCl, 40 mM EDTA) heated to 30 °C, and then incubated at room temperature for 30 min. Following incubation, 350 µl of phenol/chloroform with isoamyl (25:24:1) was added to the lysed cells. The mixture was shaken well, incubated at room temperature for 5 min, and then centrifuged for 5 min at 13,000 rpm. 200 µl of the top layer was extracted and added to 400 µl of ethyl alcohol, mixed, and incubated on ice for 30 min. Following incubation, the mixture was centrifuged for 10 min at 13,000 rpm, the supernatant was removed, and the pellet washed in 1 ml of 70 % ethanol. Finally, the extracted DNA was pelleted by centrifugation for 5 min at 13,000 rpm, the supernatant was removed, and the pellet dried by evaporation. The DNA was resuspended in 50 µl of RNase-treated H<sub>2</sub>O. Extracted DNA was sent to The Integrated Microbiome Resource at Dalhousie University, Canada for amplicon sequencing of the V4 region of the 18 rRNA gene using Illumina MiSeq technology and primers as described in (Comeau et al., 2011).

To generate the parasite OTU from Illumina data, forward and reverse reads were merged, primer sequences removed, and reads quality filtered by truncating to 350 bp using VSEARCH (Rognes et al., 2016). Then, singletons were removed, identical sequences dereplicated, chimeras checked for (none found) and finally OTUs were clustered at 97 % similarity. The V4 OTU of ThrauL4 was positively identified as an unidentified thraustochytrid in the Thraustochytriidae using the BLAST search tool (Altschul et al., 1990). The V4 region was aligned against a curated Labyrinthulomycete reference database (Pan et al., 2017) covering the Thraustochytriidae using MAFFT operating at default parameters (Kato et al., 2013). The alignment was curated and trimmed in AliView (Larsson, 2014). A Maximum Likelihood phylogeny was calculated using RAxML (Stamatakis, 2014) using the GTRCAT model and 1,000 bootstrap replicates. The phylogeny was visualised in FigTree (Andrew Rambaut: [github.com/rambaut/figtree/](https://github.com/rambaut/figtree/)).

To assess the global environmental distribution of ThrauL4, the clustered V4 OTU was searched against the 2014 and 2015 Ocean Sampling Day (Kopf et al., 2015) V4

dataset (Micro B3: [github.com/MicroB3-IS/osd-analysis](https://github.com/MicroB3-IS/osd-analysis)) using BLAST. Sites with matches of at least 97 % query coverage and 99 % percentage identity were considered positive. The Thraul4 V4 region was submitted to GenBank (submission number: SUB8326710).

### ***B.3.3 Fluorescent and electron microscopy of Chaetoceros-Thraul4***

For fluorescent labelling of subcellular structures, 250  $\mu$ l of *Chaetoceros*-Thraul4 co-culture was applied to glass bottom dishes for imaging. Cultures were incubated for 30 min at room temperature in the dark with 16.2  $\mu$ M Hoechst 33342 (to label nuclei), 4.1  $\mu$ M FM 1-43 Dye (to label membranes) and 470 nM Nile Red (NR, to label neutral lipids). Epifluorescent microscopy was conducted under a 63 x oil objective using a Leica Dmi8 microscope. Images were captured using a CMOS Camera (Prime 95B™, Photometrics). Image acquisition settings were: excitation at 395 nm and emission at 435-485 nm for Hoechst 33342; excitation at 470 nm and emission at 500-550 nm for FM 1-43; excitation at 575 nm and 575-615 nm for NR; and DIC. Chlorophyll autofluorescence was excited at 470 nm and detected at 412-448, 495-535, 575-615 and 670-770 nm using a Sp-X filter. Background fluorescence was controlled for by imaging no-stain controls using only the stain solvent DMSO (*not shown*).

For polysaccharide determination, 1 ml of each cell treatment was pipetted onto a 10  $\mu$ m cell strainer (43-50010, pluriSelect) and 1 ml of alcian blue (a stain for acidic polysaccharides) working solution (150  $\mu$ l acetic acid + 4.85 ml H<sub>2</sub>O, with 50 mg alcian blue powder) was added to the drained pellet. Cells were then washed in 20 ml of 30 kDa-filtered seawater and the pellet resuspended in 1 ml of 30 kDa-filtered seawater. Cells were imaged under a 100 x oil immersion lens. For Concanavalin A (ConA; a lectin that binds to  $\alpha$ -mannopyranosyl and  $\alpha$ -glucopyranosyl residues) staining, 960  $\mu$ l of each cell culture was added to 40  $\mu$ l of stock solution of Oregon Green 488 conjugated ConA (final concentration 100  $\mu$ g ml<sup>-1</sup>). ConA was imaged by excitation at 470 nm and emission at 500-550 nm using the same microscope and camera as previously described. Chlorophyll autofluorescence imaged as previously described. Colour DIC images were captured under a 63 x oil objective using a Leica Dmi8 microscope with a CCD camera (DFC7000 T, Leica). Scanning electron microscopy was conducted as in Chapter 5.



### **B.3.4 Quantification of diatom-thraustochyrid growth curves and host range**

To quantify diatom-thraustochyrid growth, 100 µl of sampled cells were diluted 1:10 in seawater and counted using a Sedgewick Raft Counter (02C00415, Pyser SCGI) under a Leica DM1000 (10 x objective). Parasite prevalence was quantified as the percentage of infected cells in the population, where both dead and alive cells were included in the total cell count.

To investigate the growth of ThrauL4 on different phytoplankton species, 3 x 25 ml 14 d ThrauL4-HM cultures were pelleted at 4,700 rpm for 2 min, washed of exogenous carbon in F/2, and resuspended in F/2. 7 d 25 ml phytoplankton cultures ( $n = 3$ ) were inoculated with 3 ml of this suspension and incubated as previously described. Phytoplankton cultures were selected from the Marine Biological Association Culture Collection (<https://www.mba.ac.uk/facilities/culture-collection>) based on current availability. Chosen cultures were the diatoms *Odontella sinensis* 8537, *Ditylum brightwellii* 897 and *Coscinodiscus* sp. and the dinoflagellates *Alexandrium minutum* 669 and *Procentrum minimum* 714. Parasite prevalence was quantified as above.

### **B.3.5 Live-cell imaging of Chaetoceros-ThrauL4 interactions**

The ThrauL4 lifecycle was characterised by DIC time-lapse microscopy. 250 µl of *Chaetoceros*-ThrauL4 co-culture and 500 µl of uncolonized *Chaetoceros* cells were introduced into a glass bottom dish containing 3 ml of 30 kDa-filtered natural sea water and left to settle for 1 h on the microscope stage. Time-lapse experiments were conducted for 24-48 h under a 20 x objective lens using a Leica Dmi8 microscope. Images were captured using a CMOS Camera (Prime 95B™, Photometrics). To prevent thermal and hypoxic stress during the imaging period, the dish was placed into a P-Set 2000 CT stage (PeCon, Germany) where temperature was controlled at 15 °C using an F-25 MC water bath (Julabo, Germany). The dish was covered by an optically clear film (FoilCover, Pecon) which permits gas exchange. The intensity and shutter regime of the transmitted light for DIC was set so that the imaged cells experienced a 16:8 light:dark cycle at 50 µM

s<sup>-1</sup> m<sup>-2</sup> irradiance. Development was imaged at 2.5 min intervals. Proposed life cycles in this study were reconstructed by compiling the results of multiple separate imaging sessions.

### ***B.3.6 The impact of overall *Chaetoceros* population health on *Thraul4* growth***

*Chaetoceros* cultures were exposed to varying levels of thermal stress to generate cultures of varying physiological health. For these experiments, ventilation cap culture flasks (83.3910, Sarstedt) containing 35 ml of F/2 were each inoculated with 1 ml of *Chaetoceros* culture and grown for a further 7 d. Parasitism experiments were conducted at the stationary phase of host growth. The quantum efficiency of photosystem II (Fv/Fm) was quantified using 2 ml of sampled culture with an Aquapen-C (AP100, PSI) as a proxy for culture health. There was no significant difference ( $p > 0.05$ ) in terms of cell density or Fv/Fm between treatments prior to stress treatment. Cultures were then divided into three treatments ( $n = 5$  per treatment): control (maintained at 15 °C, 'healthy'), moderate heat stress (exposure to 30 °C for 1 h, 'stressed') and lethal heat stress (exposure to 55 °C for 1 h, 'dead'). These treatments were optimised from previous, preliminary trials. Cultures were cooled on ice and returned to 15 °C for 30 min prior to inoculation to allow thermal equilibration of the growth medium. The cultures were tested for Fv/Fm prior to inoculation with *Thraul4* to quantify the success of the heat stress treatment on diatoms. Healthy control cells possessed Fv/FM values of 0.46-0.51, stressed cells of 0.30-0.36, and dead cells of 0.00-0.16. Flasks were then inoculated with 3 ml per flask of *Chaetoceros*-*Thraul4* co-cultures and incubated for 3 d prior to quantification.

### ***B.3.7 The role of individual *Chaetoceros* cell health on *Thraul4* colonisation***

To investigate the role of single cell diatom health on *Thraul4* colonisation, individual *Chaetoceros* cells were exposed to stressful laser treatments. 200 µl of 6 d post-inoculated *Chaetoceros*-*Thraul4* co-culture was allowed to settle on glass bottom dishes for 10 min on the stage of a Lecia SP8 confocal and individual cells between 25-45 µm were selected for laser treatment. Cells were divided into three treatments: Healthy (control, no laser stress), Stressed (50 % 488 nm laser power for 30 s, protoplast

structurally intact and chloroplast partially bleached), and Dead (100 % 405 nm and 488 nm laser power for 90 s, total degradation of protoplast structural integrity) (Figure B.1H). Time lapse recording of the cell was then conducted under a 20 x objective lens at 15 s intervals for 30 min using 1 % 488 nm as a light source. Cells not colonised within 30 min were considered not colonised. Chlorophyll autofluorescence was imaged by excitation at 488 nm and emission at 700-800 nm.

### ***B.3.8 The effect of Thraul4 interaction on the health of diatom populations***

500 ml Erlenmeyer flasks containing 250 ml of F/2 media were inoculated with 10 ml of *Chaetoceros* culture and grown for a further 7 d. Parasitism experiments were conducted at the stationary phase of host growth. Large culture volumes were used here to prevent depletion from repeated downstream sampling for Fv/Fm. Flasks were then inoculated with 10 ml of either *Chaetoceros*-Thraul4 co-culture (parasitized treatment,  $n = 5$ ) or control *Chaetoceros* culture (control treatment,  $n = 5$ ).

Flasks were cultured at 15 °C on a 18:6 light:dark cycle under an irradiance of 60-70  $\mu\text{M s}^{-1} \text{m}^{-2}$  and rotated daily to allow homogenous growth conditions for all treatments. Only cells with a visible intact protoplast were counted for the total population density. There was no significant difference ( $p > 0.05$ ) in terms of cell density or Fv/Fm between treatments prior to inoculation. This experiment ran for 19 d. Cultures were sampled for diatom density, Fv/Fm as a proxy for culture health, and parasite prevalence daily.

### ***B.3.9 Data analysis and statistics***

Differences in parasite growth parameters between healthy, stressed, and dead diatom populations were assessed using analysis of variance (ANOVA) testing. Differences in growth dynamics between control and parasitized diatom populations were evaluated using Welch's  $t$ -tests for each time point. Shapiro-Wilk and Levene's tests were used to assess normality and homogeneity of variance respectively. If these assumptions could not be met, then Wilcoxon Rank Sum was used as a nonparametric alternative. All data were analysed using R version 3.5.1 implemented in RStudio v1.1.456.

## B.4 Results

### ***B.4.1 Isolation of a globally distributed thraustochytrid symbiont of marine diatoms***

A heterotrophic protist was observed and isolated from a summer diatom bloom sampled at the Western Channel Observatory Station L4 in the English Channel (Figure B.1-3).

The protist was found growing epibiotically on senescent and dead *Chaetoceros* chains.

Isolation efforts achieved stable cultures of both unaffected host diatoms and the co-

culture of the protist growing associated with *Chaetoceros*. Sequencing of the V4 region of the 18S rRNA gene amplified from the co-culture placed the epibiont in the thraustochytrid family Thraustochytriidae. The epibiont was subsequently assigned the working name

'ThrauL4'. Alignment of the ThrauL4 V4 18S rRNA gene sequence against reference

Thraustochytriidae sequences revealed ThrauL4 to be most closely related to the clade

'LAB17' described by (Pan et al., 2017), a clade composed solely of currently uncultured environmental sequences (Figure B.4).



**Figure B.1** ThrauL4 was originally observed in environmental samples. Images of *Chaetoceros*-ThrauL4 (inset) observed amongst environmental plankton samples.

Arrowheads show the epibiotic thalli of ThrauL4. Images taken from samples fixed in 2.5 % formaldehyde. Main scale bars = 50  $\mu$ m. Inset scale bars = 10  $\mu$ m.

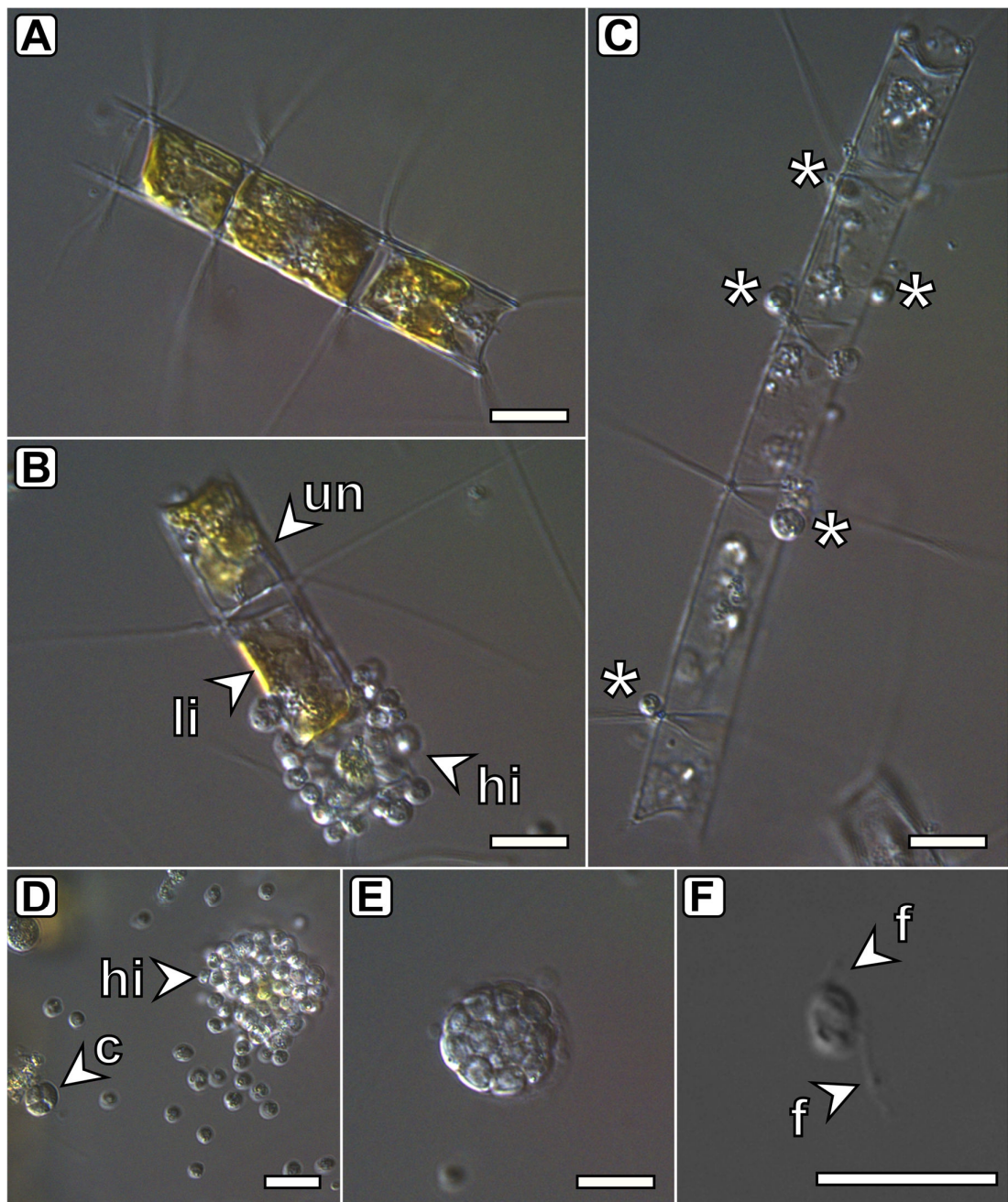


**Figure B.2** Different stages of the interaction cycle of the *Chaetoceros*-ThrauL4 symbiosis. DIC images (A-F) of *Chaetoceros*-ThrauL4 life stages. (A) A healthy *Chaetoceros* chain not associated with thraustochytrids. (B) Three *Chaetoceros* cells exhibiting different stages of ThrauL4 associations. From top to bottom these cells are uninfected (un), lightly infected (li), and heavily infected (hi). (C) Thraustochytrid thalli epibiotically attached to a chain of dead, empty diatom frustules. (D) A heavily infected cell (hi) pictured next to a cleaving, reproducing thraustochytrid thallus (c). (E) A putative

sporangial structure, probably produced by ThrauL4. (F) A biflagellate zoospore from the ThrauL4 lifecycle. Shown are flagella (f). Scale bars = 10  $\mu$ m.

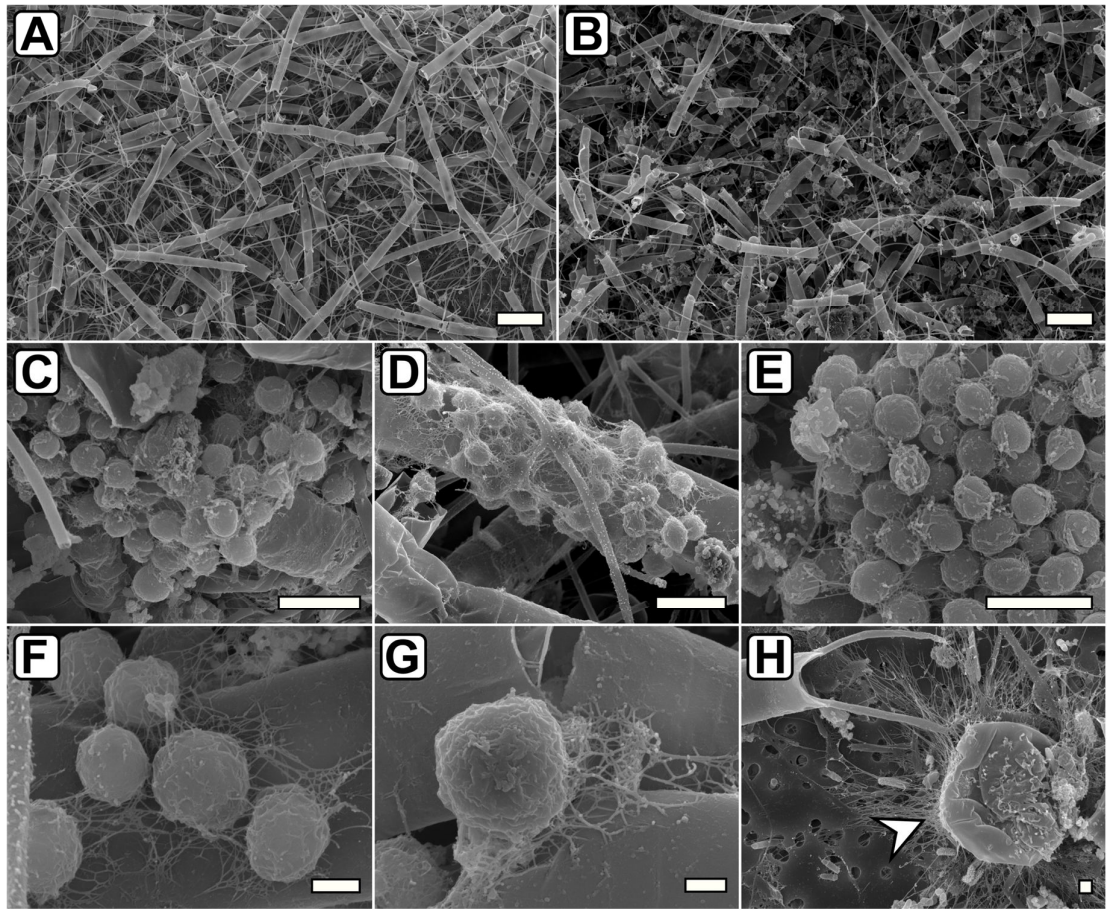


**Figure B.3 Scanning electron micrographs (SEMs) of ThrauL4 thalli attached to *Chaetoceros* diatoms.** Low magnification images of *Chaetoceros* populations not associated (A) and associated with thraustochytrids (B). Scale bars = 10  $\mu$ m. ThrauL4 thalli epibiotically attached to *Chaetoceros* frustules (C-G). Scale bars = 5  $\mu$ m (C-E) and 1  $\mu$ m (F&G). (H) A putative sporangial structure, probably produced by ThrauL4.

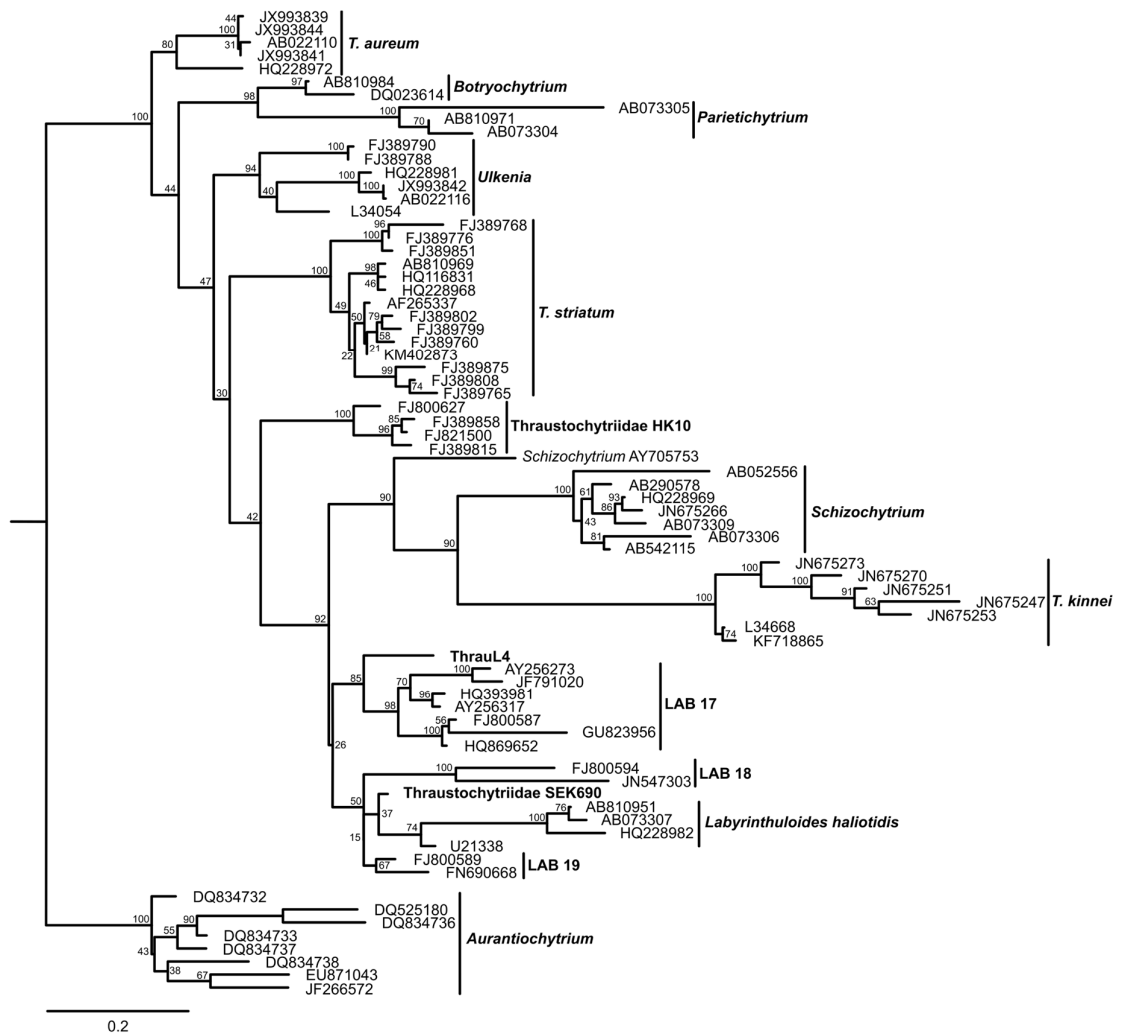


**Figure B.4 ThrauL4 is a thraustochytrid in the Thraustochytriidae associated with the LAB17 clade.** Maximum-likelihood phylogenetic tree of the ThrauL4 V4 18S rRNA gene aligned against Thraustochytriidae reference sequences. Constructed using 1,000 bootstraps. Scale bar = nucleotide substitutions per site.

ThrauL4 was found to be globally distributed in marine coastal waters and detected at 24 sites in the 2014 and 2015 Ocean Sampling Day (OSD) surveys (Figure B.5). The OSD survey sites were distributed across temperate waters in both the Northern and Southern Hemispheres, with most of the detections at sites in Western Europe. The organism was detected in coastal waters (<60 km from the coast) with a temperature distribution of 10.0-24.7 °C and a salinity range of 13.8-40.0 PSU. Over one third of the sites ( $n = 9$ ) were clustered tightly in a single ‘hotspot’ in the North Sea close to the coast of Belgium. The presence of the parasite in the 2014 OSD dataset from the sample site

used in this study, Station L4 (site OSD1), was detected, suggesting that the presence of this organism was not specific to the time of isolation.

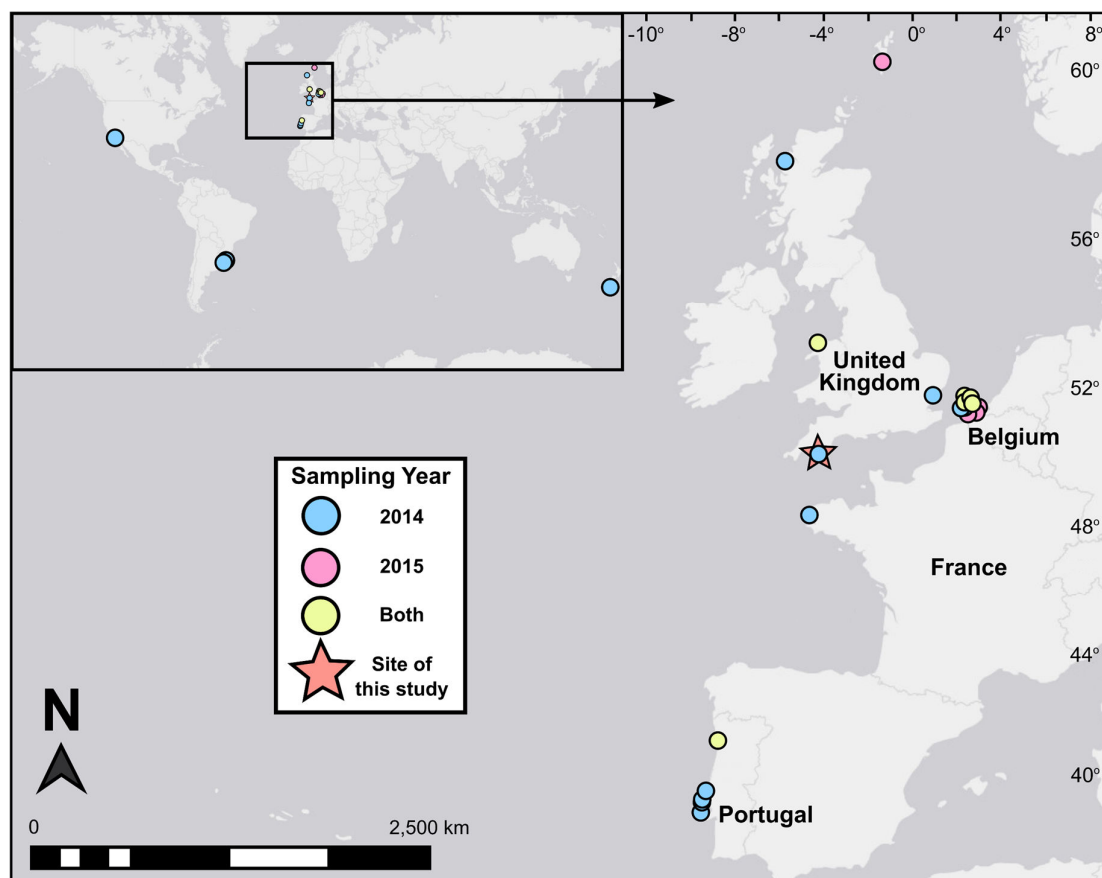


**Figure B.5 Searching of the 2014 and 2015 Ocean Sampling Day dataset for the ThrauL4 V4 sequence revealed the global distribution of this organism.** Positive sites are marked by coloured circles. Inset displays global distribution. Main figure displays higher magnification map of Western Europe where the parasite was most abundant.

#### ***B.4.2 Characterisation of the diatom-thraustochyrid interaction cycle***

Stable *Chaetoceros*-ThrauL4 co-cultures permitted the characterisation of ThrauL4 internal structures (Figure B.6&7) and growth dynamics (Figure B.8). Fluorescent labelling of individual ThrauL4 thalli showed the organism to bear a single nucleus, multiple lipid droplets and to lack chloroplasts. Labelling of swollen and enlarged thalli revealed the presence of multiple nuclei and cytoplasmic division by membrane cleavage (Figure B.6). Cells stained positive for both Concanavalin A (ConA) and Alcian Blue (AB) (Figure B.7), suggesting the presence of extracellular polysaccharides (EPS) in ThrauL4. Optical and



electron microscopy revealed that Thraul4 exists as aggregates associated with individual diatom cells at very high numbers (Figure B.2&3) which can exceed ~30-40 Thraul4 cells per diatom cell.

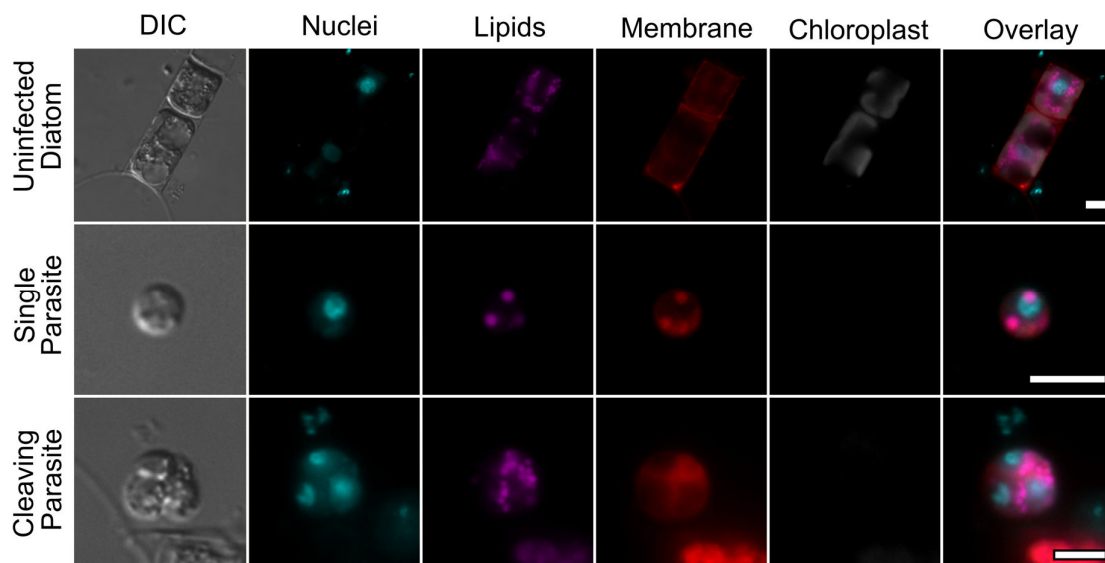


**Figure B.6 Fluorescent labelling of subcellular structures in Thraul4.**

Characterisation of the subcellular structures in different stages of the *Chaetoceros*-Thraul4 symbiosis. Note there is some coexcitation of labelled lipids in the membrane channel. Scale bars = 5  $\mu\text{m}$ .

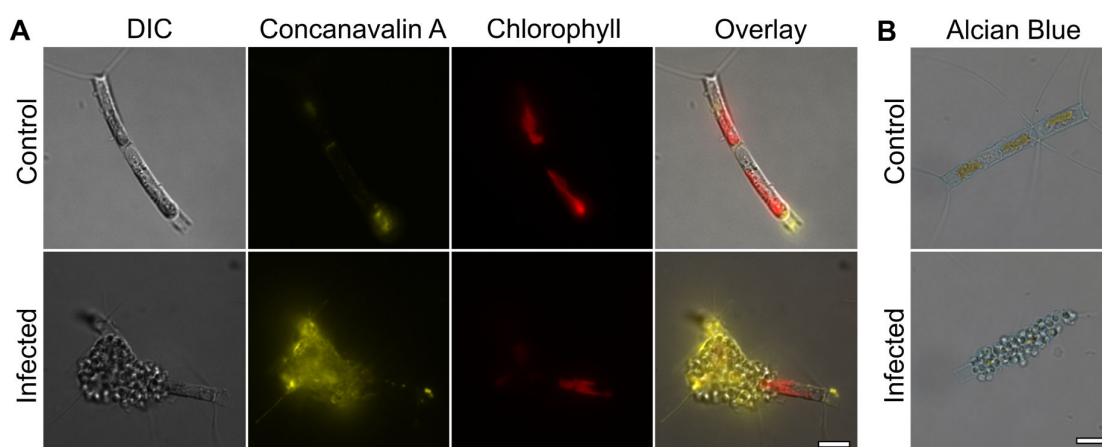


**Figure B.7 Extracellular polysaccharides (EPS) where identified associated with Thraul4.** EPS components of Thraul4 were identified by staining with 100  $\mu\text{g ml}^{-1}$  Oregon Green 488 conjugated Concanavalin A (A) and 10  $\text{mg ml}^{-1}$  Alcian Blue solution (B). Scale bars = 10  $\mu\text{m}$ .

ThrauL4 had a wide host range and grew on a selection of diatoms species, but not the tested dinoflagellates (Figure B.8A). ThrauL4 began to grow when *Chaetoceros* cells had ceased exponential growth and entered the stationary growth phases (Figure B.8B), particularly when *Chaetoceros* cell mortality exceeded division. Observations by time lapse microscopy revealed the dynamic nature of the diatom-ThrauL4 interaction (Figure B.8C). Initially, diatom cells were colonised by ~1-3 thraustochytrid thalli as a result of zoospore settlement. Diatom cells lysed rapidly following ThrauL4 colonisation, which in turn attracted swarms of new thraustochytrid cells. The swarm remained attached to the frustule, presumably consuming the organic matter from the diatom. Multiplication by cleavage of thraustochytrid cells attached to diatom frustules was also observed. Following a period of putative feeding, most of the thraustochytrid cells dispersed leaving behind the empty, cleaned diatom frustule. It appeared as if ThrauL4 targeted cells of poor health, identified by cytoplasmic blebbing prior to colonisation (Figure B.8C), which merited further investigation.

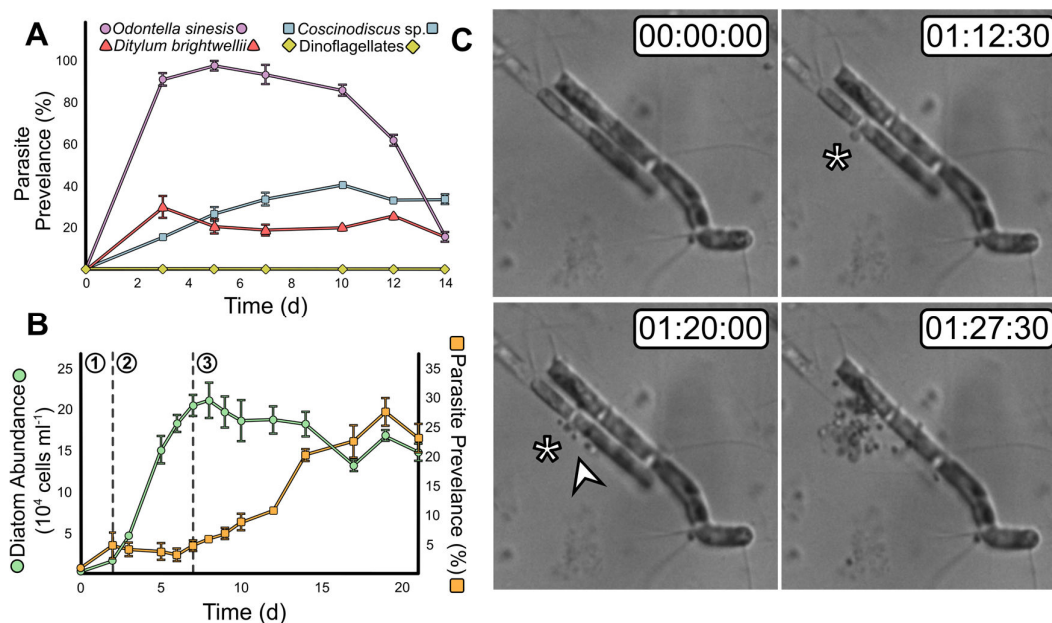


**Figure B.8 Isolation of ThrauL4 allowed the characterisation of the parasite life cycle.** (A) ThrauL4 growth dynamics on a selected range of diatoms and dinoflagellates (*Alexandrium minutum* and *Prorocentrum minimum*) ( $\pm$ SE,  $n = 3$ ). (B) *Chaetoceros* growth with ThrauL4 ( $\pm$ SE,  $n = 5$ ). Dashed lines demarcate the lag (1), exponential (2) and stationary (3) phases of *Chaetoceros* growth. (C) Time-lapse of *Chaetoceros*-ThrauL4

showing ThrauL4 colonising unhealthy cells. Asterisk = cytoplasmic bleb from unhealthy diatom. Arrowhead = initial thraustochytrid colonisation. Timestamp = HH:MM:SS

### B.4.3 Thraustochytrids preferentially target unhealthy diatom cells

Given the putative targeting of unhealthy diatoms by ThrauL4, this hypothesis was tested using population-level ecophysiology experiments. When introduced to heat-stressed diatom populations, ThrauL4 had a higher fitness (i.e. became more abundant) and infected more *Chaetoceros* cells when exposed to stressed and dead diatoms compared to healthy diatoms (Figure B.9A&B), confirming more optimal growth amongst unhealthy diatom populations. This was also demonstrated at the single cell level using laser-damaged individual cells and time lapse microscopy (Figure B.9C&D). 80 % of stressed cells and 60 % of dead cells were colonised by ThrauL4 during the experimental period, whereas not a single healthy control cell was colonised. This supports selective targeting of unhealthy diatom cells at the single cell level by ThrauL4. The *Chaetoceros*-ThrauL4 interaction cycle revealed from these experiments is diagrammatically summarised in Figure B.9E.

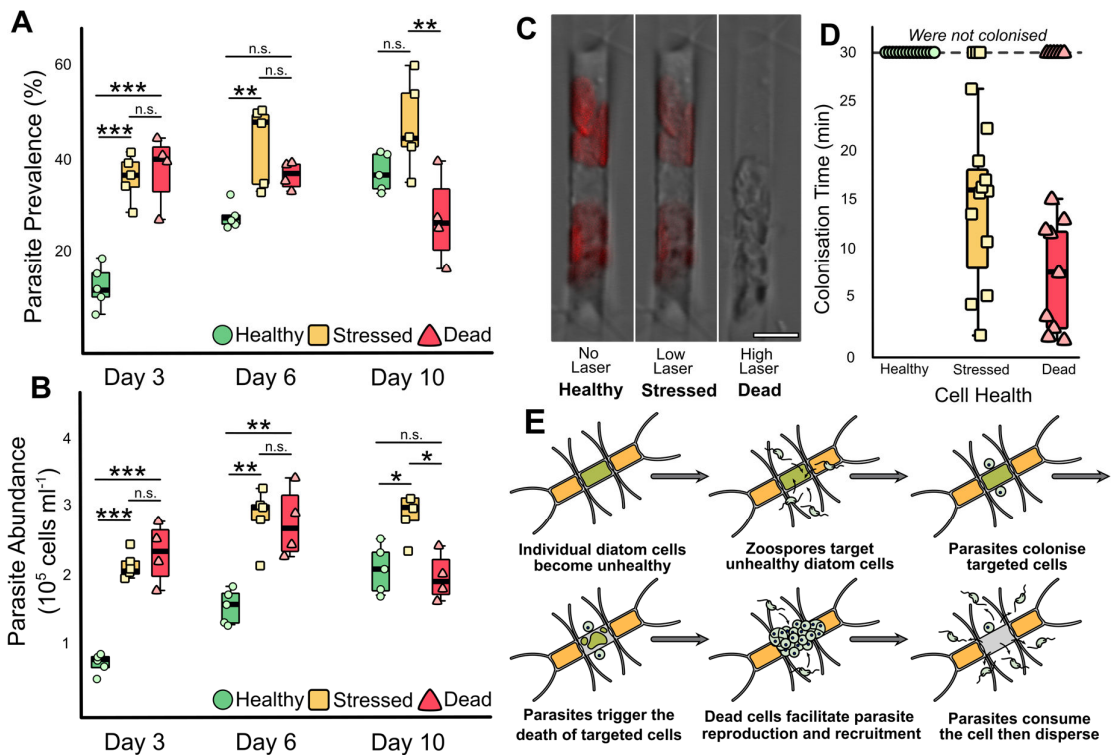


**Figure B.9 Thraustochytrids preferentially target unhealthy diatom cells. (A&B)**

Difference in the abundance (A) and prevalence (B) of parasites in healthy (control), stressed, and dead *Chaetoceros* populations ( $n = 5$ ) inoculated with ThrauL4 following heat stress exposure. n.s  $p > 0.05$  (not significant), \* $p < 0.05$ , \*\* $p < 0.01$ , \*\*\* $p < 0.001$ . (C) Example diatom exposed to different laser powers used to generate individual *Chaetoceros* cells of varying health. Red channel overlay demarks chlorophyll autofluorescence. Scale bar = 5  $\mu\text{m}$ . (D) Time taken for individual diatom cells ( $n = 15$ ) exposed to varying laser treatments to be colonised by ThrauL4. (E) Diagrammatic representation of the proposed diatom-thraustochytrid interaction cycle.

**B.4.4 Thraustochytrid parasitism increases overall diatom population health**

Once the selective parasitism on unhealthy diatom cells by the thraustochytrid had been demonstrated, the physiological impact of selective thraustochytrid parasitism on host diatom populations was investigated by comparing the dynamics of parasite exposed and non-exposed *Chaetoceros* populations (Figure B.10A-C). Using photosynthetic capacity (Fv/Fm) as a proxy for overall health, after 8 d the parasitized *Chaetoceros* populations were consistently healthier than those in the control non-exposed populations (Figure B.10A). This was associated with a brief decrease in diatom population density (Figure B.10B). The percentage of parasitized cells increased throughout the initial stages of the experiment, before stabilizing at  $32.35 \pm 4.13$  % (mean  $\pm$  SD) (Figure B.10C). In a separate experiment to investigate the role of genotype specificity in ThrauL4 parasitism, a clonal *Chaetoceros* sp. population was generated by single cell picking and exposed to ThrauL4 cultures growing independently from diatoms. Although the clonal population declined in health more rapidly overall, ThrauL4 parasitism also resulted in healthier populations (Figure B.10D&F) suggesting that these results are not an artefact of genotype specificity and succession. These results suggest a major change in the dynamics of parasitized host populations occurred after approximately 8 d. The hypothesised influence of thraustochytrid parasitism on diatom population health is diagrammatically summarised in Figure B.11.

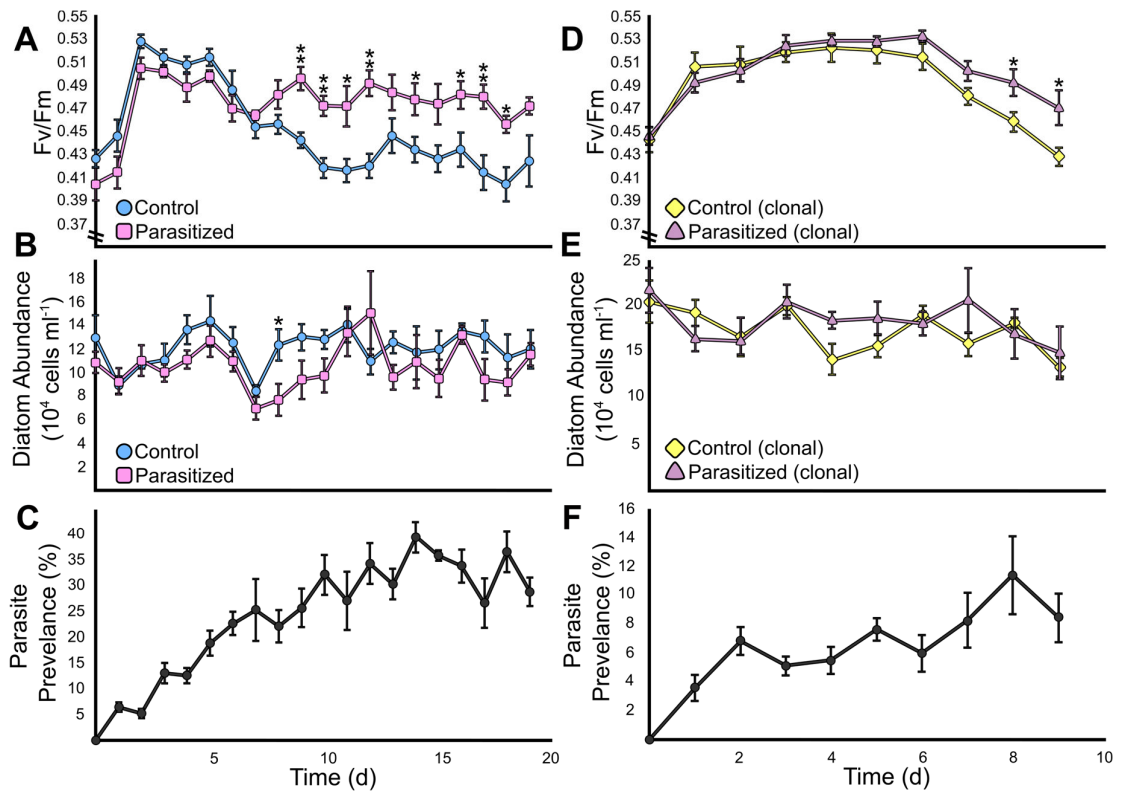


**Figure B.10 Selective targeting of unhealthy diatom cells by thraustochytrids improves the overall health of the diatom population.** (A-C) Population dynamics of the Fv/Fm (A) and total number (B) of stationary *Chaetoceros* diatoms for control and parasitized diatom populations over the experimental period ( $\pm$ SE,  $n = 5$ ). \* $p < 0.05$ , \*\* $p < 0.01$ , \*\*\* $p < 0.001$ . The parasite prevalence did not exceed about a third of the total population (C) ( $\pm$ SE,  $n = 5$ ). Parasites added at 0 d. In a separate experiment (D-F), a clonal *Chaetoceros* population was generated. Population dynamics of the Fv/Fm (D), total number (E), and infection prevalence (F) of stationary *Chaetoceros* diatoms for control and parasitized populations made clonal by single cell picking ( $\pm$ SE,  $n = 5$ ). Significance values as above. Parasites added at 0 d.

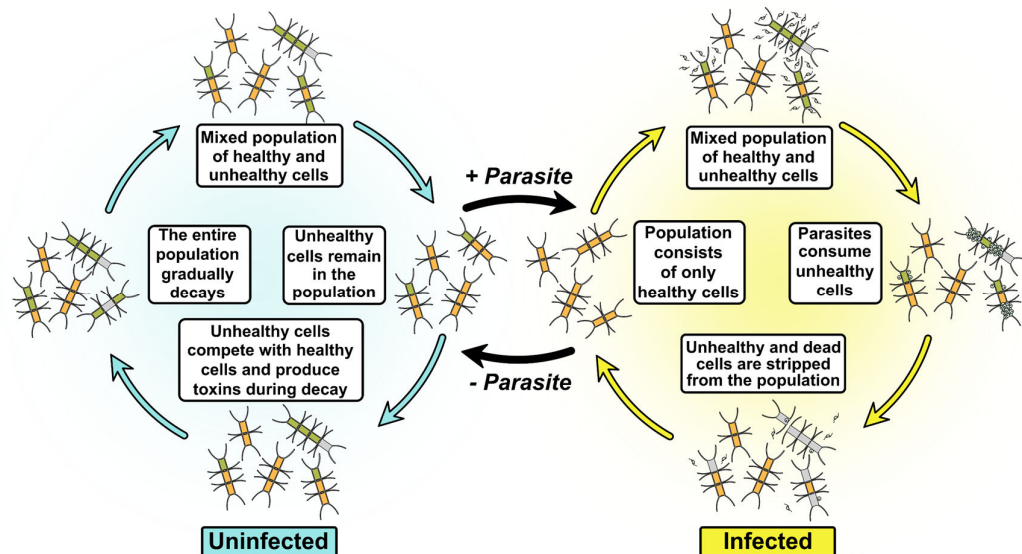


**Figure B.11** This study provides evidence for healthy herd dynamics in a protist-protist interaction. Taken together these results indicate that preferential thraustochytrid parasitism of unhealthy diatoms strengthens the overall health of the population therefore providing evidence for the 'healthy herd hypothesis' in a phytoplankton population, which is summarised diagrammatically here.

### B.5 Discussion

The isolation and stable co-culture of a widespread thraustochytrid parasite of marine diatoms and subsequent culture-based physiology experiments have both provided a major step forward in our understanding of microbial food webs in oceans and highlighted the complexity and unpredictability of microbe-microbe interactions in the plankton. The selective targeting of weak cells, their lysis, and the subsequent swarming and reproduction of cells associated with dead diatoms is indicative of osmoheterotrophic necrotrophy, previously reported in saprotrophic thraustochytrids feeding on dead mangrove leaves (Leaño et al., 2001; Phuphumirat, Ferguson and Gleason, 2016) and seaweeds (Sathe-Pathak et al., 1993). The *Chaetoceros*-ThrauL4 interaction can therefore be described as a necrotrophic parasitic symbiosis (Raghukumar, 2006), given that obligate biotrophic zoosporic parasites of diatoms do not thrive on senescent hosts. Previous environmental sampling efforts of diatom-thraustochytrid interactions have reported that thraustochytrids associate with moribund and dead diatom cells in either a

parasitic or saprotrophic manner (Gaertner, 1979; Raghukumar, 1986; Riemann and Schaumann, 1993), however due the lack of cultured isolates the exact relationship of these symbioses remained speculative. Although data for diatoms was previously lacking, in macroalgae and angiosperms thraustochytrids are typically associated with dead and dying, as opposed to living, matter (Sathe-Pathak, Raghukumar and Raghukumar, 1993; Leaño et al., 2001; Phuphumirat, Ferguson and Gleason, 2016). Indeed, the first description of a thraustochytrid was from the thallus of a moribund alga (Sparrow, 1936; Raghukumar, 2002; Fossier Marchan et al., 2018). It is thought that anti-parasite secondary metabolites synthesised by live hosts inhibit the colonisation and growth of thraustochytrids, a defence which is theoretically lost in senescent hosts (Fossier Marchan et al., 2018; Raghukumar, 2002). There is evidence to support this claim from a seagrass thraustochytrid-system, where thraustochytrids preferentially colonised senescent leaves due to the presence of high concentrations of an antimicrobial flavone glycoside in healthy specimens (Jensen et al., 1998), as well as the inhibition of thraustochytrid growth by phenolic compounds in healthy macroalgae (Raghukumar, 1992). It is therefore possible that similar metabolite synthesis, or yet unknown antifouling defence mechanisms, prevent thraustochytrid parasitism in *Chaetoceros*. The future characterisation of such mechanisms has the potential to shed light on the nature of microbe-microbe host-parasite dynamics in the phytoplankton.

The experimental evidence presented in this study shows that preferential removal of senescent and unhealthy diatoms from the population by thraustochytrid parasitism strengthens the population as a whole. I propose that by selective removal of senescent and dying cells, thraustochytrids relieve diatom-diatom competition for nutrients between unhealthy and healthy cells, which can be a major limiting factor to diatom growth and proliferation (Pinto et al., 2003; Manoylov, 2009). In addition, it is possible that thraustochytrids can 'clean' the population through the removal of dead and dying diatom matter preventing the build-up of toxic waste products or the proliferation of detrimental bacteria in the environment, in an analogous way to how carrion removal by vultures may prevent the spread of contagious diseases to large mammals (Houston and Cooper,

1975) or how invertebrate scavengers reduce the transmission of viruses in host populations (Le Sage et al., 2019).

These results illustrate that the diatom-thraustochytrid interaction provides evidence to support the 'healthy herd hypothesis', an ecological phenomenon traditionally associated with prey-predator interactions in animals (Packer et al., 2003). Like Thraustochytrid, diverse species of megafaunal predators such as lions (Schaller, 1973), mountain lions (Krumm et al., 2010), African wild dogs (Pole et al., 2004), and cougars (Husseman et al., 2003) have been shown to target prey of suboptimal health. The 'healthy herd hypothesis' states that by selective predation on unhealthy prey, predators increase the overall health of the prey population by removing potential carriers of disease and thinning the density of the prey population (Packer et al., 2003). Evidence for 'healthy herd' dynamics where predation generates healthier prey populations has also been demonstrated in sea urchin-lobster (Lafferty, 2004), waterflea-fish (Duffy et al., 2005), and grouse-fox (Hudson et al., 1992) prey-predator systems. Here, analogous supportive evidence from a protist-protist system is provided, which at the population level resembles a pseudo-mutualistic interaction. Such evidence challenges the assumption that phytoplankton-protist parasitism is inevitably detrimental to the host population and places caution in the use of such assumptions in ecosystem modelling or inference from culture-independent surveys (metabarcoding, metagenomes, etc.). These results have illustrated the potential complexity of protist-protist symbioses in the ocean and their ramifications for downstream processes, such as biogeochemical cycling, highlighting the necessity for culture-based experimentation and the future development of co-culture pathosystems in resolving complex ecological interactions.

## **B.6 Conclusion**

The recognition of the impact of protist-protist interactions, especially diatom-protist parasitism, on the ecological functioning and biogeochemical cycling of marine systems has received substantial attention in recent years, although the relatively few cultured representatives of such interactions has prevented their physiological investigation. The isolation of a diatom-thraustochytrid symbiosis in stable co-culture provides an integral



step forward in characterising the ecophysiology underpinning these ecological processes. Thraul4, a globally distributed thraustochytrid, preferentially targets unhealthy diatom cells and subsequently increases the overall health of the diatom population by selective parasitism of the weak. These results provide an analogy to the 'healthy-herd hypothesis' in a protist-protist interaction, which challenges the assumption that phytoplankton-protist parasitism is inevitably detrimental to the host population and places caution in the use of such assumptions in ecosystem modelling or inference from culture-independent surveys. These results have illustrated the potential complexity of protist-protist symbioses in the ocean and their ramifications for downstream processes, highlighting the necessity for culture-based experimentation and the development of co-culture pathosystems in resolving interactions in marine microbial ecology.

## List of abbreviations

- ANOVA - *Analysis Of Variance (test)*
- BBM – *Bold's Basal Medium*
- BF – *Brightfield (microscopy)*
- CFW – *Calcofluor White*
- CLSM - *Confocal Laser Scanning Microscopy*
- DIC - *Differential Interference Contrast (microscopy)*
- DMSO – *Dimethyl sulfoxide*
- FCS – *Foetal Calf Serum*
- LRM – *Lipid-Rumposome-Microbody (complex)*
- LTY – *LysoTracker Yellow*
- MTR – *MitoTracker Red*
- NAG - *N-Acetylglucosamine*
- NR – *Nile Red*
- PBS – *Phosphate Buffered Saline*
- PmTG – *Peptonised milk, Tryptone, Glucose (medium)*
- POM – *Particulate Organic Matter*
- SBF-SEM – *Serial Block Face Scanning Electron Microscopy*
- SEM – *Scanning Electron Microscopy*
- TEM – *Transmission Electron Microscopy*

## References

- Agha R, Saebelfeld M, Manthey C, Rohrlack T, Wolinska J. 2016. Chytrid parasitism facilitates trophic transfer between bloom-forming cyanobacteria and zooplankton (*Daphnia*). *Sci Rep* **6**:1–9. doi:10.1038/srep35039
- Ahrendt SR, Quandt CA, Ciobanu D, Clum A, Salamov A, Andreopoulos B, Cheng JF, Woyke T, Pelin A, Henrissat B, Reynolds NK, Benny GL, Smith ME, James TY, Grigoriev IV. 2018. Leveraging single-cell genomics to expand the fungal tree of life. *Nat Microbiol* **3**:1417–1428. doi:10.1038/s41564-018-0261-0
- Ahrens J, Geveci B, Law C. 2005. Paraview: An end-user tool for large data visualization. *The Visualization Handbook* **717**(8):1-17. doi: 10.1016/B978-012387582-2/50038-1
- Akinwole PO, Lefevre E, Powell MJ, Findlay RH. 2014. Unique odd-chain polyenoic phospholipid fatty acids present in chytrid fungi. *Lipids* **49**:933–942. doi:10.1007/s11745-014-3934-3
- Allen ED, Aiuto R, Sussman AS. 1980. Effects of cytochalasins on *Neurospora crassa* - I. Growth and ultrastructure. *Protoplasma* **102**:63–75. doi:10.1007/BF01276948
- Altschul SF, Gish W, Miller W, Myers EW, Lipman DJ. 1990. Basic local alignment search tool. *J Mol Biol* **215**:403–410. doi:10.1016/S0022-2836(05)80360-2
- Amend A, Burgaud G, Cunliffe M, Edgcomb VP, Ettinger CL, Gutiérrez MH, Heitman J, Hom EFY, Ianiri G, Jones AC, Kagami M, Picard KT, Quandt CA, Raghukumar S, Riquelme M, Stajich J, Vargas-Muñiz J, Walker AK, Yarden O, Gladfelter AS. 2019. Fungi in the marine environment: Open questions and unsolved problems. *MBio* **10**(2):e01189-18. doi:10.1128/mBio.01189-18
- Aramayo R, Selker EU. 2013. *Neurospora crassa*, a model system for epigenetics research. *Cold Spring Harb Perspect Biol* **5**:17921–17922. doi:10.1101/cshperspect.a017921
- Armbrust EV, Berges JA, Bowler C, Green BR, Martinez D, Putnam NH, Zhou S, Allen AE, Apt KE, Bechner M, Brzezinski MA, Chaal BK, Chiovitti A, Davis AK, Demarest MS, Detter JC, Glavina T, Goodstein D, Hadi MZ, Hellsten U, Hildebrand M, Jenkins BD, Jurka J, Kapitonov VV, Kröger N, Lau WWY, Lane TW, Larimer FW, Lippmeier JC, Lucas S, Medina M, Montsant A, Obornik M, Parker MS, Palenik B, Pazour GJ,

- Richardson PM, Ryneerson TA, Saito MA, Schwartz DC, Thamatrakoln K, Valentin K, Vardi A, Wilkerson FP, Rokhsar DS. 2004. The genome of the diatom *Thalassiosira pseudonana*: Ecology, evolution, and metabolism. *Science* **306**:79–86. doi:10.1126/science.1101156
- Arnaud MB, Costanzo MC, Skrzypek MS, Binkley G, Lane C, Miyasato SR, Sherlock G. 2005. The Candida Genome Database (CGD), a community resource for *Candida albicans* gene and protein information. *Nucleic Acids Res* **33**:D358-D363. doi:10.1093/nar/gki003
- Azimzadeh J. 2014. Exploring the evolutionary history of centrosomes. *Philos Trans R Soc B Biol Sci* **369**(1650):20130453. doi:10.1098/rstb.2013.0453
- Bago B, Azcón-Aguilar C, Goulet A, Piché Y. 1998. Branched absorbing structures (BAS): A feature of the extraradical mycelium of symbiotic arbuscular mycorrhizal fungi. *New Phytol* **139**:375–388. doi:10.1046/j.1469-8137.1998.00199.x
- Barr DJS. 2011. *Phlyctochytrium arcticum* n. sp. (Chytridiales); morphology and physiology. *Can J Bot* **48**:2279–2283. doi:10.1139/B70-330
- Barr DJS. 1986. *Allochytridium expandens* Rediscovered: Morphology, Physiology and Zoospore Ultrastructure. *Mycologia* **78**:439–448. doi:10.1080/00275514.1986.12025267
- Barr DJS. 1969. Studies on *Rhizophyidium* and *Phlyctochytrium* (Chytridiales). II Comparative physiology. *Can J Bot* **47**:999–1005. doi:10.1139/b69-140
- Barr DJS, Désaulniers NL. 1988. Precise configuration of the chytrid zoospore. *Can J Bot* **66**:869–876. doi:10.1139/b88-126
- Barr DJS, Hartmann VE. 1976. Zoospore ultrastructure of three *Chytridium* species and *Rhizoclostridium globosum*. *Can J Bot* **54**:2000–2013. doi:10.1139/b76-214
- Bates KA, Clare FC, O’Hanlon S, Bosch J, Brookes L, Hopkins K, McLaughlin EJ, Daniel O, Garner TWJ, Fisher MC, Harrison XA. 2018. Amphibian chytridiomycosis outbreak dynamics are linked with host skin bacterial community structure. *Nat Commun* **9**:1–11. doi:10.1038/s41467-018-02967-w
- Batko A, Hassan SK. 2014. A heliozoan devouring motile chytrid zoospores. *Acta Mycol* **23**:105–106. doi:10.5586/am.1987.004

- Bayne CJ. 1990. Phagocytosis and Non-Self Recognition in Invertebrates. *Bioscience* **40**:723–731. doi:10.2307/1311504
- Beakes GW, Canter HM, Jaworski GHM. 1992. Comparative ultrastructural ontogeny of zoosporangia of *Zygorhizidium affluens* and *Z. planktonicum*, chytrid parasites of the diatom *Asterionella formosa*. *Mycol Res* **96**:1047–1059. doi:10.1016/S0953-7562(09)80115-9
- Beakes GW, Canter HM, Jaworski GHM. 1988. Zoospore ultrastructure of *Zygorhizidium affluens* and *Z. planktonicum*, two chytrids parasitizing the diatom *Asterionella formosa*. *Can J Bot* **66**:1054–1067. doi:10.1139/b88-151
- Belevich I, Joensuu M, Kumar D, Vihinen H, Jokitalo E. 2016. Microscopy Image Browser: A Platform for Segmentation and Analysis of Multidimensional Datasets. *PLoS Biol* **14**:e1002340. doi:10.1371/journal.pbio.1002340
- Berbee ML, James TY, Strullu-Derrien C. 2017. Early Diverging Fungi: Diversity and Impact at the Dawn of Terrestrial Life. *Annu Rev Microbiol* **71**:41–60. doi:10.1146/annurev-micro-030117-020324
- Berger L, Hyatt AD, Speare R, Longcore JE. 2005. Life cycle stages of the amphibian chytrid *Batrachochytrium dendrobatidis*. *Dis Aquat Organ* **63**(1):51-63. doi:10.3354/dao068051
- Bertozzini E, Galluzzi L, Penna A, Magnani M. 2011. Application of the standard addition method for the absolute quantification of neutral lipids in microalgae using Nile red. *J Microbiol Methods* **87**:17–23. doi:10.1016/j.mimet.2011.06.018
- Bewick AJ, Hofmeister BT, Powers RA, Mondo SJ, Grigoriev IV, James TY, Stajich JE, Schmitz RJ. 2019. Diversity of cytosine methylation across the fungal tree of life. *Nat Ecol Evol* **3**:479–490. doi:10.1038/s41559-019-0810-9
- Bleichrodt RJ, Hulsman M, Wösten HAB, Reinders MJT. 2015. Switching from a unicellular to multicellular organization in an *Aspergillus niger* hypha. *MBio* **6**(2):e00111-15. doi:10.1128/mBio.00111-15
- Bleichrodt RJ, van Veluw GJ, Recter B, Maruyama JI, Kitamoto K, Wösten HAB. 2012. Hyphal heterogeneity in *Aspergillus oryzae* is the result of dynamic closure of septa by Woronin bodies. *Mol Microbiol* **86**:1334–1344. doi:10.1111/mmi.12077

- Bligh EG, Dyer WJ. 1959. A rapid method of total lipid extraction and purification. *Can J Biochem Physiol* **37**:911–917. doi:10.1139/o59-099
- Boddy L. 1999. Saprotrophic cord-forming fungi: meeting the challenge of heterogeneous environments. *Mycologia* **91**:13–32. doi:10.1080/00275514.1999.12060990
- Bongiorni L. 2012. Thraustochytrids, a neglected component of organic matter decomposition and food webs in marine sediments. *Prog Mol Subcell Biol* **53**:1–13. doi:10.1007/978-3-642-23342-5\_1
- Bongiorni L, Pignataro L, Santangelo G. 2004. Thraustochytrids (fungoid protist): an unexplored component of marine sediment microbiota. *Sci Mar* **68**:43–48. doi:10.3989/scimar.2004.68s143
- Booth DS, Szmidt-Middleton H, King N. 2018. Transfection of choanoflagellates illuminates their cell biology and the ancestry of animal septins. *Mol Biol Cell* **29**:3026–3038. doi:10.1091/MBC.E18-08-0514
- Boratyn GM, Schäffer AA, Agarwala R, Altschul SF, Lipman DJ, Madden TL. 2012. Domain enhanced lookup time accelerated BLAST. *Biol Direct* **7**:1–14. doi:10.1186/1745-6150-7-12
- Bourett TM, Howard RJ. 1994. Enhanced labelling of concanavalin a binding sites in fungal endomembranes using a double-sided, indirect method. *Mycol Res* **98**:769–775. doi:10.1016/S0953-7562(09)81053-8
- Bowler C, Allen AE, Badger JH, Grimwood J, Jabbari K, Kuo A, Maheswari U, Martens C, Maumus F, Otiillar RP, Rayko E, Salamov A, Vandepoele K, Beszteri B, Gruber A, Heijde M, Katinka M, Mock T, Valentin K, Verret F, Berges JA, Brownlee C, Cadoret JP, Chiovitti A, Choi CJ, Coesel S, De Martino A, Detter JC, Durkin C, Falciatore A, Fournet J, Haruta M, Huysman MJJ, Jenkins BD, Jiroutova K, Jorgensen RE, Joubert Y, Kaplan A, Kröger N, Kroth PG, La Roche J, Lindquist E, Lommer M, Martin-Jézéquel V, Lopez PJ, Lucas S, Mangogna M, McGinnis K, Medlin LK, Montsant A, Secq MPO Le, Napoli C, Obornik M, Parker MS, Petit JL, Porcel BM, Poulsen N, Robison M, Rychlewski L, Rynearson TA, Schmutz J, Shapiro H, Siaut M, Stanley M, Sussman MR, Taylor AR, Vardi A, Von Dassow P, Vyverman W, Willis A, Wyrwicz LS, Rokhsar DS, Weissenbach J, Armbrust EV, Green BR, Van De Peer Y, Grigoriev

- IV. 2008. The *Phaeodactylum* genome reveals the evolutionary history of diatom genomes. *Nature* **456**:239–244. doi:10.1038/nature07410
- Boyle D, Hyatt A, Daszak P, Berger L, Longcore J, Porter D, Hengstberger S, Olsen V. 2003. Cryo-archiving of *Batrachochytrium dendrobatidis* and other chytridiomycetes. *Dis Aquat Organ* **56**:59–64. doi:10.3354/dao056059
- Brambl RM, Van Etten JL. 1970. Protein synthesis during fungal spore germination. V. Evidence that the ungerminated conidiospores of *Botryodiplodia theobromae* contain messenger ribonucleic acid. *Arch Biochem Biophys* **137**:442–452. doi:10.1016/0003-9861(70)90461-3
- Braun A. 1856. Über Chytridium, eine Gattung einzelliger Schmarotzergewächse auf Algen und Infusorien. *Königl. Akademie der Wissenschaften*.
- Brown SP, Olson BJSC, Jumpponen A. 2015. Fungi and Algae Co-Occur in Snow: An Issue of Shared Habitat or Algal Facilitation of Heterotrophs? *Arctic, Antarct Alp Res* **47**:729–749. doi:10.1657/AAAR0014-071
- Buck JC, Truong L, Blaustein AR. 2011. Predation by zooplankton on *Batrachochytrium dendrobatidis*: Biological control of the deadly amphibian chytrid fungus? *Biodivers Conserv* **20**:3549–3553. doi:10.1007/s10531-011-0147-4
- Canter HM. 1953. Annotated list of British aquatic chytrids. *Trans Br Mycol Soc* **36**:278–301. doi:10.1016/s0007-1536(53)80023-9
- Canter HM, Lund JWG. 1948. Studies on plankton parasites. I. Fluctuation of the numbers of *Asterionella formosa* Hass. in relation to fungal epidemics. *New Phytol* **47**:238–261. doi:10.1111/j.1469-8137.1948.tb05102.x
- Cardona A, Saalfeld S, Schindelin J, Arganda-Carreras I, Preibisch S. 2012. TrakEM2 Software for Neural Circuit Reconstruction. *PLoS One* **7**:38011. doi:10.1371/journal.pone.0038011
- Carney LT, Lane TW. 2014. Parasites in algae mass culture. *Front Microbiol* **5**(278):1-4. doi:10.3389/fmicb.2014.00278
- Cathrine SJ, Raghukumar C. 2009. Anaerobic denitrification in fungi from the coastal marine sediments off Goa, India. *Mycol Res* **113**:100–109. doi:10.1016/j.mycres.2008.08.009

- Cavalier-Smith T, Allsopp MT, Chao EE. 1994. Thraustochytrids are chromists, not Fungi: 18s rRNA signatures of Heterokonta. *Philos Trans R Soc B Biol Sci* **346**:387–397. doi:10.1098/rstb.1994.0156
- Cerqueira GC, Arnaud MB, Inglis DO, Skrzypek MS, Binkley G, Simison M, Miyasato SR, Binkley J, Orvis J, Shah P, Wymore F, Sherlock G, Wortman JR. 2014. The *Aspergillus* Genome Database: Multispecies curation and incorporation of RNA-Seq data to improve structural gene annotations. *Nucleic Acids Res* **42**(D1):D705-D710. doi:10.1093/nar/gkt1029
- Cherry JM, Hong EL, Amundsen C, Balakrishnan R, Binkley G, Chan, ET, Christie KR, Costanzo MC, Dwight SS, Engel SR, Fisk DG, Hirschman JE, Hitz BC, Karra K, Krieger CJ, Miyasato SR, Nash RS, Park J, Skrzypek MS, Simison M, Weng S, Wong ED (2012). *Saccharomyces* Genome Database: the genomics resource of budding yeast. *Nucleic Acids Research* **40**(D1):D700-D705. doi: 10.1093/nar/gkr1029
- Cole GT. 1986. Models of cell differentiation in conidial fungi. *Microbiol Rev* **50**(2):95-132. doi:10.1128/membr.50.2.95-132.1986
- Comeau AM, Li WKW, Tremblay JÉ, Carmack EC, Lovejoy C. 2011. Arctic ocean microbial community structure before and after the 2007 record sea ice minimum. *PLoS One* **6**(11):e27492. doi:10.1371/journal.pone.0027492
- Comeau AM, Vincent WF, Bernier L, Lovejoy C. 2016. Novel chytrid lineages dominate fungal sequences in diverse marine and freshwater habitats. *Sci Rep* **6**:1–6. doi:10.1038/srep30120
- Connon SA, Giovannoni SJ. 2002. High-throughput methods for culturing microorganisms in very-low-nutrient media yield diverse new marine isolates. *Appl Environ Microbiol* **68**:3878–3885. doi:10.1128/AEM.68.8.3878-3885.2002
- Conway JR, Lex A, Gehlenborg N. 2017. UpSetR: an R package for the visualization of intersecting sets and their properties. *Bioinformatics* **33**(18):2938–2940. doi:10.1093/bioinformatics/btx364
- Czeczuga B, Godlewska A, Kiziewicz B. 2004. Aquatic Fungi Growing on Feathers of Wild and Domestic Bird Species in Limnologically Different Water Bodies. *Pol J Environ Stud* **13**(1):21-31.



- Dalley NE, Sonneborn DR. 1982. Evidence that *Blastocladiella emersonii* zoospore chitin synthetase is located at the plasma membrane. *Biochim Biophys Acta - Biomembr* **686**:65–76. doi:10.1016/0005-2736(82)90152-3
- Damare V, Raghukumar S. 2008. Abundance of thraustochytrids and bacteria in the equatorial Indian Ocean, in relation to transparent exopolymeric particles (TEPs). *FEMS Microbiol Ecol* **65**:40–49. doi:10.1111/j.1574-6941.2008.00500.x
- Davis WJ, Picard KT, Antonetti J, Edmonds J, Fults J, Letcher PM, Powell MJ. 2018. Inventory of chytrid diversity in two temporary forest ponds using a multiphasic approach. *Mycologia* **110**:811–821. doi:10.1080/00275514.2018.1510725
- De Vargas C, Audic S, Henry N, Decelle J, Mahé F, Logares R, Lara E, Berney C, Le Bescot N, Probert I, Carmichael M, Poulain J, Romac S, Colin S, Aury JM, Bittner L, Chaffron S, Dunthorn M, Engelen S, Flegontova O, Guidi L, Horák A, Jaillon O, Lima-Mendez G, Lukeš J, Malviya S, Morard R, Mullet M, Scalco E, Siano R, Vincent F, Zingone A, Dimier C, Picheral M, Searson S, Kandels-Lewis S, Acinas SG, Bork P, Bowler C, Gorsky G, Grimsley N, Hingamp P, Iudicone D, Not F, Ogata H, Pesant S, Raes J, Sieracki ME, Speich S, Stemmann L, Sunagawa S, Weissenbach J, Wincker P, Karsenti E, Boss E, Follows M, Karp-Boss L, Krzic U, Reynaud EG, Sardet C, Sullivan MB, Velayoudon D. 2015. Eukaryotic plankton diversity in the sunlit ocean. *Science* **348**(6237):1261605. doi:10.1126/science.1261605
- Dee JM, Mollicone M, Longcore JE, Roberson RW, Berbee ML. 2015. Cytology and molecular phylogenetics of Monoblepharidomycetes provide evidence for multiple independent origins of the hyphal habit in the Fungi. *Mycologia* **107**:710–728. doi:10.3852/14-275
- Dee JM, Landry BR, Berbee ML. 2019. Actin guides filamentous rhizoid growth and morphogenesis in the zoosporic fungus *Chytrium hyalinus*. *Mycologia* **111**:904–918. doi:10.1080/00275514.2019.1669999
- Doggett MS, Porter D. 1996. Sexual reproduction in the fungal parasite, *Zygorhizidium planktonicum*. *Mycologia* **88**:720–732. doi:10.1080/00275514.1996.12026709
- Dogma IJ. 1969. Observations on some cellulosic chytridiaceous fungi. *Arch Mikrobiol* **66**:203–219. doi:10.1007/BF00412053

- Dorward DW, Powell MJ. 1983. Cytochemical Detection of Polysaccharides and the ultrastructure of the Cell Coat of Zoospores of *Chytrium aureus* and *Chytrium hyalinus*. *Mycologia* **75**:209–220.  
doi:10.1080/00275514.1983.12021657
- Duffy MA, Hall SR, Tessier AJ, Huebner M. 2005. Selective predators and their parasitized prey: Are epidemics in zooplankton under top-down control? *Limnol Oceanogr* **50**:412–420. doi:10.4319/lo.2005.50.2.0412
- Duo Saito RA, Connell L, Rodriguez R, Redman R, Libkind D, de Garcia V. 2018. Metabarcoding analysis of the fungal biodiversity associated with Castaño Overa Glacier – Mount Tronador, Patagonia, Argentina. *Fungal Ecol* **36**:8–16.  
doi:10.1016/j.funeco.2018.07.006
- Eitzen G, Wang L, Thorngren N, Wickner W. 2002. Remodeling of organelle-bound actin is required for yeast vacuole fusion. *J Cell Biol* **158**:669–679.  
doi:10.1083/jcb.200204089
- El Ghaouth A, Arul J, Wilson C, Benhamou N. 1994. Ultrastructural and cytochemical aspects of the effect of chitosan on decay of bell pepper fruit. *Physiol Mol Plant Pathol* **44**:417–432. doi:10.1016/S0885-5765(05)80098-0
- Ellison AR, DiRenzo GV, McDonald CA, Lips KR, Zamudio KR. 2017. First in vivo *Batrachochytrium dendrobatidis* transcriptomes reveal mechanisms of host exploitation, host-specific gene expression, and expressed genotype shifts. *G3 Genes, Genomes, Genet* **7**:269–278. doi:10.1534/g3.116.035873
- Faktorová D, Nisbet RER, Fernández Robledo JA, Casacuberta E, Sudek L, Allen AE, Ares M, Aresté C, Balestreri C, Barbrook AC, Beardslee P, Bender S, Booth DS, Bouget FY, Bowler C, Breglia SA, Brownlee C, Burger G, Cerutti H, Cesaroni R, Chiurillo MA, Clemente T, Coles DB, Collier JL, Cooney EC, Coyne K, Docampo R, Dupont CL, Edgcomb V, Einarsson E, Elustondo PA, Federici F, Freire-Beneitez V, Freyria NJ, Fukuda K, García PA, Girguis PR, Gomaa F, Gornik SG, Guo J, Hampl V, Hanawa Y, Haro-Contreras ER, Hehenberger E, Highfield A, Hidakawa Y, Hopes A, Howe CJ, Hu I, Ibañez J, Irwin NAT, Ishii Y, Janowicz NE, Jones AC, Kachale A, Fujimura-Kamada K, Kaur B, Kaye JZ, Kazana E, Keeling PJ, King N, Klobutcher LA,

- Lander N, Lassadi I, Li Z, Lin S, Lozano JC, Luan F, Maruyama S, Matute T, Miceli C, Minagawa J, Moosburner M, Najle SR, Nanjappa D, Nimmo IC, Noble L, Novák Vanclová AMG, Nowacki M, Nuñez I, Pain A, Piersanti A, Pucciarelli S, Pyrih J, Rest JS, Rius M, Robertson D, Ruaud A, Ruiz-Trillo I, Sigg MA, Silver PA, Slamovits CH, Jason Smith G, Sprecher BN, Stern R, Swart EC, Tsaousis AD, Tsy-pin L, Turkewitz A, Turnšek J, Valach M, Vergé V, von Dassow P, von der Haar T, Waller RF, Wang L, Wen X, Wheeler G, Woods A, Zhang H, Mock T, Worden AZ, Lukeš J. 2020. Genetic tool development in marine protists: emerging model organisms for experimental cell biology. *Nat Methods* **17**:481–494. doi:10.1038/s41592-020-0796-x
- Farrer RA, Martel A, Verbrugghe E, Abouelleil A, Ducatelle R, Longcore JE, James TY, Pasmans F, Fisher MC, Cuomo CA. 2017. Genomic innovations linked to infection strategies across emerging pathogenic chytrid fungi. *Nat Commun* **8**:1–11. doi:10.1038/ncomms14742
- Farthing HN, Jiang J, Henwood AJ, Fenton A, Garner T, Daversa DR, Fisher MC, Montagnes DJS. 2020. Microbial grazers can control chytridiomycosis caused by aquatic zoosporic fungi. *bioRxiv* 2020.02.03.931857. doi:10.1101/2020.02.03.931857
- Field CB, Behrenfeld MJ, Randerson JT, Falkowski P. 1998. Primary production of the biosphere: Integrating terrestrial and oceanic components. *Science* **281**:237–240. doi:10.1126/science.281.5374.237
- Fisher MC, Bosch J, Yin Z, Stead DA, Walker J, Selway L, Brown AJP, Walker LA, Gow NAR, Stajich JE, Garner TWJ. 2009. Proteomic and phenotypic profiling of the amphibian pathogen *Batrachochytrium dendrobatidis* shows that genotype is linked to virulence. *Mol Ecol* **18**:415–429. doi:10.1111/j.1365-294X.2008.04041.x
- Fisher MC, Gurr SJ, Cuomo CA, Blehert DS, Jin H, Stukenbrock EH, Stajich JE, Kahmann R, Boone C, Denning DW, Gow NAR, Klein BS, Kronstad JW, Sheppard DC, Taylor JW, Wright GD, Heitman J, Casadevall A, Cowen LE. 2020. Threats posed by the fungal kingdom to humans, wildlife, and agriculture. *MBio* **11**(3):e00449-20. doi:10.1128/mBio.00449-20
- Fossier Marchan L, Lee Chang KJ, Nichols PD, Mitchell WJ, Polglase JL, Gutierrez T. 2018. Taxonomy, ecology and biotechnological applications of thraustochytrids: A

review. *Biotechnol Adv* **36**(1):26-46. doi:10.1016/j.biotechadv.2017.09.003

- Freeman KR, Martin AP, Karki D, Lynch RC, Mitter MS, Meyera AF, Longcore JE, Simmons DR, Schmidt SK. 2009. Evidence that chytrids dominate fungal communities in high-elevation soils. *Proc Natl Acad Sci USA* **106**:18315–18320. doi:10.1073/pnas.0907303106
- Frenken T, Alacid E, Berger SA, Bourne EC, Gerphagnon M, Grossart HP, Gsell AS, Ibelings BW, Kagami M, Küpper FC, Letcher PM, Loyau A, Miki T, Nejstgaard JC, Rasconi S, Reñé A, Rohrlack T, Rojas-Jimenez K, Schmeller DS, Scholz B, Seto K, Sime-Ngando T, Sukenik A, Van de Waal DB, Van den Wyngaert S, Van Donk E, Wolinska J, Wurzbacher C, Agha R. 2017. Integrating chytrid fungal parasites into plankton ecology: research gaps and needs. *Environ Microbiol* **19**:3802–3822. doi:10.1111/1462-2920.13827
- Fritz-Laylin LK, Lord SJ, Mullins RD. 2017. WASP and SCAR are evolutionarily conserved in actin-filled pseudopod-based motility. *J Cell Biol* **216**:1673–1688. doi:10.1083/jcb.201701074
- Gachet Y, Hyams JS. 2005. Endocytosis in fission yeast is spatially associated with the actin cytoskeleton during polarised cell growth and cytokinesis. *J Cell Sci* **118**:4231–4242. doi:10.1242/jcs.02530
- Gaertner A. 1979. Some fungal parasites found in the diatom populations of the Rosfjord area (South Norway) during March 1979. *Veroeff Inst Meeresforsch Bremerhaven* **18**(1):29-33.
- Galagan JE, Calvo SE, Borkovich KA, Selker EU, Read NO, Jaffe D, FitzHugh W, Ma LJ, Smirnov S, Purcell S, Rehman B, Elkins T, Engels R, Wang S, Nielsen CB, Butler J, Endrizzi M, Qui D, Ianakiev P, Bell-Pedersen D, Nelson MA, Werner-Washburne M, Selitrennikoff CP, Kinsey JA, Braun EL, Zelter A, Schulte U, Kothe GO, Jedd G, Mewes W, Staben C, Marcotte E, Greenberg D, Roy A, Foley K, Naylor J, Stange-Thomann N, Barrett R, Gnerre S, Kamal M, Kamvysselis M, Mauceli E, Bielke C, Rudd S, Frishman D, Krystofova S, Rasmussen C, Metzenberg RL, Perkins DD, Kroken S, Cogoni C, Macino G, Catcheside D, Li W, Pratt RJ, Osmani SA, DeSouza CPC, Glass L, Orbach MJ, Berglund JA, Voelker R, Yarden O, Plamann M, Seiler S,

- Dunlap J, Radford A, Aramayo R, Natvig DO, Alex LA, Mannhaupt G, Ebbole DJ, Freitag M, Paulsen I, Sachs MS, Lander ES, Nusbaum C, Birren B. 2003. The genome sequence of the filamentous fungus *Neurospora crassa*. *Nature* **422**:859–868. doi:10.1038/nature01554
- Gerloff GC, Fitzgerald GP, Skoog F. 1950. The Isolation, Purification, and Culture of Blue-Green Algae. *Am J Bot* **37**:216-218. doi:10.2307/2437904
- Gerphagnon M, Agha R, Martin-Creuzburg D, Bec A, Perriere F, Rad-Menéndez C, Gachon CMM, Wolinska J. 2019. Comparison of sterol and fatty acid profiles of chytrids and their hosts reveals trophic upgrading of nutritionally inadequate phytoplankton by fungal parasites. *Environ Microbiol* **21**:949–958. doi:10.1111/1462-2920.14489
- Gerphagnon M, Latour D, Colombet J, Sime-Ngando T. 2013. A double staining method using SYTOX green and calcofluor white for studying fungal parasites of phytoplankton. *Appl Environ Microbiol* **79**:3943–3951. doi:10.1128/AEM.00696-13
- Gladfelter AS, James TY, Amend AS. 2019. Marine fungi. *Curr Biol* **29**(6):R191-R195. doi:10.1016/j.cub.2019.02.009
- Gleason FH, Kagami M, Lefevre E, Sime-Ngando T. 2008. The ecology of chytrids in aquatic ecosystems: roles in food web dynamics. *Fungal Biol Rev* **22**(1):17-25. doi:10.1016/j.fbr.2008.02.001
- Gleason FH, Lilje O, Marano AV, Sime-Ngando T, Sullivan BK, Kirchmair M, Neuhauser S. 2014. Ecological functions of zoosporic hyperparasites. *Front Microbiol* **5**(22):1-10. doi:10.3389/fmicb.2014.00244
- Gleason FH, Mozley-Standridge SE, Porter D, Boyle DG, Hyatt AD. 2007. Preservation of Chytridiomycota in culture collections. *Mycol Res* **111**(2):129-136. doi:10.1016/j.mycres.2006.10.009
- Gleason FH, Scholz B, Jephcott TG, van Ogtrop FF, Henderson L, Lilje O, Kittelmann S, Macarthur DJ. 2017. Key Ecological Roles for Zoosporic True Fungi in Aquatic Habitats in *The Fungal Kingdom*. Washington, DC, USA: ASM Press. pp. 399–416. doi:10.1128/9781555819583.ch18
- Goffeau A, Barrell G, Bussey H, Davis RW, Dujon B, Feldmann H, Galibert F, Hoheisel

- JD, Jacq C, Johnston M, Louis EJ, Mewes HW, Murakami Y, Philippsen P, Tettelin H, Oliver SG. 1996. Life with 6000 genes. *Science* **274**:546–567.  
doi:10.1126/science.274.5287.546
- Goldstein B, King N. 2016. The Future of Cell Biology: Emerging Model Organisms. *Trends Cell Biol* **26**(11):818-824. doi:10.1016/j.tcb.2016.08.005
- Goldstein S. 1960. Degradation of Pollen by Phycomycetes. *Ecology* **41**:543–545.  
doi:10.2307/1933329
- Gow NAR, Gooday GW. 1987. Cytological aspects of dimorphism in *Candida albicans*. *Crit Rev Microbiol* **15**:73–78. doi:10.3109/10408418709104449
- Gow NAR, Latge J-P, Munro CA. 2017. The Fungal Cell Wall: Structure, Biosynthesis, and Function in *The Fungal Kingdom*. Washington, DC, USA: ASM Press. pp. 267–292. doi:10.1128/9781555819583.ch12
- Greenspan SE, Longcore JE, Calhoun AJK. 2012. Host invasion by *Batrachochytrium dendrobatidis*: Fungal and epidermal ultrastructure in model anurans. *Dis Aquat Organ* **100**:201–210. doi:10.3354/dao02483
- Grigoriev IV, Nikitin R, Haridas S, Kuo A, Ohm R, Otilar R, Riley R, Salamov A, Zhao X, Korzeniewski F, Smirnova T, Nordberg H, Dubchak I, Shabalov I. 2014. MycoCosm portal: Gearing up for 1000 fungal genomes. *Nucleic Acids Res* **42**(D1):D699-D704.  
doi:10.1093/nar/gkt1183
- Grossart HP, Van den Wyngaert S, Kagami M, Wurzbacher C, Cunliffe M, Rojas-Jimenez K. 2019. Fungi in aquatic ecosystems. *Nat Rev Microbiol* **17**(6):339-354.  
doi:10.1038/s41579-019-0175-8
- Grossart HP, Wurzbacher C, James TY, Kagami M. 2016. Discovery of dark matter fungi in aquatic ecosystems demands a reappraisal of the phylogeny and ecology of zoosporic fungi. *Fungal Ecol* **19**:28–38. doi:10.1016/j.funeco.2015.06.004
- Gruninger RJ, Puniya AK, Callaghan TM, Edwards JE, Youssef N, Dagar SS, Fliegerova K, Griffith GW, Forster R, Tsang A, McAllister T, Elshahed MS. 2014. Anaerobic fungi (phylum Neocallimastigomycota): advances in understanding their taxonomy, life cycle, ecology, role and biotechnological potential. *FEMS Microbiol Ecol* **90**(1):1-17.  
doi.org/10.1111/1574-6941.12383.

- Guillard RR, Ryther JH. 1962. Studies of marine planktonic diatoms. I. *Cyclotella nana* Hustedt, and *Detonula confervacea* (Cleve) Gran. *Can J Microbiol* **8**:229–239.  
doi:10.1139/m62-029
- Gutman J, Zarka A, Boussiba S. 2009. The host-range of *Paraphysoderma sedebokerensis*, a chytrid that infects *Haematococcus pluvialis*. *Eur J Phycol* **44**:509–514. doi:10.1080/09670260903161024
- Han Q, Wang N, Yao G, Mu C, Wang Y, Sang J. 2019. Blocking  $\beta$ -1,6-glucan synthesis by deleting *KRE6* and *SKN1* attenuates the virulence of *Candida albicans*. *Mol Microbiol* **111**:604–620. doi:10.1111/mmi.14176
- Harris SD. 2019. Hyphal branching in filamentous fungi. *Dev Biol* **451**(1):35-39.  
doi:10.1016/j.ydbio.2019.02.012
- Harris SD. 2011. Hyphal morphogenesis: An evolutionary perspective. *Fungal Biol* **115**:475–484. doi:10.1016/j.funbio.2011.02.002
- Harris SD. 2008. Branching of fungal hyphae: Regulation, mechanisms and comparison with other branching systems. *Mycologia* **100**:823–832. doi:10.3852/08-177
- Hassan MW, Catapane EJ. 2000. Physiology of two monocentric chytrids: comparative nutritional studies of *Entophlyctis* sp. and *Entophlyctis aureus* (Chytridiales). *Can J Bot* **78**:105–109. doi:10.1139/b99-167
- Hassett BT, Gradinger R. 2016. Chytrids dominate arctic marine fungal communities. *Environ Microbiol* **18**:2001–2009. doi:10.1111/1462-2920.13216
- Hérivaux A, De Bernonville TD, Roux C, Clastre M, Courdavault V, Gastebois A, Bouchara JP, James TY, Latgé JP, Martin F, Papon N. 2017. The identification of phytohormone receptor homologs in early diverging fungi suggests a role for plant sensing in land colonization by fungi. *MBio* **8**(1):e01739-16. doi:10.1128/mBio.01739-16
- Hohmann S. 2016. Nobel yeast research. *FEMS Yeast Res* **16**(8):1-3.  
doi:10.1093/femsyr/fow094
- Honda D, Yokochi T, Nakahara T, Erata M, Higashihara T. 1998. *Schizochytrium limacinum* sp. nov., a new thraustochytrid from a mangrove area in the west Pacific Ocean. *Mycol Res* **102**:439–448. doi:10.1017/S0953756297005170

- Houston DC, Cooper JE. 1975. The digestive tract of the whiteback griffon vulture and its role in disease transmission among wild ungulates. *J Wildl Dis* **11**:306–313.  
doi:10.7589/0090-3558-11.3.306
- Hudson PJ, Dobson AP, Newborn D. 1992. Do Parasites make Prey Vulnerable to Predation? Red Grouse and Parasites. *J Anim Ecol* **61**:681–692. doi:10.2307/5623
- Hurdeal VG, Gentekaki E, Hyde KD, Jeewon R. 2021. Where are the basal fungi? Current status on diversity, ecology, evolution, and taxonomy. *Biologia (Bratisl)* **76**(2):421–440. doi:10.2478/s11756-020-00642-4
- Husseman JS, Murray DL, Power G, Mack C, Wenger CR, Quigley H. 2003. Assessing differential prey selection patterns between two sympatric large carnivores. *Oikos* **101**:591–601. doi:10.1034/j.1600-0706.2003.12230.x
- Ito D, Zitouni S, Jana SC, Duarte P, Surkont J, Carvalho-Santos Z, Pereira-Leal JB, Ferreira MG, Bettencourt-Dias M. 2019. Pericentrin-mediated SAS-6 recruitment promotes centriole assembly. *Elife* **8**:e41418. doi:10.7554/eLife.41418
- Ivarsson M, Drake H, Bengtson S, Rasmussen B. 2020. A Cryptic Alternative for the Evolution of Hyphae. *BioEssays* **42**:1900183. doi:10.1002/bies.201900183
- James TY, Kauff F, Schoch CL, Matheny PB, Hofstetter V, Cox CJ, Celio G, Gueidan C, Fraker E, Miadlikowska J, Lumbsch HT, Rauhut A, Reeb V, Arnold AE, Amtoft A, Stajich JE, Hosaka K, Sung GH, Johnson D, O'Rourke B, Crockett M, Binder M, Curtis JM, Slot JC, Wang Z, Wilson AW, Schüßler A, Longcore JE, O'Donnell K, Mozley-Standridge S, Porter D, Letcher PM, Powell MJ, Taylor JW, White MM, Griffith GW, Davies DR, Humber RA, Morton JB, Sugiyama J, Rossman AY, Rogers JD, Pfister DH, Hewitt D, Hansen K, Hambleton S, Shoemaker RA, Kohlmeyer J, Volkmann-Kohlmeyer B, Spotts RA, Serdani M, Crous PW, Hughes KW, Matsuura K, Langer E, Langer G, Untereiner WA, Lücking R, Bädler B, Geiser DM, Aptroot A, Diederich P, Schmitt I, Schultz M, Yahr R, Hibbett DS, Lutzoni F, McLaughlin DJ, Spatafora JW, Vilgalys R. 2006a. Reconstructing the early evolution of Fungi using a six-gene phylogeny. *Nature* **443**:818–822. doi:10.1038/nature05110
- James TY, Letcher PM, Longcore JE, Mozley-Standridge SE, Porter D, Powell MJ, Griffith GW, Vilgalys R. 2006b. A molecular phylogeny of the flagellated fungi



- (Chytridiomycota) and description of a new phylum (Blastocladiomycota). *Mycologia* **98**:860–871. doi:10.3852/mycologia.98.6.860
- Jeffries TC, Curlevski NJ, Brown MV, Harrison DP, Doblin MA, Petrou K, Ralph PJ, Seymour JR. 2016. Partitioning of fungal assemblages across different marine habitats. *Environ Microbiol Rep* **8**:235–238. doi:10.1111/1758-2229.12373
- Jensen PR, Jenkins KM, Porter D, Fenical W. 1998. Evidence that a New Antibiotic Flavone Glycoside Chemically Defends the Sea Grass *Thalassia testudinum* against Zoosporic Fungi. *Appl Environ Microbiol* **64**:1490–6. doi: 10.1128/AEM.64.4.1490-1496.1998
- Jephcott TG, Sime-Ngando T, Gleason FH, Macarthur DJ. 2016. Host-parasite interactions in food webs: Diversity, stability, and coevolution. *Food Webs* **6**:1-8. doi:10.1016/j.fooweb.2015.12.001
- Jones GM, O'Dor RK. 1983. Ultrastructural Observations on a Thraustochytrid Fungus Parasitic in the Gills of Squid (*Illex illecebrosus* LeSueur). *J Parasitol* **69**:903 -911. doi:10.2307/3281055
- Jones MDM, Forn I, Gadelha C, Egan MJ, Bass D, Massana R, Richards TA. 2011. Discovery of novel intermediate forms redefines the fungal tree of life. *Nature* **474**:200–204. doi:10.1038/nature09984
- Joneson S, Stajich JE, Shiu SH, Rosenblum EB. 2011. Genomic transition to pathogenicity in chytrid fungi. *PLoS Pathog* **7**:e1002338. doi:10.1371/journal.ppat.1002338
- Kagami M, De Bruin A, Ibelings BW, Van Donk E. 2007. Parasitic chytrids: Their effects on phytoplankton communities and food-web dynamics. *Hydrobiologia*. Springer. pp. 113–129. doi:10.1007/s10750-006-0438-z
- Kagami M, Miki T, Takimoto G. 2014. Mycoloop: Chytrids in aquatic food webs. *Front Microbiol* **5**:166. doi:10.3389/fmicb.2014.00166
- Kagami M, Motoki Y, Masclaux H, Bec A. 2017. Carbon and nutrients of indigestible pollen are transferred to zooplankton by chytrid fungi. *Freshw Biol* **62**:954–964. doi:10.1111/fwb.12916
- Kagami M, Van Donk E, de Bruin A, Rijkeboer M, Ibelings BW. 2004. *Daphnia* can protect

- diatoms from fungal parasitism. *Limnol Oceanogr* **49**:680–685.  
doi:10.4319/lo.2004.49.3.0680
- Kanopoulos N, Vasanthavada N, Baker RL. 1988. Design of an Image Edge Detection Filter Using the Sobel Operator. *IEEE J Solid-State Circuits* **23**:358–367.  
doi:10.1109/4.996
- Karperien A, Ahammer H, Jelinek HF. 2013. Quantitating the subtleties of microglial morphology with fractal analysis. *Front Cell Neurosci* **7**(3):1-18.  
doi:10.3389/fncel.2013.00003
- Katoh K, Standley DM. 2013. MAFFT multiple sequence alignment software version 7: improvements in performance and usability. *Mol Biol Evol* **30**(4):772-780.  
doi:10.1093/molbev/mst010
- Kawachi M, Noël M. 2005. Sterilization and sterile technique in *Algal Culturing Techniques*. Academic Press. pp. 65–82. doi: 10.1016/b978-012088426-1/50002-0
- Kazama F. 1972. Development and morphology of a chytrid isolated from *Bryopsis plumosa*. *Can J Bot* **50**:499–505. doi:10.1139/b72-063
- Khomich M, Davey ML, Kauserud H, Rasconi S, Andersen T. 2017. Fungal communities in Scandinavian lakes along a longitudinal gradient. *Fungal Ecol* **27**:36–46.  
doi:10.1016/j.funeco.2017.01.008
- Kilias ES, Junges L, Šupraha L, Leonard G, Metfies K, Richards TA. 2020. Chytrid fungi distribution and co-occurrence with diatoms correlate with sea ice melt in the Arctic Ocean. *Commun Biol* **3**:1–13. doi:10.1038/s42003-020-0891-7
- Kirschner H, Aguet F, Sage D, Unser M. 2013. 3-D PSF fitting for fluorescence microscopy: implementation and localization application. *J Microsc* **249**:13–25.  
doi:10.1111/j.1365-2818.2012.03675.x
- Kiss E, Hegedüs B, Virágh M, Varga T, Merényi Z, Kószó T, Bálint B, Prasanna AN, Krizsán K, Kocsubé S, Riquelme M, Takeshita N, Nagy LG. 2019a. Comparative genomics reveals the origin of fungal hyphae and multicellularity. *Nat Commun* **10**:23955–6900. doi:10.1038/s41467-019-12085-w
- Klawonn I, Van den Wyngaert S, Parada AE, Arandia-Gorostidi N, Whitehouse MJ, Grossart HP, Dekas AE. 2021. Characterizing the “fungal shunt”: Parasitic fungi on

diatoms affect carbon flow and bacterial communities in aquatic microbial food webs.

*Proc Natl Acad Sci* **118**:e2102225118. doi:10.1073/pnas.2102225118

Kopf A, Bicak M, Kottmann R, Schnetzer J, Kostadinov I, Lehmann K, Fernandez-Guerra A, Jeanthon C, Rahav E, Ullrich M, Wichels A, Gerdts G, Polymenakou P, Kotoulas G, Siam R, Abdallah RZ, Sonnenschein EC, Cariou T, O’Gara F, Jackson S, Orlic S, Steinke M, Busch J, Duarte B, Caçador I, Canning-Clode J, Bobrova O, Marteinson V, Reynisson E, Loureiro CM, Luna GM, Quero GM, Löscher CR, Kremp A, DeLorenzo ME, Øvreås L, Tolman J, LaRoche J, Penna A, Frischer M, Davis T, Katherine B, Meyer CP, Ramos S, Magalhães C, Jude-Lemeilleur F, Aguirre-Macedo ML, Wang S, Poulton N, Jones S, Collin R, Fuhrman JA, Conan P, Alonso C, Stambler N, Goodwin K, Yakimov MM, Baltar F, Bodrossy L, Kamp J Van De, Frampton DMF, Ostrowski M, Ruth P Van, Malthouse P, Claus S, Deneudt K, Mortelmans J, Pitois S, Wallom D, Salter I, Costa R, Schroeder DC, Kandil MM, Amaral V, Biancalana F, Santana R, Pedrotti ML, Yoshida T, Ogata H, Ingleton T, Munnik K, Rodriguez-Ezpeleta N, Berteaux-Lecellier V, Wecker P, Cancio I, Vaulot D, Bienhold C, Ghazal H, Chaouni B, Essayeh S, Ettamimi S, Zaid EH, Boukhatem N, Bouali A, Chahboune R, Barrijal S, Timinouni M, Otmani FEI, Bennani M, Mea M, Todorova N, Karamfilov V, Hoopen P, Cochrane G, L’Haridon S, Bizsel KC, Vezzi A, Lauro FM, Martin P, Jensen RM, Hinks J, Gebbels S, Rosselli R, Pascale F De, Schiavon R, Santos A dos, Villar E, Pesant S, Cataletto B, Malfatti F, Edirisinghe R, Silveira JAH, Barbier M, Turk V, Tinta T, Fuller WJ, Salihoglu I, Serakinci N, Ergoren MC, Bresnan E, Iriberry J, Nyhus PAF, Bente E, Karlsen HE, Golyshin PN, Gasol JM, Moncheva S, Dzhembekova N, Johnson Z, Sinigalliano CD, Gidley ML, Zingone A, Danovaro R, Tsiamis G, Clark MS, Costa AC, Bour MEI, Martins AM, Collins RE, Ducluzeau A-L, Martinez J, Costello MJ, Amaral-Zettler LA, Gilbert JA, Davies N, Field D, Glöckner FO. 2015. The ocean sampling day consortium. *Gigascience* **4**(1):s13742-015. doi: 10.1186/s13742-015-0066-5

Krabberød A, Bjorbækmo M, Shalchian-Tabrizi K, Logares R. 2017. Exploring the oceanic microeukaryotic interactome with metaomics approaches. *Aquat Microb Ecol* **79**:1–12. doi:10.3354/ame01811

- Krings M, Dotzler N, Galtier J, Taylor TN. 2009. Microfungi from the upper Visean (Mississippian) of central France: Chytridiomycota and chytrid-like remains of uncertain affinity. *Rev Palaeobot Palynol* **156**:319–328.  
doi:10.1016/j.revpalbo.2009.03.011
- Krings M, Harper CJ, Taylor EL. 2018. Fungi and fungal interactions in the Rhynie chert: A review of the evidence, with the description of *Perexiflasca tayloriana* gen. et sp. nov. *Philos Trans R Soc B Biol Sci* **373**(1739):20160500 doi:10.1098/rstb.2016.0500
- Krings M, Kerp H. 2019. A tiny parasite of unicellular microorganisms from the Lower Devonian Rhynie and Windyfield cherts, Scotland. *Rev Palaeobot Palynol* **271**:104106. doi:10.1016/j.revpalbo.2019.104106
- Krings M, Taylor TN. 2014. An unusual fossil microfungus with suggested affinities to the Chytridiomycota from the Lower Devonian Rhynie chert. *Nov Hedwigia* **99**:403–412.  
doi:10.1127/0029-5035/2014/0205
- Krumm CE, Conner MM, Hobbs NT, Hunter DO, Miller MW. 2010. Mountain lions prey selectively on prion-infected mule deer. *Biol Lett* **6**:209–211.  
doi:10.1098/rsbl.2009.0742
- Lafferty KD. 2004. Fishing for lobsters indirectly increases epidemics in sea urchins. *Ecol Appl* **14**:1566–1573. doi:10.1890/03-5088
- Lam BA, Walton DB, Harris RN. 2011. Motile zoospores of *Batrachochytrium dendrobatidis* move away from antifungal metabolites produced by amphibian skin bacteria. *Ecohealth* **8**:36–45. doi:10.1007/s10393-011-0689-7
- Larsson A. 2014. AliView: a fast and lightweight alignment viewer and editor for large datasets. *Bioinformatics* **30**(22): 3276-3278. doi: 10.1093/bioinformatics/btu531
- Lange L, Barrett K, Pilgaard B, Gleason F, Tsang A. 2019. Enzymes of early-diverging, zoosporic fungi. *Appl Microbiol Biotechnol* **103**(17):6885-6902. doi:10.1007/s00253-019-09983-w
- Laundon D, Larson BT, McDonald K, King N, Burkhardt P. 2019. The architecture of cell differentiation in choanoflagellates and sponge choanocytes. *PLoS Biol* **17**:e3000226. doi:10.1371/journal.pbio.3000226
- Le Calvez T, Burgaud G, Mahé S, Barbier G, Vandenkoornhuyse P. 2009. Fungal

diversity in deep-sea hydrothermal ecosystems. *Appl Environ Microbiol* **75**:6415–6421. doi:10.1128/AEM.00653-09

Le Sage MJ, Towey BD, Brunner JL. 2019. Do scavengers prevent or promote disease transmission? The effect of invertebrate scavenging on Ranavirus transmission.

*Funct Ecol* **33**:1342–1350. doi:10.1111/1365-2435.13335

Leaño EM, Gapasin RSJ, Polohan B, Vrijmoed LLP. 2003. Fungal Diversity Growth and fatty acid production of thraustochytrids from Panay mangroves, Philippines. *Fungal Divers*. **12**:111-122.

Léjohn HB, Lovett JS. 1965. Ribonucleic acid and protein synthesis in *Rhizophlyctis rosea* zoospores. *J Bacteriol* **91**:709–717. doi:10.1128/jb.91.2.709-717.1966

Leonelli S, Ankeny RA. 2013. What makes a model organism? *Endeavour* **37**(4):209-212. doi:10.1016/j.endeavour.2013.06.001

Leyland B, Leu S, Boussiba S. 2017. Are Thraustochytrids algae? *Fungal Biol* **121**(10):835-840. doi:10.1016/j.funbio.2017.07.006

Lima-Mendez G, Faust K, Henry N, Decelle J, Colin S, Carcillo F, Chaffron S, Ignacio-Espinosa JC, Roux S, Vincent F, Bittner L, Darzi Y, Wang J, Audic S, Berline L, Bontempi G, Cabello AM, Coppola L, Cornejo-Castillo FM, D'Ovidio F, De Meester L, Ferrera I, Garet-Delmas MJ, Guidi L, Lara E, Pesant S, Royo-Llonch M, Salazar G, Sánchez P, Sebastian M, Souffreau C, Dimier C, Picheral M, Searson S, Kandels-Lewis S, Gorsky G, Not F, Ogata H, Speich S, Stemann L, Weissenbach J, Wincker P, Acinas SG, Sunagawa S, Bork P, Sullivan MB, Karsenti E, Bowler C, De Vargas C, Raes J, Boss E, Follows M, Grimsley N, Hingamp P, Iudicone D, Jaillon O, Karp-Boss L, Krzic U, Reynaud EG, Sardet C, Sieracki M, Velayoudon D. 2015. Determinants of community structure in the global plankton interactome. *Science* **348**(6237):1262073. doi:10.1126/science.1262073

Lodhi IJ, Semenkovich CF. 2014. Peroxisomes: A nexus for lipid metabolism and cellular signaling. *Cell Metab* **19**(3):380-392. doi:10.1016/j.cmet.2014.01.002

Lommer M, Specht M, Roy AS, Kraemer L, Andreson R, Gutowska MA, Wolf J, Bergner S V, Schilhabel MB, Klostermeier UC, Beiko RG, Rosenstiel P, Hippler M, LaRoche J. 2012. Genome and low-iron response of an oceanic diatom adapted to chronic iron

- limitation. *Genome Biol* **13**:R66. doi:10.1186/gb-2012-13-7-r66
- Longcore JE. 1995. Morphology and zoospore ultrastructure of *Entophlyctis luteolus* sp. nov. (Chytridiales): Implications for chytrid taxonomy. *Mycologia* **87**:25–33. doi:10.1080/00275514.1995.12026498
- Longcore JE, Pessier AP, Nichols DK. 1999. *Batrachochytrium dendrobatidis* gen. et sp. nov., a chytrid pathogenic to amphibians. *Mycologia* **91**:219–227. doi:10.1080/00275514.1999.12061011
- Longcore JE, Qin S, Simmons DR, James TY. 2020. *Quaeritorhiza haematococci* is a new species of parasitic chytrid of the commercially grown alga, *Haematococcus pluvialis*. *Mycologia* **112**(3):606-615. doi:10.1080/00275514.2020.1730136
- López-Franco R, Bartnicki-Garcia S, Bracker CE. 1994. Pulsed growth of fungal hyphal tips. *Proc Natl Acad Sci USA* **91**:12228–12232. doi:10.1073/pnas.91.25.12228
- Lösel DM. 1990. Lipids in the Structure and Function of Fungal Membranes in *Biochemistry of Cell Walls and Membranes in Fungi*. Springer Berlin Heidelberg. pp. 119–133. doi:10.1007/978-3-642-74215-6\_9
- Love MI, Huber W, Anders S. 2014. Moderated estimation of fold change and dispersion for RNA-seq data with DESeq2. *Genome Biol* **15**:1–21. doi:10.1186/S13059-014-0550-8
- Lovett JS. 1968. Reactivation of ribonucleic acid and protein synthesis during germination of *Blastocladiella* zoospores and the role of the ribosomal nuclear cap. *J Bacteriol* **96**:962–969. doi:10.1128/jb.96.4.962-969.1968
- Lovett JS. 1963. Chemical and physical characterization of “nuclear caps” isolated from *Blastocladiella* zoospores. *J Bacteriol* **85**:1235–1246. doi:10.1128/JB.85.6.1235-1246.1963
- Mahmoud YAG, Abou Zeid AM. 2002. Zoosporic Fungi Isolated From Four Egyptian Lakes and the Uptake of Radioactive Waste. *Mycobiology* **30**(2):76 -81. doi:10.4489/myco.2002.30.2.076
- Maier MA, Peterson TD. 2017. Prevalence of chytrid parasitism among diatom populations in the lower Columbia River (2009–2013). *Freshw Biol* **62**:414–428. doi:10.1111/fwb.12876

- Mann DG. 1999. The species concept in diatoms. *Phycologia* **38**(6):437-495.  
doi:10.2216/i0031-8884-38-6-437.1
- Manoylov KM. 2009. Intra- and interspecific competition for nutrients and light in diatom cultures. *J Freshw Ecol* **24**:145–157. doi:10.1080/02705060.2009.9664275
- McConnell G, Amos WB. 2018. Application of the Mesolens for subcellular resolution imaging of intact larval and whole adult *Drosophila*. *J Microsc* **270**:252–258.  
doi:10.1111/jmi.12693
- McConnell G, Trägårdh J, Amor R, Dempster J, Reid E, Amos WB. 2016. A novel optical microscope for imaging large embryos and tissue volumes with sub-cellular resolution throughout. *Elife* **5**:e18659. doi:10.7554/eLife.18659
- McLean N, Porter D. 1982. The Yellow-Spot Disease of *Tritonia diomedea* Bergh, 1894 (Mollusca: Gastropoda: Nudibranchia): Encapsulation of the Thraustochytriaceae Parasite by Host Amoebocytes. *J Parasitol* **68**:243-252. doi:10.2307/3281182
- Medina EM, Buchler NE. 2020. Chytrid fungi. *Curr Biol* **30**:R516–R520.  
doi:10.1016/j.cub.2020.02.076
- Medina EM, Robinson KA, Bellingham-Johnstun K, Ianiri G, Laplante C, Fritz-Laylin LK, Buchler NE. 2020. Genetic transformation of *Spizellomyces punctatus*, a resource for studying chytrid biology and evolutionary cell biology. *Elife* **9**:e52741.  
doi:10.7554/eLife.52741
- Medina EM, Turner JJ, Gordân R, Skotheim JM, Buchler NE. 2016. Punctuated evolution and transitional hybrid network in an ancestral cell cycle of fungi. *Elife* **5**:e09492.  
doi:10.7554/elife.09492
- Millay MA, Taylor TN. 1978. Chytrid-like fossils of Pennsylvanian age. *Science* **200**:1147–1149. doi:10.1126/science.200.4346.1147
- Miller CE, Dylewski DP. 1981. Syngamy and resting body development in *Chytriomycetes hyalinus* (Chytridiales). *Am J Bot*. **68**(3):342-349. doi.org/10.1002/j.1537-2197.1981.tb06371.x
- Miller CE. 1977. A developmental study with the SEM of sexual reproduction in *Chytriomycetes hyalinus*. *Bulletin de la SBF*. **124**(5-6):281-289.  
doi.org/10.1080/00378941.1977.10835753

- Mirkes PE. 1974. Polysomes, ribonucleic acid, and protein synthesis during germination of *Neurospora crassa* conidia. *J Bacteriol* **117**:196–202. doi:10.1128/jb.117.1.196-202.1974
- Mitchell RT, Deacon JW. 1986. Selective accumulation of zoospores of chytridiomycetes and oomycetes on cellulose and chitin. *Trans Br Mycol Soc* **86**:219–223. doi:10.1016/s0007-1536(86)80148-6
- Mondo SJ, Dannebaum RO, Kuo RC, Louie KB, Bewick AJ, LaButti K, Haridas S, Kuo A, Salamov A, Ahrendt SR, Lau R, Bowen BP, Lipzen A, Sullivan W, Andreopoulos BB, Clum A, Lindquist E, Daum C, Northen TR, Kunde-Ramamoorthy G, Schmitz RJ, Gryganskyi A, Culley D, Magnuson J, James TY, O'Malley MA, Stajich JE, Spatafora JW, Visel A, Grigoriev I V. 2017. Widespread adenine N6-methylation of active genes in fungi. *Nat Genet* **49**:964–968. doi:10.1038/ng.3859
- Money NP. 2016. Spore Production, Discharge, and Dispersal in *The Fungi*: Third Edition. Elsevier Inc. pp. 67–97. doi:10.1016/B978-0-12-382034-1.00003-7
- Moreno-Velásquez SD, Seidel C, Juvvadi PR, Steinbach WJ, Read ND. 2017. Caspofungin-mediated growth inhibition and paradoxical growth in *Aspergillus fumigatus* involve fungicidal hyphal tip lysis coupled with regenerative intrahyphal growth and dynamic changes in  $\beta$ -1,3-glucan synthase localization. *Antimicrob Agents Chemother* **61**:e00710-17. doi:10.1128/AAC.00710-17
- Moss AS, Reddy NS, Dortaj IM, San Francisco MJ. 2008. Chemotaxis of the amphibian pathogen *Batrachochytrium dendrobatidis* and its response to a variety of attractants. *Mycologia* **100**:1–5. doi:10.1080/15572536.2008.11832493
- Muehlstein LK, Amon JP, Leffler DL. 1988. Chemotaxis in the Marine Fungus *Rhizophydium littoreum*. *Appl Environ Microbiol* **54**:1668–1672. doi:10.1128/aem.54.7.1668-1672.1988
- Muehlstein LK, Amon JP, Leffler DL. 1987. Phototaxis in the Marine Fungus *Rhizophydium littoreum*. *Appl Environ Microbiol* **53**:1819-1821. doi:10.1128/aem.53.8.1819-1821.1987
- Murray CL, Lovett JS. 1966. Nutritional requirements of the chytrid *Karlingia asterocysta*, an obligate chitinophile. *Am J Bot* **53**:469–476. doi:10.1002/j.1537-



2197.1966.tb07359.x

Naff CS, Darcy JL, Schmidt SK. 2013. Phylogeny and biogeography of an uncultured clade of snow chytrids. *Environ Microbiol* **15**:2672–2680. doi:10.1111/1462-2920.12116

Nagahama T, Takahashi E, Nagano Y, Abdel-Wahab MA, Miyazaki M. 2011. Molecular evidence that deep-branching fungi are major fungal components in deep-sea methane cold-seep sediments. *Environ Microbiol* **13**:2359–2370. doi:10.1111/j.1462-2920.2011.02507.x

Nagy LG, Kovács GM, Krizsán K. 2018. Complex multicellularity in fungi: evolutionary convergence, single origin, or both? *Biol Rev* **93**:1778–1794. doi:10.1111/brv.12418

Nagy LG, Tóth R, Kiss E, Slot J, Gácsér A, Kovács GM. 2017. Six Key Traits of Fungi: Their Evolutionary Origins and Genetic Bases in *The Fungal Kingdom*. Washington, DC, USA: ASM Press. pp. 35–56. doi:10.1128/9781555819583.ch2

Nagy LG, Varga T, Csermetics Á, Virágh M. 2020. Fungi took a unique evolutionary route to multicellularity: Seven key challenges for fungal multicellular life. *Fungal Biol Rev* **34**(4):151-169. doi:10.1016/j.fbr.2020.07.002

Naranjo-Ortiz MA, Gabaldón T. 2019a. Fungal evolution: diversity, taxonomy and phylogeny of the Fungi. *Biol Rev* **94**:2101–2137. doi:10.1111/brv.12550

Naranjo-Ortiz MA, Gabaldón T. 2019b. Fungal evolution: major ecological adaptations and evolutionary transitions. *Biol Rev* **94**:1443–1476. doi:10.1111/brv.12510

Nelson DM, Tréguer P, Brzezinski MA, Leynaert A, Quéguiner B. 1995. Production and dissolution of biogenic silica in the ocean: Revised global estimates, comparison with regional data and relationship to biogenic sedimentation. *Global Biogeochem Cycles* **9**:359–372. doi:10.1029/95GB01070

O’Hanlon SJ, Rieux A, Farrer RA, Rosa GM, Waldman B, Bataille A, Kosch TA, Murray KA, Brankovics B, Fumagalli M, Martin MD, Wales N, Alvarado-Rybak M, Bates KA, Berger L, Böll S, Brookes L, Clare F, Courtois EA, Cunningham AA, Doherty-Bone TM, Ghosh P, Gower DJ, Hintz WE, Höglund J, Jenkinson TS, Lin CF, Laurila A, Loyau A, Martel A, Meurling S, Miaud C, Minting P, Pasmans F, Schmeller DS, Schmidt BR, Shelton JMG, Skerratt LF, Smith F, Soto-Azat C, Spagnoletti M, Tessa

- G, Toledo LF, Valenzuela-Sánchez A, Verster R, Vörös J, Webb RJ, Wierzbicki C, Wombwell E, Zamudio KR, Aanensen DM, James TY, Thomas M, Weldon C, Bosch J, Balloux F, Garner TWJ, Fisher MC. 2018. Recent Asian origin of chytrid fungi causing global amphibian declines. *Science* **360**:621–627.  
doi:10.1126/science.aar1965
- Obert M, Pfeifer P, Sernetz M. 1990. Microbial growth patterns described by fractal geometry. *J Bacteriol* **172**:1180–1185. doi:10.1128/jb.172.3.1180-1185.1990
- Ota S, Kawano S. 2015. Life cycle and lectin-binding patterns in the chytrid fungus *Chytrium hyalinus*. *Cytologia (Tokyo)* **80**:125–129. doi:10.1508/cytologia.80.125
- Otsu N. 1979. Threshold selection method from gray-level histograms. *IEEE Trans Syst Man Cybern* **SMC-9**:62–66. doi:10.1109/tsmc.1979.4310076
- Packer C, Holt RD, Hudson PJ, Lafferty KD, Dobson AP. 2003. Keeping the herds healthy and alert: Implications of predator control for infectious disease. *Ecol Lett* **6**(9):797-802. doi:10.1046/j.1461-0248.2003.00500.x
- Pan J, del Campo J, Keeling PJ. 2017. Reference Tree and Environmental Sequence Diversity of Labyrinthulomycetes. *J Eukaryot Microbiol* **64**:88–96.  
doi:10.1111/jeu.12342
- Peng H, Bria A, Zhou Z, Iannello G, Long F. 2014. Extensible visualization and analysis for multidimensional images using Vaa3D. *Nat Protoc* **9**:193–208.  
doi:10.1038/nprot.2014.011
- Phumphumirat W, Ferguson DK, Gleason FH. 2016. The colonization of palynomorphs by chytrids and thraustochytrids during pre-depositional taphonomic processes in tropical mangrove ecosystems. *Fungal Ecol* **23**:11–19.  
doi:10.1016/j.funeco.2016.05.006
- Picard KT. 2017. Coastal marine habitats harbor novel early-diverging fungal diversity. *Fungal Ecol* **25**:1–13. doi:10.1016/j.funeco.2016.10.006
- Picard KT, Letcher PM, Powell MJ. 2013. Evidence for a facultative mutualist nutritional relationship between the green coccoid alga *Bracteacoccus* sp. (Chlorophyceae) and the zoosporic fungus *Rhizidium phycophilum* (Chytridiomycota). *Fungal Biol* **117**:319–328. doi:10.1016/j.funbio.2013.03.003

- Pintoa E, Van Nieuwerburgha L, De Barros MP, Pedersén M, Colepicolo P, Snoeijs P. 2003. Density-dependent patterns of thiamine and pigment production in the diatom *Nitzschia microcephala*. *Phytochemistry* **63**:155–163. doi:10.1016/S0031-9422(03)00048-7
- Piotrowski JS, Annis SL, Longcore JE. 2004. Physiology of *Batrachochytrium dendrobatidis*, a chytrid pathogen of amphibians. *Mycologia* **96**:9–15. doi:10.1080/15572536.2005.11832990
- Pole A, Gordon IJ, Gorman ML, MacAskill M. 2004. Prey selection by African wild dogs (*Lycaon pictus*) in southern Zimbabwe. *J Zool* **262**:207–215. doi:10.1017/S0952836903004576
- Pollack JK, Li ZJ, Marten MR. 2008. Fungal mycelia show lag time before re-growth on endogenous carbon. *Biotechnol Bioeng* **100**:458–465. doi:10.1002/bit.21779
- Powell MJ. 1983. Localization of antimonate-mediated precipitates of cations in zoospores of *Chytrium hyalinus*. *Exp Mycol* **7**:266–277. doi:10.1016/0147-5975(83)90047-6
- Powell MJ. 1979. The structure of microbodies and their associations with other organelles in zoosporangia of *Entophlyctis variabilis*. *Protoplasma* **98**:177–198. doi:10.1007/BF01281439
- Powell MJ. 1977. Ultrastructural cytochemistry of the diaminobenzidine reaction in the aquatic fungus *Entophlyctis variabilis*. *Arch Microbiol* **114**:123–136. doi:10.1007/BF00410773
- Powell MJ. 1976. Ultrastructure and isolation of glyoxysomes (microbodies) in zoospores of the fungus *Entophlyctis* sp. *Protoplasma* **89**:1–27. doi:10.1007/BF01279325
- Powell MJ. 1975. Ultrastructural changes in nuclear membranes and organelle associations during mitosis of the aquatic fungus *Entophlyctis* sp. *Can J Bot* **53**:627–646. doi:10.1139/b75-078
- Powell MJ. 1974. Fine Structure of Plasmodesmata in a Chytrid. *Mycologia* **66**:606–614. doi:10.1080/00275514.1974.12019652
- Powell MJ, Gillette L. 1987. Septal Structure of the Chytrid *Rhizophlyctis harderi*. *Mycologia* **79**:635–639. doi:10.1080/00275514.1987.12025436
- Powell MJ, Letcher PM, Davis WJ, Lefèvre E, Brooks M, Longcore JE. 2019. Taxonomic

- summary of *Rhizoclostratium* and description of four new *Rhizoclostratium* species (Chytriomycetaceae, Chytridiales). *Phytologia*. **101**(2):139-163.
- Prostak SM, Robinson KA, Titus MA, Fritz-Laylin LK. 2021. The actin networks of chytrid fungi reveal evolutionary loss of cytoskeletal complexity in the fungal kingdom. *Curr Biol* **31**(6):1192-1205. doi:10.1016/j.cub.2021.01.001
- Rad-Menéndez C, Gerphagnon M, Garvetto A, Arce P, Badis Y, Sime-Ngando T, Gachon CMM. 2018. Rediscovering *Zygorhizidium affluens* Canter: Molecular taxonomy, infectious cycle, and cryopreservation of a chytrid infecting the bloom-forming diatom *Asterionella formosa*. *Appl Environ Microbiol* **84**: e01826-18. doi:10.1128/AEM.01826-18
- Rado TA, Cochrane VW. 1971. Ribosomal competence and spore germination in *Fusarium solani*. *J Bacteriol* **106**:301–304. doi:10.1128/jb.106.2.301-304.1971
- Raghukumar C. 2006. Algal-Fungal Interactions in the Marine Ecosystem: Symbiosis to Parasitism in *Recent Advances on Applied Aspects of Indian Marine Algae with Reference to Global Scenario*. CSMCRI, India. pp. 365-385.
- Raghukumar C. 1986. Thraustochytrid Fungi Associated with Marine Algae. *Indian J Mar Sci* **15**:121-122.
- Raghukumar C, Mohandass C, Cardígos F, Santos RS, Colaço A. 2008. Assemblage of benthic diatoms and culturable heterotrophs in shallow-water hydrothermal vent of the D. João de Castro Seamount, Azores in the Atlantic Ocean, *Curr Sci* **95**(12):1715-1723.
- Raghukumar S. 2002. Ecology of the marine protists, the labyrinthulomycetes (thraustochytrids and labyrinthulids). *Eur J Protistol* **38**(2):127-145. doi:10.1078/0932-4739-00832
- Raghukumar S. 1992. Bacterivory: a novel dual role for thraustochytrids in the sea. *Mar Biol* **113**:165–169. doi:10.1007/BF00367650
- Rasconi S, Jobard M, Jouve L, Sime-Ngando T. 2009. Use of calcofluor white for detection, identification, and quantification of phytoplanktonic fungal parasites. *Appl Environ Microbiol* **75**:2545–2553. doi:10.1128/AEM.02211-08
- Rasconi S, Ptacnik R, Danner S, Van den Wyngaert S, Rohrlack T, Pilecky M, Kainz MJ.

2020. Parasitic Chytrids Upgrade and Convey Primary Produced Carbon During Inedible Algae Proliferation. *Protist* **171**:125768. doi:10.1016/j.protis.2020.125768
- Refsnider JM, Poorten TJ, Langhammer PF, Burrowes PA, Rosenblum EB. 2015. Genomic correlates of virulence attenuation in the deadly amphibian chytrid fungus, *Batrachochytrium dendrobatidis*. *G3 Genes, Genomes, Genet* **5**:2291–2298. doi:10.1534/g3.115.021808
- Reisert PS, Fuller MS. 1962. Decomposition of Chitin by *Chytrium* Species. *Mycologia* **54**:647–657. doi:10.1080/00275514.1962.12025046
- Richards TA, Leonard G, Mahé F, Del Campo J, Romac S, Jones MDM, Maguire F, Dunthorn M, De Vargas C, Massana R, Chambouvet A. 2015. Molecular diversity and distribution of marine fungi across 130 european environmental samples. *Proc R Soc B Biol Sci* **282**:20152243. doi:10.1098/rspb.2015.2243
- Richards TA, Leonard G, Wideman JG. 2017. What Defines the “Kingdom” Fungi? in *The Fungal Kingdom*. Washington, DC, USA: ASM Press. pp. 57–77. doi:10.1128/9781555819583.ch3
- Richter DJ, King N. 2013. The genomic and cellular foundations of animal origins. *Annu Rev Genet* **47**:509–537. doi:10.1146/ANNUREV-GENET-111212-133456
- Riemann F, Schaumann K. 1993. Short note Thraustochytrid protists in Antarctic fast ice? *Antarct Sci* **5**:279–280. doi:10.1017/S0954102093000379
- Riquelme M, Aguirre J, Bartnicki-García S, Braus GH, Feldbrügge M, Fleig U, Hansberg W, Herrera-Estrella A, Kämper J, Kück U, Mouriño-Pérez RR, Takeshita N, Fischer R. 2018. Fungal Morphogenesis, from the Polarized Growth of Hyphae to Complex Reproduction and Infection Structures. *Microbiol Mol Biol Rev* **82**(2):e00068-17. doi:10.1128/mnbr.00068-17
- Roberts C, Allen R, Bird KE, Cunliffe M. 2020. Chytrid fungi shape bacterial communities on model particulate organic matter. *Biol Lett* **16**:20200368. doi:10.1098/rsbl.2020.0368
- Rodriguez A, Ehlenberger DB, Dickstein DL, Hof PR, Wearne SL. 2008. Automated three-dimensional detection and shape classification of dendritic spines from fluorescence microscopy images. *PLoS One* **3**(4):e1997. doi:10.1371/journal.pone.0001997

- Rodriguez A, Ehlenberger DB, Hof PR, Wearne SL. 2006. Rayburst sampling, an algorithm for automated three-dimensional shape analysis from laser scanning microscopy images. *Nat Protoc* **1**:2152–2161. doi:10.1038/nprot.2006.313
- Roemer T, Delaney S, Bussey H. 1993. *SKN1* and *KRE6* define a pair of functional homologs encoding putative membrane proteins involved in beta-glucan synthesis. *Mol Cell Biol* **13**:4039–4048. doi:10.1128/mcb.13.7.4039
- Rognes T, Flouri T, Nichols B, Quince C, Mahé F. 2016. VSEARCH: A versatile open source tool for metagenomics. *PeerJ* **2016**:e2584. doi:10.7717/peerj.2584
- Rosa SM, Galvagno MA, Vélez CG. 2011. Adjusting culture conditions to isolate thraustochytrids from temperate and cold environments in southern Argentina. *Mycoscience* **52**:242–252. doi:10.1007/s10267-010-0091-2
- Rosenblum EB, James TY, Zamudio KR, Poorten TJ, Ilut D, Rodriguez D, Eastman JM, Richards-Hrdlicka K, Joneson S, Jenkinson TS, Longcore JE, Olea GP, Toledo LF, Arellano ML, Medina EM, Restrepo S, Flechas SV, Berger L, Briggs CJ, Stajich JE. 2013. Complex history of the amphibian-killing chytrid fungus revealed with genome resequencing data. *Proc Natl Acad Sci USA* **110**:9385–9390. doi:10.1073/pnas.1300130110
- Rosenblum EB, Poorten TJ, Joneson S, Settles M. 2012. Substrate-Specific Gene Expression in *Batrachochytrium dendrobatidis*, the Chytrid Pathogen of Amphibians. *PLoS One* **7**:e49924. doi:10.1371/journal.pone.0049924
- Rosenblum EB, Stajich JE, Maddox N, Eisen MB. 2008. Global gene expression profiles for life stages of the deadly amphibian pathogen *Batrachochytrium dendrobatidis*. *Proc Natl Acad Sci USA* **105**:17034–17039. doi:10.1073/pnas.0804173105
- Ruiz-Herrera J, Ortiz-Castellanos L. 2019. Cell wall glucans of fungi. A review. *Cell Surf* **5**:100022. doi:10.1016/j.tcs.2019.100022
- Ruiz-Herrera J, Ortiz-Castellanos L. 2010. Analysis of the phylogenetic relationships and evolution of the cell walls from yeasts and fungi. *FEMS Yeast Res* **10**:225–243. doi:10.1111/j.1567-1364.2009.00589.x
- Sage D, Donati L, Soulez F, Fortun D, Schmit G, Seitz A, Guiet R, Vonesch C, Unser M. 2017. DeconvolutionLab2: An open-source software for deconvolution microscopy.

*Methods* **115**:28-41. doi:10.1016/j.ymeth.2016.12.015

Sathe-Pathak V, Raghukumar S, Raghukumar C. 1993. Thraustochytrid and fungal component of marine detritus. I-Field studies on decomposition of the brown alga *Sargassum cinereum*. *Aquat Microb Ecol* **9**(2):117-125. doi: 10.1016/0022-0981(94)90160-0.

Schaller GB. 2009. The Serengeti lion: a study of predator-prey relations. University of Chicago Press.

Scheele BC, Pasmans F, Skerratt LF, Berger L, Martel A, Beukema W, Acevedo AA, Burrowes PA, Carvalho T, Catenazzi A, De La Riva I, Fisher MC, Flechas SV, Foster CN, Frías-Álvarez P, Garner TWJ, Gratwicke B, Guayasamin JM, Hirschfeld M, Kolby JE, Kosch TA, Marca E La, Lindenmayer DB, Lips KR, Longo AV, Maneyro R, McDonald CA, Mendelson J, Palacios-Rodriguez P, Parra-Olea G, Richards-Zawacki CL, Rödel MO, Rovito SM, Soto-Azat C, Toledo LF, Voyles J, Weldon C, Whitfield SM, Wilkinson M, Zamudio KR, Canessa S. 2019. Amphibian fungal panzootic causes catastrophic and ongoing loss of biodiversity. *Science* **363**:1459–1463. doi:10.1126/science.aav0379

Schindelin J, Arganda-Carreras I, Frise E, Kaynig V, Longair M, Pietzsch T, Preibisch S, Rueden C, Saalfeld S, Schmid B, Tinevez JY, White DJ, Hartenstein V, Eliceiri K, Tomancak P, Cardona A. 2012. Fiji: An open-source platform for biological-image analysis. *Nat Methods* **9**(7):676-682. doi:10.1038/nmeth.2019

Schmoyer IR, Lovett JS. 1969. Regulation of protein synthesis in zoospores of *Blastocladiella*. *J Bacteriol* **100**:854–864. doi:10.1128/jb.100.2.854-864.1969

Scholz B, Guillou L, Marano AV, Neuhauser S, Sullivan BK, Karsten U, Küpper FC, Gleason FH. 2016a. Zoosporic parasites infecting marine diatoms-A black box that needs to be opened. *Fungal Ecol* **19**:59–76. doi:10.1016/j.funeco.2015.09.002

Scholz B, Küpper F, Vyverman W, Ólafsson H, Karsten U. 2017. Chytridiomycosis of Marine Diatoms—The Role of Stress Physiology and Resistance in Parasite-Host Recognition and Accumulation of Defense Molecules. *Mar Drugs* **15**:26-45. doi:10.3390/md15020026

Scholz B, Küpper FC, Vyverman W, Karsten U. 2016b. Effects of eukaryotic pathogens

- (Chytridiomycota and Oomycota) on marine benthic diatom communities in the Solthörn tidal flat (southern North Sea, Germany). *Eur J Phycol* **51**:253–269. doi:10.1080/09670262.2015.1134814
- Searle CL, Mendelson JR, Green LE, Duffy MA. 2013. *Daphnia* predation on the amphibian chytrid fungus and its impacts on disease risk in tadpoles. *Ecol Evol* **3**:4129–4138. doi:10.1002/ece3.777
- Semighini CP, Harris SD. 2008. Regulation of apical dominance in *Aspergillus nidulans* hyphae by reactive oxygen species. *Genetics* **179**:1919–1932. doi:10.1534/genetics.108.089318
- Seong KY, Zhao X, Xu JR, Güldener U, Kistler HC. 2008. Conidial germination in the filamentous fungus *Fusarium graminearum*. *Fungal Genet Biol* **45**:389–399. doi:10.1016/j.fgb.2007.09.002
- Sharma M, Sengupta A, Ghosh R, Agarwal G, Tarafdar A, Nagavardhini A, Pande S, Varshney RK. 2016. Genome wide transcriptome profiling of *Fusarium oxysporum* f sp. ciceris conidial germination reveals new insights into infection-related genes. *Sci Rep* **6**:1–11. doi:10.1038/srep37353
- Shertz CA, Bastidas RJ, Li W, Heitman J, Cardenas ME. 2010. Conservation, duplication, and loss of the Tor signaling pathway in the fungal kingdom. *BMC Genomics* **11**:1–14. doi:10.1186/1471-2164-11-510
- Silva S, Matz L, Elmassry MM, San Francisco MJ. 2019. Characteristics of monolayer formation in vitro by the chytrid *Batrachochytrium dendrobatidis*. *Biofilm* **1**:100009. doi:10.1016/j.biofilm.2019.100009
- Sime-Ngando T, Rasconi S, Gerphagnon M. 2013. Diagnosis of Parasitic Fungi in the Plankton: Technique for Identifying and Counting Infective Chytrids Using Epifluorescence Microscopy in *Laboratory Protocols in Fungal Biology*. Springer New York. pp. 169–174. doi:10.1007/978-1-4614-2356-0\_11
- Simmons DR, Bonds AE, Castillo BT, Clemons RA, Glasco AD, Myers JM, Thapa N, Letcher PM, Powell MJ, Longcore JE, James TY. 2020. The Collection of Zoosporic Eufungi at the University of Michigan (CZEUM): Introducing a new repository of barcoded Chytridiomycota and Blastocladiomycota cultures. *IMA Fungus* **11**:1–22.



doi:10.1186/s43008-020-00041-z

- Skovgaard A. 2014. Dirty tricks in the plankton: Diversity and role of marine parasitic protists. *Acta Protozool* **53**(1):51-62. doi:10.4467/16890027AP.14.006.1443
- Slamovits CH, Fast NM, Law JS, Keeling PJ. 2004. Genome compaction and stability in microsporidian intracellular parasites. *Curr Biol* **14**:891–896.  
doi:10.1016/j.cub.2004.04.041
- Sparrow FK. 1960. Aquatic Phycomycetes. Ann Arbor: Univ. Michigan Press.  
doi:10.5962/bhl.title.5685
- Sparrow FK. 1936. Biological Observations on the Marine Fungi of Woods Hole Waters. *Biol Bull* **70**:236–263. doi:10.2307/1537470
- Stajich JE, Berbee ML, Blackwell M, Hibbett DS, James TY, Spatafora JW, Taylor JW. 2009. The Fungi. *Curr Biol* **19**(18):R840. doi:10.1016/j.cub.2009.07.004
- Stajich JE, Harris T, Brunk BP, Brestelli J, Fischer S, Harb OS, Kissinger JC, Li W, Nayak V, Pinney DF, Stoeckert CJ, Roos DS. 2012. FungiDB: An integrated functional genomics database for fungi. *Nucleic Acids Res* **40** (D1):D675-D681.  
doi:10.1093/nar/gkr918
- Stamatakis A. 2014. RAxML version 8: a tool for phylogenetic analysis and post-analysis of large phylogenies. *Bioinformatics* **30**(9):1312-1313.  
doi:10.1093/bioinformatics/btu033
- Steinberg G, Peñalva MA, Riquelme M, Wösten HA, Harris SD. 2017. Cell Biology of Hyphal Growth in *The Fungal Kingdom*. Washington, DC, USA: ASM Press. pp. 231–265. doi:10.1128/9781555819583.ch11
- Stockley EW, Cole HM, Brown AD, Wheal HV. 1993. A system for quantitative morphological measurement and electrotonic modelling of neurons: three-dimensional reconstruction. *J Neurosci Methods* **47**:39–51. doi:10.1016/0165-0270(93)90020-R
- Strullu-Derrien C, Goral T, Longcore JE, Olesen J, Kenrick P, Edgecombe GD. 2016. A new chytridiomycete fungus intermixed with crustacean resting eggs in a 407-million-year-old continental freshwater environment. *PLoS One* **11**:e0167301.  
doi:10.1371/journal.pone.0167301

- Strullu-Derrien C, Spencer ART, Goral T, Dee J, Honegger R, Kenrick P, Longcore JE, Berbee ML. 2018. New insights into the evolutionary history of fungi from a 407 Ma Blastocladiomycota fossil showing a complex hyphal thallus. *Philos Trans R Soc B Biol Sci* **373**. doi:10.1098/rstb.2016.0502
- Swafford AJM, Hussey SP, Fritz-Laylin LK. 2020. High-efficiency electroporation of chytrid fungi. *Sci Reports* **10**:1–9. doi:10.1038/s41598-020-71618-2
- Tarling EJ, de Aguiar Vallim TQ, Edwards PA. 2013. Role of ABC transporters in lipid transport and human disease. *Trends Endocrinol Metab* **24**(7):342-350  
doi:10.1016/j.tem.2013.01.006
- Taube R, Fabian J, Van den Wyngaert S, Agha R, Baschien C, Gerphagnon M, Kagami M, Krüger A, Premke K. 2019. Potentials and limitations of quantification of fungi in freshwater environments based on PLFA profiles. *Fungal Ecol* **41**:256–268.  
doi:10.1016/j.funeco.2019.05.002
- Taylor JD, Cunliffe M. 2016. Multi-year assessment of coastal planktonic fungi reveals environmental drivers of diversity and abundance. *ISME J* **10**:2118–2128.  
doi:10.1038/ismej.2016.24
- Taylor JW, Fuller MS. 1980. Microtubules, organelle movement, and cross-wall formation at the sporangial-rhizoidal interface in the fungus, *Chytridium confervae*. *Protoplasma* **104**:201–221. doi:10.1007/BF01279768
- Taylor TN, Remy W, Hass H. 1992. Fungi from the lower Devonian Rhynie Chert: chytridiomycetes. *Am J Bot* **79**:1233–1241. doi:10.1002/j.1537-2197.1992.tb13726.x
- Tedersoo L, Sánchez-Ramírez S, Kõljalg U, Bahram M, Döring M, Schigel D, May T, Ryberg M, Abarenkov K. 2018. High-level classification of the Fungi and a tool for evolutionary ecological analyses. *Fungal Divers* **90**:135–159. doi:10.1007/s13225-018-0401-0
- Thekkiniath J, Zabet-Moghaddam M, Kottapalli KR, Pasham MR, San Francisco S, San Francisco M. 2015. Quantitative proteomics of an amphibian pathogen, *Batrachochytrium dendrobatidis*, following exposure to thyroid hormone. *PLoS One* **10**:e0123637. doi:10.1371/journal.pone.0123637
- Thekkiniath JC, Zabet-Moghaddam M, San Francisco SK, San Francisco MJ. 2013. A

novel subtilisin-like serine protease of *Batrachochytrium dendrobatidis* is induced by thyroid hormone and degrades antimicrobial peptides. *Fungal Biol* **117**:451–461.

doi:10.1016/j.funbio.2013.05.002

Tinevez JY, Perry N, Schindelin J, Hoopes GM, Reynolds GD, Laplantine E, Bednarek SY, Shorte SL, Eliceiri KW. 2017. TrackMate: An open and extensible platform for single-particle tracking. *Methods* **115**:80–90. doi:10.1016/j.ymeth.2016.09.016

Torben-Nielsen B. 2014. An efficient and extendable python library to analyze neuronal morphologies. *Neuroinformatics* **2014**: 619-622. doi:10.1007/s12021-014-9232-7

Trinci APJ. 1974. A study of the kinetics of hyphal extension and branch initiation of fungal mycelia. *J Gen Microbiol* **81**:225–236. doi:10.1099/00221287-81-1-225

Van't Padje A, Werner GDA, Kiers ET. 2021. Mycorrhizal fungi control phosphorus value in trade symbiosis with host roots when exposed to abrupt 'crashes' and 'booms' of resource availability. *New Phytol* **229**:2933–2944. doi:10.1111/nph.17055

Van De Vossenberg BTLH, Prodhomme C, Van Arkel G, Van Gent-Pelzer MPE, Bergervoet M, Brankovics B, Przetakiewicz J, Visser RGF, Van Der Lee TAJ, Vossen JH. 2019. The *Synchytrium endobioticum avrsen1* triggers a hypersensitive response in sen1 potatoes while natural variants evade detection. *Mol Plant-Microbe Interact* **32**:1536–1546. doi:10.1094/MPMI-05-19-0138-R

Van de Vossenberg BTLH, Warris S, Nguyen HDT, van Gent-Pelzer MPE, Joly DL, van de Geest HC, Bonants PJM, Smith DS, Lévesque CA, van der Lee TAJ. 2019. Comparative genomics of chytrid fungi reveal insights into the obligate biotrophic and pathogenic lifestyle of *Synchytrium endobioticum*. *Sci Rep* **9**:1–14.

doi:10.1038/s41598-019-45128-9

Van den Wyngaert S, Seto K, Rojas-Jimenez K, Kagami M, Grossart HP. 2017. A New Parasitic Chytrid, *Staurastromyces oculus* (Rhizophydiales, Staurastromycetaceae fam. nov.), Infecting the Freshwater Desmid *Staurastrum* sp. *Protist* **168**:392–407.

doi:10.1016/j.protis.2017.05.001

Van Der Walt S, Schönberger JL, Nunez-Iglesias J, Boulogne F, Warner JD, Yager N, Gouillart E, Yu T. 2014. Scikit-image: Image processing in python. *PeerJ* **2014**:e453.

doi:10.7717/peerj.453

- Van Zutphen T, Todde V, De Boer R, Kreim M, Hofbauer HF, Wolinski H, Veenhuis M, Van Der Klei IJ, Kohlwein SD. 2014. Lipid droplet autophagy in the yeast *Saccharomyces cerevisiae*. *Mol Biol Cell* **25**:290–301. doi:10.1091/mbc.E13-08-0448
- Velle KB, Fritz-Laylin LK. 2019. Diversity and evolution of actin-dependent phenotypes. *Curr Opin Genet Dev* **58**:40-48. doi:10.1016/j.gde.2019.07.016
- Velthuis M, de Senerpont Domis LN, Frenken T, Stephan S, Kazanjian G, Aben R, Hilt S, Kosten S, van Donk E, Van de Waal DB. 2017. Warming advances top-down control and reduces producer biomass in a freshwater plankton community. *Ecosphere* **8**:e01651. doi:10.1002/ecs2.1651
- Venard CM, Vasudevan KK, Stearns T. 2020. Cilium axoneme internalization and degradation in chytrid fungi. *Cytoskeleton* **77**:365–378. doi:10.1002/cm.21637
- Verbrugghe E, Adriaensen C, Martel A, Vanhaecke L, Pasmans F. 2019. Growth regulation in amphibian pathogenic chytrid fungi by the quorum sensing metabolite tryptophol. *Front Microbiol* **10**:3277. doi:10.3389/fmicb.2018.03277
- Veses V, Richards A, Gow NA. 2008. Vacuoles and fungal biology. *Curr Opin Microbiol* **11**(6):503-510. doi:10.1016/j.mib.2008.09.017
- Vevea JD, Garcia EJ, Chan RB, Zhou B, Schultz M, Di Paolo G, McCaffery JM, Pon LA. 2015. Role for Lipid Droplet Biogenesis and Microlipophagy in Adaptation to Lipid Imbalance in Yeast. *Dev Cell* **35**:584–599. doi:10.1016/j.devcel.2015.11.010
- Vinck A, Terlouw M, Pestman WR, Martens EP, Ram AF, van den Hondel CAMJJ, Wösten HAB. 2005. Hyphal differentiation in the exploring mycelium of *Aspergillus niger*. *Mol Microbiol* **58**:693–699. doi:10.1111/j.1365-2958.2005.04869.x
- Virtanen P, Gommers R, Oliphant TE, Haberland M, Reddy T, Cournapeau D, Burovski E, Peterson P, Weckesser W, Bright J, van der Walt SJ, Brett M, Wilson J, Millman KJ, Mayorov N, Nelson ARJ, Jones E, Kern R, Larson E, Carey CJ, Polat İ, Feng Y, Moore EW, VanderPlas J, Laxalde D, Perktold J, Cimrman R, Henriksen I, Quintero EA, Harris CR, Archibald AM, Ribeiro AH, Pedregosa F, van Mulbregt P, Vijaykumar A, Bardelli A, Rothberg A, Hilboll A, Kloeckner A, Scopatz A, Lee A, Rokem A, Woods CN, Fulton C, Masson C, Häggström C, Fitzgerald C, Nicholson DA, Hagen DR, Pasechnik D V, Olivetti E, Martin E, Wieser E, Silva F, Lenders F, Wilhelm F,

Young G, Price GA, Ingold GL, Allen GE, Lee GR, Audren H, Probst I, Dietrich JP, Silterra J, Webber JT, Slavič J, Nothman J, Buchner J, Kulick J, Schönberger JL, de Miranda Cardoso JV, Reimer J, Harrington J, Rodríguez JLC, Nunez-Iglesias J, Kuczynski J, Tritz K, Thoma M, Newville M, Kümmerer M, Bolingbroke M, Tartre M, Pak M, Smith NJ, Nowaczyk N, Shebanov N, Pavlyk O, Brodtkorb PA, Lee P, McGibbon RT, Feldbauer R, Lewis S, Tygier S, Sievert S, Vigna S, Peterson S, More S, Pudlik T, Oshima T, Pingel TJ, Robitaille TP, Spura T, Jones TR, Cera T, Leslie T, Zito T, Krauss T, Upadhyay U, Halchenko YO, Vázquez-Baeza Y. 2020. SciPy 1.0: fundamental algorithms for scientific computing in Python. *Nat Methods* **17**:261–272. doi:10.1038/s41592-019-0686-2

Walke JB, Becker MH, Loftus SC, House LL, Teotonio TL, Minbiole KPC, Belden LK. 2015. Community structure and function of amphibian skin microbes: An experiment with bullfrogs exposed to a chytrid fungus. *PLoS One* **10**:e0139848. doi:10.1371/journal.pone.0139848

Waller RF, Cleves PA, Rubio-Brotons M, Woods A, Bender SJ, Edgcomb V, Gann ER, Jones AC, Teytelman L, von Dassow P, Wilhelm SW, Collier JL. 2018. Strength in numbers: Collaborative science for new experimental model systems. *PLOS Biol* **16**:e2006333. doi:10.1371/journal.pbio.2006333

Wang Y, Guo X, Zheng P, Zou S, Li G, Gong J. 2017. Distinct seasonality of chytrid-dominated benthic fungal communities in the neritic oceans (Bohai Sea and North Yellow Sea). *Fungal Ecol* **30**:55–66. doi:10.1016/j.funeco.2017.08.008

Wang Y, Kim SG, Wu J, Yu S, Kang KY, Kim ST. 2011. Proteasome inhibitors affect appressorium formation and pathogenicity of the rice blast fungus, *Magnaporthe oryzae*. *Plant Pathol J* **27**:225–231. doi:10.5423/PPJ.2011.27.3.225

Watters MK, Boersma M, Johnson M, Reyes C, Westrick E, Lindamood E. 2011. A screen for *Neurospora* knockout mutants displaying growth rate dependent branch density. *Fungal Biol* **115**:296–301. doi:10.1016/J.FUNBIO.2010.12.015

Whiteside MD, Werner GDA, Caldas VEA, van't Padje A, Dupin SE, Elbers B, Bakker M, Wyatt GAK, Klein M, Hink MA, Postma M, Vaitla B, Noë R, Shimizu TS, West SA, Kiers ET. 2019. Mycorrhizal Fungi Respond to Resource Inequality by Moving

Phosphorus from Rich to Poor Patches across Networks. *Curr Biol* **29**:2043-2050.e8.

doi:10.1016/j.cub.2019.04.061

Wood V, Gwilliam R, Rajandream MA, Lyne M, Lyne R, Stewart A, Sgouros J, Peat N, Hayles J, Baker S, Basham D, Bowman S, Brooks K, Brown D, Brown S, Chillingworth T, Churcher C, Collins M, Connor R, Cronin A, Davis P, Feltwell T, Fraser A, Gentles S, Goble A, Hamlin N, Harris D, Hidalgo J, Hodgson G, Holroyd S, Hornsby T, Howarth S, Huckle EJ, Hunt S, Jagels K, James K, Jones L, Jones M, Leather S, McDonald S, McLean J, Mooney P, Moule S, Mungall K, Murphy L, Niblett D, Odell C, Oliver K, O'Neil S, Pearson D, Quail MA, Rabbinowitsch E, Rutherford K, Rutter S, Saunders D, Seeger K, Sharp S, Skelton J, Simmonds M, Squares R, Squares S, Stevens K, Taylor K, Taylor RG, Tivey A, Walsh S, Warren T, Whitehead S, Woodward J, Volckaert G, Aert R, Robben J, Grymonprez B, Weltjens I, Vanstreels E, Rieger M, Schäfer M, Müller-Auer S, Gabel C, Fuchs M, Fritzc C, Holzer E, Moestl D, Hilbert H, Borzym K, Langer I, Beck A, Lehrach H, Reinhardt R, Pohl TM, Eger P, Zimmermann W, Wedler H, Wambutt R, Purnelle B, Goffeau A, Cadieu E, Dréano S, Gloux S, Lelaure V, Mottier S, Galibert F, Aves SJ, Xiang Z, Hunt C, Moore K, Hurst SM, Lucas M, Rochet M, Gaillardin C, Tallada VA, Garzon A, Thode G, Daga RR, Cruzado L, Jimenez J, Sánchez M, del Rey F, Benito J, Domínguez A, Revuelta JL, Moreno S, Armstrong J, Forsburg SL, Cerrutti L, Lowe T, McCombie WR, Paulsen I, Potashkin J, Shpakovski GV, Ussery D, Barrell BG, Nurse P. 2002. The genome sequence of *Schizosaccharomyces pombe*. *Nature* **415**:871–880. doi:10.1038/nature724

Worden AZ, Follows MJ, Giovannoni SJ, Wilken S, Zimmerman AE, Keeling PJ. 2015.

Rethinking the marine carbon cycle: Factoring in the multifarious lifestyles of microbes. *Science* **347**:1257594. doi:10.1126/science.1257594

Wurzbacher C, Rösel S, Rychła A, Grossart HP. 2014. Importance of saprotrophic freshwater fungi for pollen degradation. *PLoS One* **9**:e94643.

doi:10.1371/journal.pone.0094643

Yarden O. 2016. Model fungi: Engines of scientific insight. *Fungal Biol Rev* **30**(2):33-35.

doi:10.1016/j.fbr.2016.05.002

- Yoshida M, Nakayama T, Inouye I. 2009. *Nuclearia thermophila* sp. nov. (Nucleariidae), a new nucleariid species isolated from Yunoko Lake in Nikko (Japan). *Eur J Protistol* **45**:147–155. doi:10.1016/j.ejop.2008.09.004
- Yu G, Wang LG, Han Y, He QY. 2012. clusterProfiler: an R package for comparing biological themes among gene clusters. *OmicS: a journal of integrative biology* **16**(5): 284-287. doi: 10.1089/omi.2011.0118
- Zhou T, Wang X, Luo J, Ye B, Zhou Y, Zhou L, Lai T. 2018. Identification of differentially expressed genes involved in spore germination of *Penicillium expansum* by comparative transcriptome and proteome approaches. *Microbiology Open* **7**:e00562. doi:10.1002/mbo3.562

## Peer-reviewed publications associated with this work

Laundon D and Cunliffe M. 2021. A call for a better understanding of aquatic chytrid biology. *Front Fungal Biol* **2**:1-8. doi:10.3389/ffunb.2021.708813

Copyright © 2021 Laundon and Cunliffe. This is an open-access article distributed under the terms of the Creative Commons Attribution License (CC BY). The use, distribution or reproduction in other forums is permitted, provided the original author(s) and the copyright owner(s) are credited and that the original publication in this journal is cited, in accordance with accepted academic practice. No use, distribution or reproduction is permitted which does not comply with these terms.





# A Call for a Better Understanding of Aquatic Chytrid Biology

Davis Laundon<sup>1,2</sup> and Michael Cunliffe<sup>1,3\*</sup>

<sup>1</sup> Marine Biological Association, The Laboratory, Citadel Hill, Plymouth, United Kingdom, <sup>2</sup> School of Environmental Sciences, University of East Anglia, Norwich, United Kingdom, <sup>3</sup> School of Biological and Marine Sciences, University of Plymouth, Plymouth, United Kingdom

## OPEN ACCESS

### Edited by:

Belle Damodara Shenoy,  
CSIR-National Institute of  
Oceanography, India

### Reviewed by:

Rajesh Jeewon,  
University of Mauritius, Mauritius  
Maiko Kagami,  
Yokohama National University, Japan  
Hyang Burm Lee,  
Chonnam National University,  
South Korea

### \*Correspondence:

Michael Cunliffe  
micnl@mba.ac.uk

### Specialty section:

This article was submitted to  
Marine and Freshwater Fungi,  
a section of the journal  
Frontiers in Fungal Biology

**Received:** 12 May 2021

**Accepted:** 09 July 2021

**Published:** 04 August 2021

### Citation:

Laundon D and Cunliffe M (2021) A  
Call for a Better Understanding of  
Aquatic Chytrid Biology.  
Front. Fungal Biol. 2:708813.  
doi: 10.3389/ffunb.2021.708813

The phylum Chytridiomycota (the “chytrids”) is an early-diverging, mostly unicellular, lineage of fungi that consists of significant aquatic saprotrophs, parasites, and pathogens, and is of evolutionary interest because its members retain biological traits considered ancestral in the fungal kingdom. While the existence of aquatic chytrids has long been known, their fundamental biology has received relatively little attention. We are beginning to establish a detailed understanding of aquatic chytrid diversity and insights into their ecological functions and prominence. However, the underpinning biology governing their aquatic ecological activities and associated core processes remain largely understudied and therefore unresolved. Many biological questions are outstanding for aquatic chytrids. What are the mechanisms that control their development and life cycle? Which core processes underpin their aquatic influence? What can their biology tell us about the evolution of fungi and the wider eukaryotic tree of life? We propose that the field of aquatic chytrid ecology could be further advanced through the improved understanding of chytrid biology, including the development of model aquatic chytrids and targeted studies using culture-independent approaches.

**Keywords:** chytrid, chytridiomycota, saprotroph, parasite, aquatic

## INTRODUCTION

The phylum Chytridiomycota (Hibbett et al., 2007) (the “chytrids”) is an early-diverging, predominantly unicellular group of fungi that use anucleate rhizoids to attach and feed on substrates, and reproduce by motile uniflagellate zoospores (Sparrow, 1960; Naranjo-Ortiz and Gabaldón, 2019) (**Figures 1A,B**). Chytrids are important components of aquatic ecosystems (**Figure 1C**), and their ecological impact has been thoroughly reviewed by previous authors (Frenken et al., 2017; Gleason et al., 2017; Grossart et al., 2019). In addition, chytrids retain biological characteristics and traits shared with their last common ancestor with hyphal fungi, making them of interest to evolutionary biologists, which has also been recently well-reviewed (Berbee et al., 2017; Nagy et al., 2017; Naranjo-Ortiz and Gabaldón, 2020). Even though aquatic chytrids have long been known to science, their fundamental biology has received relatively little attention compared to other fungi.

It is not the aim of this perspective article to review the entire fields of chytrid biology, ecology, and evolution, but to highlight recent advances related to aquatic chytrid research and knowledge gaps. It is also not within the scope of this perspective to discuss developments in chytrid taxonomy and molecular phylogeny, which have been recently covered by others (Frenken et al., 2017; Hurdeal et al., 2021). We also provide our opinion on the future direction of aquatic chytrid research, including important questions to be addressed and how this could be achieved. Our

standpoint is the importance of the fundamental biology of chytrids and how increased biological knowledge could improve understanding of the ecology and evolution of aquatic chytrids.

## BIOLOGY UNDERPINNING AQUATIC CHYTRID ECOLOGY

Motile zoospores are a major feature of aquatic chytrids, which enable the targeting of trophic substrates and hosts by the propagules in a way not possible by dikaryan spores. Dissolved molecules act as chemoattractants for zoospores (Muehlstein et al., 1988; Moss et al., 2008; Scholz et al., 2017). *Batrachochytrium dendrobatidis* Longcore et al. (1999) zoospores are attracted to amphibian thyroid hormone (Thekkiniath et al., 2013) and are repelled by antifungal metabolites produced by amphibian skin bacteria (Lam et al., 2011). Zoospores have also been shown to exhibit positive phototaxis (Muehlstein et al., 1987). Cell structures, including the enigmatic chytrid rumposome, that connect the cell surface with the flagellar apparatus have been implicated in zoospore response to environmental signals (Powell, 1983), however detailed mechanisms of environmental sensing and guided motility in aquatic chytrid zoospores are currently unknown.

While the trophic range and ecological niches are established for some chytrids [e.g., *Rhizoclostridium globosum* Petersen is a saprotroph commonly found attached to chitin-rich exuviae (Sparrow, 1960)], we know little about the degradation enzymes, mechanical processes, and physiology of nutrient assimilation. This is particularly important for degraders of recalcitrant biopolymers and hosts that are inaccessible to other heterotrophs (Kagami et al., 2014; Agha et al., 2016). Comparative genomics suggest that chytrids use a range of extracellular enzymes as part of their secretome, including carbohydrate-active enzymes (CAZymes) (Lange et al., 2019), that are yet to be characterized in any biological detail.

The biochemical development of lipid-rich zoospores is important in aquatic ecosystems because of trophic transfer through the mycology (Kagami et al., 2007a). Zoospore lipid profiling has shown enrichment in polyunsaturated fatty acids (PUFAs) and sterols (Kagami et al., 2007b; Akinwale et al., 2014). Parasitic chytrids have PUFA profiles that are similar to their hosts, indicating direct assimilation, and new sterols that are likely synthesized *de novo* (Gerphagnon et al., 2019). These details have been instrumental in quantitative aquatic ecology, allowing the modeling of C:N:P stoichiometry and nutrient flux through ecosystems (Kagami et al., 2007b). The biochemistry of lipid anabolism and intracellular transport during zoosporogenesis, and lipid catabolism during zoospore free-swimming and encystment are largely uncharacterized.

A major knowledge gap in understanding the ecological function of aquatic chytrids from a biological view is their wider role as parasites and pathogens, particularly of algae, because most of this knowledge comes from amphibian and plant hosts. Culture-based studies have characterized the impact of *B. dendrobatidis* secretions on amphibian skin (Moss et al., 2008; Rollins-Smith et al., 2019) and investigations of growth physiology have allowed for general phenotypic profiling

(Berger et al., 2005; Voyles, 2011), but quantitative biological investigations into chytrid parasites of other aquatic hosts are largely lacking.

## THE BIOLOGY OF CHYTRIDS IN TERMS OF FUNGAL TRAIT EVOLUTION

Chytrids and their close relatives represent a key transition in the fungal kingdom from generally unicellular and rhizoidal growth toward multicellularity and hyphal growth (Berbee et al., 2017; Nagy et al., 2017). As extant chytrids exhibit ancestral characteristics of the progenitors of multicellular and hyphal fungi (Berbee et al., 2017; Nagy et al., 2017), insights into their cell biology can help infer traits associated with the origin of the archetypal fungal cell form.

Of prominence are investigations into the biology of chytrid rhizoids, as it has been hypothesized that rhizoids or rhizoid-like structures were the evolutionary precursors to hyphae (Dee et al., 2015, 2019; Kiss et al., 2019; Laundon et al., 2020). Comparative genomics has suggested that hyphae evolved in the rhizoid-bearing Chytridiomycota-Blastocladiomycota-Zoopagomycota nodes of the fungal tree (Kiss et al., 2019). Monoblepharids, a sister group to the chytrids, have aseptate coenocytic hyphal growth as their predominant cell plan (Dee et al., 2015). Cytoskeleton, cytoplasmic, and vesicular organization in the hyphae of zoosporic and dikaryan fungi suggests multiple convergent origins of hyphae from rhizoid-bearing lineages (Dee et al., 2015). In chytrids, actin polymerization and cell wall synthesis guide rhizoid morphogenesis (Dee et al., 2015; Laundon et al., 2020; Medina et al., 2020), as in hyphal growth (Gow et al., 2017; Steinberg et al., 2017; Riquelme et al., 2018). Actin cables and patches are present throughout the rhizoids of several chytrid species (Dee et al., 2019; Laundon et al., 2020; Medina et al., 2020) and inhibition of normal actin polymerization disrupts rhizoid branching causing hyperbranched paramorphs (Dee et al., 2019; Laundon et al., 2020). Inhibition of cell wall synthesis also results in similarly abnormal rhizoids (Laundon et al., 2020).

Quantitative microscopy has shown that saprotrophic aquatic chytrid rhizoids are capable of developmental plasticity and functional differentiation analogous to that characteristically displayed by mycelial dikaryans (Laundon et al., 2020). Parasitic chytrids can also have outstretched rhizoids capable of finding new algal hosts (Longcore et al., 1999) and penetrating through the frustule girdle of host diatoms (Beakes et al., 1992). These few studies into the chytrid rhizoid present a promising beginning in understanding the trophic interface of the chytrid cell for both saprotrophs and parasites, and have laid the foundation for future, quantitative cell biology in rhizoid development.

## KNOWLEDGE GAPS IN AQUATIC CHYTRID BIOLOGY AND POSSIBLE FUTURE DIRECTIONS

Here we identify research questions that we think stand out as areas for investigation to help improve understanding aquatic chytrid biology, ecology, and evolution (**Figure 2**). This is not an

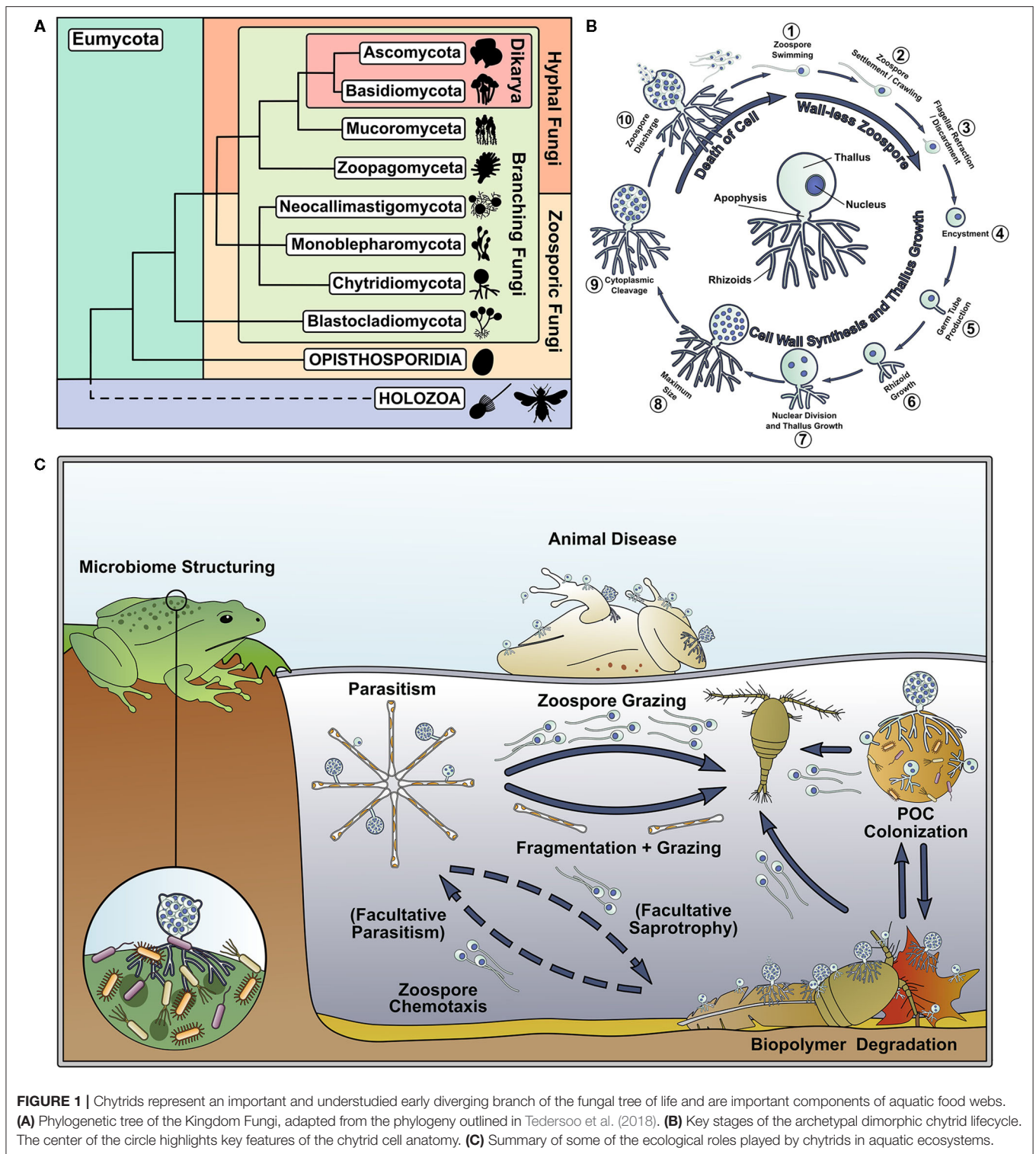
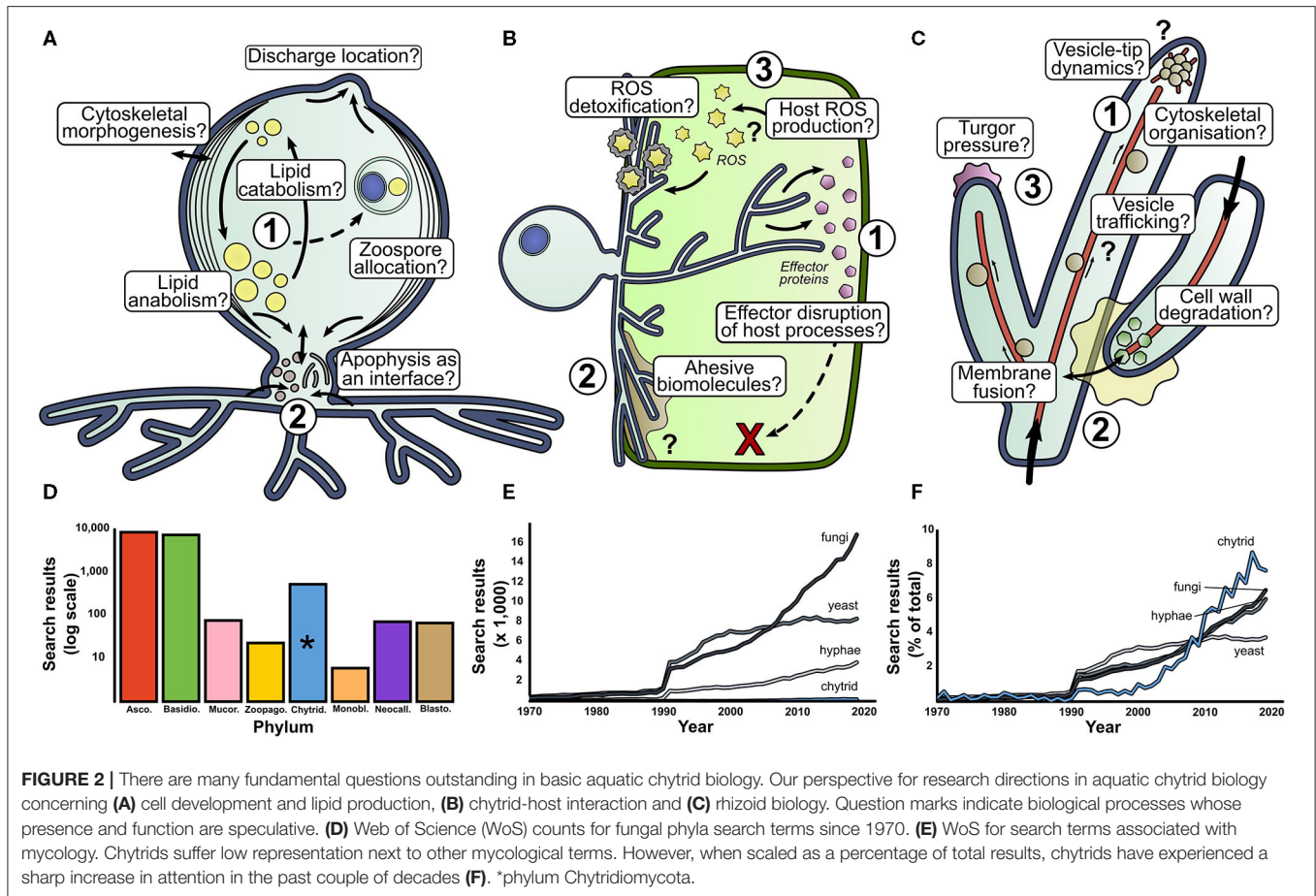


**FIGURE 1** | Chytrids represent an important and understudied early diverging branch of the fungal tree of life and are important components of aquatic food webs. **(A)** Phylogenetic tree of the Kingdom Fungi, adapted from the phylogeny outlined in Tedersoo et al. (2018). **(B)** Key stages of the archetypal dimorphic chytrid lifecycle. The center of the circle highlights key features of the chytrid cell anatomy. **(C)** Summary of some of the ecological roles played by chytrids in aquatic ecosystems.

attempt at an exhaustive list, but our perspective of knowledge gaps and future research directions that could stimulate interest and discussion.

*Chytrid cell biology important for aquatic ecology (Figure 2A)*

1. Lipid accumulation in chytrid zoospores is a key contributing factor to their ecological impact (Akinwole et al., 2014; Kagami et al., 2014; Gerphagnon et al., 2019). A large proportion of intracellular space is devoted to lipid storage, with evidence to suggest that lipid stores are dynamic throughout the zoospore



stages of the chytrid life cycle (Powell, 1976). How are lipids synthesized and what are the anabolic pathways of lipid accumulation under different trophic conditions? How are lipid stores localized, regulated, and trafficked through the chytrid cell? What cellular processes govern the distribution and allocation of lipid reserves during zoosporogenesis? How does the balance between lipid anabolism and catabolism shift over the chytrid life cycle?

2. The apophysis is the subsporangial swelling in many chytrids that links the sporangia to the substrate attaching and feeding rhizoids (Laundon et al., 2020). Fluorescent labeling of the cell wall (Ota and Kawano, 2015) and endomembrane (Laundon, unpublished) have shown increased relative brightness in the apophysis compared to the sporangium indicating elevated activity, however the structure and function of the apophysis is largely unknown. What is the role of the apophysis in aquatic chytrids, how is the apophysis formed and what does it contain? How does the apophysis link the sporangium and rhizoids? Does the apophysis act as an interface between the reproductive and feeding structures?

*The biology behind aquatic chytrid-host interaction (Figure 2B)*

1. Genomic analysis of chytrid parasites show that they have genes that encode a suite of effector proteins and pathogenicity

factors (Thekkiniath et al., 2015; Ellison et al., 2017; Farrer et al., 2017; Van de Vossenberget al., 2019a,b). What are the functions of effector proteins and where is effector protein secretion localized? What is their phenotypic impact on host defense systems? What do chytrid parasites secrete when infecting hosts?

2. The biointerface between the chytrid and host represents the frontline of pathogenic cell biology where parasite virulence meets host defense, analogous to the biotrophic complex in other fungal parasites (Yan and Talbot, 2016). What biology characterizes the physical host-parasite interface and what is the biophysical composition of this interface from a subcellular and biostructural perspective? What proteins and carbohydrates are associated with parasite adhesion? What are the roles of turgor pressure, enzymatic degradation, and cytoskeletal organization in host penetration? How do penetrating rhizoids localize in subcellular compartments of the host, and how do they migrate through host cytoplasm? Is there division of labor in parasitic rhizoids (e.g., feeding vs. attachment) as with saprotrophic chytrids (Laundon et al., 2020)?

3. Reactive Oxygen Species (ROS) molecules are implicated in fungal pathogenicity as hypersensitive host defenses, cell signaling components, and parasite development cues

(Camejo et al., 2016). What is the role of ROS in chytrid parasitic biology? Do hosts from various taxa accumulate ROS as a defense against chytrid parasitism, as earlier proposed (Canter and Jaworski, 1979)? How do chytrid parasites deal with ROS? What is the role of ROS in parasite development and virulence? Where is ROS production localized at a subcellular level?

*The rhizoid—the interface between aquatic chytrids and their substrates (Figure 2C)*

1. Our understanding of the subcellular machinery involved in hyphal development is well-characterized (Riquelme et al., 2018) and provides hypotheses to investigate similarities and differences in chytrid rhizoids (Laundon et al., 2020). Cell wall and actin proliferation have been implicated in rhizoidal development (Dee et al., 2019; Laundon et al., 2020; Medina et al., 2020), but how do these processes differ along the rhizoidal axis? To what extent do vesicle trafficking, cytoskeleton organization, and secretory machinery interact at the rhizoidal tips? Do ion gradients drive rhizoidal extension? Are dikaryan “hyphal” orthologs expressed in aquatic chytrids and how do they contribute to rhizoid morphogenesis and function?
2. Anastomosis is a rare event in chytrids and is probably associated with sexual reproduction (Miller and Dylewski, 1981). The biology of hyphal fusion is well-understood (Read et al., 2014), but what drives chytrid rhizoidal fusion? What enzymes are associated with adhesion and cell wall degradation? What intracellular processes drive membrane fusion? Are endomembrane trafficking and vesicle formation important? How are homeostasis, nutrient translocation and network resilience affected by a fused rhizoidal system?
3. In addition to a molecular understanding of hyphal development, we have a good understanding of the physical forces governing hyphal growth (Lew, 2011; Roper and Seminara, 2019) providing ground for investigations into rhizoid biophysics and fluid mechanics. Is internal turgor pressure comparable in rhizoids and, if so, how is it generated? How does cytoplasm flow through the rhizoids and what is transported with it? How elastic is the cell wall to deformation?

## DEVELOPMENT OF MODEL AQUATIC CHYTRIDS

Chytrids are understudied relative to dikaryan fungi, but the situation is starting to improve (Figures 2D–F). Of chytrid publications however, a majority are based on studies with the amphibian pathogenic batrachochytrids and plant pathogen *Synchytrium endobioticum* (Schilb.) Percival. This research is vital for the protection of global biodiversity and food security, however, as their roles as pathogens is unusual amongst the chytrids, it is unlikely that their biology is representative of most aquatic chytrids. We propose that other chytrids should also be developed as aquatic models.

Key model features include an available annotated genome, relatively easy laboratory culture (ideally under axenic

conditions), a comparatively fast life cycle, experimental and genetic tractability, and representativeness of a major functional group (Leonelli and Ankeny, 2013; Yarden, 2016). For example, *Rhizoclosmatium globosum* (order Chytridiales) is a widespread, chitinophilic saprotroph, associated with chitin-rich particulate organic matter such as arthropod exuviae (Sparrow, 1960). It is frequently isolated from freshwater habitats (Canter, 1953) and is likely an ecologically important biopolymer degrader. *Rhizoclosmatium globosum* JEL800 was isolated by chitin baiting (Powell et al., 2019) and as an experimental organism is easy to culture, amenable to live-cell microscopy (Laundon et al., 2020), and has a rapid life cycle (~11–13 h at 22°C on rich medium) (Laundon, unpublished), making it an excellent choice to study aquatic chytrid biology. The *R. globosum* JEL800 genome is available via MycoCosm (Mondo et al., 2017), and the strain has been a model in studies on flagella retraction (Venard et al., 2020), rhizoid development (Laundon et al., 2020), and chytrid-bacteria interaction (Roberts et al., 2020).

The other major functional group of aquatic chytrids is as algal parasites (Gleason et al., 2008), some of which have been isolated into culture (Frenken et al., 2017). For example, *Rhizophydium littoreum* Amon (order Rhizophidiales) was isolated from the marine macroalga *Codium* from the East coast of the USA (Amon, 1984), is amenable to laboratory experimentation (Muehlstein et al., 1988) and has a dynamic trophic spectrum, ranging from saprotrophy to parasitism (Shields, 1990). Development of *R. littoreum* into a model chytrid could therefore shed light on the biology of marine facultative parasites. Other aquatic chytrid models could also contribute to our understanding of specific biological and ecological traits of algal parasites. For example, a stable co-cultured parasite-host system for obligate chytrid biotrophs will be necessary to fully resolve the biology of chytrid parasitism, such as the recently re-isolated *Zygorhizidium affluens* Canter (order Lobulomycetales) that infects the major spring bloom-forming freshwater diatom *Asterionella formosa* Hassall (Rad-Menéndez et al., 2018). Hopefully, sometime soon, successful cultures will also be isolated of chytrids that infect sea ice diatoms from the Arctic that have so far only been studied through culture-independent approaches and microscope observation (Hassett and Gradinger, 2016).

## POTENTIAL LIMITATIONS OF CULTURE-BASED APPROACHES AND COMPLEMENTARY ALTERNATIVES TO UNDERSTAND AQUATIC CHYTRID BIOLOGY

It is likely that by studying model aquatic chytrid cultures alone we will not fully emulate the natural aquatic environment in which chytrids occur, and therefore will not develop a complete view of aquatic chytrid biology. Berbee et al. (2017) raised the point that many chytrid cultures are isolated by baiting in which a substrate [e.g., pollen, snake skin, or defatted hair (Fuller and Jaworski, 1987)] is placed in the environment for an amount of time for zoospores to attach to before the bait is retrieved

and the bait-attached chytrids subsequently isolated. Depending on the bait used, it could be difficult to be certain of the natural substrates and niches of the isolated chytrids especially if maintained on complex laboratory media. Furthermore, when chytrids models are studied under axenic conditions the potential positive and negative complex interactions that take place with other components of aquatic ecosystems, such as bacteria (Roberts et al., 2020), will not be considered.

Environmental DNA (eDNA) based assessments of aquatic ecosystems have shown a vast diversity of zoospore fungi (including chytrids) that have no cultured representatives, in some cases entire clades (Grossart et al., 2016). These cryptic chytrids that are only known from molecular surveys have been called “dark matter fungi” (Grossart et al., 2016). For example, Richards et al. (2015) surveyed marine fungal diversity across six European sites using V4 SSU sequence data and retrieved familiar operational taxonomic unit (OTU) clusters closely related to known genera including *Kappamyces* (Rhizophydiales) and *Chytridium* (Chytridiales). The molecular survey also revealed many OTU clusters from clades without cultured representatives. Some of the OTU clusters with no cultured representatives had high relative coverage in the sequence libraries suggesting that these chytrids are abundant in the samples and therefore likely important players at the various marine sites sampled. Some of the OTU clusters are part of clades that have been found in other surveys elsewhere suggesting that they are widely distributed in the marine environment. It is possible that with improved sampling effort, some chytrids only previously known via molecular surveys could be isolated into culture. A multiyear eDNA-based time-series survey of marine fungal diversity in the coastal waters off Plymouth (UK) showed that in some years a chytrid OTU (OTU 14) was prevalent only during the spring diatom bloom suggesting that the chytrid was a diatom parasite (Taylor and Cunliffe, 2016). Garvetto et al. (2019) subsequently isolated a novel species within the Rhizophydiales that infected the bloom-forming diatom *Skeletonema* and was closely related to OTU14. If we only study cultured chytrid models (as outlined above) and ignore “dark matter chytrids,” we will not be able to achieve a truly complete understanding of aquatic chytrid biology.

Alternative approaches are available to study aquatic chytrid biology that do not rely on isolated model cultures and that are able to include “dark matter chytrids.” Single-cell genomics is one option to target uncultured aquatic chytrids (Ahrendt et al., 2018). The approach is based on the isolation of a target population of cells from a complex sample, such as via fluorescence-activated cell sorting (FACS), and the subsequent extraction of DNA, genomic DNA amplification and sequencing. The approach has been used to target uncultured mycoparasitic and saprotrophic early-diverging fungi including chytrids, and because genomic-level information is retrieved, gene-based aspects of biology such as potential niche associated metabolic capability can be predicted (Ahrendt et al., 2018).

Meta-omic approaches (metagenomics, metatranscriptomics, etc.) are now widely established in aquatic microbial ecology

and allow biological understanding to be established without cultivation of target organisms. Metagenomics and metatranscriptomics have been used effectively to explore the functional biology of other uncultivated aquatic fungi, including for example the potential role of marine fungi in organic matter processing (Chrismas and Cunliffe, 2020; Baltar et al., 2021). We are not aware of any studies so far that have used meta-omic approaches to specifically target and study aquatic chytrids, however this area has great potential and warrants attention.

## CONCLUDING REMARKS

Chytrids are widespread, sometimes dominant, fungi in a range of aquatic ecosystems. In addition, they are an appealing choice for evolutionary biologists understanding the position of aquatic fungi in the eukaryotic tree of life and the origins of fungal biological trait innovations. These factors have generated an interest in chytrids and a drive to understand their biology. The current increase in sequenced genomes and comparative genomics have made major contributions, but we cannot fully understand chytrid biology by genomic approaches alone. Parallel to these investigations, it is necessary to use culture-based investigations into chytrid biology and apply targeted culture-independent tools to explore aquatic chytrids *in natura*. We have outlined our perspective to bring aquatic chytrids closer to the forefront of fungal biology. This is a call not only for aquatic chytrid researchers, but also for general cell biologists to choose chytrids in their studies and take advantage of the potential of these aquatic fungi. The community should work collaboratively to achieve a comprehensive understanding of chytrid biology by combining skillsets, from taxonomists to cell biologists, and from evolutionary biologists and paleomycologists to contemporary aquatic ecologists. In these “little pots” resides great scope for discovery.

## DATA AVAILABILITY STATEMENT

The original contributions presented in the study are included in the article, further inquiries can be directed to the corresponding author.

## AUTHOR CONTRIBUTIONS

All authors listed have made a substantial, direct and intellectual contribution to the work, and approved it for publication.

## FUNDING

DL was supported by an EnvEast Doctoral Training Partnership (DTP) PhD studentship funded from the UKRI Natural Environment Research Council (NERC Grant No. NE/L002582/1). MC was supported by the European Research Council (ERC) (MYCO-CARB project; ERC Grant Agreement No. 772584).

## REFERENCES

- Agha, R., Saebelfeld, M., Manthey, C., Rohrlack, T., and Wolinska, J. (2016). Chytrid parasitism facilitates trophic transfer between bloom-forming cyanobacteria and zooplankton (*Daphnia*). *Sci. Rep.* 6, 1–9. doi: 10.1038/srep35039
- Ahrendt, S. R., Quandt, C. A., Ciobanu, D., Clum, A., Salamov, A., Andreopoulos, B., et al. (2018). Leveraging single-cell genomics to expand the fungal tree of life. *Nat. Microbiol.* 3, 1417–1428. doi: 10.1038/s41564-018-0261-0
- Akinwale, P. O., Lefevre, E., Powell, M. J., and Findlay, R. H. (2014). Unique odd-chain polyenoic phospholipid fatty acids present in chytrid fungi. *Lipids* 49, 933–942. doi: 10.1007/s11745-014-3934-3
- Amon, J. P. (1984). *Rhizophyidium littoreum*: a chytrid from siphonaceous marine algae—an ultrastructural examination. *Mycologia* 76, 132–139. doi: 10.1080/00275514.1984.12023817
- Baltar, F., Zhao, Z., and Herndl, G. J. (2021). Potential and expression of carbohydrate utilization by marine fungi in the global ocean. *Microbiome* 9, 1–10. doi: 10.1186/s40168-021-01063-4
- Beakes, G. W., Canter, H. M., and Jaworski, G. H. M. (1992). Comparative ultrastructural ontogeny of zoosporangia of *Zygorhizidium affluens* and *Z. planktonicum*, chytrid parasites of the diatom *Asterionella formosa*. *Mycol. Res.* 96, 1047–1059. doi: 10.1016/S0953-7562(09)80115-9
- Berbee, M. L., James, T. Y., and Strullu-Derrien, C. (2017). Early diverging fungi: diversity and impact at the dawn of terrestrial life. *Annu. Rev. Microbiol.* 71, 41–60. doi: 10.1146/annurev-micro-030117-020324
- Berger, L., Hyatt, A. D., Speare, R., and Longcore, J. E. (2005). Life cycle stages of the amphibian chytrid *Batrachochytrium dendrobatidis*. *Dis. Aquat. Organ.* 68, 51–63. doi: 10.3354/dao068051
- Camejo, D., Guzmán-Cedeño, Á., and Moreno, A. (2016). Reactive oxygen species, essential molecules, during plant-pathogen interactions. *Plant Physiol. Biochem.* 103, 10–23. doi: 10.1016/j.plaphy.2016.02.035
- Canter, H. M. (1953). Annotated list of British aquatic chytrids. *Trans. Br. Mycol. Soc.* 36, 278–301. doi: 10.1016/S0007-1536(53)80023-9
- Canter, H. M., and Jaworski, G. H. M. (1979). The occurrence of a hypersensitive reaction in the planktonic diatom *Asterionella formosa* Hassall parasitized by the chytrid *Rhizophyidium planktonicum* Canter emend., in culture. *New Phytol.* 82, 187–206. doi: 10.1111/j.1469-8137.1979.tb07574.x
- Chrismas, N., and Cunliffe, M. (2020). Depth-dependent mycoplankton glycoside hydrolase gene activity in the open ocean—evidence from the Tara Oceans eukaryote metatranscriptomes. *ISME J.* 14, 2361–2365. doi: 10.1038/s41396-020-0687-2
- Dee, J. M., Landry, B. R., and Berbee, M. L. (2019). Actin guides filamentous rhizoid growth and morphogenesis in the zoosporic fungus *Chytrium hyalinus*. *Mycologia* 111, 904–918. doi: 10.1080/00275514.2019.1669999
- Dee, J. M., Mollicone, M., Longcore, J. E., Roberson, R. W., and Berbee, M. L. (2015). Cytology and molecular phylogenetics of Monoblepharidomycetes provide evidence for multiple independent origins of the hyphal habit in the fungi. *Mycologia* 107, 710–728. doi: 10.3852/14-275
- Ellison, A. R., DiRenzo, G. V., McDonald, C. A., Lips, K. R., and Zamudio, K. R. (2017). First *in vivo* *Batrachochytrium dendrobatidis* transcriptomes reveal mechanisms of host exploitation, host-specific gene expression, and expressed genotype shifts. *G3 Genes Genomes Genet.* 7, 269–278. doi: 10.1534/g3.116.035873
- Farrer, R. A., Martel, A., Verbrugge, E., Abouelleil, A., Ducatelle, R., Longcore, J. E., et al. (2017). Genomic innovations linked to infection strategies across emerging pathogenic chytrid fungi. *Nat. Commun.* 8, 1–11. doi: 10.1038/ncomms14742
- Frenken, T., Alacid, E., Berger, S. A., Bourne, E. C., Gerphagnon, M., Grossart, H. P., et al. (2017). Integrating chytrid fungal parasites into plankton ecology: research gaps and needs. *Environ. Microbiol.* 19, 3802–3822. doi: 10.1111/1462-2920.13827
- Fuller, M., and Jaworski, A. (1987). *Zoosporic Fungi in Teaching and Research*. Athens, GA: Southeastern Publishing Corporation.
- Garvetto, A., Badis, Y., Perrineau, M. M., Rad-Menéndez, C., Bresnan, E., and Gachon, C. M. (2019). Chytrid infecting the bloom-forming marine diatom *Skeletonema* sp.: morphology, phylogeny and distribution of a novel species within the Rhizophydiales. *Fungal Biology* 123, 471–480. doi: 10.1016/j.funbio.2019.04.004
- Gerphagnon, M., Agha, R., Martin-Creuzburg, D., Bec, A., Perriere, F., Rad-Menéndez, C., et al. (2019). Comparison of sterol and fatty acid profiles of chytrids and their hosts reveals trophic upgrading of nutritionally inadequate phytoplankton by fungal parasites. *Environ. Microbiol.* 21, 949–958. doi: 10.1111/1462-2920.14489
- Gleason, F. H., Kagami, M., Lefevre, E., and Sime-Ngando, T. (2008). The ecology of chytrids in aquatic ecosystems: roles in food web dynamics. *Fungal Biol. Rev.* 22, 17–25. doi: 10.1016/j.fbr.2008.02.001
- Gleason, F. H., Scholz, B., Jephcott, T. G., van Ogtrop, F. F., Henderson, L., Lilje, O., et al. (2017). “Key ecological roles for zoosporic true fungi in aquatic habitats,” in *The Fungal Kingdom* eds J. Heitman, B. J. Howlett, P. W. Crous, E. H. Stukenbrock, T. Y. James, and N. A. R. Gow (Washington, DC: ASM Press), 399–416.
- Gow, N. A. R., Latge, J.-P., and Munro, C. A. (2017). “The fungal cell wall: structure, biosynthesis, and function,” in *The Fungal Kingdom* eds J. Heitman, B. J. Howlett, P. W. Crous, E. H. Stukenbrock, T. Y. James, and N. A. R. Gow (Washington, DC: ASM Press), 267–292.
- Grossart, H. P., Van den Wyngaert, S., Kagami, M., Wurzbacher, C., Cunliffe, M., and Rojas-Jimenez, K. (2019). Fungi in aquatic ecosystems. *Nat. Rev. Microbiol.* 17, 339–354. doi: 10.1038/s41579-019-0175-8
- Grossart, H. P., Wurzbacher, C., James, T. Y., and Kagami, M. (2016). Discovery of dark matter fungi in aquatic ecosystems demands a reappraisal of the phylogeny and ecology of zoosporic fungi. *Fungal Ecol.* 19, 28–38. doi: 10.1016/j.funeco.2015.06.004
- Hassett, B. T., and Gradinger, R. (2016). Chytrids dominate arctic marine fungal communities. *Environ. Microbiol.* 18, 2001–2009. doi: 10.1111/1462-2920.13216
- Hibbett, D. S., Binder, M., Bischoff, J. F., Blackwell, M., Cannon, P. F., Eriksson, O. E., et al. (2007). A higher-level phylogenetic classification of the fungi. *Mycol. Res.* 111, 509–547. doi: 10.1016/j.mycres.2007.03.004
- Hurdeal, V. G., Gentekaki, E., Hyde, K. D., and Jeewon, R. (2021). Where are the basal fungi? Current status on diversity, ecology, evolution, and taxonomy. *Biology* 10, 421–440. doi: 10.2478/s11756-020-00642-4
- Kagami, M., Miki, T., and Takimoto, G. (2014). Mycoloop: chytrids in aquatic food webs. *Front. Microbiol.* 5:166. doi: 10.3389/fmicb.2014.00166
- Kagami, M., von Elert, E., Ibelings, B. W., de Bruin, A., and Van Donk, E. (2007b). The parasitic chytrid, *Zygorhizidium*, facilitates the growth of the cladoceran zooplankter, *Daphnia*, in cultures of the inedible alga, *Asterionella*. *Proc. R. Soc. B Biol. Sci.* 274, 1561–1566. doi: 10.1098/rspb.2007.0425
- Kagami, M., De Bruin, A., Ibelings, B. W., and Van Donk, E. (2007a). Parasitic chytrids: their effects on phytoplankton communities and food-web dynamics. *Hydrobiologia* 578, 113–129. doi: 10.1007/s10750-006-0438-z
- Kiss, E., Hegedüs, B., Virág, M., Varga, T., Merényi, Z., Kószó, T., et al. (2019). Comparative genomics reveals the origin of fungal hyphae and multicellularity. *Nat. Commun.* 10, 1–13. doi: 10.1038/s41467-019-12085-w
- Lam, B. A., Walton, D. B., and Harris, R. N. (2011). Motile zoospores of *Batrachochytrium dendrobatidis* move away from antifungal metabolites produced by amphibian skin bacteria. *Ecohealth* 8, 36–45. doi: 10.1007/s10393-011-0689-7
- Lange, L., Barrett, K., Pilgaard, B., Gleason, F., and Tsang, A. (2019). Enzymes of early-diverging, zoosporic fungi. *Appl. Microbiol. Biotechnol.* 103, 6885–6902. doi: 10.1007/s00253-019-09983-w
- Laundon, D., Chrismas, N., Wheeler, G., and Cunliffe, M. (2020). Chytrid rhizoid morphogenesis resembles hyphal development in multicellular fungi and is adaptive to resource availability. *Proc. R. Soc. B Biol. Sci.* 287:20200433. doi: 10.1098/rspb.2020.0433
- Leonelli, S., and Ankeny, R. A. (2013). What makes a model organism? *Endeavour* 37, 209–212. doi: 10.1016/j.endeavour.2013.06.001
- Lew, R. R. (2011). How does a hypha grow? The biophysics of pressurized growth in fungi. *Nat. Rev. Microbiol.* 9, 509–518. doi: 10.1038/nrmicro2591
- Longcore, J. E., Pessier, A. P., and Nichols, D. K. (1999). *Batrachochytrium dendrobatidis* gen. et sp. nov., a chytrid pathogenic to amphibians. *Mycologia* 91, 219–227. doi: 10.1080/00275514.1999.12061011
- Medina, E. M., Robinson, K. A., Bellingham-Johnstun, K., Ianiri, G., Laplante, C., Fritz-Laylin, L. K., et al. (2020). Genetic transformation of *Spizellomyces punctatus*, a resource for studying chytrid biology and evolutionary cell biology. *Elife* 9, 1–20. doi: 10.7554/eLife.52741

- Miller, C. E., and Dylewski, D. P. (1981). Syngamy and resting body development in *Chytrium hyalinus* (Chytridiales). *Am. J. Bot.* 68, 342–349. doi: 10.1002/j.1537-2197.1981.tb06371.x
- Mondo, S. J., Dannebaum, R. O., Kuo, R. C., Louie, K. B., Bewick, A. J., LaButti, K., et al. (2017). Widespread adenine N6-methylation of active genes in fungi. *Nat. Genet.* 49, 964–968. doi: 10.1038/ng.3859
- Moss, A. S., Reddy, N. S., Dortaj, I. M., and San Francisco, M. J. (2008). Chemotaxis of the amphibian pathogen *Batrachochytrium dendrobatidis* and its response to a variety of attractants. *Mycologia* 100, 1–5. doi: 10.1080/15572536.2008.11832493
- Muehlstein, L. K., Amon, J. P., and Leffler, D. L. (1987). Phototaxis in the marine fungus *Rhizophyidium littoreum*. *Appl. Environ. Microbiol.* 53, 1819–1821. doi: 10.1128/aem.53.8.1819-1821.1987
- Muehlstein, L. K., Amon, J. P., and Leffler, D. L. (1988). Chemotaxis in the marine fungus *Rhizophyidium littoreum*. *Appl. Environ. Microbiol.* 54, 1668–1672. doi: 10.1128/aem.54.7.1668-1672.1988
- Nagy, L. G., Tóth, R., Kiss, E., Slot, J., Gácsér, A., and Kovács, G. M. (2017). “Six key traits of fungi: their evolutionary origins and genetic bases,” in *The Fungal Kingdom* eds J. Heitman, B. J. Howlett, P. W. Crous, E. H. Stukenbrock, T. Y. James, and N. A. R. Gow (Washington, DC: ASM Press), 35–56.
- Naranjo-Ortiz, M. A., and Gabaldón, T. (2019). Fungal evolution: diversity, taxonomy and phylogeny of the fungi. *Biol. Rev.* 94, 2101–2137. doi: 10.1111/brv.12550
- Naranjo-Ortiz, M. A., and Gabaldón, T. (2020). Fungal evolution: cellular, genomic and metabolic complexity. *Biol. Rev.* 95, 1198–1232. doi: 10.1111/brv.12605
- Ota, S., and Kawano, S. (2015). Life cycle and lectin-binding patterns in the chytrid fungus *Chytrium hyalinus*. *Cytologia* 80, 125–129. doi: 10.1508/cytologia.80.125
- Powell, M. J. (1976). Ultrastructure and isolation of glyoxysomes (microbodies) in zoospores of the fungus *Entophlyctis* sp. *Protoplasma* 89, 1–27. doi: 10.1007/BF01279325
- Powell, M. J. (1983). Localization of antimonate-mediated precipitates of cations in zoospores of *Chytrium hyalinus*. *Exp. Mycol.* 7, 266–277. doi: 10.1016/0147-5975(83)90047-6
- Powell, M. J., Letcher, P. M., Davis, W. J., Lefèvre, E., Brooks, M., and Longcore, J. E. (2019). Taxonomic summary of *Rhizoclosmatium* and description of four new *Rhizoclosmatium* species (Chytriomycetaceae, Chytridiales). *Phytologia* 101, 139–163.
- Rad-Menéndez, C., Gerphagnon, M., Garvetto, A., Arce, P., Badis, Y., Sime-Ngando, T., et al. (2018). Rediscovering *Zygorhizidium affluens* Canter: molecular taxonomy, infectious cycle, and cryopreservation of a chytrid infecting the bloom-forming diatom *Asterionella formosa*. *Appl. Environ. Microbiol.* 84, 1826–1844. doi: 10.1128/AEM.01826-18
- Read, N. D., Fleißner, A., Roca, M. G., and Glass, N. L. (2014). “Hyphal fusion,” in *Cellular and Molecular Biology of Filamentous Fungi* eds J. Heitman, B. J. Howlett, P. W. Crous, E. H. Stukenbrock, T. Y. James, and N. A. R. Gow (Washington, DC: ASM Press), 260–273.
- Richards, T. A., Leonard, G., Mahé, F., Del Campo, J., Romac, S., Jones, M. D. M., et al. (2015). Molecular diversity and distribution of marine fungi across 130 European environmental samples. *Proc. R. Soc. B Biol. Sci.* 282:20152243. doi: 10.1098/rspb.2015.2243
- Riquelme, M., Aguirre, J., Bartnicki-García, S., Braus, G. H., Feldbrügge, M., Fleig, U., et al. (2018). Fungal morphogenesis, from the polarized growth of hyphae to complex reproduction and infection structures. *Microbiol. Mol. Biol. Rev.* 82:e00068-17. doi: 10.1128/MMBR.00068-17
- Roberts, C., Allen, R., Bird, K. E., and Cunliffe, M. (2020). Chytrid fungi shape bacterial communities on model particulate organic matter. *Biol. Lett.* 16:20200368. doi: 10.1098/rsbl.2020.0368
- Rollins-Smith, L. A., Ruzzini, A. C., Fites, J. S., Reinert, L. K., Hall, E. M., Joosse, B. A., et al. (2019). Metabolites involved in immune evasion by *Batrachochytrium dendrobatidis* include the polyamine spermidine. *Infect. Immun.* 87:e00035-19. doi: 10.1128/IAI.00035-19
- Roper, M., and Seminara, A. (2019). Mycofluidics: the fluid mechanics of fungal adaptation. *Annu. Rev. Fluid Mech.* 51, 511–538. doi: 10.1146/annurev-fluid-122316-045308
- Scholz, B., Küpper, F., Vyverman, W., Ólafsson, H., and Karsten, U. (2017). Chytridiomycosis of marine diatoms—the role of stress physiology and resistance in parasite-host recognition and accumulation of defense molecules. *Mar. Drugs* 15:26. doi: 10.3390/md15020026
- Shields, J. D. (1990). *Rhizophyidium littoreum* on the eggs of *Cancer anthonyi*: parasite or saprobe? *Biol. Bull.* 179, 201–206. doi: 10.2307/1541770
- Sparrow, F. K. (1960). *Aquatic Phycomycetes, 2nd Edn.* Ann Arbor, MI: University of Michigan Press.
- Steinberg, G., Peñalva, M. A., Riquelme, M., Wösten, H. A., and Harris, S. D. (2017). “Cell biology of hyphal growth,” in *The Fungal Kingdom* eds J. Heitman, B. J. Howlett, P. W. Crous, E. H. Stukenbrock, T. Y. James, and N. A. R. Gow (Washington, DC: ASM Press), 231–265. doi: 10.1128/9781555819583.ch11
- Taylor, J. D., and Cunliffe, M. (2016). Multi-year assessment of coastal planktonic fungi reveals environmental drivers of diversity and abundance. *ISME J.* 10, 2118–2128. doi: 10.1038/ismej.2016.24
- Tedersoo, L., Sánchez-Ramírez, S., Kõljalg, U., Bahram, M., Döring, M., Schigel, D., et al. (2018). High-level classification of the fungi and a tool for evolutionary ecological analyses. *Fungal Divers.* 90, 135–159. doi: 10.1007/s13225-018-0401-0
- Thekkiniath, J., Zabet-Moghaddam, M., Kottapalli, K. R., Pasham, M. R., San Francisco, S., and San Francisco, M. (2015). Quantitative proteomics of an amphibian pathogen, *Batrachochytrium dendrobatidis*, following exposure to thyroid hormone. *PLoS ONE* 10:e0123637. doi: 10.1371/journal.pone.0123637
- Thekkiniath, J. C., Zabet-Moghaddam, M., San Francisco, S. K., and San Francisco, M. J. (2013). A novel subtilisin-like serine protease of *Batrachochytrium dendrobatidis* is induced by thyroid hormone and degrades antimicrobial peptides. *Fungal Biol.* 117, 451–461. doi: 10.1016/j.funbio.2013.05.002
- Van de Vossen, B. T. L. H., Prodhomme, C., Van Arkel, G., Van Gent-Pelzer, M. P. E., Bergervoet, M., Brankovics, B., et al. (2019a). The *Synchytrium endobioticum* avrsen1 triggers a hypersensitive response in sen1 potatoes while natural variants evade detection. *Mol. Plant Microbe Interact.* 32, 1536–1546. doi: 10.1094/MPMI-05-19-0138-R
- Van de Vossen, B. T. L. H., Warris, S., Nguyen, H. D. T., van Gent-Pelzer, M. P. E., Joly, D. L., van de Geest, H. C., et al. (2019b). Comparative genomics of chytrid fungi reveal insights into the obligate biotrophic and pathogenic lifestyle of *Synchytrium endobioticum*. *Sci. Rep.* 9, 1–14. doi: 10.1038/s41598-019-45128-9
- Venard, C. M., Vasudevan, K. K., and Stearns, T. (2020). Cilium axoneme internalization and degradation in chytrid fungi. *Cytoskeleton* 77, 365–378. doi: 10.1002/cm.21637
- Voyles, J. (2011). Phenotypic profiling of *Batrachochytrium dendrobatidis*, a lethal fungal pathogen of amphibians. *Fungal Ecol.* 4, 196–200. doi: 10.1016/j.funeco.2010.12.003
- Yan, X., and Talbot, N. J. (2016). Investigating the cell biology of plant infection by the rice blast fungus *Magnaporthe oryzae*. *Curr. Opin. Microbiol.* 34, 147–153. doi: 10.1016/j.mib.2016.10.001
- Yarden, O. (2016). Model fungi: engines of scientific insight. *Fungal Biol. Rev.* 30, 33–35. doi: 10.1016/j.fbr.2016.05.002

**Conflict of Interest:** The authors declare that the research was conducted in the absence of any commercial or financial relationships that could be construed as a potential conflict of interest.

**Publisher’s Note:** All claims expressed in this article are solely those of the authors and do not necessarily represent those of their affiliated organizations, or those of the publisher, the editors and the reviewers. Any product that may be evaluated in this article, or claim that may be made by its manufacturer, is not guaranteed or endorsed by the publisher.

Copyright © 2021 Laundon and Cunliffe. This is an open-access article distributed under the terms of the Creative Commons Attribution License (CC BY). The use, distribution or reproduction in other forums is permitted, provided the original author(s) and the copyright owner(s) are credited and that the original publication in this journal is cited, in accordance with accepted academic practice. No use, distribution or reproduction is permitted which does not comply with these terms.



Laundon D, Christmas N, Wheeler G, and Cunliffe M. 2020. Chytrid rhizoid morphogenesis resembles hyphal development in multicellular fungi and is adaptive to resource availability. *Proc Royal Soc B* **287**(1928): p.20200433.  
doi:10.1098/rspb.2020.0433

## Research



**Cite this article:** Laundon D, Christmas N, Wheeler G, Cunliffe M. 2020 Chytrid rhizoid morphogenesis resembles hyphal development in multicellular fungi and is adaptive to resource availability. *Proc. R. Soc. B* **287**: 20200433.  
<http://dx.doi.org/10.1098/rspb.2020.0433>

Received: 26 February 2020

Accepted: 15 May 2020

**Subject Category:**

Development and physiology

**Subject Areas:**

microbiology, cellular biology, ecology

**Keywords:**

chytrids, rhizoid, hyphae, morphogenesis, plasticity, fungi

**Author for correspondence:**

Michael Cunliffe

e-mail: [micnli@mba.ac.uk](mailto:micnli@mba.ac.uk)

Electronic supplementary material is available online at <https://doi.org/10.6084/m9.figshare.c.5001059>.

# Chytrid rhizoid morphogenesis resembles hyphal development in multicellular fungi and is adaptive to resource availability

Davis Laundon<sup>1,2</sup>, Nathan Christmas<sup>1,3</sup>, Glen Wheeler<sup>1</sup> and Michael Cunliffe<sup>1,4</sup>

<sup>1</sup>Marine Biological Association of the UK, The Laboratory, Citadel Hill, Plymouth, UK

<sup>2</sup>School of Environmental Sciences, University of East Anglia, Norwich, UK

<sup>3</sup>School of Geographical Sciences, University of Bristol, Bristol, UK

<sup>4</sup>School of Biological and Marine Sciences, University of Plymouth, Plymouth, UK

MC, 0000-0002-6716-3555

Key to the ecological prominence of fungi is their distinctive cell biology, our understanding of which has been principally based on dikaryan hyphal and yeast forms. The early-diverging Chytridiomycota (chytrids) are ecologically important and a significant component of fungal diversity, yet their cell biology remains poorly understood. Unlike dikaryan hyphae, chytrids typically attach to substrates and feed osmotrophically via anucleate rhizoids. The evolution of fungal hyphae appears to have occurred from rhizoid-bearing lineages and it has been hypothesized that a rhizoid-like structure was the precursor to multicellular hyphae. Here, we show in a unicellular chytrid, *Rhizoclostridium globosum*, that rhizoid development exhibits striking similarities with dikaryan hyphae and is adaptive to resource availability. Rhizoid morphogenesis exhibits analogous patterns to hyphal growth and is controlled by  $\beta$ -glucan-dependent cell wall synthesis and actin polymerization. Chytrid rhizoids growing from individual cells also demonstrate adaptive morphological plasticity in response to resource availability, developing a searching phenotype when carbon starved and spatial differentiation when interacting with particulate organic matter. We demonstrate that the adaptive cell biology and associated developmental plasticity considered characteristic of hyphal fungi are shared more widely across the Kingdom Fungi and therefore could be conserved from their most recent common ancestor.

## 1. Introduction

Hyphae are polarized, elongating and bifurcating cellular structures that many fungi use to forage and feed (figure 1*a* and *b*). The phylum Chytridiomycota (chytrids) diverged from other fungal lineages approximately 750 Mya and, with the Blastocladiomycota, formed a critical evolutionary transition in the Kingdom Fungi dedicated to osmotrophy and the establishment of the chitin-containing cell wall [2]. Chytrids produce filamentous hyphae-like, anucleate structures called rhizoids (figure 1*a–c*) [3], which are important in their ecological functions, in terms of both attachment to substrates and osmotrophic feeding [2]. 407-million-year-old fossils from the Devonian Rhynie Chert deposit show chytrids in freshwater aquatic ecosystems physically interacting with substrates via rhizoids in a comparative mode to extant taxa [4]. Yet surprisingly, given the importance of rhizoids in both contemporary and paleo-chytrid ecology, there remains a limited understanding of chytrid rhizoid biology, including possible similarities with functionally analogous hyphae in other fungi and the potential for substrate-dependent adaptations.

Character mapping of the presence of cellular growth plans against established phylogenies reveals the multicellular hyphal form to be a derived condition, whereas rhizoid feeding structures are the basal condition within the true fungi

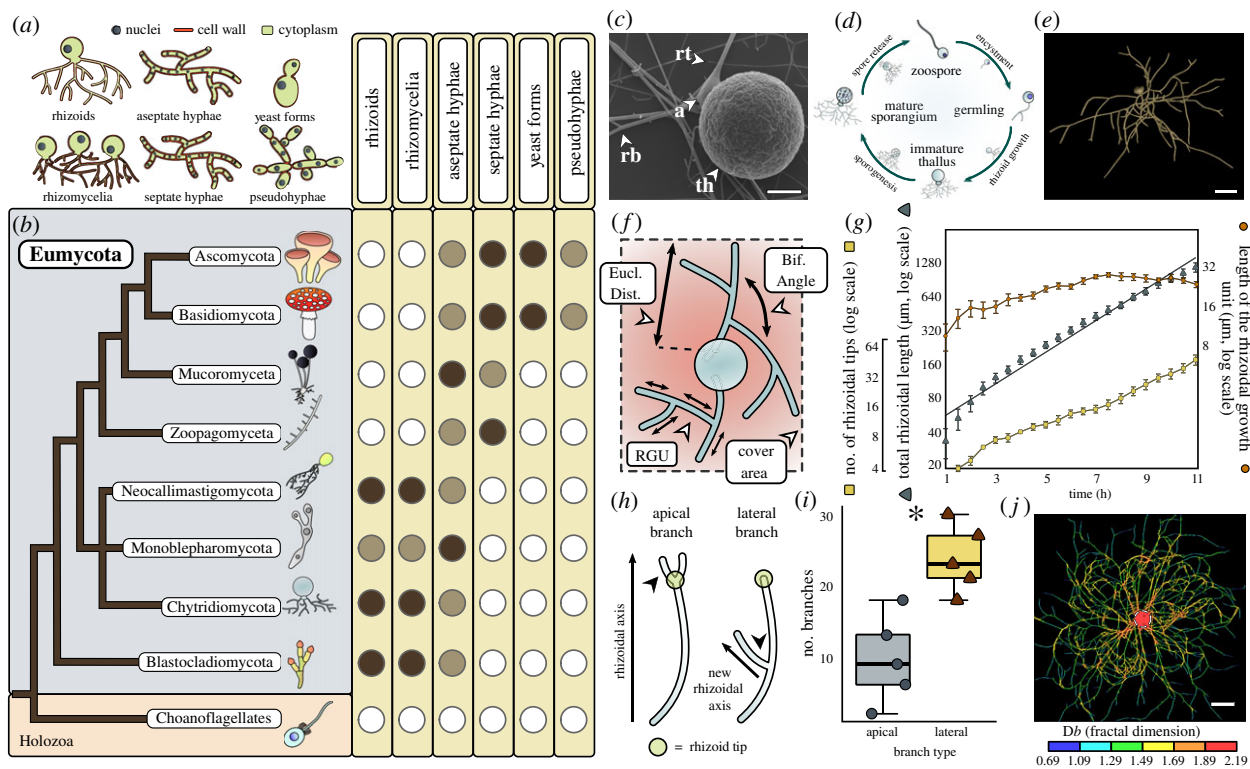


**Figure 1.** Rhizoids are the basal feeding condition within the fungal kingdom and their morphogenesis is similar to hyphal development. (a–b) Correlating the major feeding types in fungi (a) to phylogeny (b) shows rhizoids to be the basal feeding condition in the true fungi (Eumycota). White circles indicate absence of a growth plan in a taxon and dark circles indicate widespread presence. Faded circles indicate a growth plan is present within a taxon, but not widespread. Rhizoid systems bear a single thallus, whereas rhizomycelia are defined as rhizoid systems with multiple thalli. Tree based on the phylogeny outlined in [1]. (c) *R. globosum* displays a typical chytrid cell plan. Shown is the thallus (th) anchored to the substrate by threadlike rhizoids. Rhizoids emanate from a swelling termed the apophysis (a). Also shown are rhizoid bifurcations (rb) and tips (rt). Scale bar = 5  $\mu\text{m}$ . (d) *R. globosum* exhibits an archetypal chytrid life cycle. From the mature zoosporangium, multiple motile zoospores are released that swim freely for a brief period (less than 1–2 h) before encysting into germlings (i.e. losing the single flagellum and developing a chitin-containing cell wall). From the subsequent extending germtube develops the rhizoid. After a period of growth, the sporangium becomes the multinucleate zoosporangium during sporogenesis, from which the next generation of spores is released. (e) Chytrid rhizoids were reconstructed using the neuron tracing workflow outlined in electronic supplementary material, figure S3. Example of a three-dimensional reconstructed *R. globosum* rhizoid system taken from a 10 h time series. Scale bar = 20  $\mu\text{m}$ . (f) This study used morphometric parameters developed from neuron biology to describe rhizoid development in chytrids. Shown are the Euclidean distance (Eucl. Dist.), bifurcation angle (Bif. Angle), rhizoid growth unit (RGU) and cover area. Full morphometric glossary is presented in electronic supplementary material, figure S5. (g) Rhizoid growth trajectories for four-dimensional confocal time series ( $n = 5$ , mean  $\pm$  s.e.m.) of rhizoidal growth unit, total length and number of tips. (h) Apical and lateral branches occur in chytrid rhizoids. Apical branching occurs when a branch is formed at the rhizoid tip parallel to the established rhizoidal axis. Lateral branching occurs when a branch is formed distally to the rhizoidal tip, establishing a new rhizoidal axis. (i) Four-dimensional confocal imaging ( $n = 5$ , mean  $\pm$  s.e.m.) revealed that lateral branching dominates over apical branching  $*p < 0.05$ . (j) Fractal analysis of chytrid rhizoid systems shows a decrease in fractal dimension ( $Db$ ) towards the growing edge. Thallus demarcated by dashed circle. Scale bar = 50  $\mu\text{m}$ .

(Eumycota) (figure 1a and b). Aseptate hyphae represent an intermediary condition and are not typically the dominant cell type in either unicellular or multicellular fungi. Hyphal cell types are sometimes observed outside of the Eumycota, such as within the Oomycota; however, the origin of fungal hyphae within the Eumycota was independent [5,6] and has not been reported in their closest relatives the Holozoa (animals, choanoflagellates, etc.). Comparative genomics has indicated that hyphae originated within the rhizoid-bearing Chytridiomycota–Blastocladiomycota–Zoopagomycota nodes of the fungal tree [6], which is supported by fossil Blastocladiomycota and extant Monoblepharidomycetes having hyphae [5,7]. This has led to the proposition that rhizoids, or rhizoid-like structures, were the evolutionary precursors of fungal hyphae [5,6,8]; however, investigation into such hypotheses have been hindered by a relative lack of understanding of rhizoid developmental biology.

Chytrids are important aquatic fungi [9], feeding on a range of physically complex heterologous substrates, including algal cells [10], amphibian epidermises [11] and recalcitrant

particulate organic matter (POM) such as chitin and pollen [12]. Appreciation for the ecological importance of chytrids as parasites, pathogens and saprotrophs in aquatic ecosystems is greatly expanding. For example, chytrids are well-established plankton parasites [10], responsible for the global-scale amphibian panzootic [13], and have recently emerged as important components of the marine mycobiome [9]. The chytrid rhizoid is critical in all ecological functions because it is the physical interface between the fungus and substrate or host, yet there remains a limited understanding of rhizoid functional biology in terms of substrate interaction.

*Rhizoclostridium globosum* is a widespread aquatic saprotroph that is characteristically associated with chitin-rich insect exuviae and has an archetypal chytrid cell plan (figure 1c) and life cycle (figure 1d) [14]. With an available sequenced genome [15], easy laboratory culture and amenability to live cell imaging (this study), *R. globosum* JEL800 represents a promising model organism to investigate the cell and developmental biology of aquatic rhizoid-bearing, early-diverging fungi. To

study the developing rhizoid system for morphometric analyses, we established a live cell three-/four-dimensional confocal microscopy approach in combination with the application of neuron tracing software to three-dimensional reconstruct developing cells (figure 1e; electronic supplementary material, figures S3 and S4). We were subsequently able to generate a series of cell morphometrics to describe and quantify rhizoid development (figure 1f; electronic supplementary material, figure S5) under a range of experimental conditions with the aims of identifying potential similarities with hyphae in dikaryan fungi in terms of geometric organization, morphogenesis and underlying cellular control mechanisms. In addition, we set out to characterize substrate-dependent adaptations particularly in the ecological context of aquatic POM utilization.

## 2. Material and methods

Detailed materials and methods are provided as electronic supplementary material.

### (a) Rhizoid tracing and reconstruction

Chytrid plasma membranes were labelled with 8.18  $\mu\text{M}$  FM 1–43 and imaged using a Zeiss LSM 510 Meta confocal laser scanning microscope (Carl Zeiss). Z-stacks of rhizoids were imported into the neuron reconstruction software NeuronStudio [16,17] and semi-automatically traced with the ‘Build Neurite’ function. Rhizoids were morphometrically quantified using the btmorph2 library [18] run with Python 3.6.5 implemented in Jupyter Notebook 4.4.0. For visualization, reconstructed rhizoids were imported into Blender (2.79), smoothed using automatic default parameters and rendered for display only.

### (b) Chemical characterization of the rhizoid

To label F-actin and the cell wall throughout the rhizoid system, cells were fixed for 1 h in 4% formaldehyde in 1 $\times$ PBS (phosphate-buffered saline) and stained with 1 : 50 rhodamine phalloidin in PEM (100 mM PIPES (piperazine-N,N'-bis(2-ethanesulfonic acid)) buffer at pH 6.9, 1 mM EGTA (ethylene glycol tetraacetic acid), and 0.1 mM  $\text{MgSO}_4$ ) for 30 min, then with 5  $\mu\text{g ml}^{-1}$  Texas Red-conjugated wheat germ agglutinin (WGA) in PEM for 30 min.

### (c) Chemical inhibition of rhizoid growth

Casposfungin diacetate (working concentration 1–50  $\mu\text{M}$ ) was used to inhibit cell wall  $\beta$ -glucan synthesis and cytochalasin B (working concentration 0.1–10  $\mu\text{M}$ ) was used to inhibit actin filament formation. Cells were incubated for 6 h, which was found to be sufficient to observe phenotypic variation.

### (d) $\beta$ -glucan quantification

*R. globosum* was processed for  $\beta$ -glucans using a commercial  $\beta$ -glucan assay (Yeast & Mushroom) (K-YBGL, Megazyme) following the manufacturer’s protocol. Briefly, samples were processed by acid hydrolysis then enzymatic break-down and  $\beta$ -glucans were quantified spectrophotometrically with a CLARIOstar Plus microplate reader (BMG Labtech), relative to a negative control and positive  $\beta$ -glucan standard. A sample of shop-bought baker’s yeast was used as an additional positive control.

### (e) Identification of putative glucan synthase genes

All glycosyl transferase group 2 (GT2) domain-containing proteins within the *R. globosum* genome were identified using the JGI

MycCosm online portal. GT2 functional domains were identified using DELTA-BLAST [19] and aligned with MAFFT [20]. Maximum-likelihood phylogenies were calculated with RAxML [19] using the BLOSUM62 matrix and 100 bootstrap replicates.

### (f) Carbon starvation and growth on chitin beads

For carbon starvation experiments, *R. globosum* cells were grown in either carbon-free Bold’s Basal Medium supplemented with 1.89 mM ammonium sulfate and 500  $\mu\text{l l}^{-1}$  f/2 vitamin solution [21] (BBM) or BBM with 10 mM N-acetyl-D-glucosamine as a carbon source. To investigate growth on POM, chitin microbeads (New England Biolabs) were suspended in carbon-free BBM at a working concentration of 1 : 1000 stock concentration. To understand rhizoid development in a starved cell that had encountered a chitin microbead, we imaged cells that contacted a chitin microbead following development along the glass bottom of the dish.

## 3. Results

### (a) Chytrid rhizoid morphogenesis and development

During rhizoid development, we observed a continuous increase in rhizoid length ( $110.8 \pm 24.4 \mu\text{m h}^{-1}$ ) ( $n = 5$ ,  $\pm$  s.d.) and the number of rhizoid tips ( $4.6 \pm 1.2 \text{ tips h}^{-1}$ ) (figure 1g; electronic supplementary material, table S1, movies S1–S5), with an increase in the total cell surface area ( $21.1 \pm 5.2 \mu\text{m}^2 \text{ h}^{-1}$ ), rhizoid bifurcations ( $4.2 \pm 1.0 \text{ bifurcations h}^{-1}$ ), cover area ( $2,235 \pm 170.8 \mu\text{m}^2 \text{ h}^{-1}$ ) and maximum Euclidean distance ( $5.4 \pm 0.1 \mu\text{m h}^{-1}$ ) (electronic supplementary material, figure S6). The hyphal growth unit (HGU) has been used previously to describe hyphal development in dikaryan fungi and is defined as the distance between two hyphal bifurcations [22]. Adapting this metric for the chytrid rhizoid, the rhizoidal growth unit (RGU) (i.e. the distance between two rhizoid bifurcations; figure 1f) increased continuously during the first 6 h of the development period (i.e. cells became relatively less branched) before stabilizing during the later phase of growth (figure 1g). The local rhizoid bifurcation angle remained consistent at  $81.4^\circ \pm 6.3$  after approximately 2 h (electronic supplementary material, figure S6), and lateral branching was more frequent than apical branching during rhizoid development (figure 1h and i). Fractal analysis (fractal dimension =  $D_b$ ) of 24 h grown cells showed that rhizoids approximate a two-dimensional biological fractal (mean  $D_b = 1.51 \pm 0.24$ ), with rhizoids relatively more fractal at the centre of the cell (max  $D_b = 1.69$ – $2.19$ ) and less fractal towards the growing periphery (min  $D_b = 0.69$ – $1.49$ ) (figure 1j; electronic supplementary material, figure S7).

### (b) Cell wall and actin dynamics are linked to rhizoid branching

The cell wall and actin structures were present throughout the chytrid rhizoid (figure 2a). Putative actin cables ran through the rhizoid system, punctuated by actin patches. Inhibition of cell wall  $\beta$ -1,3-glucan synthesis and actin proliferation with casposfungin and cytochalasin B, respectively, induced a concentration-dependent decrease in the RGU, with the development of atypical hyperbranched rhizoids (figure 2b–d; electronic supplementary material, table S2, movies S6–S7). As with *Batrachochytrium dendrobatidis* [23,24], we confirmed that *R. globosum* JEL800 lacks an apparent  $\beta$ -1,3-glucan synthase FKS1 gene homologue (electronic supplementary material, table S3). However, the quantification of glucans in

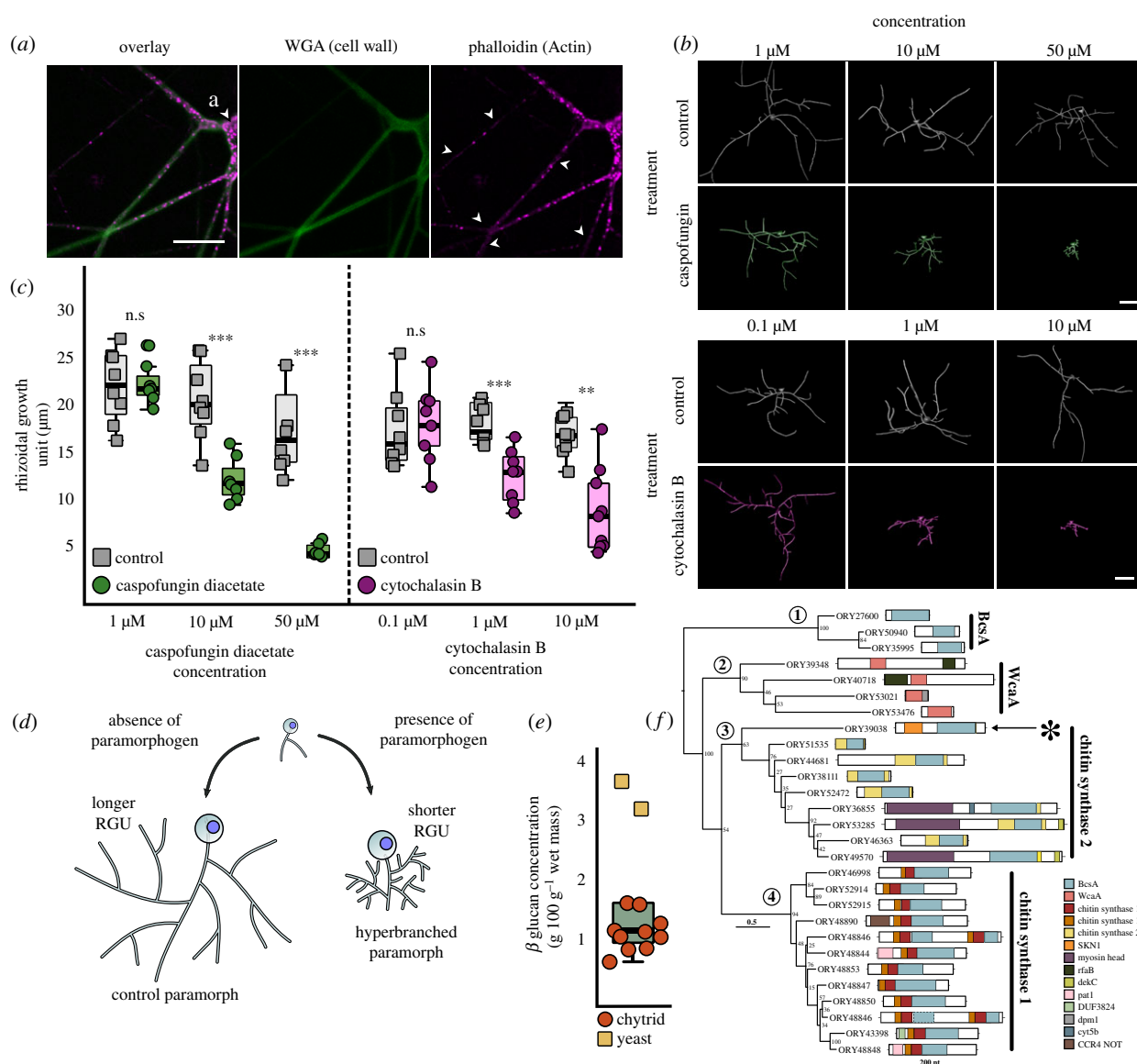


**Figure 2.** Cell wall synthesis and actin dynamics govern rhizoid branching. (a) Fluorescent labelling of cell wall and actin structures in 24 h *R. globosum* rhizoids. The cell wall and actin patches were found throughout the rhizoid. Arrowheads in the actin channel indicate putative actin cables. WGA = conjugated wheat germ agglutinin. Scale bar = 10 μm. (b) Representative three-dimensional reconstructions of 7 h *R. globosum* cells following treatment with caspofungin diacetate and cytochalasin B at stated concentrations to inhibit cell wall and actin filament biosynthesis respectively, relative to solvent only controls. Scale bar = 20 μm. (c) Application of caspofungin diacetate and cytochalasin B resulted in a concentration-dependent decrease in the rhizoidal growth unit, resulting in atypical hyperbranched rhizoids ( $n \sim 9$ ). n.s.  $p > 0.05$  (not significant), \* $p < 0.05$ , \*\* $p < 0.01$ , \*\*\* $p < 0.001$ . This differential growth is diagrammatically summarized in (d). (e)  $\beta$ -glucan concentration of *R. globosum* ( $n = 10$ ) relative to a baker's yeast control ( $n = 2$ ). (f) Maximum-likelihood phylogeny of GT2 domains (BcsA and WcaA domains) within the *R. globosum* genome (midpoint rooting). Full architecture of each protein is shown. Asterisk indicates the putative glucan synthesis protein ORY39038 containing a putative SKN1 domain.

*R. globosum* showed that they are present (figure 2e), with  $58.3 \pm 7.6\%$   $\beta$ -glucans and  $41.6 \pm 7.6\%$   $\alpha$ -glucans of total glucans.

To identify alternative putative  $\beta$ -glucan synthesis genes in *R. globosum* JEL800, we surveyed the genome and focused on GT2 encoding genes, which include typical glucan synthases in fungi. A total of 28 GT2 domains were found within 27 genes (figure 2f). Of these genes, 20 contained putative chitin synthase domains and many contained additional domains involved in transcriptional regulation. Nine encode chitin synthase 2 family proteins and 11 encode chitin synthase 1 family proteins (with two GT2 domains in ORY48846). No obvious genes for  $\beta$ -1,3-glucan or  $\beta$ -1,6-glucan synthases were found within the genome. However, the chitin synthase 2 gene ORY39038 included a putative SKN1 domain (figure 2f), which has been implicated

in  $\beta$ -1,6-glucan synthesis in the ascomycete yeasts *Saccharomyces cerevisiae* [25] and *Candida albicans* [26]. These results indicate a yet uncharacterized  $\beta$ -glucan-dependent cell wall production process in chytrids (also targeted by caspofungin) that is not currently apparent using gene/genome level assessment and warrants further study.

### (c) Rhizoids undergo adaptive development in response to carbon starvation

To examine whether chytrids are capable of modifying rhizoid development in response to changes in resource availability, we exposed *R. globosum* to carbon starvation (i.e. development in the absence of exogenous carbon). When provided with 10 mM N-acetylglucosamine (NAG) as an exogenous carbon

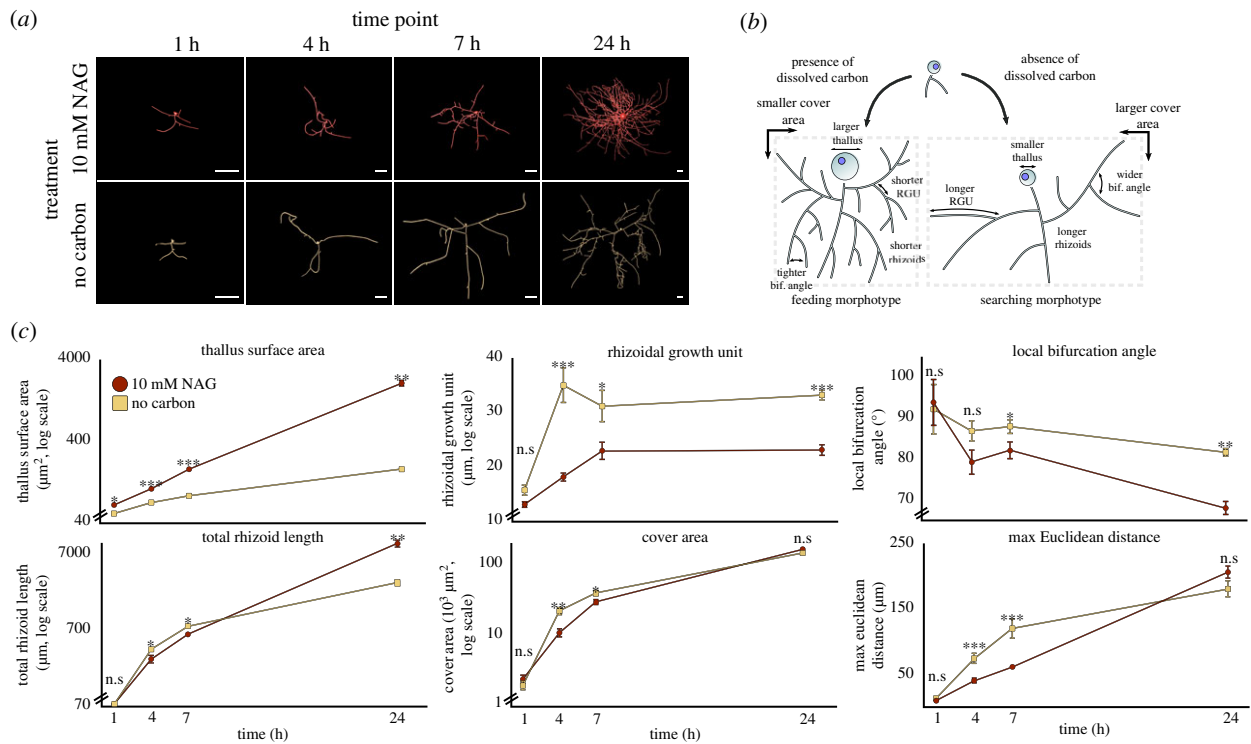


**Figure 3.** Chytrids are capable of adaptive rhizoid development under carbon starvation. (a) Representative three-dimensional reconstructions of *R. globosum* cells grown under carbon-replete or carbon-depleted conditions at different time points. Scale bar = 20  $\mu\text{m}$ . When exposed to carbon starvation, chytrids are capable of differential adaptive growth to produce a searching phenotype. This differential growth is summarized in (b). (c) Differential growth trajectories of major morphometric traits between *R. globosum* cells ( $n \sim 9$ , mean  $\pm$  s.e.m.) grown under carbon-replete and carbon-depleted conditions over time. n.s.  $p > 0.05$  (not significant), \* $p < 0.05$ , \*\* $p < 0.01$ , \*\*\* $p < 0.001$ .

source, the entire life cycle from zoospore to sporulation was completed and the rhizoids branched densely (electronic supplementary material, movie S8), indicative of a feeding phenotype. Carbon-starved cells did not produce zoospores and cell growth stopped after 14–16 h (electronic supplementary material, movie S9). Using only endogenous carbon (i.e. zoospore storage lipids), starved cells underwent differential rhizoid development compared to cells from the exogenous carbon-replete conditions to form an apparent adaptive searching phenotype (figure 3a,b; electronic supplementary material, table S4, movie S10). Under carbon starvation, *R. globosum* invested less in thallus growth than in carbon replete conditions and developed longer rhizoids with a greater maximum Euclidean distance (figure 3c). Carbon-starved cells were also less branched, had wider bifurcation angles and subsequently covered a larger surface area. These morphological changes in response to exogenous carbon starvation (summarized in figure 3b) suggest that individual chytrid cells are capable of differential reallocation of resources away from reproduction (i.e. the production of the zoosporangium) and towards an extended modified rhizoidal structure indicative of a resource searching phenotype.

#### (d) Rhizoids spatially differentiate in response to patchy resource environments

Rhizoid growth of single cells growing on chitin microbeads was quantified as experimental POM (figure 4a,b; electronic supplementary material, movie S11). Initially, rhizoids grew along the outer surface of the bead and were probably used primarily for anchorage to the substrate. Scanning electron microscopy (SEM) showed that the rhizoids growing

externally on the chitin particle formed grooves on the bead parallel to the rhizoid axis (electronic supplementary material, figure S1f,g), suggesting extracellular enzymatic chitin degradation by the rhizoid on the outer surface. Penetration of the bead occurred during the later stages of particle colonization (figure 4a; electronic supplementary material, movie S12). Branching inside the bead emanated from 'pioneer' rhizoids that penetrated the particle (figure 4c).

Given the previous results of the searching rhizoid development in response to carbon starvation, a patchy resource environment was created using the chitin microbeads randomly distributed around individual developing cells in otherwise carbon-free media to investigate how encountering POM affected rhizoid morphology (figure 4d). We observed spatial differentiation of single-cell rhizoid systems in association with POM contact. Particle-associated rhizoids were shorter than rhizoids not in particle contact, were more branched (i.e. lower RGU), had a shorter maximum Euclidean distance and covered a smaller area (figure 4e). These rhizoid morphometrics closely resembled the feeding and searching modifications of the cells grown under carbon-replete and carbon-depleted conditions previously discussed (figures 4f and 3b) but instead are displayed simultaneously with spatial regulation in individual cells linked to POM-associated and non-associated rhizoids, respectively.

## 4. Discussion

Our results provide new insights into the developmental cell biology of chytrid fungi and highlight similarities between the organization of anucleate rhizoids and multicellular hyphae. The fundamental patterns of rhizoid morphogenesis

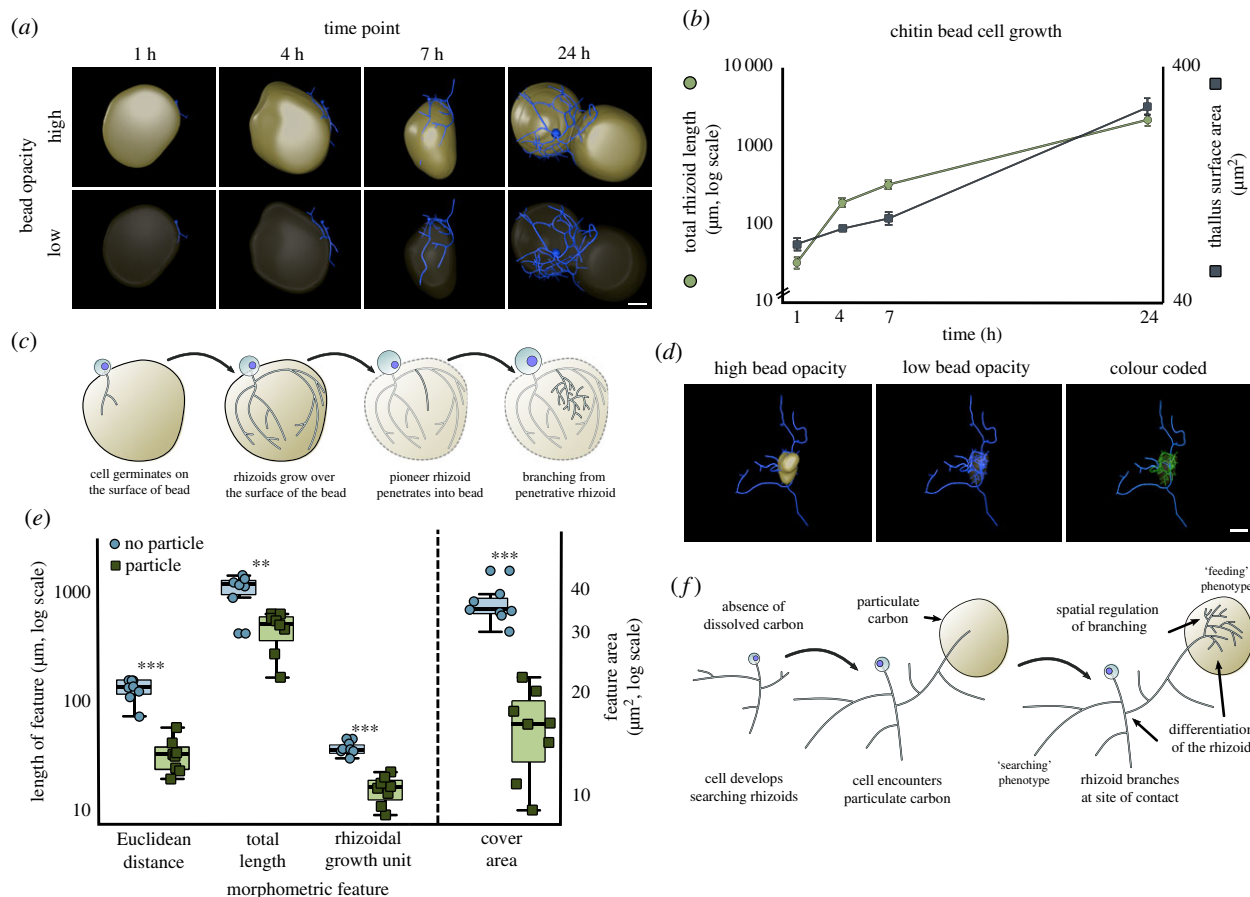


**Figure 4.** Rhizoids associated with heterogeneous particulate carbon exhibit spatial differentiation. (a) Representative three-dimensional reconstructions of *R. globosum* cells (blue) growing on chitin microbeads (beige) at different time points. Scale bar = 20  $\mu\text{m}$ . (b) Growth trajectories for total rhizoid length and thallus surface area for *R. globosum* cells growing on chitin microbeads ( $n \sim 9$ , mean  $\pm$  s.e.m.). (c) Diagrammatic summary of *R. globosum* rhizoid development on chitin microbeads. (d) Representative three-dimensional reconstruction of a 24 h searching *R. globosum* cell (blue) that has encountered a chitin microbead (beige). The colour coded panel shows parts of the rhizoid system in contact (green) and not in contact (blue) with the microbead. Scale bar = 20  $\mu\text{m}$ . (e) Comparison of rhizoids in contact or not in contact with the chitin microbead ( $n = 8$ ). (f) Diagrammatic summary of spatial differentiation in a starved, searching rhizoid that has encountered a particulate carbon patch.

that we report here for a unicellular non-hyphal fungus are comparable to those previously recorded for hyphal fungi (figure 5a) [22]. Trinci [22] assessed hyphal development in major fungal lineages (Ascomycota and Mucoromycota) and observed that the growth patterns of morphometric traits (HGU, total length and number of tips) were similar across the studied taxa. When the data from our study are directly compared to that of Trinci [22], we see that the hyphal growth pattern is also analogous to the rhizoids of the early-diverging unicellular Chytridiomycota (figure 5a). Chytrid rhizoid development in this study is also comparable to the hyphal growth rates reported by Trinci [22] (figure 5b, c), as well as the elongation rates reported by López-Franco *et al.* [27] when scaled by filament diameter (figure 5d).

Such similarities also extend to rhizoid branching patterns, where lateral branching dominates over apical branching. This branching pattern is also the predominant mode of hyphal branching, where apical branching is suppressed by a phenomenon termed 'apical dominance' [28]. These findings suggest that a form of apical dominance at the growing edge rhizoid tips may suppress apical branching to maintain rhizoid network integrity as in dikaryan hyphae [28,29]. Chytrid rhizoids also become less fractal towards the growing edge in terms of their overall morphology, and similar patterns of fractal organization are also observed in hyphae-based mycelial colonies

[30]. Taken together, these results show strong geometric analogies in the fundamental organization of unicellular chytrid rhizoid and multicellular hyphal morphogenesis.

Given the apparent hyphal-like properties of rhizoid development, we sought a greater understanding of the potential subcellular machinery underpinning rhizoid morphogenesis in *R. globosum*. Normal rhizoid branching was disrupted by inhibition of cell wall synthesis and actin polymerization, both of which are known to control branching and growth in hyphal biology [31–33]. These effects in *R. globosum* are similar to disruption of normal hyphal branching reported in *Aspergillus fumigatus* (Ascomycota) in the presence of caspofungin [34], and in *Neurospora crassa* (Ascomycota) in the presence of cytochalasins [35]. Recent studies have shown the presence of actin in the rhizoids of soil chytrids [36,37] and inhibition of actin in *Chytrium hyalinus* similarly disrupts normal rhizoid branching [36]. In this study, our quantitative characterization of cell wall and actin inhibited rhizoid paramorphs provides support that  $\beta$ -1,3-glucan-dependent cell wall synthesis and actin dynamics also govern branching in chytrid rhizoids as in multicellular hyphae.

We also show that rhizoid development is plastic to resource availability, with chytrid cells displaying an adaptive searching phenotype under carbon starvation. Adaptive foraging strategies are well described in multicellular hyphae [38,39], and our data support the existence of analogous strategies in

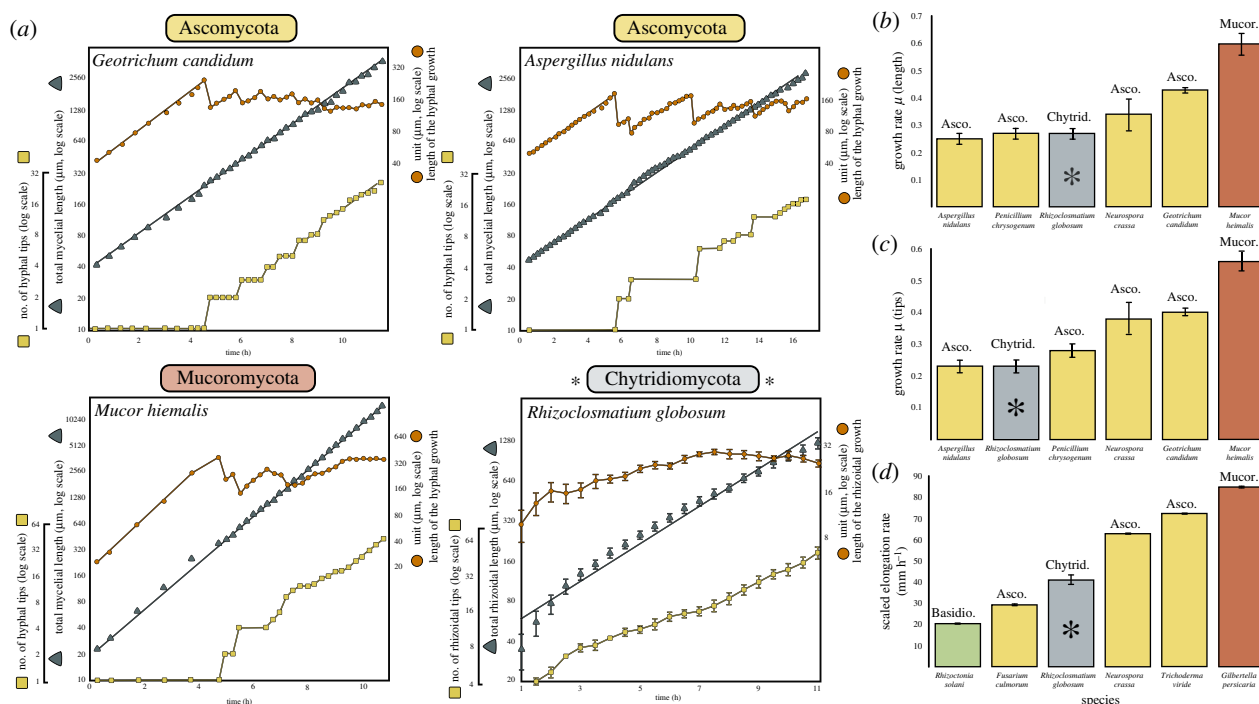


**Figure 5.** Development of chytrid rhizoids fundamentally resembles mycelial development in hyphal fungi. Comparison of rhizoid development from this study (asterisks) with other studies on hyphal fungi [22,27]. (a) Growth trajectories of the growth unit, total length and number of tips of rhizoids and hyphae. Data for other fungi are reproduced as new figures directly from [22]. For *R. globosum*  $n = 5$  biological replicates. Error bars denote  $\pm$  s.e.m. (b,c) *R. globosum* has similar growth rates regarding total length (b) and tip production (c) to hyphal fungi. Rhizoid growth rates ( $\mu$ ) calculated as increase in the total rhizoid length or tip number as in [22]. Data for Ascomycota and Mucoromycota fungi are from [22]. For *R. globosum*  $n = 5$  biological replicates. Mean  $\pm$  s.d. (d) *R. globosum* rhizoids when scaled by diameter have a comparable elongation rate to hyphae. Rhizoid elongation rates (the speed at which individual rhizoid compartments extend) were quantified by measurement of extending rhizoid compartments (10 rhizoids for each biological replicate) separated by a 30 min interval on maximum intensity projected z-stacks in Fiji. Data for other fungi are from [27]. For *R. globosum*  $n = 5$  biological replicates. Mean  $\pm$  s.e.m.

rhizoidal fungi. Dense branching zones in dikaryan mycelia are known to improve colonization of trophic substrates and feeding by increasing surface area for osmotrophy, while more linear ‘exploring’ zones cover greater area and search for new resources [39]. Similar morphometrics are displayed by *R. globosum* exhibiting feeding and searching phenotypes, respectively. In addition, exogenous carbon starvation has also been shown to be associated with a decrease in branching in the multicellular dikaryan fungus *Aspergillus oryzae* (Ascomycota) [40]. Overall, these results highlight that adaptive search strategies are more widely spread than previously known in the Kingdom Fungi.

Finally, we report the spatial and functional differentiation of feeding and searching sections of anucleate rhizoid systems from individual cells. The simultaneous display of both rhizoid types in the same cell indicates a controlled spatial regulation of branching and differentiation of labour within single chytrid rhizoid networks. Functional division of labour is prevalently seen in multicellular mycelial fungi [38,39] including the development of specialized branching structures for increased surface area and nutrient uptake, as in the plant symbiont mycorrhiza (Glomeromycota) [41]. Our observation of similarly complex development in a unicellular chytrid suggests that multicellularity is not a prerequisite for adaptive spatial differentiation in fungi.

## 5. Conclusion

The improved understanding of chytrid rhizoid biology related to substrate attachment and feeding we present here opens the door to a greater insight into the functional ecology of chytrids

and their environmental potency. Our approach of combining live cell confocal microscopy with three-dimensional rhizoid reconstruction provides a powerful toolkit for morphometric quantification of chytrid cell development and could shed light on the biology underpinning chytrid ecological prevalence. In the future, the application of this approach to different systems could provide a detailed understanding of chytrid parasitism and host interaction, development under different nutrient regimes and degradation of diverse carbon sources.

From an evolutionary perspective, the early-diverging fungi are a critical component of the eukaryotic tree of life [42,43], including an origin of multicellularity and the establishment of the archetypal fungal hyphal form, which is responsible in part for the subsequent colonization of land by fungi, diversity expansion and interaction with plants [2]. Our cell biology focused approach advances this developing paradigm by showing that a representative unicellular, rhizoid-bearing (i.e. non-hyphal) chytrid displays hyphal-like morphogenesis, with evidence that the cell structuring mechanisms (e.g. apical dominance) underpinning chytrid rhizoid development are equivalent to reciprocal mechanisms in dikaryan fungi.

Perhaps our key discovery is that the anucleate chytrid rhizoid shows considerable developmental plasticity. *R. globosum* is able to control rhizoid morphogenesis to produce a searching form in response to carbon starvation and, from an individual cell, is capable of spatial differentiation in adaptation to patchy substrate availability indicating functional division of labour. The potential for convergent evolution aside, we propose by parsimony from the presence of analogous complex cell developmental features in an extant representative chytrid



and dikaryan fungi that adaptive rhizoids are a shared feature of their most recent common ancestor.

**Data accessibility.** All data that support the findings of this study are included in the electronic supplementary material of this paper.

**Authors' contributions.** D.L. and M.C. conceived the study. D.L. conducted the laboratory work and data analysis. N.C. analysed the *R. globosum* JEL800 genome. G.W. provided support with microscopy. M.C. secured the funding. D.L. and M.C. critically assessed and interpreted the findings. D.L. and M.C. wrote the manuscript, with the help of N.C. and G.W.

**Competing interests.** The authors declare no competing interests.

**Funding.** D.L. is supported by an EnvEast Doctoral Training Partnership (DTP) PhD studentship funded from the UK Natural Environment Research Council (NERC grant no. NE/L002582/1). M.C. is supported by the European Research Council (ERC) (MYCO-CARB project; ERC grant agreement no. 772584). N.C. is supported by NERC (Marine-DNA project; NERC grant no. NE/N006151/1). G.W. is supported by an MBA Senior Research Fellowship.

**Acknowledgements.** The authors would like to thank Glenn Harper, Alex Strachan and the team at the Plymouth Electron Microscopy Centre (PEMC) for their assistance. We are indebted to Joyce Longcore (University of Maine) for providing *R. globosum* JEL800 from her chytrid culture collection (now curated by the Collection of Zoosporic Eufungi at the University of Michigan).

## References

1. Tedersoo L, Sánchez-Ramírez S, Kõljalg U, Bahram M, Döring M, Schigel D, May T, Ryberg M, Abarenkov K. 2018 High-level classification of the Fungi and a tool for evolutionary ecological analyses. *Fungal Divers.* **90**, 135–159. (doi:10.1007/s13225-018-0401-0)
2. Berbee ML, James TY, Strullu-Derrien C. 2017 Early diverging fungi: diversity and impact at the dawn of terrestrial life. *Annu. Rev. Microbiol.* **71**, 41–60. (doi:10.1146/annurev-micro-030117-020324)
3. Stajich JE, Berbee ML, Blackwell M, Hibbett DS, James TY, Spatafora JW, Taylor JW. 2009 The Fungi. *Curr. Biol.* **19**, R840–R845. (doi:10.1016/j.cub.2009.07.004)
4. Strullu-Derrien C, Goral T, Longcore JE, Olesen J, Kenrick P, Edgecombe GD. 2016 A new chytridiomycete fungus intermixed with crustacean resting eggs in a 407-million-year-old continental freshwater environment. *PLoS ONE* **11**, e0167301. (doi:10.1371/journal.pone.0167301)
5. Dee JM, Mollicone M, Longcore JE, Roberson RW, Berbee ML. 2015 Cytology and molecular phylogenetics of Monoblepharidomycetes provide evidence for multiple independent origins of the hyphal habit in the Fungi. *Mycologia* **107**, 710–728. (doi:10.3852/14-275)
6. Kiss E *et al.* 2019 Comparative genomics reveals the origin of fungal hyphae and multicellularity. *Nat. Commun.* **10**, 4080. (doi:10.1038/s41467-019-12085-w)
7. Strullu-Derrien C, Spencer ART, Goral T, Dee J, Honegger R, Kenrick P, Longcore JE, Berbee ML. 2018 New insights into the evolutionary history of Fungi from a 407 Ma Blastocladiomycota fossil showing a complex hyphal thallus. *Phil. Trans. R. Soc. B* **373**, 20160502. (doi:10.1098/rstb.2016.0502)
8. Harris SD. 2011 Hyphal morphogenesis: an evolutionary perspective. *Fungal Biol.* **115**, 475–484. (doi:10.1016/j.funbio.2011.02.002)
9. Grossart H-P, Van Den Wyngaert S, Kagami M, Wurzbacher C, Cunliffe M, Rojas-Jimenez K. 2019 Fungi in aquatic ecosystems. *Nat. Rev. Microbiol.* **17**, 339–354. (doi:10.1038/s41579-019-0175-8)
10. Frenken T *et al.* 2017 Integrating chytrid fungal parasites into plankton ecology: research gaps and needs. *Environ. Microbiol.* **19**, 3802–3822. (doi:10.1111/1462-2920.13827)
11. Longcore JE, Pessier AP, Nichols DK. 1999 *Batrachochytrium dendrobatidis* gen. et sp. nov., a chytrid pathogenic to amphibians. *Mycologia* **91**, 219–227. (doi:10.1080/00275514.1999.12061011)
12. Gleason FH, Kagami M, Lefevre E, Sime-Ngando T. 2008 The ecology of chytrids in aquatic ecosystems: roles in food web dynamics. *Fungal Biol. Rev.* **22**, 17–25. (doi:10.1016/j.fbr.2008.02.001)
13. O'Hanlon SJ *et al.* 2018 Recent Asian origin of chytrid fungi causing global amphibian declines. *Science* **360**, 621–627. (doi:10.1126/science.aar1965)
14. Sparrow FK. 1960 *Aquatic phycomycetes*. Ann Arbor, MI: University of Michigan Press.
15. Mondo SJ *et al.* 2017 Widespread adenine N6-methylation of active genes in fungi. *Nat. Genet.* **49**, 964–968. (doi:10.1038/ng.3859)
16. Rodriguez A, Ehlenberger DB, Dickstein DL, Hof PR, Wearne SL. 2008 Automated three-dimensional detection and shape classification of dendritic spines from fluorescence microscopy images. *PLoS ONE* **3**, e1997. (doi:10.1371/journal.pone.0001997)
17. Rodriguez A, Ehlenberger DB, Hof PR, Wearne SL. 2006 Rayburst sampling, an algorithm for automated three-dimensional shape analysis from laser scanning microscopy images. *Nat. Protoc.* **1**, 2152–2161. (doi:10.1038/nprot.2006.313)
18. Torben-Nielsen B. 2014 An efficient and extendable python library to analyze neuronal morphologies. *Neuroinformatics* **12**, 619–622. (doi:10.1007/s12021-014-9232-7)
19. Stamatakis A. 2014 RAxML version 8: a tool for phylogenetic analysis and post-analysis of large phylogenies. *Bioinformatics* **30**, 1312–1313. (doi:10.1093/bioinformatics/btu033)
20. Katoh K, Standley DM. 2013 MAFFT Multiple Sequence Alignment Software Version 7: improvements in performance and usability. *Mol. Biol. Evol.* **30**, 772–780. (doi:10.1093/molbev/mst010)
21. Guillard RRL, Ryther JH. 1967 Studies of marine planktonic diatoms. I. *Cyclotella nana* Hustedt and *Detonula confervaceae* (Cleve) Gran. *Can. J. Microbiol.* **8**, 229–239. (doi:10.1139/m62-029)
22. Trinci APJ. 1974 A study of the kinetics of hyphal extension and branch initiation of fungal mycelia. *Microbiology* **81**, 225–236. (doi:10.1099/0021287-81-1-225)
23. Ruiz-Herrera J, Ortiz-Castellanos L. 2010 Analysis of the phylogenetic relationships and evolution of the cell walls from yeasts and fungi. *FEMS Yeast Res.* **10**, 225–243. (doi:10.1111/j.1567-1364.2009.00589.x)
24. Richards TA, Leonard G, Wideman JG. 2017 What defines the 'kingdom' Fungi? *Microbiol. Spectr.* **5**, FUNK-0044-2017.
25. Roemer T, Delaney S, Bussey H. 1993 SKN1 and KRE6 define a pair of functional homologs encoding putative membrane proteins involved in beta-glucan synthesis. *Mol. Cell. Biol.* **13**, 4039–4048. (doi:10.1128/MCB.13.7.4039)
26. Han Q, Wang N, Yao G, Mu C, Wang Y, Sang J. 2019 Blocking  $\beta$ -1,6-glucan synthesis by deleting KRE6 and SKN1 attenuates the virulence of *Candida albicans*. *Mol. Microbiol.* **111**, 604–620. (doi:10.1111/mmi.14176)
27. López-Franco R, Bartnicki-Garcia S, Bracker CE. 1994 Pulsed growth of fungal hyphal tips. *Proc. Natl Acad. Sci. USA* **91**, 12 228–12 232. (doi:10.1073/pnas.91.25.12228)
28. Harris SD. 2019 Hyphal branching in filamentous fungi. *Dev. Biol.* **451**, 35–39. (doi:10.1016/j.ydbio.2019.02.012)
29. Semighini CP, Harris SD. 2008 Regulation of apical dominance in *Aspergillus nidulans* hyphae by reactive oxygen species. *Genetics* **179**, 1919–1932. (doi:10.1534/genetics.108.089318)
30. Obert M, Pfeifer P, Sernetz M. 1990 Microbial growth patterns described by fractal geometry. *J. Bacteriol.* **172**, 1180–1185. (doi:10.1128/JB.172.3.1180-1185.1990)
31. Gow NAR, Latge J-P, Munro CA. 2017 The fungal cell wall: structure, biosynthesis, and function. *Microbiol. Spectr.* **5**, FUNK-0035-2016.
32. Steinberg G, Peñalva MA, Riquelme M, Wösten HA, Harris SD. 2017 Cell biology of hyphal growth. *Microbiol. Spectr.* **5**, FUNK-0034-2016.
33. Riquelme M *et al.* 2018 Fungal morphogenesis, from the polarized growth of hyphae to complex reproduction and infection structures. *Microbiol. Mol. Biol. Rev.* **82**, e00068-17. (doi:10.1128/MMBR.00068-17)
34. Moreno-Velázquez SD, Seidel C, Juvvadi PR, Steinbach WJ, Read ND. 2017 Caspofungin-mediated growth inhibition and paradoxical growth



- in *Aspergillus fumigatus* involve fungicidal hyphal tip lysis coupled with regenerative intrahyphal growth and dynamic changes in  $\beta$ -1,3-glucan synthase localization. *Antimicrob. Agents Chemother.* **61**, e00710-17. (doi:10.1128/AAC.00710-17)
35. Allen ED, Aiuto R, Sussman AS. 1980 Effects of cytochalasins on *Neurospora crassa*. *Protoplasma* **102**, 63–75. (doi:10.1007/BF01276948)
36. Dee JM, Landry BR, Berbee ML. 2019 Actin guides filamentous rhizoid growth and morphogenesis in the zoospore fungus *Chytrium hyalinus*. *Mycologia* **111**, 904–918. (doi:10.1080/00275514.2019.1669999)
37. Medina EM, Robinson KA, Bellingham-Johnstun K, Ianiri G, Laplante C, Fritz-Laylin LK, Buchler NE. 2019 Genetic transformation and live-cell nuclear and actin dynamics during the life cycle of a chytrid. bioRxiv 787945. (doi:10.1101/787945)
38. Boddy L. 1999 Saprotrophic cord-forming fungi: meeting the challenge of heterogeneous environments. *Mycologia* **91**, 13–32. (doi:10.1080/00275514.1999.12060990)
39. Vinck A, Terlou M, Pestman WR, Martens EP, Ram AF, Van Den Hondel CAMJJ, Wösten HAB. 2005 Hyphal differentiation in the exploring mycelium of *Aspergillus niger*. *Mol. Microbiol.* **58**, 693–699. (doi:10.1111/j.1365-2958.2005.04869.x)
40. Pollack JK, Li ZJ, Marten MR. 2008 Fungal mycelia show lag time before re-growth on endogenous carbon. *Biotechnol. Bioeng.* **100**, 458–465. (doi:10.1002/bit.21779)
41. Bago B, Azcon-Aguilar C, Goulet A, Piche Y. 1998 Branched absorbing structures (BAS): a feature of the extraradical mycelium of symbiotic arbuscular mycorrhizal fungi. *New Phytol.* **139**, 375–388. (doi:10.1046/j.1469-8137.1998.00199.x)
42. James TY *et al.* 2006 Reconstructing the early evolution of Fungi using a six-gene phylogeny. *Nature* **443**, 818–822. (doi:10.1038/nature05110)
43. Jones MDM, Forn I, Gadelha C, Egan MJ, Bass D, Massana R, Richards TA. 2011 Discovery of novel intermediate forms redefines the fungal tree of life. *Nature* **474**, 200–203. (doi:10.1038/nature09984)

Laundon D, Mock T, Wheeler G, and Cunliffe M. 2021. Healthy herds in the phytoplankton: the benefit of selective parasitism. *ISME J* **15**:2163-2166.  
doi:10.1038/s41396-021-00936-8

© The Author(s), under exclusive licence to International Society for Microbial Ecology 2021. Material from: 'Laundon et al., *Healthy herds in the phytoplankton: the benefit of selective parasitism.*, ISME J., 2021, Springer Nature.



# Healthy herds in the phytoplankton: the benefit of selective parasitism

Davis Laundon<sup>1,2</sup> · Thomas Mock<sup>2</sup>  · Glen Wheeler<sup>1</sup> · Michael Cunliffe<sup>1,3</sup> 

Received: 27 October 2020 / Revised: 8 February 2021 / Accepted: 10 February 2021  
© The Author(s), under exclusive licence to International Society for Microbial Ecology 2021

## Abstract

The impact of selective predation of weaker individuals on the general health of prey populations is well-established in animal ecology. Analogous processes have not been considered at microbial scales despite the ubiquity of microbe-microbe interactions, such as parasitism. Here we present insights into the biotic interactions between a widespread marine thraustochytrid and a diatom from the ecologically important genus *Chaetoceros*. Physiological experiments show the thraustochytrid targets senescent diatom cells in a similar way to selective animal predation on weaker prey individuals. This physiology-selective targeting of ‘unhealthy’ cells appears to improve the overall health (i.e., increased photosynthetic quantum yield) of the diatom population without impacting density, providing support for ‘healthy herd’ dynamics in a protist–protist interaction, a phenomenon typically associated with animal predators and their prey. Thus, our study suggests caution against the assumption that protist–protist parasitism is always detrimental to the host population and highlights the complexity of microbial interactions.

Animal predators can exert overall positive effects on the health of prey populations by removing individuals with suboptimal health [1, 2] in a manner that has been termed ‘healthy herd’ dynamics [3]. While such top-down processes are well-established in animal ecology [1–3], they have largely been unconsidered in microbe-microbe interactions.

Protist–protist parasitism is widespread in the marine environment [4] and is generally considered to be detrimental to host populations [5, 6]. However, despite their ubiquity, the ecophysiological impact of protist–protist parasitism remains poorly understood. An important case

that necessitates investigation is protist parasitism of diatoms, which have limited representation with culture-dependent model systems despite the significance of diatoms in marine ecosystem functioning and global primary production [7].

We observed and isolated a heterotrophic protist growing epibiotically on moribund and dead *Chaetoceros* sp. diatoms from a summer bloom at Station L4 in the Western English Channel off Plymouth (UK) (Fig. 1A, B; Supplementary Figs. 1 and 2; Supplementary Methods). Single-cell picking achieved diatom and parasite co-cultures and uninfected host diatoms. The 18 S rRNA gene V4 region of the protist (termed ‘ThrauL4’) identified the epibiont as a novel thraustochytrid (Stramenopila; Labyrinthulomycota; Thraustochytrida) (Supplementary Fig. 3). Searching for ThrauL4 18 S rRNA gene homologues in the Ocean Sampling Day dataset revealed that the parasite has a wide distribution in coastal temperate regions (Supplementary Fig. 4).

Stable *Chaetoceros*-ThrauL4 co-cultures permitted the characterisation of ThrauL4 internal structures (Supplementary Figs. 5 and 6), epibiotic growth (Fig. 1A, B; Supplementary Figs. 7 and 8) and infection dynamics (Fig. 1C, D). ThrauL4 also attached to other diatoms (*Odontella sinensis*, *Ditylum brightwellii* and *Coscindodiscus* sp.) in a similar manner to *Chaetoceros* sp. but not dinoflagellates (Fig. 1C; Supplementary Fig. 9).

---

**Supplementary information** The online version contains supplementary material available at <https://doi.org/10.1038/s41396-021-00936-8>.

✉ Michael Cunliffe  
micnli@mba.ac.uk

<sup>1</sup> Marine Biological Association of the UK, The Laboratory, Citadel Hill, Plymouth, UK

<sup>2</sup> School of Environmental Sciences, University of East Anglia, Norwich, UK

<sup>3</sup> School of Biological and Marine Sciences, University of Plymouth, Plymouth, UK

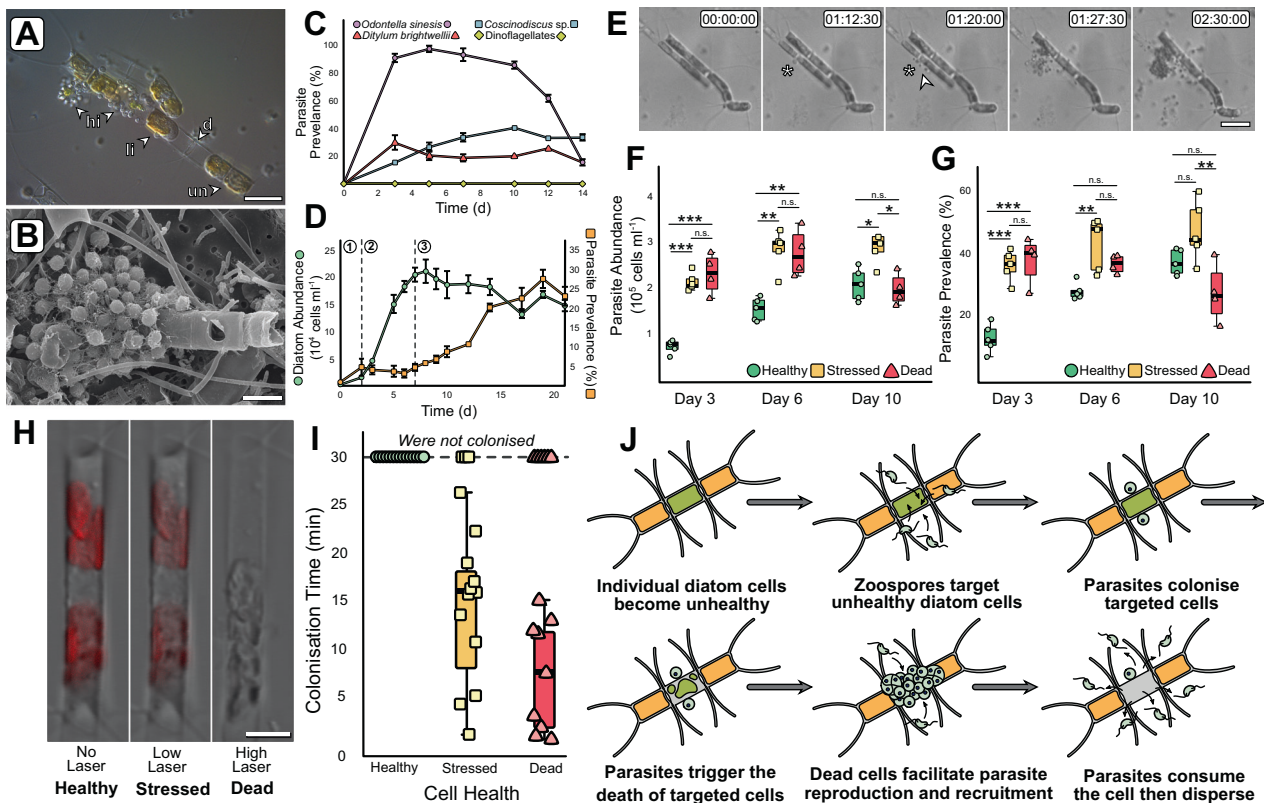


**Fig. 1** Growth experiments demonstrate that thraustochytrids preferentially target and grow on unhealthy diatom cells. **A** Differential interference contrast (DIC) image of *Chaetoceros* chain exhibiting different degrees of infection by Thraul4. Uninfected cell (un), a lightly infected cell (li), heavily infected cells (hi) and a dead, empty frustule (d). Scale bar = 20  $\mu\text{m}$ . **B** Scanning Electron Micrograph (SEM) of a *Chaetoceros* diatom swarmed by Thraul4. Scale bar = 5  $\mu\text{m}$ . **C** Thraul4 growth dynamics on a selected range of diatoms and dinoflagellates (*Alexandrium minutum* and *Prorocentrum minimum*) ( $\pm$ SEM,  $n = 3$ ). **D** *Chaetoceros* growth with Thraul4 ( $\pm$ SEM,  $n = 5$ ). Dashed lines demarcate the lag (1), exponential (2) and stationary (3) phases of *Chaetoceros* growth. **E** Time-lapse of *Chaetoceros*-Thraul4 showing Thraul4 colonising unhealthy cells. Asterisk = cytoplasmic bleb from

unhealthy diatom. Arrowhead = initial thraustochytrid colonisation. Timestamp = HH:MM:SS. Difference in the abundance (**F**) and prevalence (**G**) of parasites in healthy (control), stressed and dead *Chaetoceros* populations ( $n = 5$ ) inoculated with Thraul4 following heat stress exposure. ANOVA Tukey's HSD  $n.s.p > 0.05$  (not significant),  $*p < 0.05$ ,  $**p < 0.01$ ,  $***p < 0.001$ . **H** Example diatom exposed to different laser powers used to generate individual *Chaetoceros* cells of varying health. Red channel overlay demarks chlorophyll autofluorescence. Scale bar = 5  $\mu\text{m}$ . **I** Time taken for individual diatom cells ( $n = 15$ ) exposed to varying laser treatments to be colonised by Thraul4. **J** Diagrammatic representation of the proposed diatom-thraustochytrid interaction cycle based on time-lapse microscopy observations (see Supplementary Videos).

The proportion of diatom cells with Thraul4 attached increased when *Chaetoceros* sp. cells entered the stationary growth phase (Fig. 1D). Time-lapse microscopy revealed the dynamic nature of the Thraul4-diatom interaction (Fig. 1E, Supplementary Movies 1–6), with the motile Thraul4 apparently targeting physiologically ‘unhealthy’ cells identified by cytoplasmic blebbing prior to colonisation (Fig. 1E).

We set out to test the hypothesis that Thraul4 targeted unhealthy diatoms using population-level ecophysiology experiments. When introduced to heat-stressed diatom populations, Thraul4 had a higher fitness (i.e. became more abundant) and infected more *Chaetoceros* sp. cells than when exposed to healthy un-stressed diatoms (Fig. 1F, G), confirming more optimal growth of the parasite amongst unhealthy diatom populations. Furthermore, selective

targeting was also demonstrated at the single-cell level using laser-damaged individual cells and time-lapse microscopy (Fig. 1H, I). 80% of stressed cells and 60% of dead cells were colonised by Thraul4 during the 30 min experimental period, whereas diatoms in healthy control populations were un-colonised.

These results led us to investigate the physiological impact of thraustochytrid parasitism on host diatom populations by comparing the dynamics and health of parasite exposed and non-exposed *Chaetoceros* sp. populations (Fig. 2A–C). Based on the previous growth experiments showing Thraul4 proliferation during the diatom stationary phase (Fig. 1D), *Chaetoceros* sp. cultures grown to their stationary phase after 7 d were chosen to mimic environmental bloom decline. Using the photosynthetic quantum yield (Fv/Fm) as a proxy for overall diatom health [8], after

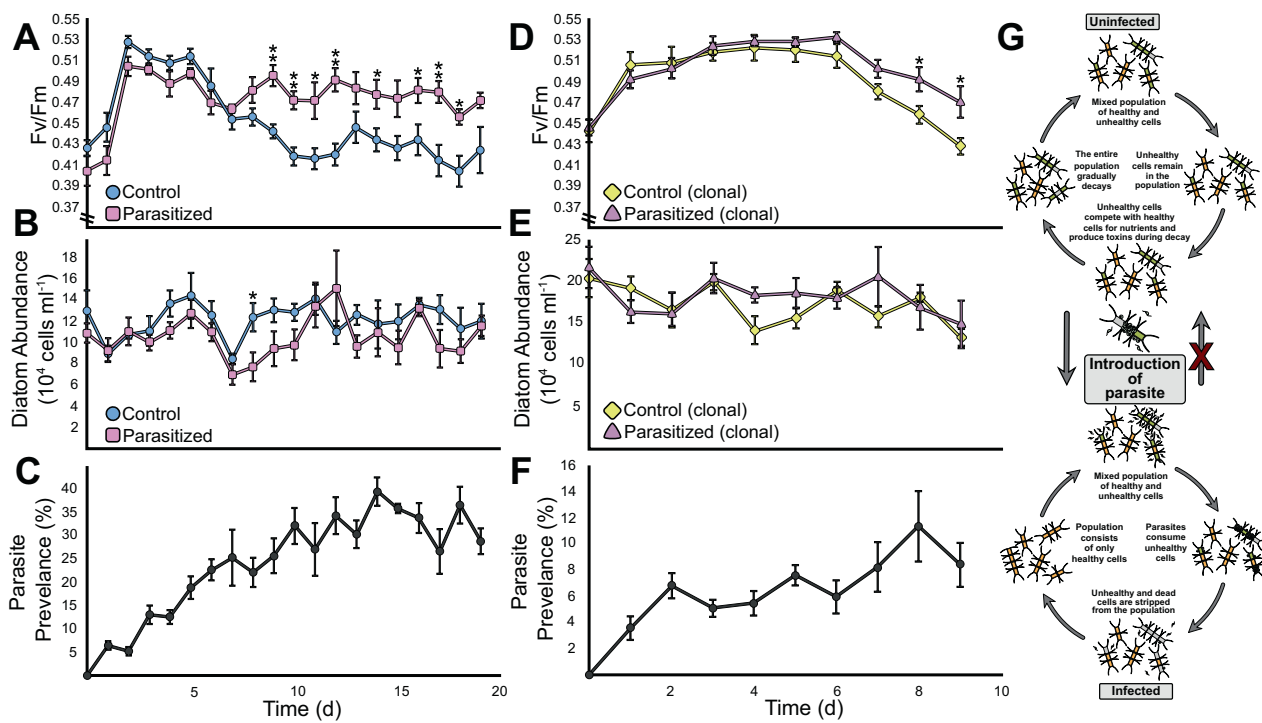


**Fig. 2** Selective targeting of unhealthy diatom cells by thraustochytrids improves the overall health of the diatom population. A–C Population dynamics of the Fv/Fm (A) and total number (B) of stationary *Chaetoceros* diatoms for control and parasitized diatom populations over the experimental period ( $\pm$ SEM,  $n = 5$ ). Welch's *t*-test \* $p < 0.05$ , \*\* $p < 0.01$ , \*\*\* $p < 0.001$ . The parasite prevalence did not exceed about a third of the total population (C) ( $\pm$ SEM,  $n = 5$ ). Parasites added at 0 d. In a separate experiment (D–F), a clonal *Chaetoceros* population was generated. Population dynamics of the

Fv/Fm (D), total number (E) and infection prevalence (F) of stationary *Chaetoceros* diatoms for control and parasitized populations made clonal by single-cell picking ( $\pm$ SEM,  $n = 5$ ). Significance values as above. Parasites added at 0 day. Taken together these results indicate that preferential thraustochytrid parasitism of unhealthy diatoms strengthens the overall health of the population therefore providing evidence for the 'healthy herd' hypothesis in a phytoplankton population, which is summarised diagrammatically in (G).

8 d, the parasitized *Chaetoceros* sp. populations were consistently healthier than those in the control non-exposed populations (Fig. 2A). Diatom population density was similar in both treatments (Fig. 2B) and parasite prevalence peaked after 8 days (Fig. 2C). In a separate experiment to investigate the role of genotype specificity in ThrauL4 parasitism, we generated a clonal *Chaetoceros* sp. population by single-cell picking and exposed the population to ThrauL4 cultures growing independently from diatoms. Although the clonal population declined in health more rapidly overall, ThrauL4 parasitism also resulted in healthier populations (Fig. 2D–F) suggesting that these results are not an artefact of genotype specificity and succession.

By removing physiologically weaker individuals from the population, the remaining cells will constitute an overall healthier population. However, other mechanisms may also promote an overall healthier diatom population. It may be that selective parasitism relieves nutrient competition between unhealthy and healthy individuals. In the natural environment, diatom-diatom competition is a major growth limiting factor [9, 10] and removing the pressure exerted by weaker cells may allow the population to be more robust. It

is also possible that the thraustochytrid could be 'cleaning' the population by preventing the build-up of toxic waste products or the proliferation of detrimental co-culture bacteria in an analogous way to how carrion removal by vultures prevents the spread of diseases to mammals [11]. In addition, thraustochytrid parasitism could accelerate nutrient recycling by releasing nutrients from dying cells. The consequences of physiology-selective diatom parasitism should be assessed in the marine environment, including impacts at the community scale and in the context of ecosystem functioning.

The proposed influence of thraustochytrid parasitism on diatom population health is summarised in Fig. 2G. We suggest that this thraustochytrid-diatom interaction provides evidence of 'healthy herd' dynamics in a protist–protist interaction, an ecological phenomenon typically associated with animal predator–prey interactions [3]. As we show here with ThrauL4, animal predators such as lions [12], cougars [13], African wild dogs [14], and wolves [15] have been shown to target prey with suboptimal health. The 'healthy herd' hypothesis states that by selective predation on unhealthy prey,

predators increase the overall health of the prey population by increasing resource availability or by removing potential carriers of disease [3]. Evidence for ‘healthy herd’ dynamics where predation generates healthier prey populations has also been demonstrated in lobster-sea urchin [16], fish-*Daphnia* [17], and fox-grouse [18] predator–prey systems. Here, we provide analogous supportive evidence from a marine protist–protist system.

‘Healthy herd’ dynamics between protists challenges the assumption that protist–protist parasitism is always detrimental to the host population and raises caution in this assumption in ecosystem modelling or inference from molecular ecology surveys (e.g., metabarcoding). Our results have demonstrated the potential complexity of protist–protist symbioses, highlighting the value of culture-based experimentation and the importance of developing model co-culture systems in resolving complex ecological interactions. The underpinning biology and ecological importance *in natura* of such interactions now require further investigation.

**Acknowledgements** We thank the crew of the *RV Sepia* for sampling and Angela Ward and Claire Hopkins (MBA) for their guidance with isolation and culturing. We also thank Glenn Harper, Alex Strachan and the team at the Plymouth Electron Microscopy Centre (PEMC) for their assistance with SEM. We are indebted to Jingwen Pan (University of British Columbia) and Javier del Campo (Institute of Evolutionary Biology, Spain) for providing the reference sequences used in building phylogenetic trees in this study, as well as to Daniel Vaultot (Station Biologique de Roscoff) for help in interpreting the Ocean Sampling Day data. Nathan Christmas (MBA) is also thanked for bioinformatic support.

## Compliance with ethical standards

**Conflict of interest** The author declares no competing interests.

**Publisher’s note** Springer Nature remains neutral with regard to jurisdictional claims in published maps and institutional affiliations.

## References

1. Slobodkin LB. Prudent predation does not require group selection. *Am Nat.* 1974;108:665–78.

2. Williams PD. Unhealthy herds: some epidemiological consequences of host heterogeneity in predator-host-parasite systems. *J Theor Biol.* 2008;253:500–7.
3. Packer C, Holt RD, Hudson PJ, Lafferty KD, Dobson AP. Keeping the herds healthy and alert: Implications of predator control for infectious disease. *Ecol Lett.* 2003;6:797–802.
4. Lima-Mendez G, Faust K, Henry N, Decelle J, Colin S, Carcillo F, et al. Determinants of community structure in the global plankton interactome. *Science* 2015;348:1262073.
5. Skovgaard A. Dirty tricks in the plankton: Diversity and role of marine parasitic protists. *Acta Protozool.* 2014;53:51–62.
6. Jephcott TG, Sime-Ngando T, Gleason FH, MacArthur DJ. Host-parasite interactions in food webs: Diversity, stability, and coevolution. *Food Webs.* 2016;6:1–8.
7. Nelson DM, Tréguer P, Brzezinski MA, Leynaert A, Quéguiner B. Production and dissolution of biogenic silica in the ocean: Revised global estimates, comparison with regional data and relationship to biogenic sedimentation. *Glob Biogeochem Cycles.* 1995;9:359–72.
8. Timmermans KR, Veldhuis MJ, Brussaard CP. Cell death in three marine diatom species in response to different irradiance levels, silicate, or iron concentrations. *Aquat Micro Ecol.* 2007;46:253–61.
9. Pinto E, Van Nieuwerburgh L, De Barros MP, Pedersén M, Colepicolo P, Snoeijls P. Density-dependent patterns of thiamine and pigment production in the diatom *Nitzschia microcephala*. *Phytochemistry.* 2003;63:155–63.
10. Manoylov KM. Intra- and interspecific competition for nutrients and light in diatom cultures. *J Freshw Ecol.* 2009;24:145–57.
11. Houston DC, Cooper JE. The digestive tract of the whiteback griffon vulture and its role in disease transmission among wild ungulates. *J Wildl Dis.* 1975;11:306–13.
12. Schaller G. *The Serengeti lion: a study of predator-prey relations.* London: University of Chicago Press; 1972.
13. Krumm CE, Conner MM, Hobbs NT, Hunter DO, Miller MW. Mountain lions prey selectively on prion-infected mule deer. *Biol Lett.* 2010;6:209–11.
14. Pole A, Gordon IJ, Gorman ML, MacAskill M. Prey selection by African wild dogs (*Lycaon pictus*) in southern Zimbabwe. *J Zool.* 2004;262:207–15.
15. Husseman JS, Murray DL, Power G, Mack C, Wenger CR, Quigley H. Assessing differential prey selection patterns between two sympatric large carnivores. *Oikos.* 2003;101:591–601.
16. Lafferty KD. Fishing for lobsters indirectly increases epidemics in sea urchins. *Ecol Appl.* 2004;14:1566–73.
17. Duffy MA, Hall SR, Tessier AJ, Huebner M. Selective predators and their parasitized prey: Are epidemics in zooplankton under top-down control? *Limnol Oceanogr.* 2005;50:412–20.
18. Hudson PJ, Dobson AP, Newborn D. Do parasites make prey vulnerable to predation? Red grouse and parasites. *J Anim Ecol.* 1992;61:681.